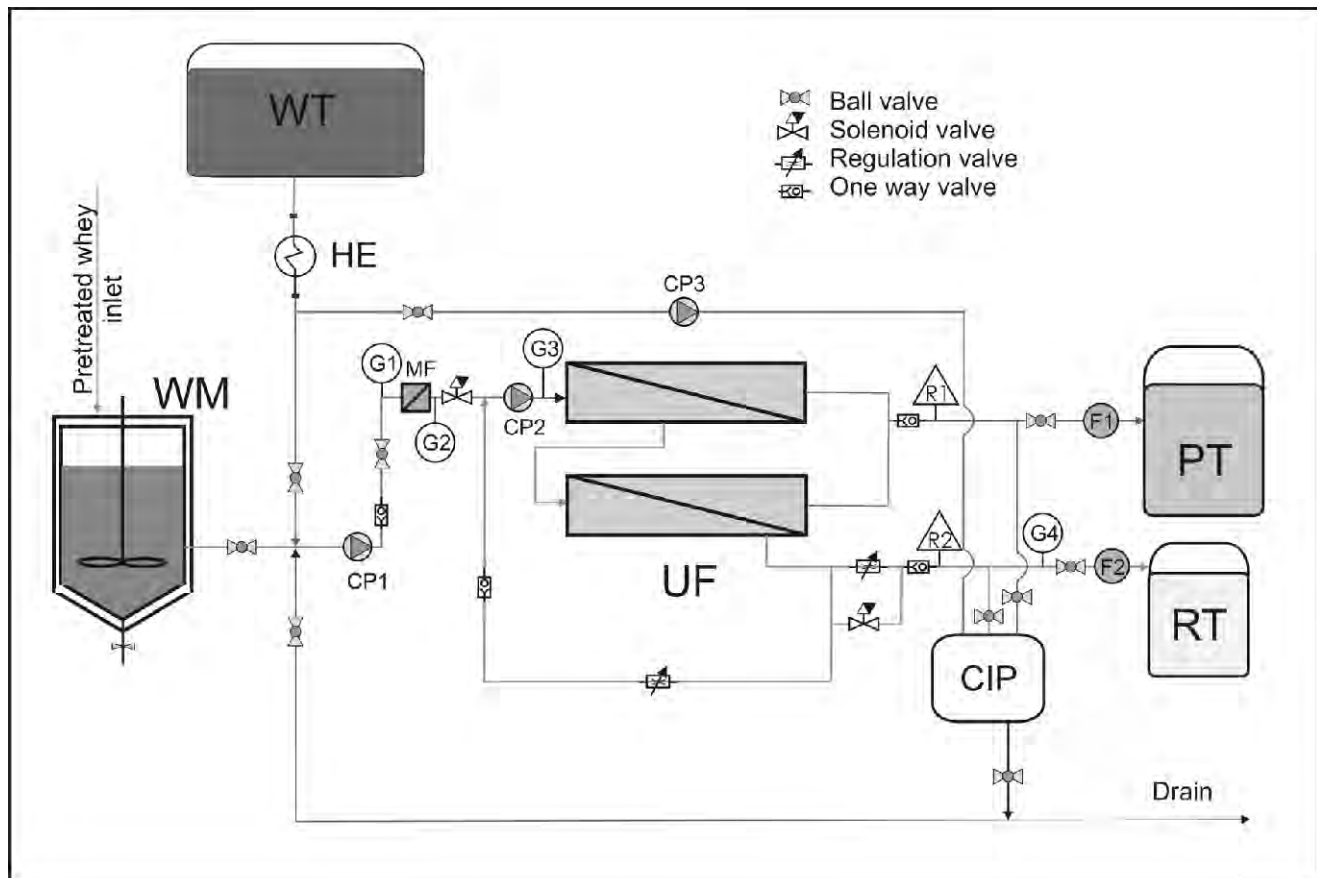


5

Hemijska industrija

Vol. 67

Časopis Saveza hemijskih inženjera
Chemical Industry



GENERALNI POKROVITELJ



HEMOFARM KONCERN

VRŠAC, Beogradski put bb, tel. 013/821-345, 821-027, 821-129
BEOGRAD, Prote Mateje 70, tel. 011/344-26-63, faks: 344-17-87
E-pošta: info@hemofarm.com

IZDAVANJE ČASOPISA POMOGLA JE:



INŽENJERSKA KOMORA SRBIJE
Bulevar vojvode Mišića 37
11000 Beograd

SUIZDAVAČI



Tehnološko-metalurški fakultet
Univerziteta u Beogradu, Beograd



Prirodno-matematički fakultet Univerziteta
u Novom Sadu, Novi Sad



Hemijski fakultet
Univerziteta u Beogradu
Beograd



Institut za tehnologiju nuklearnih i drugih
mineralnih sirovina, Beograd



HIP Petrohemija a.d. Pančevo



Tehnološki fakultet Univerziteta
u Novom Sadu, Novi Sad



NU Institut za hemiju,
tehnologiju i metalurgiju
Univerziteta u Beogradu,
Beograd



Tehnološki fakultet Univerziteta
u Nišu, Leskovac



„Nevena Color“ d.o.o.
Leskovac



DCP Hemigal, Leskovac



Chemical Industry

Химическая промышленность

Hemijska industrija

Časopis Saveza hemijskih inženjera Srbije

Journal of the Association of Chemical Engineers of Serbia

Журнал Союза химических инженеров Сербии

VOL. 67

Beograd, septembar–oktobar 2013

Broj 5

Izdavač

Savez hemijskih inženjera Srbije
Beograd, Kneza Miloša 9/1

Glavni urednik

Branko Bugarski

Urednici

Katarina Jeremić, Ivana Banković-Ilić, Maja Obradović,
Dušan Mijin

Članovi uredništva

Milorad Cakić, Željko Čupić, Željko Grbavčić, Katarina
Jeremić, Miodrag Lazić, Slobodan Petrović, Milovan
Purenović, Aleksandar Spasić, Dragoslav Stojiljković,
Radmila Šećerov-Sokolović, Slobodan Šerbanović,
Nikola Nikačević, Svetomir Milojević

Članovi uredništva iz inostranstva

Dragomir Bukur (SAD), Jiri Hanika (Češka Republika),
Valerij Meshalkin (Rusija), Ljubiša Radović (SAD),
Constantinos Vayenas (Grčka)

Likovno-grafičko rešenje naslovne strane

Milan Jovanović

Redakcija

11000 Beograd, Kneza Miloša 9/1
Tel/fax: 011/3240-018
E-pošta: shi@yubc.net
www.ache.org.rs

Izlazi dvomesečno, rukopisi se ne vraćaju

Za izdavača

Tatijana Duduković

Sekretar redakcije

Slavica Desnica

Izdavanje časopisa pomaže

Republika Srbija, Ministarstvo prosvete, nauke i
tehnološkog razvoja

Upłata preplate i oglasnog prostora vrši se na tekući
račun Saveza hemijskih inženjera Srbije, Beograd, broj
205-2172-71, Komercijalna banka a.d., Beograd

Kompjuterska priprema

Vladimir Panić

Štampa

Razvojno-istraživački centar grafičkog inženjerstva,
Tehnološko-metalurški fakultet, Univerzitet u
Beogradu, Karnegijeva 4, 11000 Beograd

Indeksiranje

Radovi koji se publikuju u časopisu *Hemijska Industrija*
ideksiraju se preko *Thompson Reuters Scietific®* servisa
Science Citation Index - Expanded™ i *Journal Citation
Report (JCR)*, kao i domaćeg *SCIndeks* servisa Centra za
evaluaciju u obrazovanju i nauci

SADRŽAJ

Jovana N. Trbojević, Aleksandra S. Dimitrijević, Dušan V. Veličković, Marija Gavrović-Jankulović, Nenad B. Milosavić, Isolation of <i>Candida rugosa</i> lipase isoforms 703
Ljubica M. Radović, Milutin Z. Nikičević, Branka M. Jordović, Some aspects of microstructure and properties of Al-Mg alloys after shear spinning and cold rolling 707
Vesna M. Marjanović, Slavica S. Lazarević, Ivona M. Janković-Častvan, Bojan M. Jokić, Andelika Z. Bjelajac, Đorđe T. Janačković, Rada D. Petrović, Functionalization of thermo-acid activated sepiolite by amine-silane and mercapto-silane for chromium(VI) adsorption from aqueous solutions 715
Dragica M. Kisić, Saša R. Miletić, Vladimir D. Radonjić, Sanja B. Radanović, Jelena Z. Filipović, Ivan A. Gržetić, Prirodna radioaktivnost uglja i letećeg pepela u termoelektrani „Nikola Tesla B“ 729
Marija Z. Šljivić-Ivanović, Ivana D. Smičiklas, Jelena P. Marković, Aleksandra S. Milenković, Analiza faktora koji utiču na sorpciju Cu(II) jona klinoptilolitom 739
Aleksandar Z. Fišteš, Dušan Z. Rakić, Biljana S. Pajin, Ljubica P. Dokić, Ivana R. Nikolić, The effect of processing parameters on energy consumption of ball mill refiner for chocolate 747
Marija D. Mihailović, Aleksandra S. Patarić, Zvonko P. Gulišija, Zoran V. Janjušević, Miroslav D. Sokić, Mogućnosti primene atmosferskog plazma-sprej postupka za dobijanje prevlaka hidroksiapatita na uzorcima od nerđajućeg čelika 753
Krešimir Osman, Dragi Stamenković, Mihailo Lazarević, Integration of system design and production processes in robust mechatronic product architectures development – extended M-FBPP framework 759
Ivana S. Kostić, Tatjana D. Andelković, Ružica S. Nikolić, Tatjana P. Cvetković, Dušica D. Pavlović, Aleksandar Lj. Bojić, Comparative study of binding strengths of heavy metals with humic acid 773
Jovanka V. Popov-Raljić, Jovanka G. Laličić-Petronijević, Etelka B. Dimić, Vladimir S. Popov, Vesna B. Vujasinović, Ivana V. Blešić, Milijanko J. Portić, Change of sensory characteristics and some quality parameters of mixed milk and cocoa spreads during storage up to 180 days 781
Sanela M. Đorđević, Nebojša D. Cekić, Tanja M. Isailović, Jela R. Milić, Gordana M. Vučeta, Miodrag L. Lazić, Snežana D. Savić, Nanoemulzije dobijene variranjem tipa emulgatora i udela masne faze: Uticaj formulacije i procesnih parametara na karakteristike i fizičku stabilnost 795

SADRŽAJ nastavak

Milica V. Arsenović, Lato L. Pezo, Zagorka M. Radojević, Slavka M. Stanković, Serbian heavy clays behavior: Application in rough ceramics	811
Svetlana Vujović, Srđan Kolaković, Milena Bečelić-Tomin, Procena kvaliteta vode značajno izmenjenih vodnih tela na teritoriji Vojvodine primenom multivarijacionih statističkih metoda	823
Miroslav Đ. Kukučka, Nikoleta M. Kukučka, Investigation of whey protein concentration by ultrafiltration elements designed for water treatment	835
Svetomir Ž. Milojević, Dragana B. Radosavljević, Vladimir P. Pavicević, Srđan Pejanović, Vlada B. Veljković, Modeling the kinetics of essential oil hydrodistillation from plant materials	843

CONTENTS

Jovana N. Trbojević, Aleksandra S. Dimitrijević, Dušan V. Veličković, Marija Gavrović-Jankulović, Nenad B. Milosavić, Isolation of <i>Candida rugosa</i> lipase isoforms	703
Ljubica M. Radović, Milutin Z. Nikachević, Branka M. Jordović, Some aspects of microstructure and properties of Al–Mg alloys after shear spinning and cold rolling	707
Vesna M. Marjanović, Slavica S. Lazarević, Ivona M. Janković-Častvan, Bojan M. Jokić, Andelika Z. Bjelajac, Đorđe T. Janačković, Rada D. Petrović, Functionalization of thermo-acid activated sepiolite by amine-silane and mercapto-silane for chromium(VI) adsorption from aqueous solutions	715
Dragica M. Kisić, Saša R. Miletić, Vladimir D. Radonjić, Sanja B. Radanović, Jelena Z. Filipovic, Ivan A. Gržetić, Natural radioactivity of coal and fly ash at the Nikola Tesla B TPP	729
Marija Z. Šljivić-Ivanović, Ivana D. Smičiklas, Jelena P. Marković, Aleksandra S. Milenković, Analysis of factors influencing Cu(II) sorption by clinoptiolite	739
Aleksandar Z. Fišteš, Dušan Z. Rakić, Biljana S. Pajin, Ljubica P. Dokić, Ivana R. Nikolić, The effect of processing parameters on energy consumption of ball mill refiner for chocolate	747
Marija D. Mihailović, Aleksandra S. Patarić, Zvonko P. Gulišija, Zoran V. Janjušević, Miroslav D. Sokić, The possibilities of atmospheric plasma-spraying application to obtain hydroxyapatite coatings on the stainless steel samples	753
Krešimir Osman, Dragi Stamenović, Mihailo Lazarević, Integration of system design and production processes in robust mechatronic product architectures development – extended M-FBPP framework	759
Ivana S. Kostić, Tatjana D. Andelković, Ružica S. Nikolić, Tatjana P. Cvetković, Dušica D. Pavlović, Aleksandar Lj. Bojić, Comparative study of binding strengths of heavy metals with humic acid	773
Jovanka V. Popov-Raljić, Jovanka G. Laličić-Petronijević, Etelka B. Dimić, Vladimir S. Popov, Vesna B. Vujasinović, Ivana V. Blešić, Milijanko J. Portić, Change of sensory characteristics and some quality parameters of mixed milk and cocoa spreads during storage up to 180 days	781
Sanela M. Đorđević, Nebojša D. Čekić, Tanja M. Isailović, Jela R. Milić, Gordana M. Vučeta, Miodrag L. Lazić, Snežana D. Savić, Nanoemulsions produced by varying the type of emulsifier and oil content: Effect of formulation and process parameters on the characteristics and physical stability	795

CONTENTS Continued

Milica V. Arsenović, Lato L. Pezo, Zagorka M. Radojević, Slavka M. Stanković, Serbian heavy clays behavior: Application in rough ceramics.....	811
Svetlana Vujović, Srđan Kolaković, Milena Bečelić-Tomin, Evaluation of heavily modified water bodies in Vojvodina by using multivariate statistical techniques.....	823
Miroslav Đ. Kukučka, Nikoleta M. Kukučka, Investigation of whey protein concentration by ultrafiltration elements designed for water treatment	835
Svetomir Ž. Milojević, Dragana B. Radosavljević, Vladimir P. Pavicević, Srđan Pejanović, Vlada B. Veljković, Modeling the kinetics of essential oil hydrodistillation from plant materials.....	843

Isolation of *Candida rugosa* lipase isoforms

Jovana N. Trbojević¹, Aleksandra S. Dimitrijević², Dušan V. Veličković², Marija Gavrović-Jankulović², Nenad B. Milosavić²

¹Innovation Center of Faculty of Chemistry, University of Belgrade, Serbia

²Faculty of Chemistry, University of Belgrade, Serbia

Abstract

The yeast *Candida rugosa* is a convenient source of lipases for science and industry. Crude preparation of *Candida rugosa* lipase (CRL) consists of several extracellular lipases. Isoenzyme profile depends on the culture or fermentation conditions. All isoforms are coded by the lip pseudogene family; they are monomers of 534 amino acids and molecular weight of about 60 kDa. They share the same catalytic mechanism and interfacial mode of activation. Isoenzymes differ in isoelectric points, post-translational modifications, substrate specificity and hydrophobicity. The presence of different lipase isoforms and other substances (*i.e.*, inhibitors) in crude preparation leads to lack of their productivity in biocatalytic reactions. Purification of specific isoform improves its overall performance and stability. This paper provides an overview of different methods for purification of CRL isoenzymes up to date, their advantages and disadvantages.

Keywords: Lipases, *Candida rugosa*, isoforms, purification.

Available online at the Journal website: <http://www.ache.org.rs/HI/>

Lipases (E.C.3.1.1.3, glycerol ester hydrolase) catalyze the hydrolysis of an ester bond between a fatty acid and glycerol. They are among the most important biocatalysts in modern science and industry. Many plant, animal and microbial cells produce lipases. Microbial lipases (fungal, bacterial or yeast) have more importance over animal and plant lipases, because they can be easily grown on inexpensive agricultural waste materials: sugarcane, plant or animal fats and oils, etc. [1–6].

Yeast *Candida rugosa* (formerly known as *Candida cylindracea*) is a non-sporogenous, pseudofilamentous, unicellular yeast and imperfect hemiascomycete. It grows aerobically in nutritive media with different carbon and nitrogen source. *C. rugosa* is non-pathogenic microorganism, and its lipases do not show genotoxic or cancerogenic effects on human health. Because of that, the species is generally regarded as safe (*it has GRAS status*), and classified as biological safety level 1 [7–9].

CRL are decoded by lip pseudogene family. Each isoenzyme is a product of the expression of an individual gene, and each of the lip genes is transcriptionally active [7]. *C. rugosa* can produce 5–7 lipase isoforms, depending on the culture or fermentation conditions. All of them are glycosylated monomers of 534 amino acids and approximate molecular weight of 60 kDa and have the same catalytic triad (Ser, His, Glu or Asp). Iso-

PROFESSIONAL PAPER

UDC 663.12:577.152.311:66.097.3:60

Hem. Ind. **67** (5) 703–706 (2013)

doi: 10.2298/HEMIND120828113T

enzymes differ in their isoelectric points, carbohydrate content, substrate specificity and hydrophobicity.

C. rugosa lipases are very important biocatalytic tool in different fields of industry (food processing, cosmetic and pharmaceutical preparations, biodiesel production and detergent industry) and science (environmental sciences, analytical chemistry and medicine) [10–17].

EXPERIMENTAL

Crude preparation of CRL is a mixture of several different lipases and esterases. Activity of one of these enzymes affects the others in the preparation (*i.e.*, in a competitive way), so it is necessary to purify the individual isoform in order to improve its catalytic properties [18].

Multi-step approach

Pernas *et al.* purified an esterase of about 43 kDa and reported separation of lipase isoforms 2 and 3 from crude CRL preparation [19]. The crude sample was prepared in two ways: in the first preparation, the sample was simply dissolved in buffer and centrifuged. That supernatant was subjected to hydrophobic interaction chromatography (HIC) on phenyl-sepharose, followed by anion-exchange chromatography on DEAE-sephacel and gel-filtration on sephacryl S-200. The second preparation was slightly different, since the crude sample was dissolved in a buffer that contains ammonium sulphate. After stirring and centrifugation, obtained supernatant was subjected to HIC on phenyl-sepharose HR5/5, followed by anion-exchange chroma-

Correspondence: N.B. Milosavić, Faculty of Chemistry, University of Belgrade, Serbia.

E-mail: nenadmil@chem.bg.ac.rs

Paper received: 28 August, 2012

Paper accepted: 3 December, 2012

tography on Source 15Q HR5/5 and gel-filtration on sephacryl S-200.

Sailas and Pandey described purification method for three distinct fractions of lipases from crude fermentation material, designated as lipase A, B and C [20]. The purification scheme consists of: ammonium-sulphate precipitation, dialysis, ultrafiltration and gel-filtration on sephadex G-200.

Combining chromatography on agarose-mercurial column and desalting step on sephadex G-25, Tai *et al.* reported separation of two main lipase fractions from crude sample [21].

Combination of anion-exchange chromatography on DEAE-Sepharose CL-6B and "hydrophobic interfacial affinity chromatography" resulted in fine resolution of CRL isoenzymes, according to Xin *et al.* [22]. The anion-exchange step serves for crude separation of two main lipase fractions: CRL A and CRL B. HIC on nucleosil C4 column allowed fine separation of different isoforms, present within the main fractions. Accordingly, both CRL A and CRL B were further resolved to 4 isoenzymes, which slightly differ in their hydrophobicity pattern and hence cannot be separated by conventional HIC methods (*i.e.*, HIC on phenyl-sepharose). In isoelectric focusing, however, CRL A fraction only gave a single band of approximate $pI = 5.6$ and CRL B fraction also gave a single band of an approximate $pI = 4.2$.

Lipase 3 isoenzyme is reported to act on cholester-yl-esters. In order to investigate its activity on different plant steryl-esters it was necessary to obtain it from crude preparation. Tenkanen *et al.* describe a method for purification of this lipase isoform, based on combination of classical pre-purification procedure, HIC on phenyl-sepharose FF and ion-exchange chromatography on DEAE-Sepharose [23].

Blends of alginate and gelatin, additionally functionalized with succinic anhydride, can be used for separation of lipases, according to procedure described by Fadnavis *et al.* [24].

One-step approach

In recent years there has been a growing interest for developing new, more economic one-step purification strategies. In the further text, some of them will be presented.

Lv and associates have reported a one-step method for successful resolution of *Candida* sp. lipase into four distinct fractions [26]. In this approach, they used ion-exchange chromatography on polyethyleneimine monoliths.

Solanki and Gupta [26] have reported simultaneous immobilization and purification of CRL, for the use in transesterification. Lipase was adsorbed on a Fe_3O_4 nanoparticles and coated with polyethyleneimine (PEI). It is believed that purification is achieved because of selective binding property of PEI.

RESULTS AND DISCUSSION

The general advantage of a multi-step purification approach is that there are well established purification protocols, which are freely available. Also, a great advantage is the use of classic purification techniques, such as ion-exchange chromatography, HIC, gel-filtration, precipitations, etc.

On the other hand, the main disadvantage of such purification methods is the low yield of purified isoenzymes. Table 1 summarizes some of the previously mentioned methods with purification yields. According to data from the table, the highest yield is achieved after purification strategy described in literature [20]. However, in terms of industrial use, the yields are too low, so the described methods are not profitable for large-scale production. Apart from the low yield, the duration of purification process is also a problem, because at least 3 steps are needed for purification of an isoenzyme of interest.

One-step purification methods are convenient for modern approach in isolation of lipases from their sources. They are usually easy to perform, fast and

Table 1. Purification yields of different multi-step purification strategies

Purification steps	Purified isoenzyme	Yield, %	Reference
Precipitation, sodium-cholate treatment, ethanol/ether, anion-exchange	Lip 2 Lip 3	4.3 4.9	19
Ammonium-sulphate precipitation, dialysis, ultrafiltration, gel-filtration	Lip A Lip B Lip C	11.62 1.15 3.64	20
Chromatography on agarose-mercurial column	CRL I CRL II CRL III	Not defined	21
Ion-exchange chromatography, hydrophobic interfacial affinity chromatography	CRL A CRL B	Not defined	22
Pre-purification, HIC, ion-exchange	Lip 3	7	23

inexpensive. In the term of yield, the represented one-step strategies are compared in Table 2.

172049, 046010 and 451-03-00605/2012-16/51) and FP7 Reg Pot FCUB ERA, GA No. 256716.

Table 2. Purification yields of different one-step purification strategies

Purification steps	Purified Isoenzyme	Yield, %	Reference
Ion-exchange chromatography on polyethyleneimine monolith	Lipase A	3.50	25
	Lipase B	19.8	
	Lipase C	16.6	
	Lipase D	12.3	
Simultaneous immobilization and purification	Not defined	Not defined	26

CONCLUSION

Within the last decade, interest for microbial lipases, especially those produced by *C. rugosa*, has increased and will probably continue in that trend even more so in the future. Because of their numerous applications, especially in different fields of industry, it is necessary to find a way to purify these valuable biocatalysts from the crude preparations, which are most commonly used as starting material. Purification increases biocatalytic performances of an enzyme, since it is released from impurities, which can have inhibitory effects on its activity. Having in mind different approaches, described in this paper, it is possible to conclude what their advantages or disadvantages are.

Different multi-step methods have been described and developed, but their major disadvantage is a great loss in the yield during several purification steps. This disables the use of such approaches in large-scale purification, since it is expensive, time-consuming and gives poor yield of the enzyme of interest.

One-step approaches have also been developed. They are less time consuming, but not all of them are cost-effective, since some of them use expensive affinity ligands, or matrices, which cannot be used in large-scale production. The purification yield of such approaches can be improved by developing new, more selective purification procedures.

Nomenclature

CRL – *Candida rugosa* lipase

DEAE – Diethylaminoethyl group

EC – Enzyme Commission

FF – Fast flow

HIC – Hydrophobic interaction chromatography

HR – High resolution

Lip – Lipase

PEI - Polyethyleneimine

Acknowledgments

The authors are grateful for the financial support of the Ministry of Education, Science and Technological Development of the Republic of Serbia (Project Nos.

REFERENCES

- [1] K. Long, Unlocking the miracle of lipase, Research Inaugural Lecture Presented at MARDI, Serdang, 2010, pp. 1–46.
- [2] M.M. Zheng, Y. Lu, L. Dong, G. Ping-Mei, D. Quian-Chun, L. Wen-Lin, F. Yu-Qi, H. Feng-Hong, Immobilization of *Candida rugosa* lipase on hydrophobic/strong cation exchange silica particles for biocatalytic synthesis of phytosterol esters, *Biores. Technol.* **115** (2012) 141–146.
- [3] A. Rajan, D.R. Soban Kumar, A.J. Nair, Isolation of a novel alkaline lipase producing fungus *Aspergillus fumigatus* MTCC 9657 from aged and crude rice bran oil and quantification by HPTLC, *Int. J. Biol. Chem.* **5** (2011) 116–126.
- [4] K.J. Patil, M.Z. Chopda, R.T. Mahajan, Lipase biodiversity, *Ind. J. Sci. Technol.* **4** (2011) 971–982
- [5] L.L. Lock, V.A. Corbellini, P. Valente, Lipases produced by yeasts: powerful biocatalysts for industrial purposes, *Techno-Logica* **11** (2007) 18–25
- [6] B. Dias Ribeiro, A. Machado de Castro, M.A. Zarur Coelho, D.M. Guimaraes Freire, Production and use of lipases in bioenergy: a review from the feedstocks to biodiesel production, *Enz. Res.* (2011), doi: 10.4061/ /2011/615803.
- [7] B. Sailas, P. Ashok, *Candida rugosa* lipases: molecular biology and versatility in biotechnology, *Yeast* **14** (1998) 1069–1087.
- [8] M.T. Flood, M. Kondo, Safety evaluation of lipase produced from *Candida rugosa*: summary of toxicological data, *Reg. Toxicol. Pharmacol.* **33** (2001) 157–164.
- [9] http://www.bcrc.firdi.org.tw/fungi/fungal_detail.jsp?id=FU200802060045 (accessed 12 July, 2012).
- [10] F. Kartal, A. Kilinc, S. Timur, Lipase biosensor for tributyrin and pesticide detection, *Int. J. Environ. Analyt. Chem.* **87** (2007) 715–722.
- [11] J.F. Liang, Y.T. Li, V.C. Yang, Biomedical application of immobilized enzymes, *J. Pharm. Sci.* **89** (2000) 979–990.
- [12] A.A. Khan, M.A. Alzohairy, Recent advantages and applications of immobilized enzyme technologies: A review, *Res. J. Biol. Sci.* **5** (2010); 565–575.
- [13] M.R. Talukder, J.C. Wu, L. Pen-Lin Chua, Conversion of waste cooking oil to biodiesel via enzymatic hydrolysis followed by chemical esterification, *Energ. Fuel.* **24** (2010) 2016–2019.

- [14] A. Rajendran, A. Palanisamy, A. Thangavelu, Lipase catalyzed ester synthesis for food processing industries, *Braz. Arch. Biol. Technol.* **52** (2009) 207–219.
- [15] http://www.epa.gov/greenchemistry/pubs/pgcc/winner_s/gspa09.html (accessed 12 July 2012).
- [16] P. Winayanuwattikun, C. Kaewpiboon, K. Piriyakananon, W. Chulalaksananukul, T. Yongvanich, J. Svasti, Immobilized lipase from potential lyophilic microbes for catalyzing biodiesel production using palm oil as feedstock, *Afric. J. Biotechnol.* **10** (2011) 1666–1673.
- [17] S. Zhu, Y. Wu, Z. Yu, Immobilization of *Candida rugosa* lipase on a pH-sensitive support for enantioselective hydrolysis of ketoprofen ester, *J. Biotechnol.* **116** (2005) 397–401.
- [18] C.C. Akoh, G.C. Lee, J.F. Shaw, Protein engineering and applications of *Candida rugosa* lipase isoforms, *Lip.* **39** (2004) 513–526.
- [19] M.A. Pernas, C. Lopez, L. Pastrana, M.L. Rua, Purification and characterization of Lip2 and Lip3 isoenzymes from a *Candida rugosa* pilot-plant scale fed-batch fermentation, *J. Biotechnol.* **84** (2000) 163–174.
- [20] B. Sailas, P. Ashok, Isolation and characterization of three distinct forms of lipases from *Candida rugosa* produced in solid state fermentation, *Braz. Arch. Biol. Technol.* **43** (2000) 453–460.
- [21] D.F. Tai, Y.F. Chang, T.W. Chiou, Purification of *Candida rugosa* lipase on agarose-mercurial column, *J. Chin. Chem. Soc.* **49** (2002) 957–960.
- [22] J.Y. Xin, Y.X. Hu, J.R. Cui, S.B. Li, C.G. Xia, L.M. Zhu, Fine separation and characterization of *Candida rugosa* lipase isoenzymes, *J. Basic Microbiol.* **42** (2002) 355–363.
- [23] M. Tenkanen, H. Kontkanen, R. Isonemi, P. Spetz, B. Holmbom, Hydrolysis of sterol esters by a lipase (Lip 3) from *Candida rugosa*, *Appl. Microbiol. Biotechnol.* **60** (2002) 120–127.
- [24] N.W. Fadnavis, G. Sheelu, B. Mani Kumaar, M.U. Bhale-rao, A.A. Desphande, Gelatin blends with alginate: gels for lipase immobilization and purification, *Biotechnol. Prog.* **19** (2003) 557–564.
- [25] G. Bassani, P. Fucinos, G. Pico, B. Farruggia, *Candida rugosa* lipase Lip1-polyethyleneglycol interaction and the relation with its partition in aqueous and two-phase system, *Colloids Surfaces, B* **75** (2010) 532–537.
- [26] Y.Q. Lv, D.Y. Fu, T.W. Tan, M.Y. Wang, One-step purification of YLLIP2 isoforms from *Candida* sp. 99–125 by polyethyleneimine modified poly(glycidyl methacrylate-co-ethyleneglycol dimethacrylate) monolith, *J. Mol. Catal., B* **62** (2010) 149–154.
- [27] K. Solanki, M.N. Gupta, Simultaneous purification and immobilization of *Candida rugosa* lipase on superparamagnetic Fe₃O₄ nanoparticles for catalyzing transesterification reactions, *New J. Chem.* **35** (2011) 2551–2556.

IZVOD

IZOLOVANJE IZOFORMI LIPAZE IZ *Candida rugosa*

Jovana N. Trbojević¹, Aleksandra S. Dimitrijević², Dušan V. Veličković², Marija Gavrović-Jankulović², Nenad B. Milosavić²

¹Inovacioni Centar Hemijskog fakulteta, Univerzitet u Beogradu

²Hemijski fakultet, Univerzitet u Beogradu

(Stručni rad)

Lipaze (hidrolaze estara glicerola, E.C.3.1.3.3) su važna grupa enzima, široko rasprostranjenih u prirodi. Mogu se izolovati iz materijala biljnog, životinjskog ili mikrobnog porekla. Zahvaljujući svojim karakteristikama, pobuđuju sve više pažnje kao efikasni biokatalizatori u različitim sintetičkim i hidrolitičkim procesima. Među lipazama, poreklom iz mikroorganizama, posebno su značajne one koje produkuje kvasac *Candida rugosa*. Komercijalni preparat lipaza iz *C. rugosa* može sadržati 5–7 izoformi ekstracelularnih lipaza. Sve te izoforme kodirane su od strane *lip* familije pseudogena, a na njihovu ekspresiju utiču uslovi u kojima se mikroorganizam gaji (sastav hranljive podloge je najvažniji). Ekstracelularne lipaze, koje proizvodi *C. rugosa* su monomerni glikoproteini, molekulske mase od oko 60 kDa, sa 534 aminokiseline. Za sve izoforme je karakterističan isti složeni mehanizam aktivacije na granici faza i mehanizam katalize, kakav se sreće i kod serin-proteaza. Izoenzimi se međusobno razlikuju po post-translacionim modifikacijama (udelu ugljohidratne komponente), supstratnoj specifičnosti, izoelektričnim tačkama i hidrofobnosti. Prisustvo više izoformi lipaza u komercijalnom preparatu utiče na njihovu produktivnost u reakcijama koje katalizuju. Takvi preparati često sadrže i druge supstance koje mogu uticati na aktivnost enzima (na primer inhibitore). Razdvajanjem pojedinačnih izoformi iz komercijalnog preparata poboljšavaju se njihova enantioselektivnost, specifična aktivnost i stabilnost enzima, što je od izuzetnog značaja za njihovu dalju primenu. U ovom radu su predstavljeni različiti pristupi u razdvajaju pojedinačnih izoformi vanćelijskih lipaza iz komercijalnog preparata *C. rugosa*, njihove prednosti i nedostaci.

Ključne reči: Lipaze • *Candida rugosa* • Izoforme • Prečišćavanje

Some aspects of microstructure and properties of Al–Mg alloys after shear spinning and cold rolling

Ljubica M. Radović¹, Milutin Z. Nikičević¹, Branka M. Jordović²

¹Military Technical Institute, Belgrade, Serbia

²Faculty of Technical Sciences, Čačak, University of Kragujevac, Serbia

Abstract

Three commercial Al–Mg alloys containing 3 to 6 mass% of Mg (AlMg3, AlMg4.5Mn and AlMg6Mn) were subjected to different forming processes: shear spinning and cold rolling. The effect of Mg content and reduction in thickness on the tensile properties and microstructure evolution of Al–Mg alloys were studied. Both optical (OM) and transmission electron microscopy (TEM) were used for the microstructure characterization. The results show that the addition of Mg in these alloys increases the yield strength (YS) and ultimate tensile strength (UTS) in both cold rolled and spun specimens. The strength of all Al–Mg alloys after shear spinning was lower compared to the strength after cold rolling for the same strain. This effect was attributed to the occurrence of dynamic recovery during shear spinning and confirmed by transmission electron microscopy.

Keywords: Al–Mg alloys, shear spinning, cold rolling, mechanical properties, microstructure, dynamic recovery.

Available online at the Journal website: <http://www.ache.org.rs/HI/>

Spinning deformation processing is an advanced local metal forming process, which is widely used in many fields [1–9]. Generally, it refers to a group of processes for transforming flat sheet metal blanks or other preforms into hollow seamless, axisymmetric shapes (cylinders, cones, hemispheres or the other circular shapes) by a combination of rotation and force. The most often used terms are: conventional spinning, shear spinning (shear forming) and tube (cylindrical) flow forming. The main difference between these forming processes is in the wall thickness of the formed part. While in conventional spinning the wall thickness remains nearly constant throughout the process, in shear spinning and tube forming the wall thickness is considerably reduced.

During shear spinning a blank of the initial thickness (t_0) is reduced to a thickness (t) by a roller moving along a cone-shaped mandrel defined by an half angle, α . During shear forming, the material is displaced along an axis parallel to the mandrel's rotational axis, as shown in Figure 1. The principal deformation process is assumed to be one of the simple shears in plane strain and hence the name, shear forming [7]. The final wall thickness (t) is determined by initial thickness (t_0), and half-angle of the mandrel (α), according to the „sine“ law:

$$t = t_0 \sin \alpha \quad (1)$$

SCIENTIFIC PAPER

UDC 669.715.017:620.18

Hem. Ind. 67 (5) 707–714 (2013)

doi: 10.2298/HEMIND121023116R

The reduction in the wall thickness is calculated by:

$$r = 100(t - t_0)/t_0 (\%) \quad (2)$$

Therefore, the smaller the angle, the higher will be the reduction in wall thickness.

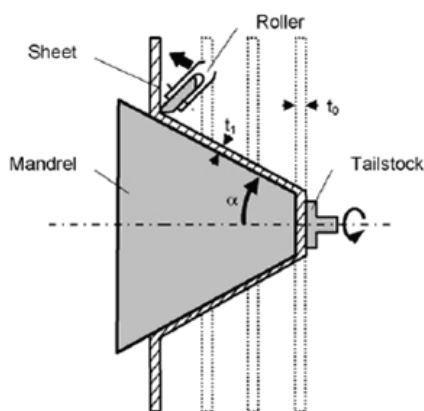


Figure 1. Schematic illustration of the shear spinning process [9].

Shear spinning and flow forming are used to manufacture the high-strength and high-precision thin-wall parts [10,11]. During shear spinning, the deformation of the preform takes place in localized volume in the small contact regions beneath the rollers. Therefore, the force required for deformation is significantly reduced compared to conventional press forming.

The force distribution in shear spinning has been analysed previously [7,8,12]. The differences between these forces and those in conventional cold rolling are evident [12–14]. Moreover, due to work hardening, significant improvement in mechanical properties can

Correspondence: Lj. Radović, Military Technical Institute, Belgrade, Ratka Resanovića 1, 11030 Belgrade, Serbia.

E-mail: ljubica.radovic@vti.vs.rs

Paper received: 23 October, 2012

Paper accepted: 4 December, 2012

be achieved. Shear spinning has other advantages compared to alternative manufacturing methods (such as press forming, machining, welding, etc.) of axisymmetric sheet metal components: low forming forces, simple tools, high surface quality and dimensional accuracy, small and large scale products, shorter production times, etc. In many cases, only a single-pass is required to produce the final component, without further production steps.

The processes with wall thickness reduction are very significant especially in aerospace and automotive applications and missile parts production (ballistic cap, warhead shells, jet engine parts, rocket nose cones, rocket nozzles, tubes of the tank, liquid or gas tanks and parts of turbines and many other parts).

Aluminium alloys are the most commonly used materials for advanced applications, due to their high strength/weight ratio, corrosion resistance and good formability. Recently, some experimental studies on shear spinning and tube forming were performed on aluminium and both heat treatable and non-heat treatable aluminium alloys [15–19]. High strength aluminum alloys used in the aerospace industry exhibit problems like consistency of tolerances introduced by quenching. Using non-heat treatable alloys (solid solution hardened) this problem is eliminated. Additionally, non-heat treatable Al alloys have better corrosion resistance and good formability. In this respect Al–Mg alloys are the most often used among solid solution hardening alloys. Good formability of Al–Mg alloys is achieved due to high solubility of Mg in solid solution and the solute-dislocation interaction. The effect of solute element on work hardening characteristics and deformation microstructure has received considerable interest [20–24], but the results describing the influence of

shear spinning on deformation behaviour are lacking.

The aim of this work is to evaluate the influence of processing technology (shear spinning or conventional cold rolling) on microstructure and mechanical properties of commercial Al–Mg alloys containing different contents of Mg and Mn.

EXPERIMENTAL

The material used in this study was industrially produced. As received hot rolled plates were further laboratory cold rolled and fully annealed. Annealed Al–Mg alloy sheets (0-temper) with initial thickness of 3 mm and average grain size of approximately 15 µm, were finally processed by shear spinning and conventional cold rolling. The chemical compositions of the alloys are given in Table 1.

Shear spinning experiments were carried out on a LEIFELD St 400 DK spinning machine. The preforms were flat sheet metal square blanks with dimensions of 130 mm×130 mm and initial thickness $S_0 = 3$ mm. Mandrels with different angles 2α of 90, 60, 40 and 20° were used, achieving the reductions in the wall thickness of $r \approx 30, 50, 66$ and 84%, respectively. The process parameters during shear spinning were: mandrel revolution, $n = 400$ rev/min for 2α of 90 and 60°, and $n = 660$ rev/min for 2α of 40 and 18°. The shear spun cones are presented in Figure 2.

Table 1. The chemical composition of Al–Mg alloys (mass%)

Alloy	Mg	Mn	Si	Cu	Fe	Zn	Ni	Al
AlMg3	3.10	0.03	0.09	0.01	0.31	0.04	0.01	Bal.
AlMg4,5Mn	4.50	0.47	0.16	0.02	0.42	0.02	0.01	Bal.
AlMg6Mn	6.02	0.54	0.12	0.015	0.36	0.07	0.01	Bal.

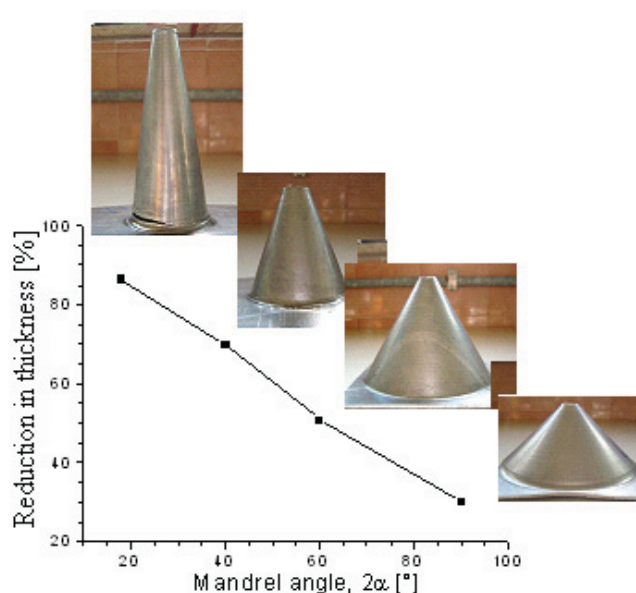


Figure 2. Effect of the mandrel angle on the reduction in the wall thickness and spun cones.

Conventional cold rolling was performed on laboratory rolling mill at a relatively low strain rate. Tensile tests were carried out at room temperature, with strain rate of $\dot{\varepsilon} = 6.7 \times 10^{-3} \text{ s}^{-1}$, on a "Zwick" testing machine, using a small ASTM tension specimen with a 25 mm gauge length [25].

The initial microstructure of annealed specimens and microstructure after deformation by shear spinning and cold rolling was characterized by optical microscopy (OM), as well as transmission electron microscopy (TEM) using a Jeol 100CX microscope operating at 100 kV. Specimens for OM were prepared by mechanical grinding and polishing techniques up to 1 μm diamond paste. To reveal the grain structure, after electrolytic polishing in perchloric acid, the samples were etched in Barker's solution (25 ml HBF₄ (40%), 1000 ml distilled water). Thin foils for TEM were prepared by a twin-jet polishing technique using a mixture of 30% nitric acid and 70% methanol at 30 °C. The microstructures of both spun and cold rolled specimens

were characterized (OM and TEM) on the cone/sheet surface, i.e., L-T plane.

RESULTS AND DISCUSSION

The influences of the reduction in the wall thickness on the microstructure and mechanical properties of the shear spun specimens were studied compared to the cold rolled specimens.

Mechanical properties

The yield strength (YS) and the ultimate tensile strength (UTS) dependence on the reduction of Al-Mg alloys after shear spinning and cold rolling are shown in Figures 3 and 4. The YS and UTS were enhanced after shear spinning and cold rolling. They increase with increase in the reduction of thickness. This behaviour is attributed to work hardening during deformation, together with influence of the elements in solid solution (mainly Mg and Mn), as well as second phase

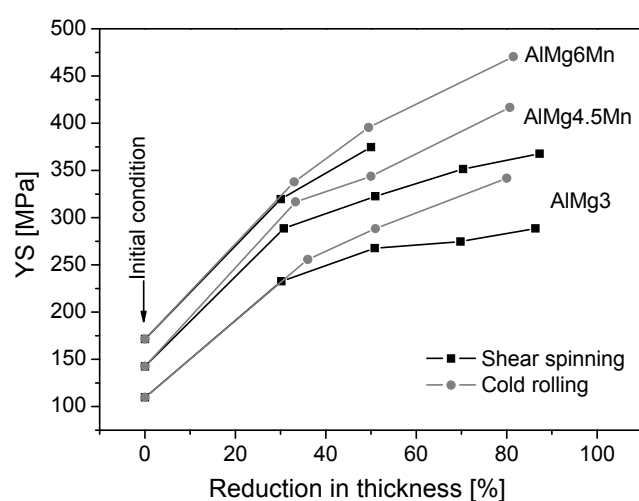


Figure 3. Effect of reduction in thickness on the yield strength (YS) of Al-Mg alloys deformed by shear spinning and cold rolling.

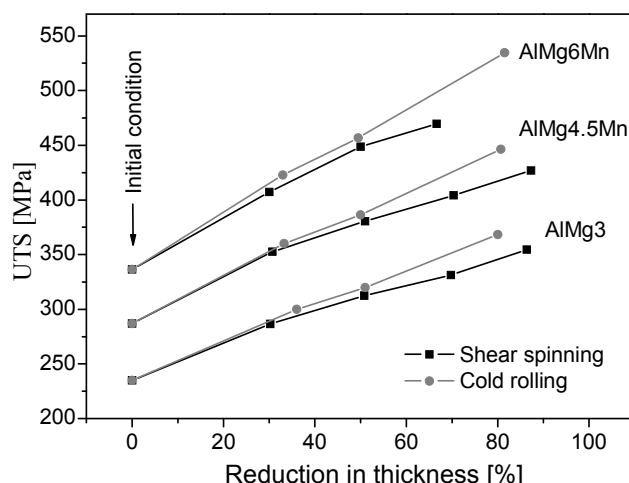


Figure 4. Effect of reduction in thickness on ultimate tensile strength (UTS) of Al-Mg alloys deformed by shear spinning and cold rolling.

particles, as already published [20,24]. Also, both YS and UTS of the shear spun specimens were lower compared to cold rolled specimens at the same reduction. The decline in the values of YS and UTS is more pronounced with increasing reduction in all alloys.

The differences in mechanical properties of spun and cold rolled specimens indicate that some softening occurred during shear spinning. During processing by shear spinning, the dynamic recovery becomes more efficient, resulting in decreased work hardening.

The effect of reduction on the total elongation during tensile tests of both shear spun and cold rolled specimens is shown in Figure 5. Elongation generally decreases with increase of applied reduction. This trend is observed in cold rolled specimens for all tested alloys. However, while elongation in the spun specimen of the AlMg3 alloy follows this trend, elongation of the other two alloys rapidly drops up to 30% reduction, decreases more slowly up to 50% reduction, and then even slightly increases. In other words, applying higher reduction during shear spinning leads to an increase of the total elongation in AlMg4.5Mn and AlMg6Mn alloys.

About 70% reduction in the wall thickness of the cones is achieved using a mandrel with $2\alpha = 40^\circ$.

Dimensional measurement showed that the final wall thickness was less than predicted by Eq. (1), indicating that the tested material was over-reduced [26]. Over-reduction has a great effect on the state of stress in the deformation zone and therefore on plasticity: over-reduction increased the plasticity of a material [27].

The effect of Mg content on the mechanical properties of Al-Mg alloys is summarized in Figure 6. The strength increased at any given reduction with increase of Mg content. This behaviour is in agreement with previously published results, confirming that magnesium addition in solid solution increases considerably the work hardening ability of aluminium [19,22,24]. The solid solution hardening is a result of an interaction between the mobile dislocations and the solute atoms.

Microstructure

Microstructural characterization of the tested alloys was performed in order to understand the difference in tensile properties of spun and cold rolled specimens. An optical micrograph of the AlMg3 sample in the initial annealed condition is shown in Figure 7a. The microstructure was characterized by equiaxial grains, implying that full recrystallization occurred. The results of

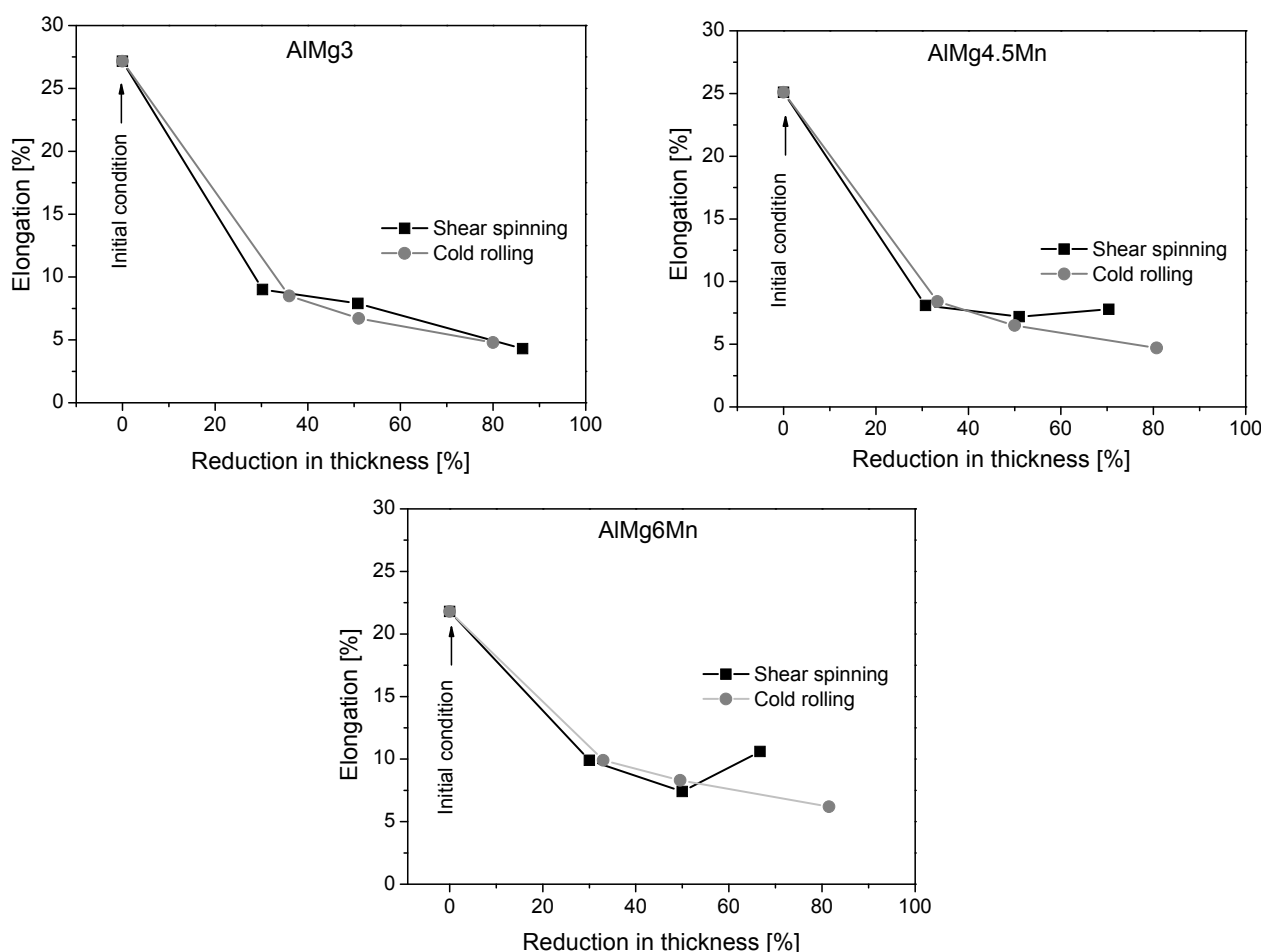


Figure 5. Effect of reduction in thickness on the total elongation of Al-Mg alloys deformed by shear spinning and cold rolling.

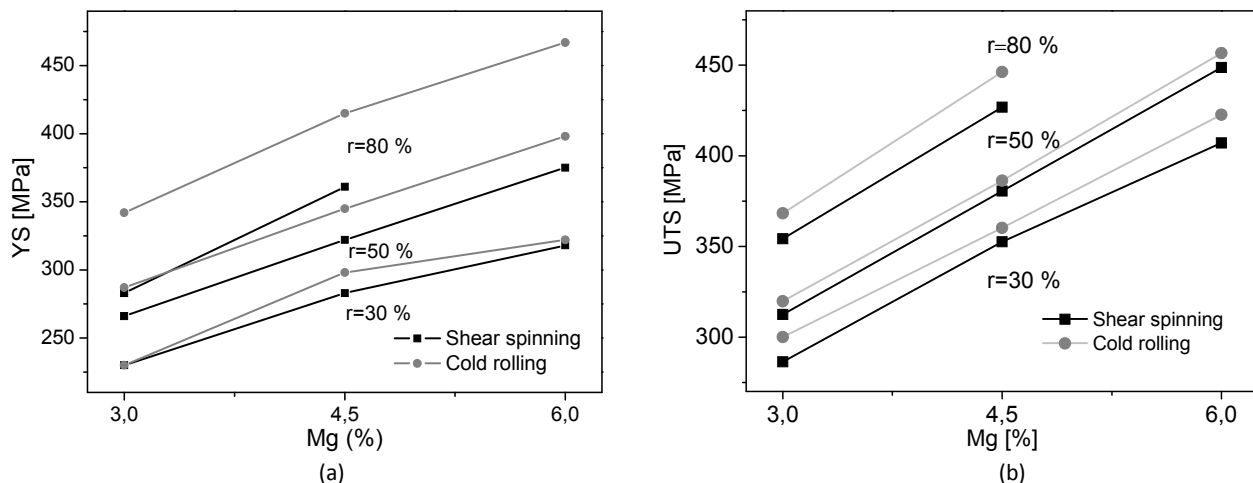


Figure 6. The influence of Mg content on tensile properties of Al-Mg alloys deformed by shear spinning and cold rolling.
a) Yield strength (YS); b) ultimate tensile strength (UTS).

microstructural investigation of deformed Al-Mg alloys by optical microscopy showed that the microstructures after both shear spinning and cold rolling are very similar. The grains became elongated with increasing reduction in thickness during shear spinning and cold rolling. Since during shear spinning the material is displaced axially, along an axis parallel to the mandrel's rotational axis the grains become elongated (Figure 7b). Very similar microstructure is observed after cold rolling (Figure 7c). Optical micrographs of AlMg6Mn and AlMg4.5Mn alloys after shear spinning and cold rolling show similar features [19,26]. Therefore, based on this observation it was not possible to explain obvious differences between the applied modes of deformation.

In order to clarify difference in strength, further analysis using TEM on AlMg3 alloy was performed after deformation at applied 80% reduction by shear spinning and cold rolling (Figure 8). The substructure after shear spinning is characterized by a well-defined cell band (Figure 8a). The band walls are well-defined in one direction, while formation of cell structure by arranging dislocations into cell walls is visible in the other direction.

The TEM micrograph in Figure 8b illustrates the cold rolled microstructure of AlMg3 alloy. A high level of residual stress is observed, therefore the individual dislocations are not visible. The fragmentation of the microstructure and reduction of dislocation density in the center of the fragment occurred. This is evidence of the first stage of dynamic recovery, as reported previously [20,21,23,24,28,29]. However, well-defined cell substructure was not formed, which indicates low recovery level and significant residual stress. Well defined cell walls and subgrains, as shown in Figure 8b, were observed only in a few cases.

This is in good correlation with the lower values of the strength after shear spinning than cold rolling and increasing plasticity. It was supposed that the formation of the subgrains and continually increasing subgrain boundaries misorientation, due to the annihilation of dislocations, leading to grain refinement near the original grain boundaries. The newly formed grains can accommodate deformation by mechanism of grain boundary sliding and thus contribute to increased ductility [30].

The dislocation density inside the subgrains after cold rolling is much higher compared to shear spinning.

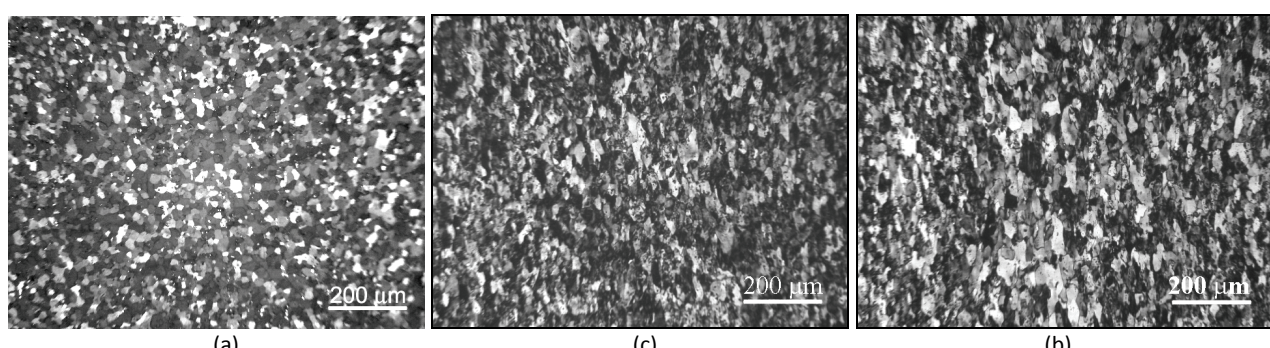


Figure 7. Optical micrographs of AlMg3 alloy. a) Initial annealed condition; b) processed by shear spinning ($r = 50\%$); c) processed by cold rolling ($r = 50\%$).

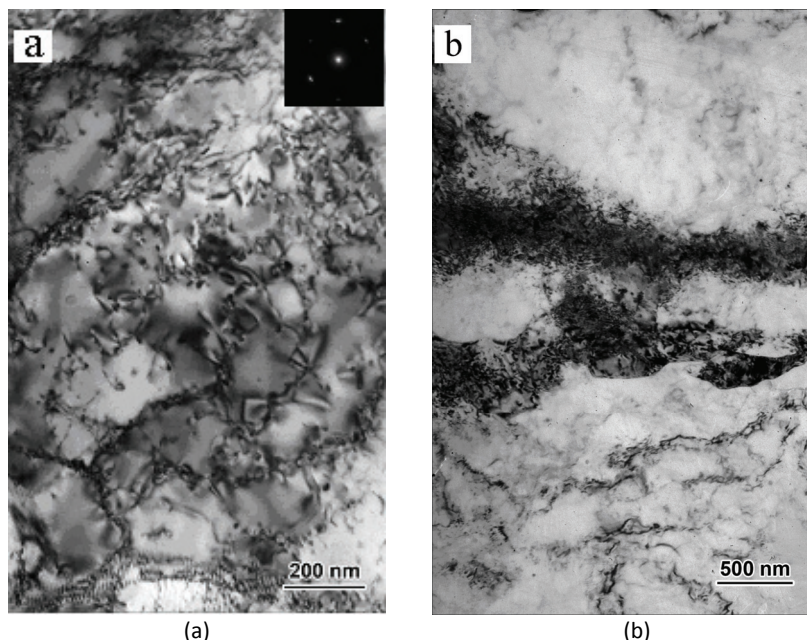


Figure 8. TEM Micrographs of dislocation substructure in AlMg3 alloy a) after shear spinning ($r = 85\%$) and b) after cold rolling ($r = 80\%$).

The difference in mechanical properties is attributed to dynamic recovery in shear spun samples.

TEM microstructures obtained for AlMg3 alloy show typical recovered structure. The lower values of tensile properties (YS and UTS) of spun compared to cold rolled specimens in the other two studied alloys (AlMg4.5Mn and AlMg6Mn) can be also attributed to dynamic recovery due to suppression of dynamic recrystallization in alloys with higher Mg content. Similar behaviour showing typically recovered microstructure is reported for Al–Cu–Mg alloy during tube spinning [31].

During dynamic recovery, simultaneously with generation of new dislocations, rearrangement of all dislocations occurs. This feature leads to dislocation placement characterized with longer free distance for dislocation glide [28,29]. Easier dislocation glide results in lower strength.

CONCLUSION

Three commercial Al–Mg alloys containing 3 to 6 mass% of Mg (AlMg3, AlMg4.5Mn and AlMg6Mn) were processed by shear spinning and cold rolling. The effect of Mg content and spinning/rolling reduction in wall thickness on the tensile properties and microstructure evolution of Al–Mg alloys was studied. Optical (OM) and transmission electron microscopy (TEM) were used for the microstructure characterization.

The tensile properties (YS and UTS) were enhanced with increasing of a reduction in thickness as well as increase of Mg content. The YS and UTS of the shear spun specimens were lower compared to cold rolled

specimens at the same reductions. These differences in strength increase with increase of reduction in all alloys.

Optical micrograph revealed that the structure becomes elongated after shear spinning and cold rolling. The difference in grain size obtained in the two processes was not significant.

However, TEM characterization of spun specimens showed typical features for dynamic recovery, which were not observed in cold rolled specimens. This resulted in lower strength level of AlMg3 alloy after shear spinning compared to cold rolled specimens.

Acknowledgment

The authors are indebted to the Ministry of Education, Science and Technological Development of the Republic of Serbia for financial support through Project TR-34018.

REFERENCES

- [1] <http://www.acmemetalspinning.com>
- [2] <http://www.leifeldms.de>
- [3] <http://www.metal-spinners.co.uk>
- [4] <http://www.precisionmetalspinning.com>
- [5] <http://www.spincraft.net>
- [6] <http://www.toledometalspinning.com/metal-spinnin-products>
- [7] S. Kalpakcioglu, A study of shear-spinnability of metals, Trans. ASME-J. Eng. Ind. **83** (1961) 478–484.
- [8] S. Kobayashi, E. G. Thomsen, A theory of shear spinning of cones, Trans. ASME-J. Eng. Ind. **83** (1961) 485–495.

- [9] O. Music, J.M. Allwooda, K. Kawai, A review of the mechanics of metal spinning, *J. Mater. Proc. Tech.* **210** (2010) 3–23.
- [10] C.C. Wong, T.A. Dean and J. Lin, A review of spinning, shear forming and flow forming processes, *Int. J. Mach. Tool Manu.* **43** (2003) 1419–1435.
- [11] ASM Metals Handbook, Forming and Forging, Vol. 14, Ninth ed., ASM Metals Park, OH, 1988.
- [12] M.-D. Chen, R.-Q. Hsu, K.-H. Fuh, An analysis of force distribution in shear spinning of cone, *Int. J. Mech. Sci.* **47** (2005) 902–921.
- [13] B. Avitzur, *Handbook of Metal-Forming Processes*, John Wiley and Sons, Inc., Toronto, 1983.
- [14] E. Romhanji, *Mechanics and Metallurgy of Metal Forming*, Faculty of Technology and Metallurgy, Belgrade, 2001.
- [15] M. -D. Chen, R. -Q. Hsua, K. -H. Fuh, Effects of over-roll thickness on cone surface, *J. Mater. Proc. Tech.* **159** (2005) 1–8.
- [16] K. Kawai, L. N. Yang, H. Kudo, A flexible shear spinning of truncated conical shells with a general-purpose mandrel, *J. Mater. Proc. Tech.* **113** (2001) 28–33.
- [17] S.-C. Chang, C.-C. Wang, C.-A. Huang, Y. Chang, T.-L. Chen, Fabrication of 2024 aluminum spun tube, *J. Mater. Proc. Tech.* **108** (2001) 294–299.
- [18] S. -C. Chang, C.-C. Wang, C. -A. Huang, Y. Chang, T. -L. Chen, Fabrication of 2024 aluminum spun tube, *J. Mater. Proc. Tech.* **108** (2001) 294–299.
- [19] Lj. Radović, M. Nikačević, B. Jordović, Deformation behaviour and microstructure evolution of AlMg6Mn alloy during shear spinning, *Trans. Nonferr. Metal. Soc.* **22** (2012) 991–1000.
- [20] Ø. Ryen, O. Nijs, E. Sjölander, B. Holmedal, H.-E. Eks-töm, E. Nes, Strengthening Mechanisms in Solid Solution Aluminum Alloys, *Metall. Mater. Trans., A* **37** (2006) 1999–2006.
- [21] J.M. Robinson, M.P. Shaw, Observations on deformation characteristics and microstructure in an Al–Mg alloy during serrated flow, *Mater. Sci. Eng., A* **174** (1994) 1–7.
- [22] D.J. Lloyd, The Deformation of Commercial Aluminium-Magnesium Alloys, *Metall. Trans., A* **34** (1986) 1999–2009.
- [23] W. Wen, J.G. Morris, An investigation of serrated yielding in 5000 series aluminum alloys, *Mater. Sci. Eng., A* **354** (2003) 279–285.
- [24] D.J. Lloyd, D. Kenny, The Large Strain Deformation of some Aluminium Alloys, *Metall. Trans., A* **13** (1982) 1445–1452.
- [25] ASTM E 8-04, Standard Test Methods for Tension Testing of Metallic Materials.
- [26] Lj. Radović, M. Nikačević, Osobine rotaciono valjanih konusnih delova od Al legura u funkciji sadržaja Mg i stepena deformacije, 3rd International Scientific Conference on Defensive Technologies, OTEH 2009, Belgrade, Military Technical Institute, Proceedings on CD, 2009.
- [27] R. L. Kegg, A new test method for determination of spinnability of metals, *Trans. ASME-J. Eng. Ind.* **83** (1961) 119–124.
- [28] F.J. Humphreys, M. Hatherely, *Recrystallization and Related Annealing Phenomena*, Elsevier Science Inc., New York, 1996.
- [29] N. Ryum, J. D. Embury, A comment on the recrystallization behaviour of Al–Mg alloys, *Scand. J. Metall.* **11** (1982) 51–54.
- [30] W.A. Soer, A.R. Chezan, J.Th.M. De Hosson, Deformation and reconstruction mechanisms in coarse-grained superplastic Al–Mg alloys, *Acta Mater.* **54** (2006) 3827–3833.
- [31] Z.L. Hu, S.J. Yuan, X.S. Wang, G. Liu, H.J. Liu, Microstructure and mechanical properties of Al–Cu–Mg alloy tube fabricated by friction stir welding and tube spinning, *Scripta Mater.* **66** (2012) 427–430.

IZVOD

MIKROSTRUKTURA I SVOJSTVA Al–Mg LEGURA DEFORMISANIH ROTACIONIM VALJANJEM I KONVENTIONALNIM HLADNIM VALJANJEM

Ljubica M. Radović¹, Milutin Z. Nikičević¹, Branka M. Jordović²

¹Vojnotehnički institut, Beograd, Srbija

²Fakultet tehničkih nauka, Čačak, Univerzitet u Kragujevcu, Srbija

(Naučni rad)

U ovom radu ispitane su tri komercijalne Al–Mg legure sa različitim sadržajem Mg od 3 do 6 mas.% (AlMg3, AlMg4.5Mn i AlMg6Mn) su deformisane postupcima rotacionog valjanja konusa i konvencionalnim hladnim valjanjem glatkim valjcima. Korišćenjem konusnih trnova sa različitim uglovima ($2\alpha = 90, 60, 40$ i 18°) pri rotacionom valjanju ostvareni su stepeni deformacije, tj. redukcije debljine zida konusa od 30 do 86%. Kod Al–Mg limova koji su deformisani hladnim valjanjem glatkim valjcima, postignuti su stepeni redukcije od 30 do oko 85%. Ispitan je uticaj sadržaja Mg i stepena deformacije na mikrostrukturalne promene i zatezna svojstva Al–Mg legura. Za ispitivanje mikrostrukture primenjene su metode optičke mikroskopije (OM) i transmisione elektronske mikroskopije (TEM). Zatezne osobine su ispitane u testu jednoosnim zatezanjem na sobnoj temperaturi. Rezultati su pokazali da se sa povećanjem sadržaja Mg u leguri i stepena redukcije napon tečenja ($R_{p0.2}$) i zatezna čvrstoća (R_m) povećavaju, dok duktilnost pada kod oba primenjena procesa. Međutim, čvrstoća uzorka rotaciono valjanih konusa je manja u poređenju sa uzorcima koji su deformisani valjanjem glatkim valjcima sa približno istim stepenima redukcije. Pretpostavljeno je da je usled lokalizovanja deformacije pri rotacionom valjanju konusa, tj. znatno manje zone deformacije u odnosu na konvencionalno hladno valjanje, došlo do oporavljanja u toku deformacije (dinamičkog oporavljanja). Optičkom mikroskopijom nisu uočene razlike u mikrostrukturi uzoraka deformisanih rotacionim valjanjem i konvencionalnim hladnim valjanjem sa približno istim stepenom redukcije. Pojava dinamičkog oporavljanja je potvrđena primenom transmisione elektronske mikroskopije.

Ključne reči: Al–Mg legure • Rotaciono valjanje konusa • Hladno valjanje glatkim valjcima • Mehaničke osobine • Mikrostruktura • Dinamičko oporavljanje

Functionalization of thermo-acid activated sepiolite by amine-silane and mercapto-silane for chromium(VI) adsorption from aqueous solutions

Vesna M. Marjanović¹, Slavica S. Lazarević², Ivona M. Janković-Častvar², Bojan M. Jokić², Andelika Z. Bjelajac², Đorđe T. Janačković², Rada D. Petrović²

¹High Business-Technical School of Užice, 31000 Užice, Trg Sv. Save 34, Serbia

²Faculty of Technology and Metallurgy, University of Belgrade, 11000 Belgrade, Karnegijeva 4, Serbia

Abstract

Chromium(VI) adsorption from aqueous solutions onto thermo-acid activated sepiolite functionalized with (3-mercaptopropyl)trimethoxy-silane and [3-(2-aminoethylamino)propyl]trimethoxy-silane was investigated. Scanning electron microscopy, X-ray diffraction, Fourier transform infrared spectroscopy, thermogravimetric and differential thermal analysis, nitrogen adsorption-desorption, and determination of the point of zero charge were used to characterize the obtained adsorbents. It has been established that the silanes were successfully grafted on the thermo-acid activated sepiolite surfaces and that the structure of parent material was preserved during the functionalization. The adsorption of Cr(VI) onto functionalized thermo-acid activated sepiolite was tested as a function of initial pH values at 298 K. The amine functionalized thermo-acid activated sepiolite showed a higher adsorption capacity than the mercapto functionalized thermo-acid activated sepiolite at all studied initial pH values, especially at the initial pH 2.

Keywords: thermo-acid activated sepiolite, functionalization, (3-mercaptopropyl)trimethoxy-silane, [3-(2-aminoethylamino)propyl]trimethoxy-silane, adsorption, chromium(VI).

Available online at the Journal website: <http://www.ache.org.rs/HI/>

In the environment, chromium originates from geochemical and anthropogenic sources (industry, energy, mines and smelters). The most stable forms of chromium in the environment are trivalent chromium, Cr(III), and hexavalent chromium, Cr(VI), whereas Cr(VI) is more toxic, carcinogenic and mutagenic to the living organisms [1]. In aqueous solutions, Cr(VI) occurs in several stable forms, such as: $\text{Cr}_2\text{O}_7^{2-}$, H_2CrO_4 , HCrO_4^- and CrO_4^{2-} . The relative abundance of those forms mainly depends on the pH value of the solution and Cr(VI) concentration. H_2CrO_4 generally exists at pH less than about 1.0; HCrO_4^- predominates at pH values between 2.0 and 6.0; and when pH increases to above 6.8, CrO_4^{2-} is the primary form. The dichromate ion, $\text{Cr}_2\text{O}_7^{2-}$, forms when the concentration of chromium exceeds approximately 1 g/dm³ [1].

A simple, effective and inexpensive method for the Cr(VI) removal from aqueous solutions, like polluted water, is the adsorption, where the key factor is the selection of a proper adsorbent. The adsorption of Cr(VI) oxyanions from aqueous solutions by natural clay minerals was not given much attention, mainly due to the fact that clays are negatively charged and moreover unfunctionalized clay mineral surface shows no affinity for Cr(VI) oxyanions [2]. In order to use natural clay

SCIENTIFIC PAPER

UDC 546.766:66.081.3:546.281:547.7

Hem. Ind. **67** (5) 715–728 (2013)

doi: 10.2298/HEMIND121026117M

minerals for the adsorption of anionic species of Cr(VI) from aqueous solutions, it is necessary to change the character of their surface, which can be achieved via functionalization processes by adsorption of quaternary ammonium salts or amines and by organosilane grafting, through reaction with surface silanol groups. The study of Cr(VI) adsorption from aqueous solutions by functionalized clay minerals (kaolinite, montmorillonite, stevensite, rectorite, etc.) was the object of several researches [3–12]. To the best of our knowledge, there are no studies about Cr(VI) removal from aqueous solutions by functionalized sepiolite, except our previous studies, where natural and acid activated sepiolites were functionalized by using (3-mercaptopropyl)trimethoxy-silane [13] and [3-(2-aminoethylamino)propyl]trimethoxy-silane [14]. It was shown that functionalized partially acid activated sepiolite has a higher degree of functionalization and a higher adsorption capacity for anionic species of Cr(VI) compared to functionalized natural sepiolite [13,14].

Our further studies were directed to the investigation of the removal of Cr(VI) by using fully-acid activated sepiolite functionalized with both (3-mercaptopropyl)trimethoxy-silane and [3-(2-aminoethylamino)propyl]trimethoxy-silane. It was shown [15–19] that during acid treatments of sepiolite, variable amounts of structural Mg²⁺ were removed, depending on the intensity of the acid treatment. If the treatment is aggressive enough, as during acid activation at elevated temperature, the octahedral cations are completely dissolved,

Correspondence: R.D. Petrović, University of Belgrade, Faculty of Technology and Metallurgy, 11000 Belgrade, Serbia.

E-mail: radaab@tmf.bg.ac.rs

Paper received: 26 October, 2012

Paper accepted: 10 December, 2012

while the tetrahedral sheets form free amorphous silica of high surface area and high mesoporosity [20]. It was expected that high density of silanol groups on the surface of thusly activated sepiolite can provide good functionalization through reaction between surface silanol groups and alkoxyl groups of organosilane $R'-(CH_2)_3-SiX_3$, where X is alkoxyl group (usually methoxy, $-OCH_3$, or ethoxy, $-OC_2H_5$) and R' is reactive vinyl ($-HC=CH_2$), amine ($-NH_2$) or mercapto ($-SH$) groups.

In this study, the influence of type of functionalization of fully-acid activated sepiolite on its physicochemical properties and Cr(VI) adsorption from aqueous solutions of the produced materials was investigated. Physicochemical characterization of the adsorbents was performed using N_2 adsorption, FTIR, DTA, SEM and XRD measurements, as well as by determination of the point of zero charge. Cr(VI) adsorption was studied at different initial pH values and the dominant mechanisms of adsorption were proposed.

MATERIALS AND METHODS

Starting material

A fraction < 250 μm of natural sepiolite (SEP) from Andrić, Čačak (Serbia), was used as the starting material [15]. An acid treatment was performed at elevated temperature (thermo-acid activation) as follows [20]: 10 g of sepiolite was suspended in 100 cm^3 of 4 mol/dm³ HCl solution and heated at 65±1 °C in a stirred reaction flask for 10 h. Then, the mixture was filtered, washed with hot distilled water until it became Cl^- free and dried at 110 °C for 2 h. Hereinafter, sepiolite activated by acid at elevated temperature was marked as TASEP.

With the determination of the chemical composition of TASEP by AAS, Perkin Elmer 730 (89.6 wt.% SiO_2 , 0.12 wt.% MgO , < 0.03 wt.% Al_2O_3 , 0.08 wt.% Fe_2O_3 , < 0.05 wt.% CaO and 8.66 wt.% LOI) it was shown that there was almost complete magnesium leaching from sepiolite structure during applied thermo-acid activation.

Functionalization of the thermo-acid activated sepiolite by organosilane

The TASEP sample was functionalized with organosilane, 99.99% purity, manufactured by Sigma-Aldrich: *i*) (3-Mercaptopropyl)trimethoxysilane ($HS-(CH_2)_3-Si-(OCH_3)_3$) or shortly named mercapto-silane and *ii*) [3-(2-aminoethylamino)propyl]trimethoxy-silane or amine-silane, with the chemical formula $(CH_3O)_3Si-(CH_2)_3-NH-(CH_2)_2-NH_2$. The functionalization reactions were performed according to previous studies [13,14]. The mercapto and amine functionalized

samples were denoted as MTASEP and APT-TASEP, respectively.

Characterization

The morphology of the TASEP, MTASEP and APT-TASEP powders was analysed by scanning electron microscopy (SEM) on a TESCAN MIRA 3 XMU microscope operating at 20 kV.

The phase compositions of TASEP, MTASEP and APT-TASEP were determined using a conventional powder diffractometer (Ital Structures APD 2000) with Bragg-Brentano geometry and $CuK_{\alpha 1,2}$ radiation (Ni filter) with a 0.02° 2θ step and a 2 s counting time per data point.

FT-IR analyses of the samples were performed on a 100 MB Boman Hartmann & Brown instrument in the wave number range from 400 to 4000 cm^{-1} . The samples were prepared by the KBr method, at a ratio of the sample:KBr = 1:100.

Simultaneous thermogravimetric and differential thermal analysis (TG/DTA) of the samples (approximately 5 mg) were performed in a flowing air atmosphere using a TA thermogravimetric analyzer (TA Instruments, New Castle, USA), model SDT Q600. The samples were heated up to 1000 °C at a heating rate of 20 °C/min.

The specific surface area, pore volume and pore size distribution of the samples were determined on the basis of nitrogen adsorption-desorption isotherms, using a Micromeritics ASAP 2020 instrument for measurements. Before the sorption measurement, the samples were degassed at 150 °C for 12 h, in vacuum. Then, adsorption of nitrogen (purity 99.9%) on the free surfaces of the samples was performed at a temperature of liquid nitrogen (-196 °C). Desorption of nitrogen was carried out at liquid nitrogen temperature. The specific surface area of each sample was calculated according to the Brunauer-Emmett-Teller (BET) method from the linear part of the nitrogen adsorption isotherm. The volume of the mesopores and pore size distribution were calculated according to the Barrett, Joyner and Halenda method [21] from the desorption branch of isotherm. The Dubinin-Radushkevich method [22] was used for analyzing of micropores.

The point of zero charge of the samples was determined using previously described batch equilibration technique [13–15,23] in KNO_3 solution (concentration 0.1 or 0.01 mol/dm³). In all experiments, a series of samples of 25 cm^3 KNO_3 solution, with the concentration of 0.1 and 0.01 mol/dm³ and the preset adjusted pH values ($pH_{initial}$) of approximately 2.0 to approximately 11.0, were equilibrated with 0.05 g of sepiolite sample, during 24 h at 25 °C with constant shaking. In the case of TASEP and MTASEP samples, equilibration was performed for the two ratios of solid/liquid (0.05 and 0.10 g/25 cm^3). After achieving equilibrium, the suspensions were filtered through filter paper, and the

pH value of the filtrate (pH_{final}) was measured. The point of zero charge (pH_{pzC}) was determined from the dependence of the pH_{final} vs. $\text{pH}_{\text{initial}}$, as the pH value of plateau or as the pH value of the curve inflection [13–15,23].

Adsorption experiments

The aqueous solutions of Cr(VI) anions were prepared by dissolving $\text{K}_2\text{Cr}_2\text{O}_7$ in demineralized water.

The Cr(VI) adsorption was investigated at batch conditions at a constant temperature in a thermostat with a shaker (MEMMERT), where the temperature was maintained at $25 \pm 0.01^\circ\text{C}$. The measured mass quantities of MTASEP or APT-TASEP were mixed with solutions of Cr(VI), at the preset pH values ($\text{pH}_{\text{initial}}$) in PVC vessels. Upon expiration of the required mixing time in the thermostat, the suspensions were filtered and further, the concentrations of Cr(VI) in solution and the final pH value of the solution (pH_{final}) were determined. In order to determinate the concentration of Cr(VI) in the solution, atomic absorption spectroscopy (AAS) was performed using a Perkin Elmer 730 instrument, while the pH value of the solution was measured by a pH meter (InoLab WTW series pH 720). To adjust the initial pH values of solutions, solutions of HCl or KOH of 0.1 mol/dm³ concentration were used.

The adsorption of Cr(VI) on MTASEP or APT-TASEP was investigated at different initial concentrations of Cr(VI) solution of 5 to 205 mg/dm³ and at different initial pH values: 4.5, 3.0 and 2.0 ± 0.1 . The ratio of adsorbent/solution was 0.10 g/25 cm³ for MTASEP and 0.05 g/25 cm³ for APT-TASEP.

The amounts of Cr(VI) ions adsorbed per unit mass of functionalized sepiolite were calculated using Eq. (1):

$$q_e = \frac{c_i - c_e}{w} V \quad (1)$$

where: c_i – initial concentration of Cr(VI) in solution (mg/dm³); c_e – the equilibrium concentration of Cr(VI) in solution (mg/dm³) w – mass of adsorbent (g), V – volume of Cr(VI) solution (dm³).

All adsorption experiments were repeated twice. The presented results represent the mean of two measurements.

RESULTS AND DISCUSSION

Characterization of the unfunctionalized and functionalized thermo-acid activated sepiolites

Figure 1 shows micrographs of TASEP (a), MTASEP (b) and APT-TASEP (c). It can be seen that the thermo-acid activated sepiolite (TASEP) has a fibrous structure (Figure 1a) like a natural sepiolite [24], but the difference is that TASEP fibres are shorter (Figure 1a). What is more, the fibre structure of MTASEP and APT-TASEP

samples was preserved during functionalization (Figure 1b and c), whereby the fibres were more connected comparing to the parent material (Figure 1a).

The diffraction patterns of TASEP, MTASEP and APT-TASEP are given in Figure 2. The X-ray diffractogram of the TASEP sample shows almost completely amorphous structure. The appearance of the broad diffraction peak at $2\theta = 23^\circ$ indicates the formation of amorphous silica. There are no differences between diffractograms of functionalized (MTASEP and APT-TASEP) and parent sample (TASEP), which indicates that functionalized samples retained the structure of unfunctionalized one.

FT-IR spectra of the TASEP, MTASEP and APT-TASEP samples are shown in Figure 3. The spectrum of MTASEP is very similar to the spectrum of TASEP, but there is the difference in the intensity of the bands in the 2950–2840 cm⁻¹ range, which can be assigned to vibration of C–H bonds in mercapto-silane [13,14,25–27].

Also, FT-IR spectrum of APT-TASEP is generally similar to FT-IR spectrum of TASEP, but the intensity of the bands in the 2950–2840 cm⁻¹ range in the spectrum of APT-TASEP is higher than in the spectrum of TASEP. In addition, there is a band at around 1500 cm⁻¹, which is characteristic of amine groups in amine-silane [25,28–34].

In order to assess the differences between the functionalized and unfunctionalized samples, the results of FT-IR spectroscopy of TASEP, MTASEP and APT-TASEP were presented in the range between 3200 and 2500 cm⁻¹ (Figure 4).

From the Figure 4, it can be seen that there are the bands at about 2936 and 2857 cm⁻¹ which can be assigned to the C–H vibration of methoxy (OCH_3) and methylene (CH_2) groups, respectively [13,14,25–27]. These bands cannot be observed in the FT-IR spectrum of TASEP. The presence of methoxy groups in the functionalized samples indicates that the silanes do not bind to the surface by reaction of all (three) methoxy groups, but probably by reaction of one OCH_3 with one silanol group at the surface of TASEP [26,35]. The intensities of the both bands are higher for APT-TASEP than for MTASEP, which indicates that the content of CH_2 and OCH_3 groups is higher in APT-TASEP than in MTASEP, supposing it is due to the fact that the amine-silane contains five CH_2 groups, while mercapto-silane contains only three. However, higher content of OCH_3 groups in APT-TASEP is an indicator of better functionalization of TASEP by amine-silane than by mercapto-silane.

Figure 5 shows TG/DTA curves of the TASEP, MTASEP and APT-TASEP sepiolite samples. It should be noted that there is no exothermic peak at about 820°C [15] on DTA curves, which would correspond to the phase transformation of sepiolite to enstatite. This is indica-

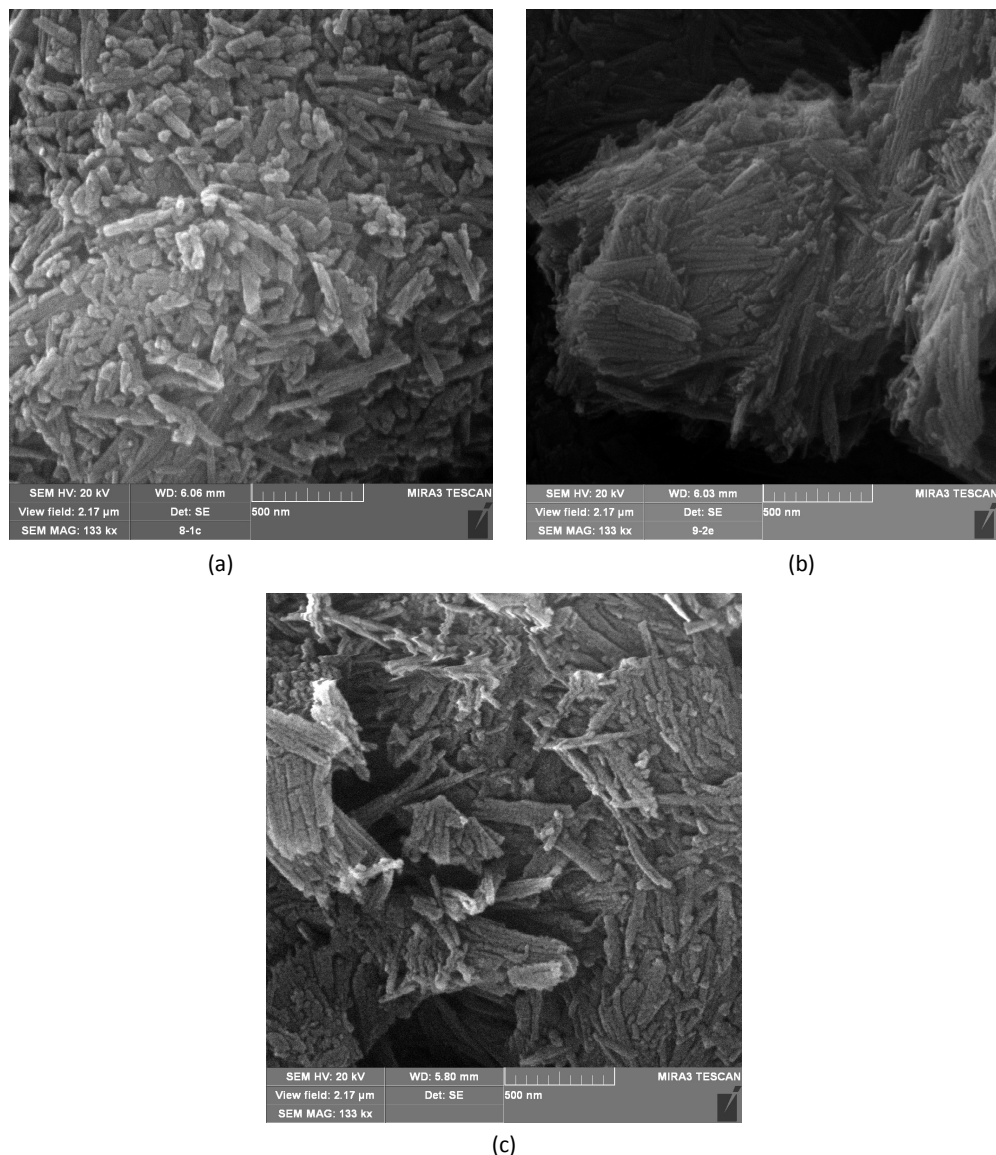


Figure 1. SEM Micrographs of TASEP (a), MTASEP (b) and APT-TASEP (c).

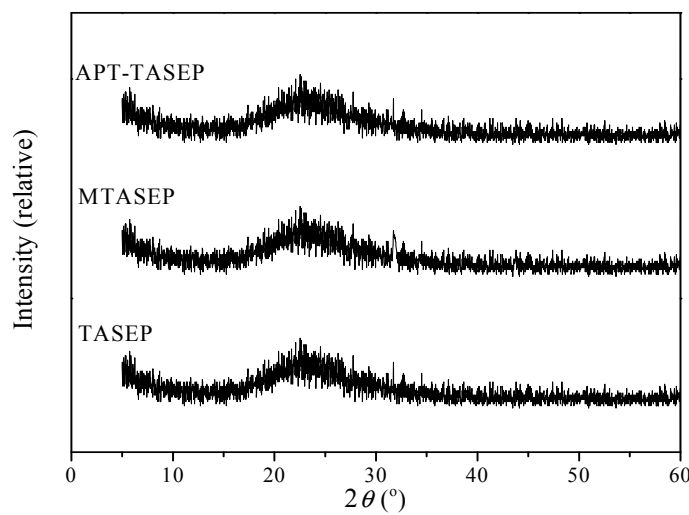


Figure 2. X-Ray diffractograms of the TASEP, MTASEP, and APT-TASEP samples.

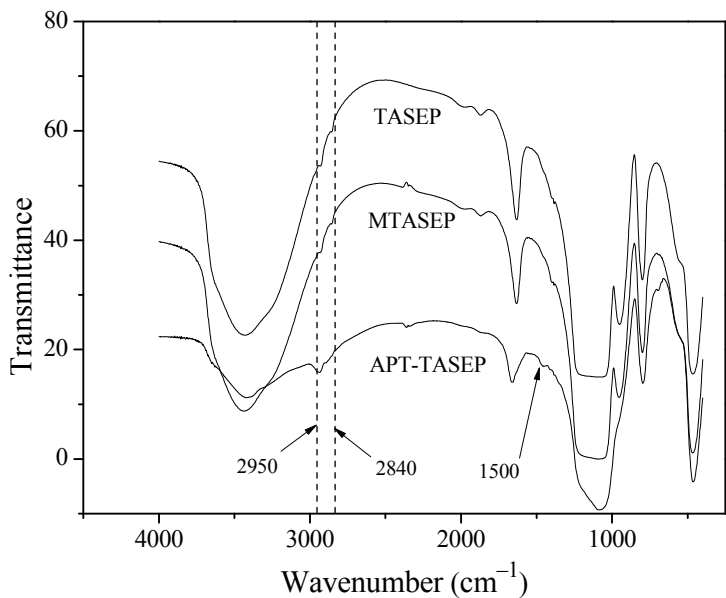


Figure 3. FT-IR spectra of the TASEP, MTASEP and APT-TASEP samples.

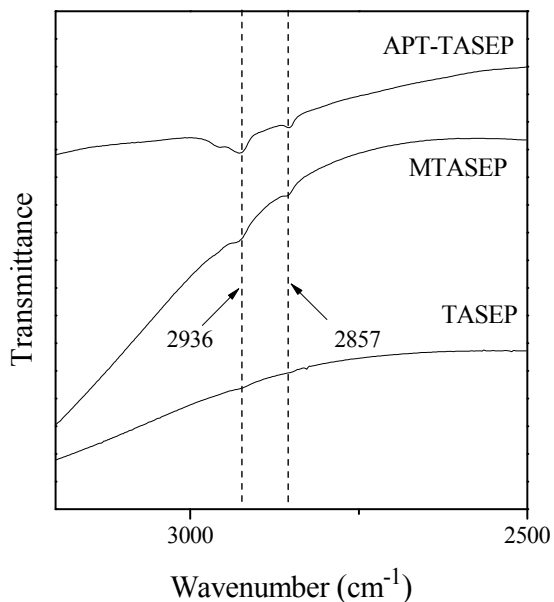


Figure 4. $3200\text{--}2500\text{ cm}^{-1}$ region of the FT-IR spectra of TASEP, MTASEP, and APT-TASEP.

tion of destruction of sepiolite structure during thermal-acid activation.

According to DTA curves in Figure 5, the two characteristic regions can be noticed: endothermic, from room temperature to $\sim 200\text{ }^{\circ}\text{C}$, and exothermic, from ~ 200 to approximately $\sim 700\text{ }^{\circ}\text{C}$. The weight loss in the first region, due to dehydratation [26,36], is approximately the same for all samples, but slightly lower for APT-TASEP (3.5 wt.%) than for TASEP (4.2 wt.%) and MTASEP (5.6 wt.%). On the other hand, the weight loss in the second region is much higher for APT-TASEP (16.6 wt.%) than for TASEP (4.0 wt.%) and MTASEP (5.3 wt.%). The weight loss in the second

region is primarily due to combustion of the organic matter, *i.e.*, amine-silane or mercapto-silane [28,33,37]. Bearing in mind the molar mass of amine-silane, 209 g/mol, and mercapto-silane, 185 g/mol, it can be said that higher weight loss of APT-TASEP in the second region compared to MTASEP is primarily the result of much better functionalization of TASEP by amine-silane than by mercapto-silane.

Table 1 shows the textural properties of the TASEP, MTASEP and APT-TASEP samples. The results show that mercapto functionalization of TASEP leads to slight decreases in specific surface area, mesopore volume and micropore volume, while amine functionalization leads to significant decrease of these parameters.

Such changes of the textural parameters of TASEP by functionalization, especially micropore volume, can be explained by the size of organosilane molecules, *i.e.*, the possibility of organosilane molecule to enter into the pores of TASEP.

In the case of APT-TASEP, it can be assumed that the large molecules of amine-silane entered and closed micropores [28,37–39] of TASEP during amine functionalization which caused a decrease of porosity, mainly microporosity, and consequently specific surface area. The decrease of microporosity of APT-TASEP compared to the TASEP causes the increase of the maximum and mean pore diameter of the APT-TASEP compared to the TASEP. Due to micropore closing, the content of pore water in APT-TASEP is lower than in TASEP and MTASEP, and consequently weight loss is lower due to dehydration (Figure 5).

According to the textural parameters of the MTASEP and TASEP (Table 1), a slight decrease of porosity of MTASEP compared to TASEP can be seen, so it could be

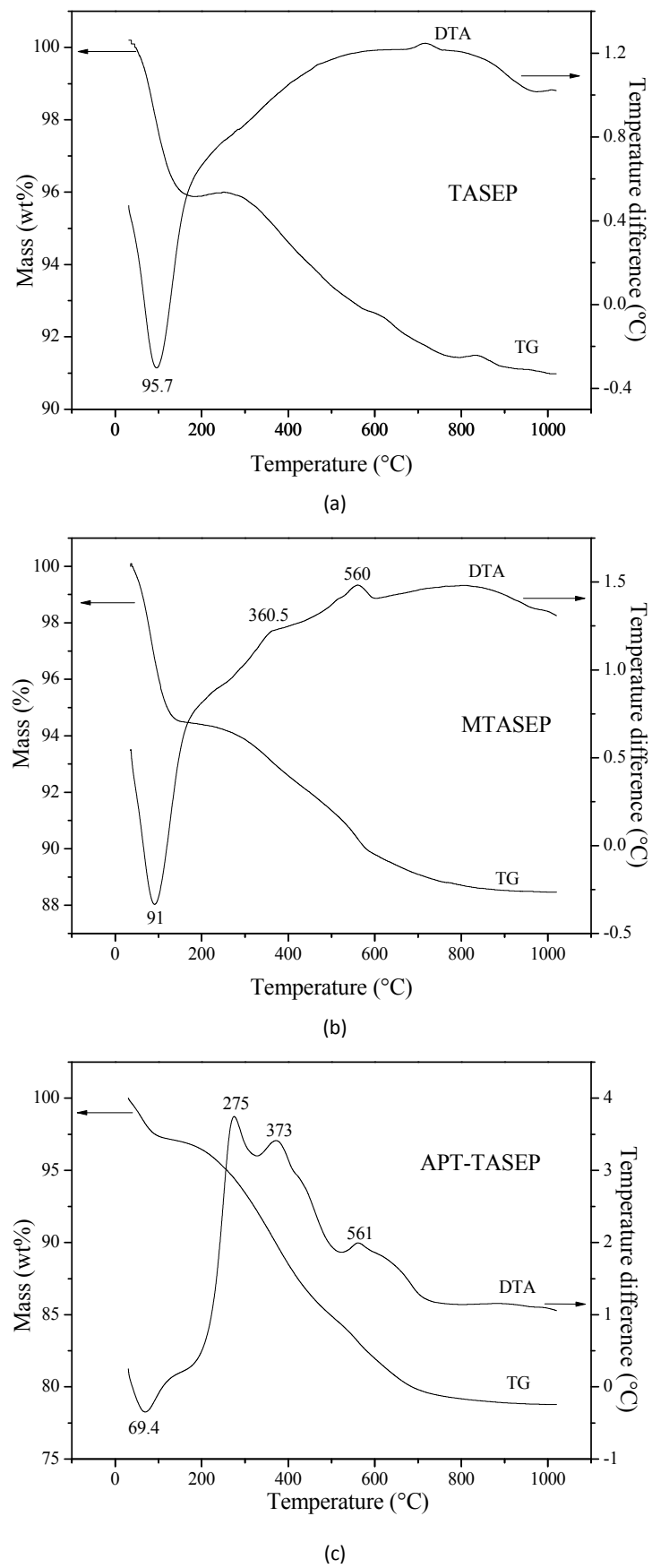


Figure 5. TG/DTA curves of the a) TASEP, b) MTASEP and c) APT-TASEP samples.

Table 1. The textural parameters of the TASEP, MTASEP, and APT-TASEP samples

Parameter	TASEP	MTASEP	APT-TASEP
Specific surface area, $S_{\text{BET}} / \text{m}^2 \text{g}^{-1}$	449	403	33
Micropore volume, $V_{\text{micropore}} / \text{cm}^3 \text{g}^{-1}$	0.415	0.349	0.058
Mesopore volume, $V_{\text{mesopore}} / \text{cm}^3 \text{g}^{-1}$	0.571	0.396	0.133
Maximum pore diameter, $D_{\text{max}} / \text{nm}$	3	4	8
Mean pore diameter, $D_{\text{mean}} / \text{nm}$	7	6	11

assumed that the entry of relatively small molecules mercapto-silane in pores of TASEP did not cause a significant reduction in volume of micropores and mesopores. The maximum and mean pore diameters of MTASEP are similar to those of TASEP indicating that micropores of the TASEP were not closed during the mercapto functionalization of TASEP.

The results of determination of the point of zero charge, pH_{pzc} for the samples TASEP, MTASEP and APT-TASEP are shown in Figure 6. The pH_{pzc} of APT-SEP (Figure 6c) was determined as the pH value of the plateau of pH_{final} vs. $\text{pH}_{\text{initial}}$ dependence, while the pH_{pzc} of TASEP and MTASEP was obtained as pH_{final} vs. $\text{pH}_{\text{initial}}$ curves inflection (Figure 6a and b, respectively). To precisely define the curve inflection, the pH_{pzc} of TASEP and MTASEP were determined for two solid/liquid ratio.

From Figure 6 it is obvious that the pH value of the plateau or inflexion of the pH_{final} vs. $\text{pH}_{\text{initial}}$ dependence remains constant with changing concentration of KNO_3 solution, which means that KNO_3 is an indifferent electrolyte. In that way, the common plateau obtained at a pH value of 9.5 ± 0.1 for APT-TASEP corresponds to the pH_{pzc} of the APT-TASEP. In addition, in the case of pH_{pzc} of TASEP and MTASEP determination, the position of curve inflection was independent of solid/liquid ratio and values of pH_{pzc} of TASEP and MTASEP were determined as 5.0 ± 0.1 and 4.7 ± 0.1 , respectively.

The results of determination of the point of zero charge showed that acid-base properties of functionalized sepiolite were very much depended on the type of organosilane used for functionalization. The value of the point of zero charge of APT-TASEP was much higher than that of MTASEP, because amine-silane contains more basic groups ($-\text{NH}_2$ and $-\text{NH}-$) than mercapto-silane ($-\text{SH}$). The acid-base properties of MTASEP are very similar to that of TASEP, because ($-\text{SH}$) group has similar acidity as ($-\text{OH}$) group. In addition, the buffer capacity APT-TASEP is much higher than that of MTASEP and TASEP. In the wide range of $\text{pH}_{\text{initial}}$, the final pH values were constant and equal to pH_{pzc} of APT-TASEP. Just in the range below the initial pH ~ 4.0 , the final pH values were less than pH_{pzc} for APT-TASEP and the surface charge of APT-TASEP could become positive.

The adsorption of Cr(VI) onto mercapto-silane and amine-silane functionalized thermo-acid activated sepiolite samples

The results of preliminary experiments showed that adsorption capacity of TASEP for Cr(VI) is very low, as in the case of natural and acid-activated sepiolite [13]. Therefore, adsorption onto functionalized samples MTASEP and APT-TASEP was investigated and presented in this study.

The adsorption experiments were done at different initial pH values. During equilibration of adsorbent with ion solution, the pH value of solution can be changed due to: protonation/deprotonation of surface functional groups of adsorbent, interaction of H^+/OH^- with ions in the solution, specific adsorption of adsorbent, etc. Therefore, in order to assess the influence of pH on adsorption, it is not enough to adjust initial pH value, but it is necessary to follow the changes of pH during adsorption.

The dependence of the final solution pH value (pH_{final}), during equilibration of the Cr(VI) solution with MTASEP and APT-TASEP samples on the initial concentration of Cr(VI) solution are shown in Figure 7a and b, respectively. The dependence of the adsorbed amount of Cr(VI), q_e , on the equilibrium concentration of Cr(VI) solution, c_e , is shown on Figure 8a for MTASEP and 8b for APT-TASEP.

During equilibration of the Cr(VI) solutions with MTASEP and APT-TASEP at $\text{pH}_{\text{initial}}$ 2.0 (Figure 7), the pH_{final} remained nearly constant with an increase in initial Cr(VI) concentration and approximately equal to $\text{pH}_{\text{initial}}$, due to high acid conditions in the suspension of both samples. The similar dependence of pH_{final} on Cr(VI) concentration was obtained for MTASEP for $\text{pH}_{\text{initial}}$ 3.0. But, in the case of APT-TASEP at $\text{pH}_{\text{initial}}$ 3.0, as well as at $\text{pH}_{\text{initial}}$ 4.5, pH_{final} was much higher due to high buffer capacity of APT-TASEP. At low Cr(VI) concentration, pH_{final} was equal to pH_{pzc} of APT-TASEP, but with the increase of Cr(VI) concentration pH_{final} decreased, which can be explained by deprotonation of HCrO_4^- ions at $\text{pH} > 6.8$ ($\text{HCrO}_4^- \rightleftharpoons \text{H}^+ + \text{CrO}_4^{2-}$) [1]. During Cr(VI) adsorption on MTASEP at $\text{pH}_{\text{initial}}$ 4.5, final pH values were not much higher than the initial pH, because of low buffer capacity of the adsorbent. A slight increase of pH_{final} with the increase of Cr(VI) con-

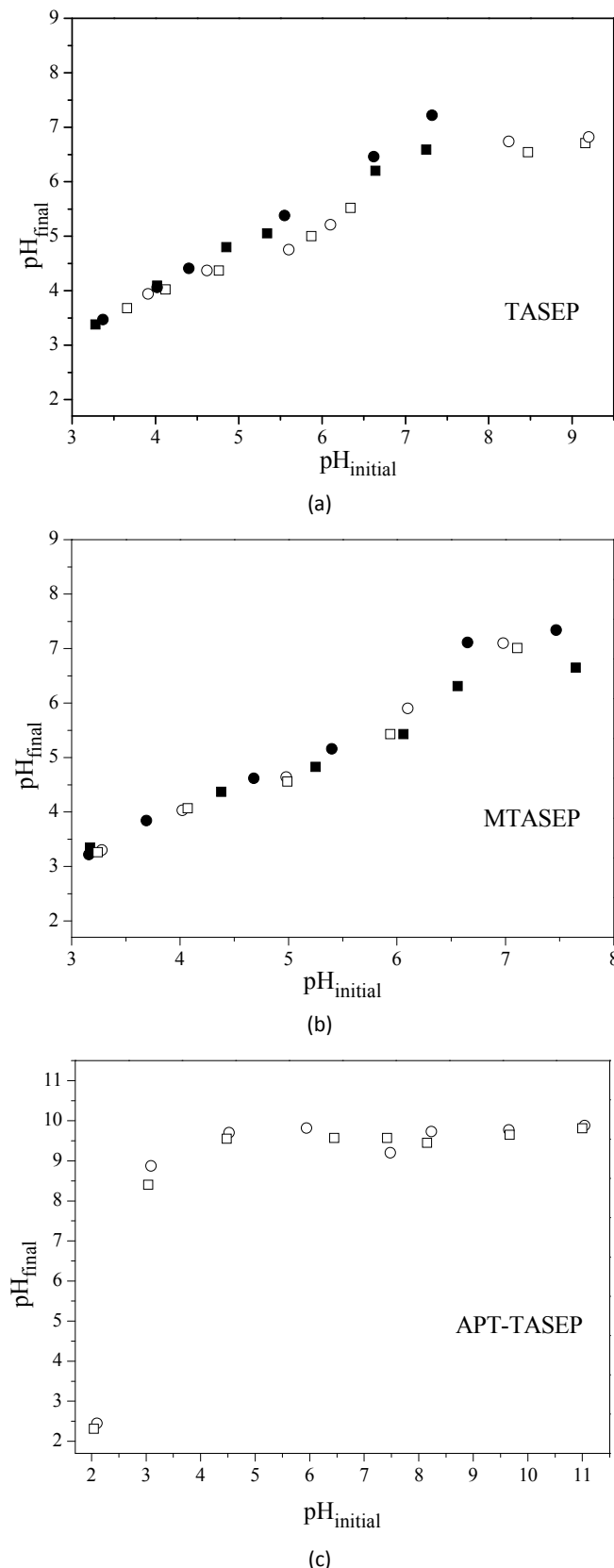


Figure 6. Dependence of pH_{final} on $pH_{initial}$ during the equilibration: a) of 0.1 g of TASEP with 25 cm^3 solution of (■) 0.1 M KNO_3 , (●) 0.01 M KNO_3 and 0.05 g of TASEP with 25 cm^3 solution of (□) 0.1 M KNO_3 , (○) 0.01 M KNO_3 ; b) of 0.1 g of MTASEP with 25 cm^3 solution of (■) 0.1 M KNO_3 , (●) 0.01 M KNO_3 and 0.05 g of MTASEP with 25 cm^3 solution of (□) 0.1 M KNO_3 , (○) 0.01 M KNO_3 ; c) of 0.05 g of APT-TASEP with 25 cm^3 solution of (□) 0.1 M KNO_3 , (○) 0.01 M KNO_3 .

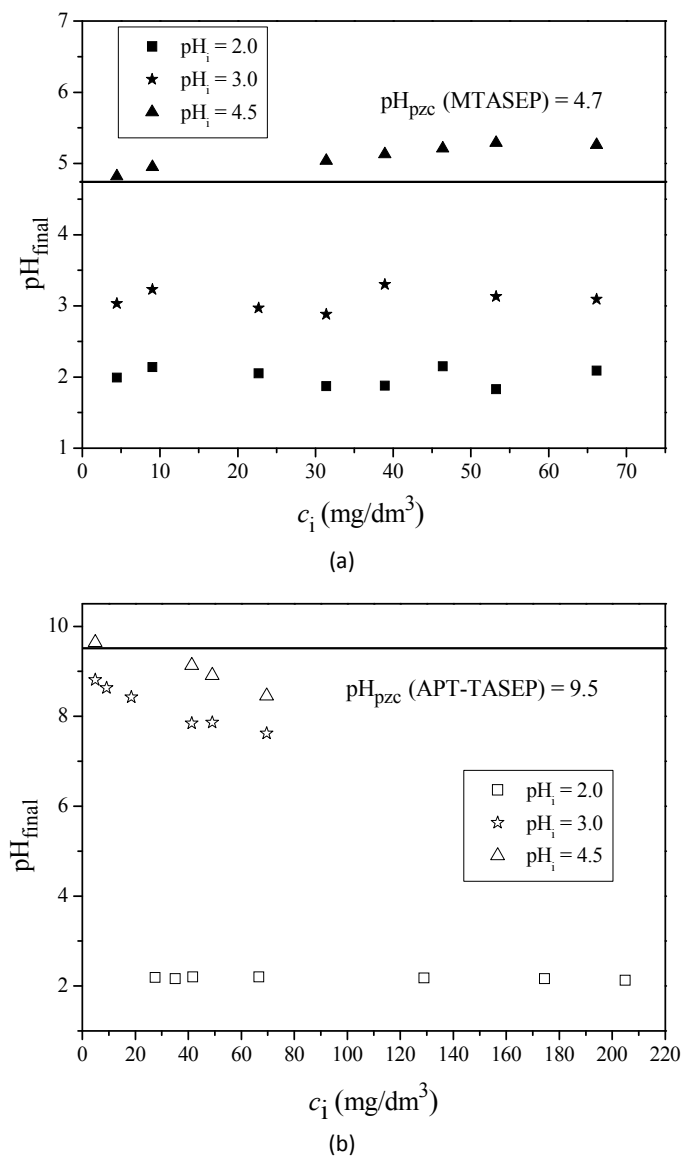


Figure 7. a) Dependence of the final solution pH value on the initial Cr(VI) concentration during the equilibration of 25 cm³ of Cr(VI) solution with 0.1 g of MTASEP at initial pH values 2.0, 3.0 and 4.5; b) dependence of the final solution pH value on the initial Cr(VI) concentration during the equilibration of 25 cm³ of Cr(VI) solution with 0.05 g of APT-TASEP at initial pH values of 2.0, 3.0 and 4.5.

centration can be explained by the increase of content of HCrO₄⁻ instead of CrO₄²⁻ at lower pH values (~ 5).

The adsorption of Cr(VI) on functionalized sepiolites is dependent on pH of the solution which affects the surface charge of the adsorbent and the predominant species of Cr(VI) in solution.

It was found (Figure 8) that the amount of Cr(VI) ions adsorbed onto MTASEP slightly increased with pH_{final} decreasing from 5.2 (at pH_{initial} 4.5) to 3.1 (at pH_{initial} 3.0) and 2.1 (at pH_{initial} 2.0). Thus, the amount of adsorbed Cr(VI) was higher at lower pHs (around 3.0 and 2.0) than at higher pHs (around 5.0), but the sorption capacity of MTASEP was a bit higher at pHs ~ 3.0 than at pHs ~ 2.0.

The results, shown in Figure 7a, indicate that at pH_{initial} of 2.0 and 3.0, pH_{final} were lower than pH_{pzc} of

MTASEP (4.7), which means that the surface of MTASEP was positively charged due to protonation of the surface mercapto (-SH) groups. As the pH_{final} was lower than the pH_{pzc} of MTASEP, the surface was more positively charged, due to the large number of protonated mercapto groups (-SH₂⁺). A higher positive charge of the surface of MTASEP cause higher electrostatic attraction between MTASEP surface [13,40–44] and HCrO₄⁻, which is predominant form of Cr(VI) in the solution of examined pH range [1].

It was shown [13,45–47] that in very acidic conditions, at pH < 3, mercapto groups can reduce Cr(VI) to Cr(III), whereby the mercapto groups are oxidized into sulfonic groups (-SO₃H) of high acidity. It can be supposed that at pH_{initial} 2.0, due to very acidic conditions, sulfonic groups were weakly ionized, and Cr³⁺, formed

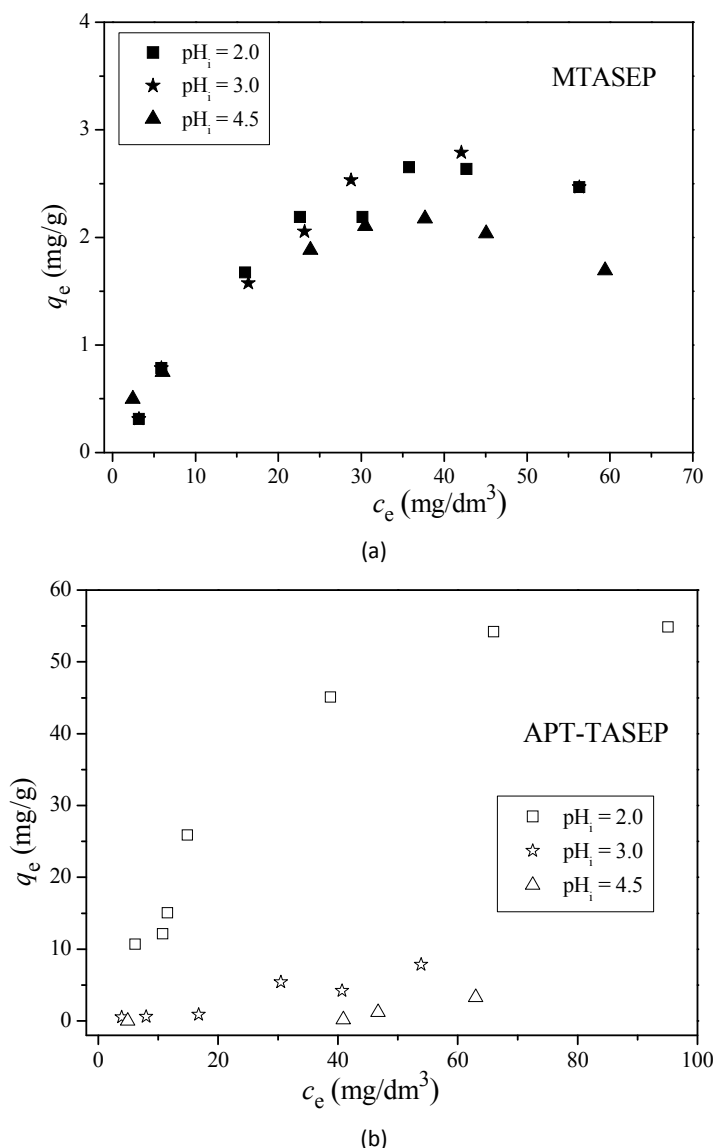


Figure 8. The adsorption isotherms of Cr(VI): a) on MTASEP at initial pHs 2.0, 3.0 and 4.5 and b) on APT-TASEP at initial pHs 2.0, 3.0 and 4.5.

by reduction of Cr(VI), were weakly adsorbed on the surface MTASEP, due to a very small number of $-\text{SO}_2\text{O}^-$ groups, that could bind the Cr^{3+} through electrostatic attraction. According to that, it was assumed that the predominant mechanism of removal of Cr(VI) from aqueous solutions, at initial pH value of 2.0, was the electrostatic attraction between HCrO_4^- from the solution and protonated mercapto ($-\text{SH}_2^+$) groups on the surface of the MTASEP.

On the other hand, at $\text{pH}_{\text{initial}}$ 3.0, the reduction of Cr(VI) to Cr^{3+} was lower than at $\text{pH}_{\text{initial}}$ 2.0, but due to a higher number of $-\text{SO}_2\text{O}^-$ groups, formed by ionization of the $-\text{SO}_3\text{H}$ groups at higher pH value, it can be suppose that Cr^{3+} were better adsorbed on the surface MTASEP due to the electrostatic attraction between the Cr^{3+} and $-\text{SO}_2\text{O}^-$ groups. Thus, it was assumed that

the reduction of Cr(VI) to Cr(III) followed by removal of resulted Cr^{3+} gave the contribution to adsorption of chromium onto MTASEP at $\text{pH}_{\text{initial}}$ 3.0. Therefore, the electrostatic attraction between HCrO_4^- and the protonated $-\text{SH}_2^+$ groups on the MTASEP surface, as well as reduction of Cr(VI) to Cr(III) followed by electrostatic attraction between Cr^{3+} and $-\text{SO}_2\text{O}^-$ groups were possible mechanisms of Cr(VI) removal from solution at initial $\text{pH}_{\text{initial}}$ 3.0.

It can be seen from Figure 8b that Cr(VI) adsorption onto APT-TASEP significantly increased with initial and final pH value decreasing to $\text{pH} \sim 2$ and ~ 2.2 , respectively. During the equilibration of APT-TASEP with Cr(VI) solution at $\text{pH}_{\text{initial}}$ 2.0, the final pH values were much lower than pH_{pcz} of APT-TASEP, which means that the surface of APT-TASEP had high positive charge, due to

protonation of the surface amine groups ($-\text{NH}-$ and $-\text{NH}_2$) [29,30,34,39,40,48–50]. The presence of a large number of protonated amine groups on the surfaces of the APT-TASEP favoured HCrO_4^- adsorption by electrostatic attraction [8,13,29,40,48–50].

At higher $\text{pH}_{\text{initial}}$, 3.0 and 4.5, the pH_{final} of solutions were near the pH_{pzc} of the APT-TASEP and the surface of APT-TASEP was less positively charged. Thus, electrostatic attractions between the surface and Cr(VI) anions were lower than at $\text{pH}_{\text{initial}}$ 2.0 and the amount of Cr(VI) removed from solution was also lower. The possible mechanism of Cr(VI) removal at those pH values is also the formation of hydrogen bonding between oxygen atoms of CrO_4^{2-} (which is a predominant form of Cr(VI) at pHs approximately equal to pH_{pzc} for APT-TASEP) and hydrogen atoms of non-protonated amine groups [29,40].

According to the reported results, the amine functionalized thermo-acid activated sepiolite is a more effective adsorbent than mercapto functionalized thermo-acid activated sepiolite for Cr(VI), at all investigated initial solution pH values, especially at lower pHs. Although TASEP mercapto functionalization leads to a slight decrease in the specific surface area and porosity, while the amino functionalization leads to a significant reduction in these parameters, the APT-TASEP showed a higher adsorption capacity than the MTASEP. It is obvious that the type of silane used for modification, e.g., its chain length and basicity of groups in silane that could be protonated, has a pronounced influence on adsorption capacity for Cr(VI). Similar results were obtained in our previous studies for the functionalised natural and acid-activated sepiolites [13,14]: adsorption capacities of amine-functionalized sepiolites were much higher than of mercapto functionalized sepiolites. The maximum adsorption capacities of the functionalized thermo-acid activated sepiolites are higher than those of the functionalized natural sepiolites [13,14], but lower than those of the functionalized acid activated sepiolite, at the same conditions (pH and temperature). In this study, it was assumed that by thermo-acid activation of sepiolite, silica with high content of silanol groups at the surface could be obtained, which could enable higher degree of functionalization by covalent grafting of silane and consequently higher adsorption capacity for anionic species of chromium (VI) compared to functionalized acid activated and natural sepiolite. However, this was not the case. The lower adsorption capacities of functionalized thermo-acid activated sepiolites compared to functionalized acid activated sepiolites can be explained by the higher degree of condensation of surface silanol groups of thermo-acid activated sepiolites, which caused a decrease in the number of silanol groups at the surface for silane grafting.

CONCLUSION

The removal of Cr(VI) from aqueous solution using adsorbents obtained by covalent grafting of mercapto-silane and amine-silane onto thermo-acid activated sepiolite was studied.

Based on the presented results, it was concluded that the structure as well as fibre morphology of the thermo-acid activated sepiolite were preserved during organosilane functionalization.

FT-IR and DTA/TG results showed much better functionalization of thermo-acid activated sepiolite by amine-silane than by mercapto-silane.

According to the value of the point of zero charge, pH_{pzc} , it was shown that amine-silane gave a basic character to the surface and caused the pH_{pzc} shift from 5.0 (pH_{pzc} of unfunctionalized sample) to 9.5 (pH_{pzc} of amine-functionalized sample), while the pH_{pzc} of mercapto-silane functionalized sample (4.7) is slightly lower than pH_{pzc} of unfunctionalized sample, due to similar acidity of their surface groups ($-\text{SH}$ and $-\text{OH}$).

In addition, the specific surface area, pore volume, maximum and mean pore diameters of amine functionalized sample were reduced, while these textural parameters of the mercapto functionalized sample were similar to those of parent sample.

The amine functionalized thermo-acid activated sepiolite showed a higher adsorption capacity for Cr(VI) than the mercapto functionalized sample at all the studied initial pH values, especially at lower initial pH values. The electrostatic attraction of anionic Cr(VI) species with protonated amine/mercapto groups of functionalized samples is a possible mechanism of Cr(VI) removal, at pH values of solution below the point of zero charge of adsorbent. The formation of hydrogen bonds between oxygen atoms of oxyanion species of Cr(VI) and hydrogen atoms of amine groups, at pH values of solution close to the pH_{pzc} of amine functionalized sample could be another possible mechanisms of Cr(VI) removal by amine-silane functionalised sample. In the case of mercapto-functionalized sample, the reduction of Cr(VI) by mercapto groups to Cr^{3+} , followed by their electrostatic interaction with the sulfonate group, obtained by oxidation of the mercapto groups, is a possible mechanism at lower solution pH values.

Acknowledgements

The authors wish to acknowledge the financial support for this research from the Ministry of Education, Science and Technological Development of the Republic of Serbia through the project III45019.

REFERENCES

- [1] D. Mohan, C.U. Pittman Jr., Review: activated carbons and low cost adsorbents for remediation of tri- and

- hexavalent chromium from water, *J. Hazard. Mater.*, **B 137** (2006) 762–811.
- [2] M.B. Fritzen, A.J. Souza, T.A. G. Silva, L. Souza, R.A. Nome, H.D. Fiedler, F. Nome, Distribution of hexavalent Cr species across the clay mineral surface–water interface, *J. Colloid Interf. Sci.* **296** (2006) 465–471.
- [3] B.S. Krishna, D.S.R. Murty, B.S. Prakash Jai, Surfactant-modified clay as adsorbent for chromate, *Appl. Clay Sci.* **20** (2001) 65–71.
- [4] O. Maryuk, S. Pikus, E. Olszewska, M. Majdan, H. Skrzypek, E. Zięba, Benzylidimethyloctadecylammonium bentonite in chromates adsorption, *Mater. Lett.* **59** (2005) 2015–2017.
- [5] Y. Bayrak, Y. Yesiloglu, U. Gecgel, Adsorption behavior of Cr(VI) on activated hazelnut shell ash and activated bentonite, *Micropor. Mesopor. Mat.* **91** (2006) 107–110.
- [6] B. Sarkar, Y. Xi, M. Megharaj, G.S.R. Krishnamurti, D. Rajarathnam, R. Naidu, Remediation of hexavalent chromium through adsorption by bentonite based Arquad® 2HT-75 organoclays, *J. Hazard. Mater.* **183** (2010) 87–97.
- [7] A. A. Atia, Adsorption of chromate and molybdate by cetylpyridinium bentonite, *Appl. Clay Sci.* **41** (2008) 73–84.
- [8] P. Yuan, M. Fan, D. Yanga, H. He, D. Liua, A. Yuan, J.X. Zhu, T.H. Chen, Montmorillonite-supported magnetite nanoparticles for the removal of hexavalent chromium [Cr(VI)] from aqueous solutions, *J. Hazard. Mater.* **166** (2009) 821–829.
- [9] N. Rajesh, B.G. Mishra, P.K. Pareek, Solid phase extraction of chromium(VI) from aqueous solutions by adsorption of its diphenylcarbazide complex on a mixed bed adsorbent (acid activated montmorillonite–silica gel) column, *Spectrochim. Acta, A* **69** (2008) 612–618.
- [10] A. Benhammou, A. Yaacoubi, L. Nibou, B. Tanouti, Chromium(VI) adsorption from aqueous solution onto Moroccan Al-pillared and cationic surfactant stevensite, *J. Hazard. Mater.* **140** (2007) 104–109.
- [11] Y. Huang, X. Ma, G. Liang, Y. Yan, S. Wang, Adsorption behavior of Cr(VI) on organic-modified rectorite, *Chem. Eng. J.* **138** (2008) 187–193.
- [12] H. Hong, W.-T. Jiang, X. Zhang, L. Tie, Z. Li, Adsorption of Cr(VI) on STAC-modified rectorite, *Appl. Clay Sci.* **42** (2008) 292–299.
- [13] V. Marjanović, S. Lazarević, I. Janković-Častvan, B. Potkonjak, Đ. Janačković, R. Petrović, Chromium(VI) removal from aqueous solutions using mercaptosilane functionalized sepiolites, *Chem. Eng. J.* **166** (2011) 198–206.
- [14] V. Marjanović, S. Lazarević, I. Janković-Častvan, B. Jokić, Dj. Janačković, R. Petrović, Adsorption of chromium(VI) from aqueous solutions onto amine-functionalized natural and acid-activated sepiolites, *Appl. Clay Sci.*, submitted.
- [15] S. Lazarević, I. Janković-Častvan, D. Jovanović, S. Milonjić, Dj. Janačković, R. Petrović, Adsorption of Pb²⁺, Cd²⁺ and Sr²⁺ onto natural and acid-activated sepiolites, *Appl. Clay Sci.* **37** (2007) 47–57.
- [16] M. Radojević, V. Jović, D. Vitorović, Study of sepiolite from Goleš (Kosovo, Yugoslavia). I. Sorption capacity, *J. Serb. Chem. Soc.* **67**(7) (2002) 489–497.
- [17] M. Radojević, V. Jović, D. Karaulić, D. Vitorović, Study of sepiolite from Goleš (Kosovo, Yugoslavia). II. Acid activation, *J. Serb. Chem. Soc.* **67**(7) (2002) 499–506.
- [18] J. L. Valentín, M. A. López-Manchado, A. Rodríguez, P. Posadas, L. Ibarra, Novel anhydrous unfolded structure by heating of acid pre-treated sepiolite, *Appl. Clay Sci.* **36** (2007) 245–255.
- [19] M.A. Vicente Rodriguez, J. de D. Lopez Gonzalez, M.A. Bañares Muñoz, Acid activation of a Spanish sepiolite: physicochemical characterization, free silica content and surface areaof products obtained, *Clay Miner.* **29** (1994) 361–367.
- [20] A.J. Aznar, E. Gutiérrez, P. Díaz, A. Alvarez, G. Poncelet, Silica from sepiolite: Preparation, textural properties, and use as support to catalysts, *Micropor. Mat.* **6** (1996) 105–114.
- [21] E.P. Barrett, L.G. Joyner, P.P. Halenda, The deter–mi–nation of pore volume and area distributions in porous substances. I. Computations from nitrogen isotherms, *J. Am. Chem. Soc.* **73** (1951) 373–380.
- [22] M.L. Pinto, A.S. Mestre, A.P. Carvalho, J. Pires, Comparison of methods to obtain micropore size distributions of carbonaceous materials from CO₂ adsorption based on the Dubinin-Radushkevich isotherm, *Ind. Eng. Chem. Res.* **49** (2010) 4726–4730.
- [23] S.K. Milonjić, A.Lj. Ruvarac, M.V. Šušić, The Heat Immersion of Natural Magnetite in Aqueous Solution, *Thermochim. Acta* **11** (1975) 261–266.
- [24] S. Lazarević, Ž. Radovanović, Dj. Veljović, A. Onjia, Dj. Janačković, R. Petrović, Characterization of sepiolite by inverse gas chromatography at infinite and finite surface coverage, *Appl. Clay Sci.* **43** (2009) 41–48.
- [25] M. Alkan, G. Tekin, H. Namli, FTIR and zeta potential measurements of sepiolite treated with some organo-silanes, *Micropor. Mesopor. Mat.* **84** (2005) 75–83.
- [26] M. Doğan, Y. Turhan, M. Alkan, H. Namli, P. Turan, Ö. Demirbaş, Functionalized sepiolite for heavy metal ions adsorption, *Desalination* **230** (2008) 248–268.
- [27] C. del Hoyo, C. Dorado, M.S. Rodríguez-Cruz, M.J. Sánchez-Martín, Physico-chemical study of selected surfactant-clay mineral systems, *J. Therm. Anal. Calorim.* **94** (2008) 227–234.
- [28] B. Lee, Y. Kim, H. Lee, J. Yi, Synthesis of functionalized porous silica via templating method as heavy metal ion adsorbents: the introduction of surface hydrophilicity onto the surface of adsorbents, *Micropor. Mesopor. Mat.* **50** (2001) 77–90.
- [29] S. Denga, R. Bai, Removal of trivalent and hexavalent chromium with aminated polyacrylonitrile fibers: performance and mechanisms, *Water Res.* **38**(9) (2004) 2424–2432.
- [30] H. Yoshitake, E. Koiso, H. Horie, H. Yoshimura, Polyamine-functionalized mesoporous silicas: Preparation, structural analysis and oxyanion adsorption, *Micropor. Mesopor. Mat.* **85** (2005) 183–194.

- [31] H. Yang, R. Xu, X. Xue, F. Li, G. Li, Hybrid surfactant-templated mesoporous silica formed in ethanol and its application for heavy metal removal, *J. Hazard. Mater.* **152** (2008) 690–698.
- [32] X. Xu, B-Y. Gao, Q-Y. Yue, Q-Q. Zhong, Preparation and utilization of wheat straw bearing amine groups for the sorption of acid and reactive dyes from aqueous solutions, *J. Hazard. Mater.* **182** (2010) 1–9.
- [33] P. Yin, Q. Xu, R. Qu, G. Zhao, Removal of transition metal ions from aqueous solutions by adsorption onto a novel silica gel matrix composite adsorbent, *J. Hazard. Mater.* **169** (2009) 228–232.
- [34] M. Manzano, V. Aina, C.O. Areán, F. Balas, V. Cauda, M. Colilla, M.R. Delgado, M. Vallet-Regí, Studies on MCM-41 mesoporous silica for drug delivery: Effect of particle morphology and amine functionalization, *Chem. Eng. J.* **137** (2008) 30–37.
- [35] H. Sayılkın, S. Erdemoğlu, Ş. Şener, F. Sayılkın, M. Akarsu, M. Erdemoğlu, Surface modification of pyrophyllite with amino silane coupling agent for the removal of 4-nitrophenol from aqueous solutions, *J. Colloid Interf. Sci.* **275** (2004) 530–538.
- [36] G. Tartaglione, D. Tabuani, G. Camino, Thermall and morphological characterisation of organically modified sepiolite, *Micropor. Mesopor. Mat.* **107** (2008) 161–168.
- [37] V. Zeleňák, M. Badaníčová, D. Halamová, J. Čejka, A. Zukal, N. Murafa, G. Goerigk, Amine-modified ordered mesoporous silica: Effect of pore size on carbon dioxide capture, *Chem. Eng. J.* **144** (2008) 336–342.
- [38] L. Niu, S. Deng, G. Yu, J. Huang, Efficient removal of Cu(II), Pb(II), Cr(VI) and As(V) from aqueous solution using an aminated resin prepared by surface-initiated atom transfer radical polymerization, *Chem. Eng. J.* **165** (2010) 751–757.
- [39] J. Li, X. Miao, Y. Hao, J. Zhao, X. Sun, L. Wang, Synthesis, amino-functionalization of mesoporous silica and its adsorption of Cr(VI), *J. Colloid Interf. Sci.* **318** (2008) 309–314.
- [40] J. Qiu, Z. Wang, H. Li, L. Xua, J. Peng, M. Zhai, C. Yang, J. Li, G. Wei, Adsorption of Cr(VI) using silica-based adsorbent prepared by radiation-induced grafting, *J. Hazard. Mater.* **166** (2009) 270–276.
- [41] W. Liu, J. Zhang, C. Zhang, Y. Wang, Y. Li, Adsorptive removal of Cr (VI) by Fe-modified activated carbon prepared from *Trapa natans* husk, *Chem. Eng. J.* **162** (2010) 677–684.
- [42] S. Edebali, E. Pehlivan, Evaluation of Amberlite IRA96 and Dowex 1×8 ion-exchange resins for the removal of Cr(VI) from aqueous solution, *Chem. Eng. J.* **161** (2010) 161–166.
- [43] G. Moussavi, B. Barikbin, Biosorption of chromium(VI) from industrial wastewater onto pistachio hull waste biomass, *Chem. Eng. J.* **162** (2010) 893–900.
- [44] G. Blázquez, F. Hernández, M. Calero, M.A. Martín-Lara, G. Tenorio, The effect of pH on the biosorption of Cr (III) and Cr (VI) with olive stone, *Chem. Eng. J.* **148** (2009) 473–479.
- [45] T. Bai, X. Cheng, Preparation and characterization of 3-mercaptopropyl trimethoxysilane self-assembled monolayers, *J. Univ. Sci. Technol.*, B **15** (2008) 192.
- [46] S. Shylesh, Sahida Sharma, S.P. Mirajkar, A.P. Singh, Silica functionalised sulphonic acid groups: synthesis, characterization and catalytic activity in acetalization and acetylation reactions, *J. Mol. Catal.*, A **212** (2004) 219–228.
- [47] J. Zhe, C. Xianhua, Characterization and tribological investigation of self-assembled MPTS-MPTES/RE composite films, *J. Rare Earths* **27** (2009) 490–495.
- [48] K. Barquist, S. C. Larsen, Chromate adsorption on amine-functionalized nanocrystalline silicalite-1, *Micropor. Mesopor. Mater.* **116** (2008) 365–369.
- [49] Z. Yong-Gang, S. Hao-Yu, P. Sheng-Dong, H. Mei-Qin, Synthesis, characterization and properties of ethylene-diamine-functionalized Fe_3O_4 magnetic polymers for removal of Cr(VI) in wastewater, *J. Hazard. Mater.* **182** (2010) 295–302.
- [50] P.A. Kumar, M. Rayb, S. Chakraborty, Hexavalent chromium removal from wastewater using aniline formaldehyde condensate coated silica gel, *J. Hazard. Mater.* **143** (2007) 24–32.

IZVOD**ADSORPCIJA HROMA(VI) IZ VODENIH RASTVORA NA TERMO-KISELINSKI AKTIVIRANOM SEPIOLITU FUNKCIONALIZOVANOM AMINO-SILANOM I MERKAPTO-SILANOM**

Vesna M. Marjanović¹, Slavica S. Lazarević², Ivona M. Janković-Častvan², Bojan M. Jokić², Anđelika Z. Bjelajac², Đorđe T. Janačković², Rada D. Petrović²

¹Visoka poslovno-tehnička škola strukovnih studija, 31000 Užice, Srbija

²Tehnološko-metalurški fakultet Univerziteta u Beogradu, 11000 Beograd, Srbija

(Naučni rad)

Predmet ovog rada je funkcionalizacija termo-kiselinski aktiviranog sepiolita primenom (3-merkaptopropil)trimetoksilan ili merkapto-silan i [3-(2-aminoetil-amino)propil]trimetoksilan ili amino-silan, određivanje fizičko-hemijskih svojstava i proučavanje adsorpcije Cr(VI) iz vodenih rastvora na funkcionalizovanim materijalima pri različitim početnim pH vrednostima (2,0, 3,0 i 4,5). Za karakterizaciju funkcionalizovanih adsorbenata korišćene su: rendgenska difrakcionala analiza (XRD), infracrvena spektroskopska analiza (FT-IR), termogravimetrijska i diferencijalno-termijska analiza (TG/DTA), skenirajuća elektronska mikroskopija (SEM), dok su adsorpciono-desorpционne izoterme azota korišćene za određivanje specifične površine, zapremine i raspodele veličina pora. Tačka nultog naielektisanja adsorbenata je određena metodom uravnotežavanja posebnih proba. Rezultati karakterizacije su pokazali da je bolja funkcionalizacija termo-kiselinski aktiviranog sepiolita postignuta primenom amino-silan. Tokom funkcionalizacije organosilanima sačuvana je struktura i vlaknasta morfologija termo-kiselinski aktiviranog sepiolita. Kovalentnim vezivanjem amino-silan za površinu termo-kiselinski aktiviranog sepiolita povećava se bazni karakter površine, dok se u slučaju vezivanja merkapto-silan kiselo-bazna svojstva ne menjaju značajno. Specifična površina, zapremina i prečnici pora amino-silaniziranog uzorka su značajno manji u odnosu na nefunkcionalizovan uzorak, dok su kod merkapto-silaniziranog sepiolita približno isti kao kod polaznog materijala. Kapacitet adsorpcije Cr(VI) amino-silaniziranog adsorbenta je veći od kapaciteta merkapto-silaniziranog uzorka na svim ispitivanim početnim pH vrednostima Cr(VI) rastvora i naročito pri veoma niskoj početnoj pH vrednosti (2,0). Dominantan mehanizam adsorpcije Cr(VI) pri početnoj pH rastvora 2,0 na amino-silaniziranom adsorbentu je elektrostaticko privlačenje između Cr(VI) anjona i protonovanih amino grupa, a pri višim početnim pH rastvora moguće je obrazovanje vodoničnih veza između CrO₄²⁻ i amino grupa. Adsorpcija Cr(VI) na merkapto-silaniziranom adsorbentu se zasniva na elektrostatickim interakcijama između Cr(VI) anjona i protonovanih merkapto grupa, kao i redukciji Cr(VI) do Cr³⁺ merkapto grupama, uz elektrostaticko privlačenje redukcijom nastalih Cr³⁺ i sulfonatnih grupa dobijenih oksidacijom merkapto grupa.

Ključne reči: Termo-kiselinski aktiviran sepiolit • Funkcionalizacija • (3-Merkaptopropil)trimetoksi-silan • [3-(2-Aminoetilamino)propil]trimetoksi-silan • Adsorpcija • Hrom(VI)

Prirodna radioaktivnost uglja i letećeg pepela u termoelektrani „Nikola Tesla B“

Dragica M. Kisić¹, Saša R. Miletić¹, Vladimir D. Radonjić¹, Sanja B. Radanović², Jelena Z. Filipović³, Ivan A. Gržetić⁴

¹Javno preduzeće Elektroprivreda Srbije, Beograd, Srbija

²Privredno društvo Rudarski basen Kolubara, Srbija

³Institut za nuklearne nauke Vinča, Beograd, Univerzitet u Beogradu, Srbija

⁴Hemski fakultet Univerziteta u Beogradu, Srbija

Izvod

U termoelektranama (TE) Javnog preduzeća „Elektroprivreda Srbije“ (JP EPS) koje u kotlovima sagorevaju lignit, kao nus produkat nastaje godišnje oko 6 miliona tona letećeg pepela. Potencijalno tržište za upotrebu letećeg pepela postoji, ali ga za sada koriste isključivo cementare. Radioaktivnost letećeg pepela može da predstavlja jedan od važnih razloga protiv njegove šire upotrebe u građevinskoj industriji Srbije. Merenje radioaktivnosti u termoelektranama redovno se sprovodi od 1990. godine. U radu su prikazani rezultati dvadesetogodišnjih merenja radioaktivnosti letećeg pepela u termoelektrani Nikola Tesla B (TENT B) u Obrenovcu. Uporedno su prikazani podaci o sadržaju prirodnih radionuklida u uglju koji se sagoreva u kotlovima TENT B poreklom iz kolubarskog basena i pepelu koji nastaje prilikom sagorevanja uglja. Na osnovu dobijenih rezultata o sadržaju prirodnih radionuklida zaključuje se da se pepeo iz termoelektrane Nikola Tesla B može odlagati u životnu sredinu. Pepeo se može koristiti i u građevinarstvu, u niskogradnji. Kod primene u visokoj gradnji ideo pepela kao dodataka drugim građevinskim materijalima zavisi kako od njegovih fizičkih i hemijskih karakteristika, tako i od specifične aktivnosti ^{226}Ra , ^{232}Th i ^{40}K .

Ključne reči: termoelektrane u Srbiji, leteći pepeo, merenje radioaktivnosti, prirodni radio-nuklidi, ^{238}U , ^{232}Th , ^{226}Ra , građevinska industrija.

Dostupno na Internetu sa adrese časopisa: <http://www.ache.org.rs/HI/>

U kotlovima termoelektrana Javnog preduzeća Elektroprivrede Srbije godišnje se sagori u proseku oko 32 000 000 t lignita poreklom iz ugljenih basena Kolubara i Kostolac, pri čemu godišnje nastaje oko 6 000 000 t letećeg pepela. TENT B se sastoji od dva bloka sa instalisanom električnom snagom od po 620 MW. snabdevanje ugljem vrši se iz kolubarskog basena i to iz kopa Tamnava zapadno polje (80%) i polja E (20%). Zavisno od količine sagorelog uglja, godišnja količina pepela koja se izdvoji u elektrofiltrima u TENT B iznosi oko 1 800 000 t. Posle izdvajanja u elektrofiltrima leteći pepeo se sakuplja u silosima. Pepeo koji se ne isporučuje građevinskoj industriji meša se sa vodom u odnosu 1:1 i pomoću pumpi transportuje cevovodima na otvoreno odlagalište tj. deponiju pepela i šljake (u daljem tekstu deponija). Šljaka koja pada na dno kotla (kracer) takođe se sakuplja u poseban silos, odakle se odvodi u miksere i zajedno sa letećim pepelom meša sa vodom te pumpama transportuje na deponiju.

Blokovi B1 i B2 TENT B su tokom remonata 2009./2010. godine priključeni na novi sistem sakupljanja,

Prepiska: D.M. Kisić, Javno preduzeće Elektroprivreda Srbije, Vojvode Stepe 412, 11000 Beograd, Srbija.

E-pošta: dragica.kisic@eps.rs

Rad primljen: 16. oktobar, 2012

Rad prihvaćen: 7. decembar, 2012

STRUČNI RAD

UDK 621.311(497.11Obrenovac):
662.613:504:691

Hem. Ind. 67 (5) 729–738 (2013)

doi: 10.2298/HEMIND121016120K

transporta i odlaganja pepela i šljake (pepeo čini 90% čvrste smeše) u skladu sa novom tehnologijom, u vidu guste mešavine (odnos čvrste faze i vode 1:1) [1].

Primenom nove tehnologije omogućeno je sakupljanje suvog pepela u silosima spremnog za njegovu isporuku za potrebe industrije, što je nedavno ostvaren u TENT B, TE Kolubara A i TE Kostolac B, koje predstavljaju termoelektrane sa najvećom proizvodnjom električne energije u Republici Srbiji.

Deponija TENT B zauzima veliku površinu, oko 600 ha, od čega je odlaganje pepela do sada vršeno na 400 ha, a preostalih 200 ha je predviđeno za slučaj gradnje novih blokova. Deponija okružena naseljima i obradivim površinama, predstavlja difuzioni izvori zagađivanja vazduha, vode i tla [2]. Rešavanje ekoloških problema koji nastaju zbog negativnog uticaja deponija zahteva stalnu primenu odgovarajućih mera zaštite koje se moraju unaprediti, što iziskuje velika finansijska sredstva. Pored navedenih troškova, daleko veći troškovi nastaju u toku skupljanja, transporta i odlaganja pepela. Svi navedeni troškovi značajno poskupljuju proizvodnju električne energije [3].

Primena pepela u građevinarstvu, pre svega niskogradnji (gradnja puteva), zatim u visokoj gradnji (proizvodnja cementa, građevinske opeke), i u druge svrhe (korekcija pH vrednosti zemljišta) značajno bi smanjila

ekološke probleme, jer bi se smanjila količina odloženog pepela. Pored toga, upotreboom pepela, smanjila bi se eksploatacija prirodnih materijala sličnog hemijskog sastava, kao što je pesak [3].

Kolubarski ugljunosni basen

Kolubarski basen kao glavni snabdevač termoelektrana ugljem u Srbiji, nalazi se 30 km jugozapadno od Beograda i pokriva totalnu površinu od oko 600 km², obuhvata srednji i donji tok reke Kolubare i njene glavne pritoke Peštan, Turija, Tamnava i Ub. Morfološki gledano, to je ravan teren sa od 186 do 250 m nadmorske visine. Prostire se oko 55 km u pravcu zapad–istok i 15 km u pravcu sever–jug. U geološko-ekonomskom i morfološkom pogledu donjo-pliocenski sedimenti nose velike rezerve lignita.

Geološka građa obuhvata donjo-pliocenske sedimente koji leže transgresivno i u kontinuitetu preko panonskih sedimenata, a ređe su donjo-pliocenski sedimenti diskordantni preko starih paleozojskih i mezozojskih članova i dacito-andezitskih stena. Debljina donjo-pliocenske ugljene serije je izmedju 250 i 300 m.

Obrazovanje ugljene serije započelo je krajem donjeg ponta, a završilo se u gornjem pontu. Tokom ovog perioda, postojali su optimalni uslovi za život močvarne vegetacije na lokaciji izmedju mesta Rudovci, Veliki Crljeni, Radljevo i Koceljevo. Ova močvarna vegetacija (velike močvarne šume) dala je bazičnu masu za formiranje lignita. Petrografske analize pokazale su dominantno prisustvo ksilitiske komponente (20–80%). Srednji sadržaj ksilita je 33,0 %. Zastupljeni su ksilit siromašan celulozom ($X_A = 17\%$), ksilit bogat celulozom ($X_R = 6\%$) i gelificirani ksilit ($X_V = 10\%$). Gelificiranog ksilita više ima u podinskom ugljenom sloju [4].

Kolubarski basen je podeljen na istočni i zapadni deo koji su produktivni i severni deo koji je neproduktivan. Produktivni deo Kolubarskog ugljenog basena pokriva oko 600 km². Istočni deo basena čini oko 20% totalne proizvodnje površine, tj. nekih 120 km² i sastoji se iz četiri površinska kopa (eksploataciona polja) A, B, C i D. Polje A je iscrpljeno pre mnogo godina, a i ostala polja su pri kraju. Tokom prvih godina rudarenja postojala je podzemna eksploatacija, ali današnja eksploatacija je striktno površinska. Zapadni deo basena (odvojen od istočnog rekom Kolubarom) perspektivan je za budućnost i pokriva 80% basena ili 480 km². Unutar ovog polja nalazi se i najveće polje – polje Tamnava.

Prirodni radionuklidi u uglju

Ugalj je većim delom sačinjen od organske materije, ali neki elementi u tragovima u uglju su prirodno radioaktivni i čine prirodno prisutni radioaktivni materijal (*Normally Occurring Radioactive Material* – NORM). Ovi radioaktivni elementi uključuju uranijum (U), torijum (Th), njihove brojne produkte raspadanja, uključujući radijum (Ra) i radon (Rn). Tokom sagorevanja uglja

većina U i Th i njihovih produkata raspadanja odlazi iz njegove strukture i rasporedjuje se izmedju gasne faze i čvrstih produkata sagorevanja. Skoro celokupan gas radon prisutan u gorivnom uglju prelazi u gasnu fazu i gubi se u emisiji. Nasuprot njemu, manje gasoviti elementi, kao što su Th i U i većina produkata njihovog raspada zadržavaju se u čvrstom otpadu koji nastaje u procesu sagorevanja.

EKSPERIMENTALNI DEO

Kontrola prirodnih radionuklida u uglju Kolubarskog basena

Ispitivanja sadržaja prirodnih radionuklida u uzorcima uglja Kolubaskog basena vršena su 2003. i 2005. godine, u okviru projekta Geohemijska ispitivanja u funkciji pronalaženja novih ležišta fosilnih goriva i zaštite životne sredine. Projekat je finansiran od strane Ministarstva nauke i zaštite životne sredine Republike Srbije, a realizovao ga je Rudarsko-geološki fakultet Univerziteta u Beogradu. Tom prilikom izvršeno je ispitivanje sadržaja uranijuma 238 (^{238}U) i torijuma 232 (^{232}Th) u 95 uzoraka iz 8 basena uglja lignita u Srbiji i Crnoj Gori [5].

Za potrebe analize, uzorci su razloženi pomoću tehnike mikrotalasa. U ovom ispitivanju, uranijum i torijum su analizirani pomoću plazma masenog spektroskopa koji je induktivno spojen sa ICP-MS korišćenjem NIST standarda u laboratoriji BGR u Saveznom zavodu za geonauke i mineralne sirovine (*Bundesanstalt für Geowissenschaften und Rohstoffe*; BGR) u Hanoveru (Nemačka). Analizirani uzorki su takođe provereni na XRF analizatoru [6].

U cilju ujednačavanja kvaliteta uglja koji se isporučuje termoelektranama, u rudarskom basenu Kolubara je tokom 2008. godine uveden sistem selektivnog otkopavanja i homogenizacije uglja. Jedan od osnovnih elemenata u ovom sistemu bili su kontinualni (online) analizatori kvaliteta uglja čiji je rad zasnovan na merenju prirodne radioaktivnosti mineralnih materija u uglju. Merenjem intenziteta ukupne radioaktivnosti prirodnih radioizotopa ili pojedinačnog intenziteta radioaktivnosti radionuklida iz uranijumovog ili torijumovog niza, odnosno kalijuma 40, prisutnih u mineralnim materijama u uglju, a uz pomoć poznatih kalibracionih postupaka sprovedenih za svaki tip uglja, moguće je odrediti maseni sadržaj mineralnih materija u uglju. Shodno tome tokom 2008. godine obavljeno je uzorkovanje 22 uzoraka uglja površinskog kopa Tamnava-Zapadno polje i urađeno ispitivanje na specifičnu aktivnost i sadržaj uranijuma 238, torijuma 232 i kalijuma 40, metodom gama-spektrometrijske analize uz pomoć poluprovodničkog HPGe detektora (GEM30-70, SV-GEM, S/N: AMETEK-AMT ORTEC-SAD) relativne efikasnosti 37% i rezolucije 1,66 keV [7].

Obrada spektara izvršena je pomoću softverskog programa Genie 2000 (Canberra), a obrada rezultata merenja pomoću originalnog programa koji je razvijen u okviru programa Mathematica 5.2 (Wolfram Research, Inc.) [7].

Uzorci uglja koji su prethodno pripremljeni na odgovarajući način (sušenjem i sitnjenjem) stavljeni su u plastične Marinelli posude zapremine 500 ml. Masa uzorka koji su stavljeni u Marinelli posude varirala je od 298.21 g do 473.11 g u zavisnosti od gustine samog uzorka. Ove posude su zatopljene prirodnim voskom. Svrha zatapanja posuda sa uzorcima je da se onemogüći da radioaktivni gasovi, pre svega ^{222}Rn , difunduju, odnosno da se omogući uspostavljanje ravnoteže između radionuklida čvrste i gasovite faze. Ravnoteža se uspostavlja nakon približno 40 dana od zatapanja, što podrazumeva da je uspostavljen stalni odnos nuklidnog pretka i njegovih potomaka u uranovoј seriji, odnosno ista aktivnost svih članova radioaktivnog niza. Na taj način omogućava se kvalitativna i kvantitativna analiza uzorka [7].

Kvalitetna analiza ispitivanih uzorka zahteva dobru kalibraciju i adekvatnu kalibraciju efikasnosti. Pod adekvatnom kalibracijom efikasnosti podrazumeva se da kalibracioni standard i mereni uzorak imaju identičnu geometriju merenja i da je njihov hemijski sastav i specifična gustina što je moguće približniji [7]. Vreme merenja pojedinačnog uzorka obično traje, u zavisnosti od uslova merenja, između 70 000 i 350 000 s. Nakon 40 dana od zatapanja uzorka, ponovljena su merenja istih uzorka, koja su trajala između 74 000 i 246 000 s [7].

Kontrola prirodne radioaktivnosti u okolini TENT B

Prirodni radionuklidi se u toku procesa sagorevanja uglja koncentrišu prevashodno u čvrstim produktima sagorevanja uglja (nus produkat), u pepelu i šljaci, koji predstavljaju industrijski otpad termoelektrana. Na taj način, pepeo i šljaka mogu biti obogaćeni, tj. imati povećane količine prirodnih radionuklida. U takvim slučajevima radi se o tehnološki povišenoj prirodnoj radioaktivnosti (*Technologically Enhanced Occurring Radioactive Material* – TENORM) industrijskog otpada. Ovakav otpad se, kako smo rekli, deponuje na odlagalište, na otvorenu deponiju ili se može koristiti kao dodatak građevinskog materijala.

Ciljano ispitivanje sadržaja prirodnih radionuklida uranijmovog (^{238}U i ^{226}Ra) i torijumovog niza (^{232}Th) i kalijuma (^{40}K), izvršeno je 1996. godine da bi se utvrdila potencijalna radioaktivna kontaminacija zemljišta i podzemnih voda poreklom iz industrijskog otpada termoelektrane i to iz pepela i šljake TENT Obrenovac. Tom prilikom uočene su značajne, ali ne i visoke vrednosti sadržaja ovih radionuklida [8].

U naknadnim istraživanju, sprovedenom od 2005. do 2007. godine potvrđen je nizak sadržaj prirodnih radionuklida u okolini TENT B [9]. Izmerene specifične

aktivnosti radona i torona u okolini deponije TENT B, na 28 mernih mesta u zemljištu na dubini od 80 cm, daju srednje vrednosti specifične aktivnosti radioaktivnih gasova ispod $10\ 000 \text{ Bq} \cdot \text{m}^{-3}$, uz log-normalnu raspodelu specifične aktivnosti radona. Dobijeni rezultati identificuju okolinu deponije kao zonu sa niskim nivoom osnovnog zračenja iz prirode [9].

Počevši od 1990. godine, za TENT B vrše se redovne kontrole (jedanput godišnje) radioaktivnosti u životnoj i radnoj sredini od strane ovlašćenih institucija.

Cilj kontrole je procena prirodne radioaktivnosti iznad prirodnog fona neposredno i u okolini TENT B, zatim procena odgovarajućeg efekta tehnološki izmenjene prirodne radioaktivnosti na zdravlje populacije koja živi i radi u toj životnoj sredini i da se pronađe i ustanovi poreklo eventualno lokalnog izvora veštačke radioaktivnosti [10].

Kontrola obuhvata gama-spektrometrijsku analizu uzorka: uglja, šljake, elektrofiltarskog pepela iz procesa proizvodnje; šljake i pepela odloženih na depozitima, zemljišta u neposrednoj okolini deponije, poljoprivrednog zemljišta u krugu prečnika 10 km od elektrane (obradivo). Pored toga kontrolom su bile obuhvачene biljne kulture sa deponije i biljne kulture sa odgovarajućem zemljištem, rečne vode (reka Sava pre i posle ispuštanja otpadnih voda) i otpadne vode sa deponija.

Vršena su merenja specifične aktivnosti prirodnih radionuklida uranijumovog (^{238}U i ^{226}Ra) i torijumovog niza (^{232}Th) i ^{40}K , aktvacionih radionuklida (^{51}Cr , ^{54}Mn , ^{59}Fe , ^{60}Co i ^{65}Zn), proizvedenih radionuklida poreklom iz fallout-a (^{95}Zr , ^{95}Nb , ^{103}Ru , ^{106}Ru , ^{141}Ce , ^{144}Ce , ^{134}Cs i ^{137}Cs) i kosmogenog radionuklida (^{7}Be). Istovremeno sa uzimanjem uzorka, od 1992. do 2011. godine, vršeno je merenje jačine apsorbovane doze gama zračenja u vazduhu na jednom metru iznad površine tla. Takođe je urađena i kontrola ukupne alfa i ukupne beta aktivnosti otpadnih voda i vode reke Save [10,11].

Uzorci uglja, pepela i zemljišta su sušeni na 105°C , odmereni, zaptiveni pčelinjim voskom u plastične kutije od 100 g. Radi uspostavljanja radioaktivne ravnoteže pripremljeni su uzorci čuvani u laboratoriji 30 dana pre nego što je rađena spektrometrija - gama emitera [11].

Spektrometrija gama-emitera urađena je na HPGe detektorima relativne efikasnosti 20 i 23%, firme Canberra i ORTEC. Rezolucija detektora je 1.8 keV na energiji od 1332 keV.

Kalibracija detektora sprovedena je sekundarnim referentnim radioaktivnim materijalom u matriksu zemlje, a materijal je potom odložen u plastične kutije od 100 g. Sekundarni referentni materijal dobijen je od primarnog referentnog materijala, koga je proizveo: National office of Measures, Budapest, matriksa zemlje, nakapanim ^{22}Na , ^{57}Co , ^{60}Co , ^{89}Y , ^{133}Ba i ^{137}Cs , ukupne specifične aktivnosti 1500 Bq/kg , na dan 01.07.1991. godine i Czech Metrological institute, Praha, 9031-OL-

116/8 type erx, ukupne aktivnosti 114,9 kBq na dan 03.03.2008.godine (^{241}Am , ^{109}Cd , ^{139}Ce , ^{57}Co , ^{60}Co , ^{88}Y , ^{113}Sn , ^{137}Cs i ^{210}Pb) [12]. Vreme merenja uzorka trajalo je 52 000 s [12].

REZULTATI MERENJA I DISKUSIJA

Statistička obrada podataka dobijenih hemijskim ispitivanjem sadržaja uranijuma (^{238}U) i torijuma (^{232}Th) u 95 uzoraka iz 8 basena uglja lignita u Srbiji i Crnoj Gori je prikazana je u tabeli 1 [5]. U odnosu na ugljeve navedenih basena u Republici Srbiji, ugalj Kolubarskog basena ima nizak sadržaj uranijuma 238 (^{238}U), dok je sadržaj torijuma 232 (^{232}Th) viši, što je takođe slučaj sa ugljem basena Krepoljin.

Ugalj iz basena Krepoljin ima viši sadržaj uranijuma i najveći sadržaj torijuma u odnosu na sav proučavan ugalj. Sadržaj uranijuma i torijuma u uglju iz basena Sjenica i Soko Banje je nizak. Karakteristike uglja iz basena Senje-Resavica je niska koncentracija uranijuma i torijuma. Ugalj iz basena Pljevlja (Crna Gora) pokazuje veoma nisku koncentraciju uranijuma i torijuma [5].

Laboratorijska gama – spektrometrijska merenja prirodnih radionuklida u uglju Tamnava-Zapadno polje, obavljena tokom 2008. godine prikazana su u tabeli 2 i pokazuju nizak sadržaj radionuklida [7]. Vrednosti specifične aktivnost i sadržaja prirodnih radionuklida iznose su:

- uranijum 238 (^{238}U): 0,46–32,9 Bq/kg, odnosno izmerene koncentracije se kreću u intervalu 0,036–2,69 mg/kg;
- torijum 232 (^{232}Th): 3,8–20,42 Bq/kg, odnosno izmerene koncentracije se kreću u intervalu 0,84–5,05 mg/kg;
- kalijuma 40 (^{40}K): 10,57–100,6 Bq/kg, odnosno izmerene koncentracije se kreću u intervalu 350–3330 mg/kg.

Na osnovu gama-spektrometrijskih merenja obavljenih u periodu od 1990. do 2011. godine u tabeli 3 dati su rezultati spektrometrije gama-emitera za TENT B. Prikazane su minimalne i maksimalne vrednosti, vrednosti aritmetičkih i geometrijskih sredina i mediana, specifične aktivnosti prirodnih radionuklida uranijumovog (^{238}U i ^{226}Ra) i torijumovog niza (^{232}Th) i kalijuma 40 (^{40}K) [11,12].

Analiza rezultata merenja koncentracija prirodnih radionuklida u uglju, kotlovske šljake, letećem pepelu i pepelu sa deponije prikazanih u tabeli 3 pokazuje sledeće:

- U uzorcima uglja, kotlovske šljake, letećem pepelu, pepelu sa deponije, detektovani su prirodni radionuklidi uranijum 238 i uranijum 235 (^{238}U i ^{235}U), radijum 226 (^{226}Ra) i torijum 232 (^{232}Th) kao i kalijum 40 (^{40}K).
- Leteći pepeo obogaćen je prirodnim radionuklidima, pri čemu prosečne specifične aktivnosti ^{232}Th u uglju iznose 25,2 Bq/kg, a u letećem pepelu 84,2 Bq/kg;

Tabela 1. Sadržaj prirodnih radionuklida ^{238}U , ^{226}Ra , ^{232}Th i ^{40}K u ugljevima Srbije, uporedno sa ugljem Crne Gore [5]; MD – medijana
Table 1. Natural radionuclides content ^{238}U , ^{226}Ra , ^{232}Th and ^{40}K in coal in the Republic of Serbia compared with coal in the Republic of Montenegro [5]; MD – median values

Ugljeni basen	^{238}U , mg/kg			^{232}Th , mg/kg		
	Min	Max	MD	Min	Max	MD
Kostolac	0,60	70,10	0,95	0,20	2,60	1,08
Kolubara	0,65	3,20	1,84	0,84	6,57	3,18
Krepoljin	0,95	6,59	2,99	1,48	6,48	3,65
Sjenica	1,20	6,05	3,11	0,12	2,71	1,18
Soko Banja	0,80	6,66	3,17	0,13	4,95	0,80
Bogovina-Istočno polje	0,18	89,90	13,55	0,14	3,48	0,33
Senje-Resavica	0,19	4,14	1,35	0,29	3,56	0,90
Pljevlja	0,28	3,52	1,30	0,17	1,89	0,78

Tabela 2. Prirodni radionuklidi ^{238}U , ^{232}Th i ^{40}K u uglju Kolubarskog basena, sa kopa Tamnava-Zapadno polje [7]
Table 2. Natural radionuclides ^{238}U , ^{232}Th and ^{40}K in coal in the Kolubara Mining Basin, from the Tamnava West Field OCM [7]

Vrednost	Specifična aktivnost, Bq/kg			Sadržaj, mg/kg		
	^{238}U	^{232}Th	^{40}K	^{238}U	^{232}Th	^{40}K
Min	0,46	3,38	10,57	0,036	0,84	350
Max	32,9	20,42	100,6	2,69	5,05	3330
Aritmetička sredina	16,265	11,75091	60,0681	1,328909	2,928182	1988,095
Medijana	14,61	10,475	60,63	1,195	2,635	2000
Geometrijska sredina	12,82906	10,90072	51,56194	1,046321	2,721521	1706,418

Tabela 3. Rezultati merenja gama-spektrometrije u periodu 1990–2011.godina – TENT B [11–13]; AM – aritmetička srednja vrednost, MD – mediana, GS – geometrijska sredina
 Table 3. Gamma spectrometry measurements results, in period 1990–2011 – TPP Nikola Tesla B [11–13]

Merno mesto	^{232}Th , Bq/kg						^{226}Ra , Bq/kg						^{238}U , Bq/kg						^{40}K , Bq/kg							
	Min	Max	AM	MD	GS	Min	Max	AM	MD	GS	Min	Max	AM	MD	GS	Min	Max	AM	MD	GS	Min	Max	AM	MD	GS	
Ugalj sa dodavača ^a	10,6	66,8	25,2	20,9	22,8	14,1	86,8	36,3	31,0	32,5	11,0	68,9	38,3	37,5	33,8	36,2	376,9	112,2	92,5	97,7						
Šljaka ispod kracer-a	19,8	91,6	59,0	60,2	55,2	28,9	276,2	88,6	84	79,5	18,9	160,3	81,2	78,0	73,9	118,0	472,4	294,4	326	277,4						
Leteći pepeo ^a	71,0	104,0	84,2	79,5	83,3	91,0	152	127,1	130	125,5	114,0	174,0	142,6	141,	141,2	357	473,0	415,6	405	413,2						
Pepeo ^a	Aktivna kaset-a	11,3	143,0	75,3	74,5	71,6	46,0	318,8	120,9	106	110,9	19,1	284,5	110,7	106	97,4	81,3	693,4	343,2	339,4	331,9					
Pasivna kaset-a	12,4	109,0	73,9	74,1	70,4	27,0	279,9	117,8	116	109,6	15,5	241,0	119,5	119	108,1	241,0	241,0	669,0	398,2	397,3	390,4					
Ugalj sa odlagališta ^b			23±1				33±2										70±3									
Pepeo sa deponije ^b			75±4				111±5										–									
																	317±15									

^aMerenja su vršena od strane ovlašćenih institucija: Institut za medicinu rada i radioološku zaštitu „Dr. Dragomir Karađorđević“, Beograd (1990–2002, 2005, 2006 i 2011) i Institut za nuklearne nauke „Vinča“, Beograd, (2003, 2004, 2007–2010); ^bmerenja obavljena 2004. godine (projekat INTALRISK, EU FP 6, 2004–2007)

^{238}U u uglju iznose 38,3 Bq/kg, a u letećem pepelu 142,60 Bq/kg; ^{40}K u uglju iznose 112,2 Bq/kg, a u letećem pepelu 415,60 Bq/kg.

- Ne postoji velika razlika u sadržaju radionuklida na aktivnim (deo deponije gde se privremeno odlaže pepeo) i pasivnim kasetama u posmatranom periodu. To se može objasniti time da se uloga aktivnih i pasivnih kaseti menja tokom godina, tj. aktivne postaju pasivne i obrnuto.

Ukoliko se uporede rezultati spektrometrije gama – emitera uglja i letećeg pepela TPP Nikola Tesla B sa podacima iz literature objavljenim u drugim delovima sveta (SAD, bivši SSSR, Poljska, Indija i Turska), prikazanim u tabeli 4 [11,12,14–19], primećuje se da su vrednosti uporedive, odnosno istog reda veličine.

Termoelektrane koje sagorevaju kolubarski ugalj, a to se odnosi i na TPP B, redovno su (jedanput godišnje) vršile ispitivanja specifične aktivnosti prirodnih radionuklida u uglju, letećem pepelu, pepelu i šljaci odlaganim na deponijama, okolnom zemljištu, te na biljnim kulturama zasejanim na deponijama u cilju biološke rekultivacije, biljnim kulturama na okolnom zemljištu, površinskim i podzemnim vodama. Međutim, rudarski basen Kolubara nije vršio redovna ispitivanja sadržaja prirodnih radionuklida u uglju na kopovima kolubarskog basena. Shodno tome, postojeće programe ispitivanja karakteristika uglja kopova kolubarskog basena – kojima su obuhvaćeni: petrografska ispitivanja, ispitivanje mineraloškog sastava, tehnička i elementarna analiza

uglja, ispitivanje sadržaja makro- i mikro-elemenata, te ukupnog i sagorljivog sumpora, potrebno je dopuniti ispitivanjem sadržaja i specifične aktivnosti prirodnih radionuklida uranijumovog (^{238}U i ^{226}Ra) i torijumovog niza (^{232}Th), kao i kalijuma (^{40}K). Dosadašnja ispitivanja sadržaja uranijuma i torijuma u ugljevima Srbije i Crne Gore pokazuju da nema osnova za nepovoljan uticaj na prirodu [5].

Upotreba pepela u građevinskoj industriji

Prema raspoloživim podacima, u Srbiji je upotreba pepela u metalurgiji, poljoprivredi, građevinskoj i hemijskoj industriji prilično mala. Upotreba pepela poboljšava karakteristike cementnih proizvoda – smanjuje njihovu poroznost i otpornost na degradaciju. Prilikom izgradnje puteva ugrađuje se u podlogu puta što smanjuje potrošnju konvencionalnih sirovina za ove svrhe. To umanjuje cenu izgradnje i štedi izvore – smanjuje eksploataciju prirodnih resursa – konvencionalnih sirovina za ove svrhe (peska, koji ima slične karakteristike, ili kamena).

Da bi se proširila upotreba pepela u industrijske svrhe, potrebno je primeniti nove tehnologije u pojedinim industrijskim granama. Naročito je značajna upotreba pepela u izgradnji puteva, jer ona omogućava njegovo korišćenje u velikim količinima [2]. Kako sadržaj prirodnih radionuklida u pepelu može da ograniči njegovu upotrebu u građevinskoj industriji, neophodno je poznavanje podataka o sadržaju prirodnih radionuk-

Tabela 4. Specifična aktivnost radionuklida u uglju i letećem pepelu, uporedno TPP Nikola Tesla B sa nekim zemljama u svetu i (Bq/kg) [11,12,14–19]

Table 4. Comparison of coal and fly ash specific radionuclides activity between TPP Nikola Tesla B and some world countries (Bq/kg) [11,12,14–19]

Država		^{232}Th		^{226}Ra		^{238}U		^{40}K	
		Min	Max	Min	Max	Min	Max	Min	Max
SAD	Pepeo	78	122	42	141	111	204	259	370
	Ugalj	8	23	1	30	16	30	52	120
Bivši SSSR	Pepeo	185		185		–		1850	
	Ugalj	–		28		–		120	
Poljska	Pepeo	47	92	75	120	–	–	448	759
	Ugalj	8	21	13	29	38	43	43	181
Indija	Pepeo	96	178	40	152	–	–	148	840
	Ugalj	–	–	11	67	–	–	14	445
Turska	Pepeo	58		149		–		94	
	Ugalj	11		14		–		123	
Kina	Pepeo	119	196	76	166	–	–	262	521
	Ugalj	34	38	23	30	–	–	93	110
Nemačka	Pepeo	88		118		133		514	
	Ugalj	<20		20		<40		–	
Srbija	Pepeo	71	104	91	152	114	178	311	509
		84		130		143		408	
	Ugalj	11	27	14	38	18	68	48	157
		20		25		35		101	

lida. Pored ispitivanja radioaktivnosti pepela i šljake, radi njihovog odlaganja u životnu sredinu, ispituje se i mogućnost njihove upotrebe u građevinarstvu, u niskogradnji i visokoj gradnji. Naročito je povoljna upotreba letećeg pepela u građevinarsvu ako je specifična aktivnost građevinskih proizvoda u okviru granica dozvoljenog.

Na osnovu višegodišnjih ispitivanja potvrđena je mogućnost upotrebe pepela u industriji [2]. Zbog povećane prirodne radioaktivnosti u uzorcima pepela i šljake, obavezna je stalna kontrola industrijskih proizvoda i ulaznih komponenti koji bi se koristili u građevinarstvu. Propisani su različiti kriterijumi graničnih vrednosti sadržaja radionuklida u građevinskom materijalu. Ovi kriterijumi dati su u tabeli 5, a odnose se na građevinske materijale koji se upotrebljavaju u visokoj gradnji za enterijer i eksterijer, te u niskogradnji za podloge za puteve, igrališta i ostalu niskogradnju (ispod sloja za prekrivanje) [20].

Da bi neki materijal mogao da se koristi u građevinarstvu, specifične aktivnosti ^{226}Ra , ^{232}Th i ^{40}K moraju da zadovolje sledeću relaciju:

$$\frac{C_{\text{Ra}}}{\text{Max(Ra)}} + \frac{C_{\text{Th}}}{\text{Max(Th)}} + \frac{C_K}{\text{Max(K)}} < 1 \quad (1)$$

gde su sa C_x označene koncentracije odgovarajućih radionuklida, a sa Max(x) su označene granice sadržaja radionuklida (tabela 5) za odgovarajuću kategoriju primene materijala u visokoj gradnji (enterijer i eksterijer) i niskogradnji (putevi i igrališta).

Tabela 5. Granice sadržaja radionuklida u građevinskom materijalu [20]

Table 5. Radionuclides content limits in the construction material [20]

Propisana vrednost	^{226}Ra , Bq/kg	^{232}Th , Bq/kg	^{40}K , Bq/kg
Za enterijer	300	200	3000
Za eksterijer	400	300	5000
Za podloge za puteve i igrališta	700	500	8000

Tabela 6. Specifična aktivnost prirodnih radionuklida (Bq/kg) u letećem pepelu u TENT B [11,12]

Table 6. Fly ash specific radionuclides activity (Bq/kg) in TPP Nikola Tesla B [11,12]

Godina ispitivanja	^{232}Th	^{226}Ra	^{40}K
2004	104	152	363
2005	98	152	311
2006	99	147	509
2007	71	112	405
2008	72	120	357
2009	79	138	382
2010	80	130	461
2011	71	91	473
Min	71	91	311
Max	104	152	509
Srednja vrednost	84,24	130,25	407,63
Medijana	79,5	134	393,5
Geometrijska sredina	83,27	128,54	402,73

Na osnovu podataka o specifičnoj aktivnosti prirodnih radionuklida u letećem pepelu u TENT B (tabela 6) i korišenjem relacije (1) izračunati su gama indeksi za leteći pepeo u slučaju korišćenja u visokoj gradnji i niskogradnji, koji iznose manje od jedan (tabela 7) [21].

Na osnovu prikazanih rezultata u tabelama 6 i 7 o sadržaju prirodnih radionuklida i izračunatom gama indeksu može se zaključiti da se pepeo iz TENT B može koristiti i u građevinarstvu (u niskogradnji), pošto je gama-indeks manji od jedan [21]. Kod primene u visokoj gradnji ideo pepela, kao dodataka drugim građevinskim materijalima, zavisi od njegovih fizičkih i hemijskih karakteristika, a zavisi i od specifične aktivnosti ^{226}Ra , ^{232}Th i ^{40}K . Shodno tome, neophodna je redovna kontrola sadržaja prirodnih radionuklida svih ulaznih komponenti (sirovina), kao i finalnog proizvoda.

Korišćenje elektrofiltrarskog pepela poreklom iz TENT B isplativo je i ekološki opravdano za ekotroprirednu iz sledećih razloga: 1) Manjeg iznosa obavezne novčane naknade za odlaganje otpada, 2) ostvarenja dobiti od prodaje pepela, 3) umanjenja troškova za transport i odlaganje (manja je količina pepela koji se odlaže na deponije), 4) produženja radnog veka depozite, 5) manje eksploatacije prirodnih resursa (peska, koji ima slične karakteristike), kao i 6) redukcije ekoloških problema [2]. Primena nove tehnologije sakupljanja, malovodnog transporta i odlaganja pepela i šljake u TENT B i drugim termoelektranama, omogućila je zasebno skladištenje šljake i suvog pepela u silosima, te isporuku suvog letećeg pepela građevinskoj industriji

Tabela 7. Gama indeks za leteći pepeo TENT B za slučaj upotrebe u visokoj gradnji i niskogradnji [21]
Table 7. Fly ash gamma index in TPP Nikola Tesla B in case of use in building construction and civil engineering [21]

Godina	Visoka gradnja		Niskogradnja
	Za energetičar	Za eksterijer	Za podlove za puteve i igrališta
2007.	0,86	0,60	0,35
2008.	0,88	0,61	0,36
2009.	0,98	0,68	0,40
2010.	0,99	0,68	0,40
2011.	0,82	0,56	0,33
Min.	0,82	0,56	0,33
Max.	0,99	0,68	0,40
Sr.vred.	0,91	0,63	0,37

pomoću auto-cisterni. Tokom 2011. godine TENT B je na osnovu ugovora isporučio suvi leteći pepeo i to: 40336 t cementari Lafarge, Beočin, i 3045 t cementari Titan, Kosjerić. Pored toga, isporučeno je i 5267 t šljake Javnog preduzeću za izgradnju Obrenovca, koja je upotrebljena kao podloga za izradu nekategorisanih puteva.

ZAKLJUČAK

1. U uzorcima uglja, letećeg pepela, pepela sa depozite, detektovani su prirodni radionuklidi uranijum 238 U i uranijum 235 U (^{238}U i ^{235}U), radijum 226 Ra), torijum 232 Th (^{232}Th).

2. Leteći pepeo koji nastaje u kotlovima TENT ima povećanu koncentraciju prirodnih radionuklida u odnosu na ugalj. Radi se o tehnološki povišenoj prirodnoj radioaktivnosti (*Technologically Enhanced Occurring Radioactive Material – TENORM*) industrijskog otpada, pri čemu prosečne specifične aktivnosti ^{232}Th u uglju iznose 25,2, a u letećem pepelu 84,2 Bq/kg. Specifične aktivnosti ^{238}U u uglju iznose 38,3, a u letećem pepelu 142,60 Bq/kg. Specifične aktivnosti ^{40}K u uglju iznose 112,2, a u letećem pepelu 415,60 Bq/kg.

3. Pepeo se može koristiti u niskogradnji, pošto je gama-indeks manji od jedan. Kod primene u visokoj gradnji udeo pepela kao dodataka drugim građevinskim materijalima zavisi kako od njegovih fizičkih i hemijskih karakteristika, tako i od specifične aktivnosti ^{266}Ra , ^{232}Th i ^{40}K .

4. Postojeće programe ispitivanja karakteristika ugljeva rudarskog basena Kolubara, potrebno je dopuniti ispitivanjima specifične aktivnosti i sadržaja prirodnih radionuklida uranijumovog (^{238}U i ^{226}Ra) i torijumovog niza (^{232}Th) i kalijuma 40 (^{40}K).

5. Ispitivanja koja se odnose na prirodne radionuklide u uglju i pepelu Kolubarskog basena treba nastaviti. Dalja studijska istraživanja zahtevaju multidisciplinarni pristup koji uključuje i procenu uticaja na zdravlje ljudi.

LITERATURA

- [1] D. Kisić, Z. Cokić, N. Milićević, D. Mađarac, I. Radovanović, V. Radonjić, Prilagođavanje mera zaštite životne sredine u TE "Nikola Tesla" B, saglasno novoj tehnologiji malovodnog transporta i odlaganja pepela i šljake, III savetovanje sa međunarodnim učešćem – Stanje i perspektive deponija pepela, šljake i jalovine u termoelektranama i rudnicima, Palić, 2011, str. 42–52.
- [2] D. Kisić, M. Gavrić, N. Milićević, D. Mađarac, S. Cojić, P. Cvijanović, Mere zaštite preduzete u termoenergetskim postrojenjima jp eps u cilju smanjenja emisije praškastih materija u vazduh, Simpozijun sa međunarodnim učešćem „Zaštita vazduha 2010“ – Kvalitet vazduha i zakonska regulativa u zaštiti životne sredine, Subotica, 2010, str. 124–134.
- [3] D. Kisić, Z. Žbogar, S. Marinković, A. Kostić-Pulek, S. Cmiljanić, Mogućnost korišćenja elektrofiltratskog pepela PD TENT d.o.o. Obrenovac u niskoj i visokoj gradnji, Prva regionalna naučno-stručna konferencija o upravljanju industrijskim otpadom – Industrijski otpad, Kopaonik, 2007.
- [4] M. Kezović, Ugljunosnost Kolubarskog basena, Elektroprivreda **2** (2011) 154–163.
- [5] D. Životić, I. Gržetić, H. Lorenz, V. Simić, U and Th in Some Brown Coals of Serbia and Montenegro and Their Environmental Impact, Environ Sci Pollut Res **15** (2008) 155–161.
- [6] A.L. Meier, F.E. Lichte, P.H. Biggs, J.J. Bullock, In: B.F. Arbogast (ed.), Analysis of Coal Ash by Inductively Coupled Plasma-Mass Spectrometry: Analytical Methods for the Mineral Resources Surveys Program, U.S. Geological Survey Open File 96–525, 1996, pp. 109–125.
- [7] Izveštaj: Laboratorijsko ispitivanje zavisnosti Prirodne radioaktivnosti uzorka uglja PK „Tamnava-Zapadno polje“ od sadržaja pepela, Institut za nuklearne nauke Vinča, 2009.
- [8] Ž. Vuković, M. Mandić, D. Vuković, Natural radioactivity of ground waters and soil in the vicinity of the ash repository of the coal-fired power plant "Nikola Tesla" A, Obrenovac (Yugoslavia), J. Environ. Radioact. **33** (1996) 41–48.
- [9] D. Kisić, N. Veselinović, S. Tokonami, I. Čeliković, Z. Stojanović, O. Čuknić, N. Nemčević, R. Simović, Z. Žunić,

- Norm u okolini TE „Nikola Tesla“ B – eksperimentalni rezultati, XXV simpozijum Društva za zaštitu od zračenja Srbije i Crne Gore, Zbotnik radova, Kopaonik, 2009, str. 47–52.
- [10] G. Pantelić, M. Eremić-Savković, M. Tanasković, Lj. Javorina, V. Vuletić, D. Kisić, Ispitivanje povećane prirodne radioaktivnosti u radnoj životnoj sredini termoelektrana u Obrenovcu, Zbornik radova, Međunarodna konferencija Elektra II-ISO 14000, Tara, 2002, str. 294–296.
- [11] Elaborat: Kontrola radioaktivnosti u radnoj i životnoj sredini TE "Nikola Tesla " B (1990–2002, 2005, 2006 i 2011. godina), Institut za medicinu rada i radiološku zaštitu "Dr. Dragomir Karajović", Beograd.
- [12] Elaborati – Kontrola radioaktivnosti u radnoj i životnoj sredini TE "Nikola Tesla " B (2003, 2004, 2007–2010. godina), Institut za nuklearne nauke "Vinča", Beograd.
- [13] Međunarodni Projekat INTAILRISK, EU FP 6, 2004–2007, „Procena rizika na životnu sredinu zbog upotrebe radioaktivnog kontaminiranog industrijskog otpada“.
- [14] United Nations Scentific Committee on the Effetcts of Atomic Radiation (UNCEAR), 1988, Report of the General Assembly,with annexes, Sources, Effects and Risks of Ionizing Radiation, United Nations, New, York, 1988.
- [15] G. Rosner, K. Bunzl, H. Hotzl, R. Winkler, Low Level Measurements of Natural Radionuclides in Soil Samples around A Coal – Fired Power Plant, *Nucl. Instrum. Methods* **223** (1984) 585–589.
- [16] U.C.Mishira, Environmenal Impact of Coal Industry and Thermal Power Plants in India, *Journal of Environmenal Radioactivity* **72** (2004) 35–40.
- [17] T. Momdal, D. Sengupt, A. Mandal, Natural Radioactivity of Ash and Coal in Major Thermal Power Plants of West Bengal, India, *Curr. Sci. India* **91** (2006) 1387–1393.
- [18] R. Kljajić, V. Šipka, M. Radenković, R. Mitrović, Ugljevi i mineralna đubriva kao izvori tehnološkog povećanja prirodne radioaktivnosti, Jonizujuća zračenja iz prirode, Beograd, 1995, str. 95–11.
- [19] U. Cevik, N. Damla, S. Nezir, Radiological Characterization of Cayirhan Coal-fired Power Plant in Turkey, *Fuel* **86** (2007) 2509–2513.
- [20] Pravilnik o granicama sadržaja radionuklida u vodi za piće, životnim namirnicama, stočnoj hrani, lekovima, predmetima opšte upotrebe, građeviskom materijalu i drugoj robi koja se stavlja u promet, Službeni list RS br. 86/2011.
- [21] D. Kisić, S. Miletić, Đ. Janaćković, D. Todorović, V. Radonjić, Prirodna radioaktivnost letećeg pepela iz termoelektrane Nikola Tesla B, kao jedna od značajnih karakteristika kod primene u građevinskoj industriji, I simpozijum Odsumporavanje dimnih gasova, IV savetovanje deponije pepela i šljake i jalovine u termoelektranama i rudnicima, sa međunarodnim učešćem, Palić, 2012, str. 217–227.

SUMMARY

NATURAL RADIOACTIVITY OF COAL AND FLY ASH AT THE NIKOLA TESLA B TPP

Dragica M. Kisić¹, Saša R. Miletić¹, Vladimir D Radonjić¹, Sanja B. Radanović², Jelena Z. Filipović³, Ivan A. Gržetić⁴

¹*Public Enterprise Electric Power Industry of Serbia, Serbia*

²*Kolubara Mining Basin, Serbia*

³*Vinča Institute of Nuclear Sciences, University of Belgrade, Serbia*

⁴*University of Belgrade, Faculty of Chemistry, Serbia*

(Professional paper)

Serbian thermal power plants (TPPs) produce siliceous fly ash from lignite in the quantity of approximately 6 million tons per year. The potential market for the use of fly ash is operational, but for the time being, only used by cement producers. Fly ash radioactivity could be one of the major points of concern when larger use of fly ash is planned, particularly in the Serbian construction industry. Radioactivity measurements have been conducted regularly from 1980. This paper presents the results of a ten-year fly ash radioactivity measurements at the Nikola Tesla B TPP located in Obrenovac. In addition, the paper compares the natural radionuclides coal content data combusted by the Nikola Tesla B TPP boilers coming from the Kolubara Basin and ash created during coal combustion. Fly ash created in the Nikola Tesla TPPs boilers is characterised by the increased concentration of the natural radionuclides content compared to coal. This is the so-called technologically enhanced natural radioactivity (Technologically Enhanced Occurring Radioactive Material – TENORM) of industrial waste, whereas the average specific activities: ^{232}Th in coal amount to 25.2 Bq/kg, and in fly ash and coal 84.2 Bq/kg and ^{238}U 38.3 Bq/kg, respectively. Following the obtained natural radionuclides content results it may be concluded that the Nikola Tesla B TPP ash may be disposed into the environment. Ash may be used also in the construction industry (civil engineering). In building construction applications, ash share as the additive to other building materials depends from its physical and chemical characteristics, as well as from the radionuclides activity: ^{226}Ra , ^{232}Th and ^{40}K . Unlike the thermal power plants regularly (once a year) testing the specific natural radionuclides activity in the combusted coal and boiler fly ash, the Electric Power Industry of Serbia has not performed large-scale investigations of the natural radionuclides content in coal within the Kolubara Mining Basin. Natural radionuclides content in fly ash is compared to the combusted coal some 3–4 times higher and may present a limitation for applying ash in the construction industry. In view of the above, and considering the construction industry interests in using the Nikola Tesla B TPP ash, regular investigations of the natural radionuclides content in ash created in the thermal power plants should be carried out, together with the Kolubara Mining Basin coal combusted by the Nikola Tesla B TPP and other PE EPS thermal power plants. The current Kolubara Mining Basin coal characteristics investigation programme should be supplemented by the natural radionuclides content of the uranium (^{238}U and ^{226}Ra) and thorium series (^{232}Th) and potassium 40 (^{40}K).

Keywords: Serbian power plants • Fly ash

• Radioactivity measurements • Natural radionuclides ^{238}U , ^{232}Th , ^{226}Ra • Construction industry

Analiza faktora koji utiču na sorpciju Cu(II) jona klinoptilolitom

Marija Z. Šljivić-Ivanović, Ivana D. Smičiklas, Jelena P. Marković, Aleksandra S. Milenković

Univerzitet u Beogradu, Institut za nuklearne nauke „Vinča”, Beograd, Srbija

Izvod

U ovom radu su izračunati i upoređeni efekti procesnih parametara na sorpciju Cu(II)-jona klinoptilolitom. Varirani su inicijalna koncentracija Cu(II)-jona, pH vrednost rastvora, masa i veličina čestica sorbenta, a kao odgovor sistema posmatrana je rezidualna koncentracija jona metala u rastvoru. Primenom punog faktorijalnog dizajna, na dva nivoa faktora, pokazano je da su pri izabranom intervalu poverenja od 95%, statistički značajni efekti promene početne koncentracije jona metala i mase sorbenta, kao i efekat interakcije ova dva parametra. Efekat interakcije je izraženiji pri višem nivou koncentracije jona Cu(II). Izračunati su efekti glavnih varijabila, a regresiona analiza je korišćena za fitovanje odgovora sistema. Analizom dobijenih podataka definisan je matematički model koji verodostojno opisuje eksperimentalno dobijene vrednosti ($R^2 > 0,99$).

Ključne reči: klinoptilolit, Cu(II), sorpcija, eksperimentalni dizajn.

Dostupno na Internetu sa adrese časopisa: <http://www.ache.org.rs/HI/>

Procesi i fenomeni koji se dešavaju u laboratorijskim i industrijskim sistemima, kao i oni u prirodi, uzrokovani su nizom faktora. Za razumevanje ovih procesa, neophodno je ispitati uzajamne veze između faktora i odgovora sistema. Eksperimentalni dizajn i optimizacija su alati koji se koriste da bi se sistematizovano rešili različiti tipovi problema sa širokom primenom na svim poljima nauke (hemija, biologija, fizika,...), kao i u industriji (prehrabenoj, farmaceutskoj,...) [1]. Generalno, umesto variranja jednog faktora pri ostalim constantnim uslovima, eksperimentalni dizajn omogućava simultano variranje svih faktora i dobijanje velikog broja informacija o ispitivanom procesu uz relativno mali broj eksperimentalnih pokušaja. Na taj način se izvode preliminarna istraživanja (*screening* faktora), optimizacija procesa, ispitivanje robustnosti i preciznosti, kao i definisanje empirijskih matematičkih modela koji opisuju ispitivane procese. Postoji niz metoda planiranja tj. dizajniranja eksperimenta, kao što su jednostavan uporedni dizajn, nasumični "blok" dizajn, dizajn latinskih kvadrata, faktorijalni dizajn, itd. [1]. Ispravnim odabirom nezavisnih promenljivih, njihovim variranjem i praćenjem odgovora sistema, definiše se uticaj faktora, kao i uticaj njihovih međusobnih interakcija. Skrining eksperimenti se izvode u cilju definisanja faktora čija promena značajno utiče na odgovor sistema, veličine uticaja glavnih faktora i interakcija. Za ovakva preliminarna istraživanja koristi se pun ili delimični (frakcionisani) faktorski dizajn. Pun faktorski dizajn daje najpotpuniju sliku o uticaju faktora, s obzirom na to da se na

NAUČNI RAD

UDK 546.562:66.081:549.67.02

Hem. Ind. 67 (5) 739–745 (2013)

doi: 10.2298/HEMIND121123121S

ovaj način ispituju sve kombinacije faktora, pri svim nivoima.

Zbog univerzalnog pristupa u postavci eksperimenta i statističkoj obradi rezultata, primena eksperimentalnog dizajna u svim granama nauke značajno raste poslednjih dvadeset godina. Ova metodologija je našla primenu i u ispitivanju i optimizaciji različitih sorpcionih procesa, među kojima i sorpcije teških metala [2–4] i radionuklida [5,6] iz vodenih rastvora. Imobilizacija navedenih jona zavisi od prirode sorbenta i sorbata, kao i od niza eksperimentalnih uslova u kojima se proces odvija (pH, koncentracija sorbenta i sorbata, vreme kontakta, temperatura, jonska jačina, prisustvo drugih hemijskih vrsta u rastvoru, itd.). Standardna eksperimentalna procedura koja podrazumeva variranje samo jedne promenljive, ne omogućava izračunavanje i poređenje efekata promene faktora, pa se sve češće koristi eksperimentalni dizajn. Pregled literature pokazuje da se metodologija planiranih eksperimenta i statističke analize primenjuju kako za povećanje fundamentalnih znanja o procesima sorpcije i njihovim mehanizmima [7], tako i za analizu faktora [6,8] i optimizaciju procesnih parametara [9,10].

U prethodno publikovanim radovima, ispitivana je ravnoteža sorpcije Cu(II)-jona zeolitom, u funkciji početne pH vrednosti rastvora i koncentracije metala u rastvoru [11], kao i kinetika procesa u šaržnom sistemu [12]. Zeolit je okarakterisan kao jeftina, domaća sirovina pogodna za uklanjanje jona bakra iz rastvora. U ovom radu, ispitivanja su upotpunjena primenom punog faktorskog dizajna, pri dva nivoa faktora, pri čemu su prethodno stečena saznanja omogućila selekciju nivoa faktora. Kao nezavisne promenljive posmatrane su početna pH vrednost rastvora, početna koncentracija jona metala, masa i granulacija sorbenta, a kao odgovor sistema koncentracija jona Cu(II) u rastvoru nakon sorpcije. Cilj ovog rada je analiza i poređenje efe-

Prepiska: M. Šljivić-Ivanović, Univerzitet u Beogradu, Institut za nuklearne nauke „Vinča”, p.pr. 522, Beograd, Srbija.

E-pošta: marijasljivic@vinca.rs

Rad primljen: 23. novembar, 2012

Rad prihvaćen: 13. decembar, 2012

kata procesnih varijabila na sorpciju zeolitom, kao i definisanje matematičkog modela koji daje vezu između faktora i odgovora sistema.

EKSPERIMENTALNI DEO

Kao sorbent je korišćen zeolit iz rudnika zeolita Vranjska Banja, Srbija. Prethodno publikovana istraživanja [11], pokazala su da je ispitivani materijal mezoporozne strukture i da se sastoji od klinoptilolita, sa primesama albita i kvarca. Tačka nultog nanelektrisanja ovog sorbenta (pH_{PZC}) iznosila je 7,5 [11].

Sorpcioni eksperimenti izvođeni su u šaržnim uslovima. Odgovarajuće količine sorbenta su uravnotežavane sa fiksnom zapreminom rastvora $\text{Cu}(\text{NO}_3)_2 \cdot 3\text{H}_2\text{O}$ (p.a. Merk) (20,00 mL) u zatvorenim PVC posudama od 50mL. Suspenzije su uravnotežavane na horizontalnom šejkeru (120 rpm), na sobnoj temperaturi ($20 \pm 1^\circ\text{C}$). Kao nezavisne promenljive uzeti su parametri dati u tabeli 1. Variranjem faktora između dva nivoa, dobija se matrica prikazana u tabeli 2, a koja predstavlja kodirane eksperimentalne uslove dobijene punim faktorskim dizajnom. Nakon 48 h, suspenzije su proceđene, i rezidualne koncentracije Cu(II)-jona u rastvoru su izmerene metodom ICP-OES (optička emisiona spektrometrija sa induktivno spregnutom plazmom) na instrumentu tipa Perkin Elmer emission spectrometer Plasma 400, na $\lambda = 222,78 \text{ nm}$.

Tabela 1. Promenljive i njihovi nivoi
Table 1. Variables and their levels

Faktor	Nivo	
	-1	+1
A - inicijalna pH	3	5
B – masa sorbenta, g	0,1000	0,4000
C - inicijalna koncentracija Cu(II), mol/L	0,0002	0,005
D- veličina čestica, mm	<0,1	1–3

Generalno, u ovom tipu dizajna, svi faktori se variraju u širokim opsezima od značaja za dati proces. Masa sorbenta varirana je između 5,00 i 20,00 g/L, što predstavlja najčešće ispitivani opseg datog parametra [13,14]. Minimalna i maksimalna koncentracija jona metala izabrane su na osnovu izoterme sorpcije [11], uzimajući u obzir početni deo izoterme i njen plato. U eksperimentima su korišćene najsitnija i najkrupnija od dostupnih komercijalnih granulacija zeolita. Zbog specifične sorpcije Cu(II)-jona, tačka nultog nanelektrisanja izučavanog zeolita, opadala je sa porastom koncentracije Cu(II)-jona, a hidroliza jona metala uslovila je skraćenje puferske oblasti na opseg inicijalnih pH vrednosti 4–6 [11]. Minimalna pH vrednost u ovoj studiji (pH 3) izabana je kao tačka van puferske oblasti sorbenta, pri kojoj ne dolazi do značajne dealuminacije, a time i značajnih strukturalnih promena sorbenta [15], a maksimal-

na (pH 5) da bi se izbegla precipitacija hidroksida bakra. Inicijalne pH vrednosti rastvora su podešene dodavanjem minimalnih količina 0,1 M HNO_3 i KOH. pH vrednosti su određivane WTW pH-metrom, uz upotrebu elektrode Sentix 41 sa temperaturnom kompenzacijom.

Za statističku obradu rezultata je korišćen programski paket MINITAB.

Tabela 2. Matrica dobijena eksperimentalnim dizajnom (kodirane vrednosti)
Table 2. Experimental design matrix (coded units)

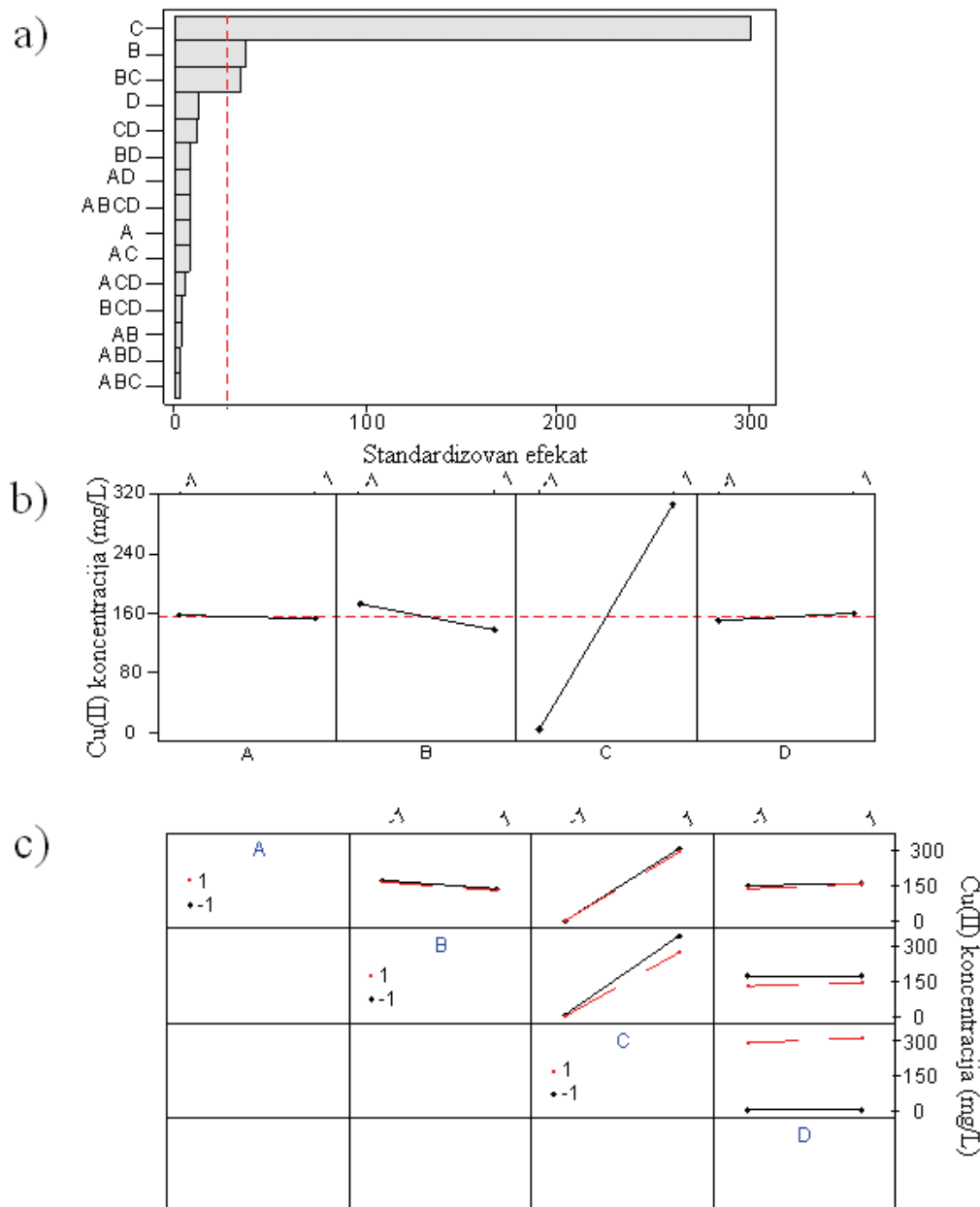
A	B	C	D	Faktor	Odgovor (Y)
				Cu koncentracija, mg/L	
1	-1	-1	-1		4,01
1	1	1	1		289,71
1	1	1	-1		233,18
-1	1	1	1		286,39
1	1	-1	1		3,91
-1	1	-1	1		7,21
-1	-1	1	-1		341,47
1	-1	1	-1		328,9
-1	-1	1	1		350,82
-1	-1	-1	-1		10,97
1	-1	-1	1		8,27
-1	1	1	-1		274,16
1	1	-1	-1		1,66
-1	-1	-1	1		0,05
-1	1	-1	-1		0,04
1	-1	1	1		343,94

REZULTATI I DISKUSIJA

Interpretacija rezultata eksperimentalnog dizajna

Efekat promene nivoa nezavisno promenljive, dovodi do promene u odgovoru sistema. Važnost i apsolutne vrednosti efekata promenljivih su date Pareto grafikom (slika 1a). Dužina bara je proporcionalna standardizovanom efektu (izračunati efekat podeljen njegovom standardnom devijacijom), a faktori su poređani po opadajućem apsolutnom efektu. Vertikalna linija na grafiku pokazuje granicu koju prelaze statistički značajni efekti, u odabranom intervalu poverenja od 95% ($\alpha = 0,05$).

Takođe, konstruisan je grafik glavnih efekata (slika 1b) koji pokazuje da li promena varijabli između dva nivoa utiče na smanjenje ili povećanje odgovora sistema. Tačke na grafiku glavnih efekata predstavljaju srednju vrednost odgovora sistema pri nižem, odnosno višem nivou posmatranog parametra. Srednje vrednosti odgovora za različite nivoje faktora su povezane pravom linijom. Horizontalna linija na grafiku predstavlja sveukupnu srednju vrednost odgovora sistema, za sve faktore, pri oba nivoa, tako da veće odstupanje od hori-



Slika 1. a) Pareto grafik, b) grafik glavnih efekata i c) grafik interakcija za rezidualnu koncentraciju Cu(II)-jona u rastvoru.
Figure 1. a) Pareto chart, b) main effect plot and c) interaction plot for residual Cu(II) concentrations.

zontalne linije ukazuje na to da je efekat promene date varijabile veći.

Uočava se da su početna koncentracija metala i masa sorbenta najuticajniji parametri, dok je efekat početne pH vrednosti, kao i granulacije sorbenta zanemarljiv. Sniženje početne koncentracije i porast mase sorbenta (slika 1b) redukuju koncentraciju Cu(II) jona u tečnoj fazi. Generalno, veća količina sorbenta vezuje veću količinu jona metala, saglasno većoj raspoloživoj površini. Porast koncentracije sorbata daje isti efekat kao i sniženje koncentracije sorbenta, jer takođe dovodi do opadanja odnosa čvrsto/tečno.

Na slici 1a se uočava da efekat promene pH vrednosti nije statistički značajan. Sam opseg selektovanih pH vrednosti je relativno uzak, kako bi reflektovao isključivo promene koncentracije Cu(II) jona usled sorpcije klinoptilolitom. Takođe, puferska svojstva sorbenta [11] doprinose smanjenju efekta promene inicijalne pH na finalno pH, a time i na sorbovanu količinu. Promena veličine čestica sorbenta ne utiče na praćeni odgovor sistema, što ukazuje na to da su sorpcioni sistemi pri svim kombinacijama faktora bili blizu ravnoteže, ili je ravnoteža dostignuta.

Interakcije između faktora mogu značajno uticati na smanjenje ili povećanje efekata glavnih faktora. Grafik interakcija (slika 1c) pokazuje da je jedino statistički značajna dvofaktorska interakcija početne koncentracije jona metala i mase sorbenta. Promena količine sorbenta u suspenziji značajnije utiče na odgovor sistema pri višem nego pri nižem nivou koncentracije jona metala u rastvoru.

Uticaji promena koncentracije jona, mase sorbenta i njihovo međudejstvo pokazali su se statistički značajni i pri izučavanju sorpcije Co(II)-jona koštanim pepelom [6]. Pregled literature ukazuje na različitu osetljivost sorpcije Cu(II)-jona na promene procesnih parametara, u zavisnosti od njihovih selektovanih nivoa i prirode sorbenta. Pun faktorski dizajn primjenjen je i na izučavanje sorpcije Cu(II)-jona ilitom, u funkciji pH rastvora, vremena uravnotežavanja i mase sorbenta [16], gde je kao odgovor sistema posmatrana efikasnost sorpcije (%). Pokazano je da su statistički značajne varijabile pH vrednost rastvora, masa sorbenta i njihova interakcija. U ovom istraživanju pH vrednost je varirana u opsegu 2–7, pa je mehanizam precipitacije prouzrokovao veći uticaj pH. Dizajn sa četiri varijabile na dva nivoa je primjenjen pri ispitivanju sorpcije Cu(II)-jona funkcionalizovanim silikatom (SBA 15) [17]. Kako je uočeno da promena varijabila između nivoa uzrokuje nelinearni odgovor sistema, primjenjena je i metoda odzivne površine (eng. *response surface methodology*), što je omogućilo optimizaciju procesa. Uticaj temperature, početne pH vrednosti i koncentracije rastvora, kao i njihovih interakcija na sorpciju Cu(II)-jona morskim algama ispitana je

Box-Behnken dizajnom u sprezi sa metodom odzivne površine [18]. Pokazano je da je u ispitivanom opsegu parametara maksimalna sorpcija od 70 mg/g postignuta pri pH 5,0, početnoj koncentraciji rastvora od 150 mg Cu(II)/L i temperaturi od 40 °C. Frakcionisanim dizajnom je istražen efekat promene početne koncentracije jona u rastvoru (*A*), pH vrednosti (*B*), temperature (*C*), vremena kontakta (*E*), kao i tipa sorbenta (*D*), gde su korišćeni komercijalni aktivni ugalj i aktivni ugalj proizveden od kore kokosove palme [4]. Sorpcija Cu(II)-jona je u najvećoj meri zavisila od glavnih faktora *A*, *B* i *D*, dok su statistički značajne bile i interakcije *AB*, *AD*, *BD* i *CE*, a dat je i matematički model koji sa visokom tačnošću opisuje dobijene rezultate.

Statistička analiza

Ponašanje sistema se može opisati multilinearnim regresionim modelom:

$$Y = b_0 + \sum b_i x_i \quad (1)$$

gde je *Y* predskazana vrednost odgovora sistema, *b*₀ vrednost odgovora u centralnoj tački dizajna, *b*_{*i*} izračunati koeficijenti regresije, a *x*_{*i*} varijabile koje mogu biti glavni faktori (*x*_{*i*} = *A*, *B*, *C*,...) ili neka od njihovih interakcija (*x*_{*i*} = *A*·*B*, *A*·*B*·*C*,...). Model je linearan u smislu da se nepoznati regresioni koeficijenti pojavljuju u linearном obliku [19].

Uzimajući u obzir da interakcije između tri i četiri faktora nisu pokatale statistički značajne efekte (slika 1a) u proračun su uključeni samo glavni faktori i interakcije između dva faktora (Tabela 3).

Tabela 3. Izračunati efekti i koeficijenti za rezidualnu koncentraciju Cu(II)-jona, kao odgovor sistema (kodirane vrednosti)
Table 3. Estimated effects and coefficients for residual Cu(II) concentration (coded units)

Faktor	Član					
	Efekat	Koeficijent	SE koef	T		
Konstanta	–	155,3	2,236	69,44		
<i>A</i>	–7,19	–3,6	2,236	–1,61		
<i>B</i>	–36,52	–18,26	2,236	–8,17		
<i>C</i>	301,55	150,78	2,236	67,42		
<i>D</i>	11,99	5,99	2,236	2,68		
<i>AB</i>	–2,65	–1,32	2,236	–0,59		
<i>AC</i>	–7,09	–3,54	2,236	–1,58		
<i>AD</i>	7,53	3,77	2,236	1,68		
<i>BC</i>	–33,9	–16,95	2,236	–7,58		
<i>BD</i>	7,56	3,78	2,236	1,69		
<i>CD</i>	11,3	5,65	2,236	2,53		
Analiza varijanse						
Parametar	Br. stepeni slobode	Sekv. SS	Podešena SS	Podešena MS	F	P
Glavni efekti	4	369857	369857	92464,3	1000	0
Interakcije	6	5792	5792	965,4	12,06	0,008
Ostatak	5	400	400	80	–	–
Ukupno	15	15	–	–	–	–

Efekat svake varijabile je određen Yates-ovim algoritmom [20], kao razlika između srednjih vrednosti odgovora za eksperimente pri višem nivou (+1) i srednjih vrednosti za eksperimente pri nižem nivou (-1). Pozitivan znak ukazuje na povećanje odgovora sistema.

Regresiona analiza je korišćena za fitovanje eksperimentalnih podataka. Regresioni koeficijenti za svaki parametar su izračunati pomoću standardne greške koeficijenta (SE koeficijent), Studentovog T -testa i verovatnoće (p -vrednosti). Standardne greške omogućavaju jednostavno merenje nepouzdanosti izračunatih vrednosti. T -vrednost se dobija kada se koeficijent podeli njegovom standardnom greškom, te veće apsolutne T vrednosti označavaju manju mogućnost da je vrednost koeficijenta nula. p -vrednost je definisana kao najniži nivo pouzdanosti koji vodi do odbacivanja nulte hipoteze i koristi se za definisanje statistički značajnih varijabli. Generalno, što je viša T -vrednost i niža p -vrednost, član je statistički značajniji.

Vrednosti $p < 0,05$ potvrđuju da su statistički značajne samo promene početne koncentracije Cu(II)-jona i masa zeolita, kao i njihova interakcija (tabela 3).

Uzimajući u obzir samo statistički značajne parametre, dobija se sledeći matematički model:

$$Y = 155,3 - 18,26B + 150,78C - 16,95BC \quad (2)$$

Adekvatnost regresije je određena korišćenjem analize varianse ANOVA (tabela 3), čiji je osnovni princip razdvajanje vrednosti odgovora sistema na komponente koje su uzrokovane različitim nivoima faktora. U tabeli 3 su date funkcije greške, u cilju definisanja značaja članova, vrednosti parametara i matematičkog modela koji verodostojno opisuje eksperimentalne rezultate. Suma kvadrata (SS) za svaki faktor kvantificuje nje-

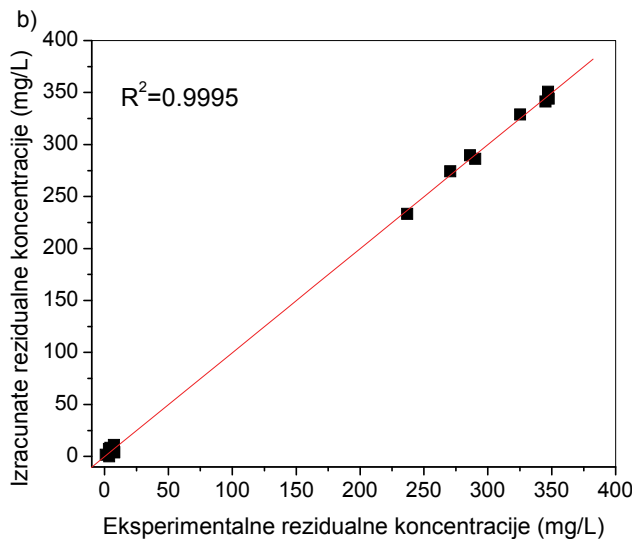
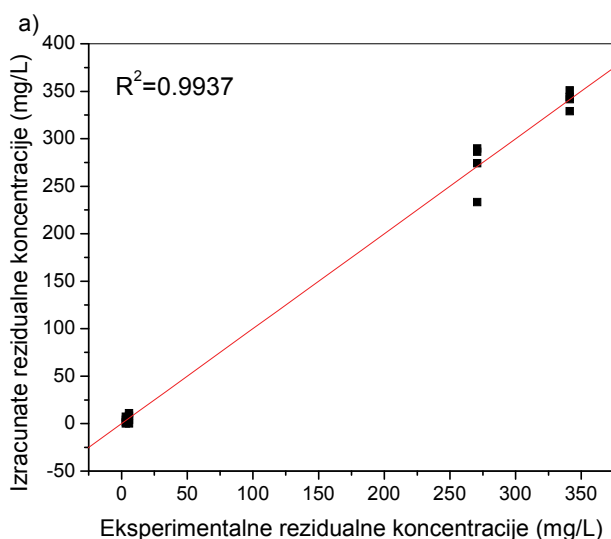
gov značaj i što je njegova vrednost veća veći je i značaj faktora, a dobija se kao suma kvadrata razlika između eksperimentalne i izračunate vrednosti. Takođe je definisana srednja kvadratna vrednost, kao količnik sume kvadrata i odgovarajućeg broja stepeni slobode. Fisherovim testom je izračunata F -vrednost, kao odnos srednje kvadratne greške usled regresije i srednje kvadratne greške usled reziduala. Veća F -vrednost ukazuje na veći značaj člana.

Korišćenjem jednačine (2) izračunate su rezidualne koncentracije, a grafik zavisnosti izračunatih i eksperimentalnih vrednosti dat je na slici 2a. Poređenja radi, ukoliko se uzme matematički model koji u obzir uzima sve interakcije drugog i trećeg reda, model predskazuje vrednosti date na slici 2b.

Dispasija tačaka oko prave nagiba 1 je veoma mala što ukazuje na dobro slaganje modela i eksperimenta. Visoka vrednost R^2 , kao i prob $<F$ manje od 0,001 ukazuju na veoma visok stepen korelacije između modela datog jednačinom 2 i eksperimentalnih vrednosti.

ZAKLJUČAK

Dizajniranje eksperimenata i statistička analiza primjeni su u analizi efekata parametara koji utiču na sorpciju Cu (II)-jona klinoptilolitom. Korišćenjem punog faktorijalnog dizajna ispitana je i upoređen uticaj promena procesnih varijabila (početna pH rastvora, početna koncentracija metala, masa i veličina čestica sorbenta). Statistički značajni efekti glavnih faktora su promena početne koncentracije jona metala i uticaj mase sorbenta. Značajnim se pokazao i efekat interakcije između ova dva faktora, pri čemu povećanje mase sorbenta značajnije utiče na efikasnost procesa pri višem nivou



Slika 2. Zavisnost između eksperimentalno dobijenih koncentracija Cu(II)-jona u rastvoru i vrednosti izračunatih primenom: a) jednačine (2) i b) modela koji u obzir uzima glavne efekte i interakcije dva i tri faktora.

Figure 2. Dependances between experimentally obtained Cu(II) residual concentrations and concentrations calculated using: a) Eq. (2) and b) model considering main effects, 2-way and 3-way interactions.

konzentracije Cu(II)-jona. Definisan je empirijski matematički model pogodan za opisivanje procesa, a na osnovu koga se može predvideti odgovor sistema unutar izabranih nivoa varijabila.

Zahvalnica

Ovaj rad je finansiralo Ministarstvo prosvete, nauke i tehnološkog razvoja Republike Srbije (Projekat broj 43009).

LITERATURA

- [1] Ž. Lazić, Design of experiments in chemical engineering, Wiley-VCH Verlag GmbH&Co. KGaA, Weinheim, Germany, 2004.
- [2] A.R. Cestari , E.F.S. Vieira, I.A. de Oliveira, R.E. Bruns, The removal of Cu(II) and Co(II) from aqueous solutions using cross-linked chitosan – Evaluation by the factorial design methodology, *J.Hazard. Mater.* **143** (2007) 8–16.
- [3] C.G. Passos, F.S. Ribaski, N.M. Simon, A. A. dos Santos Jr., J.C.P. Vaghetto, E.V. Benvenutti, É. Lima, Use of statistical design of experiments to evaluate the sorption capacity of 7-amino-4-azaheptyl silica and 10-amino-4-azadecyl silica for Cu(II), Pb(II), and Fe(III) adsorption, *J. Colloid Interface Sci.* **302** (2006) 396–407.
- [4] L.S. de Lima, M.D.M Araujo, S.P. Quináia, D.W. Migliorine, J.R. Garcia, Adsorption modeling of Cr, Cd and Cu on activated carbon of different origins by using fractional factorial design, *Chem. Eng. J.* **166** (2011) 881–889.
- [5] C. Kutahyal, B. Çetinkaya, M.B. Acar, N.O. Işık, I. Cireli, Investigation of strontium sorption onto Kula volcanics using central composite design, *J.Hazard.Mater.* **201–202** (2012) 115–124.
- [6] I. Smičiklas, M. Šljivić-Ivanović, Evaluation of factors influencing Co²⁺ removal by calcinated bone sorbent using experimental design methodology, *J. Environ. Sci. Health. A Tox. Hazard. Subst. Environ. Eng.* **47** (2012) 896–908.
- [7] C. Echeverria, M.T. Morera, C. Mazkarin, J.J. Garrido, Competitive sorption of heavy metal by soils. Isotherms and fractional factorial experiments, *Environ. Pollut.* **101** (1998) 275–284.
- [8] S. Al-Asheh, N. Abdel-Jabar, F. Banat, Packed-bed sorption of copper using spent animal bones: factorial expe-
- rimental design, desorption and column regeneration, *Adv. Environ.Res.* **6** (2002) 221–227.
- [9] S. Inan, Y. Altas, Preparation of zirconium–manganese oxide/polyacrylonitrile (Zr–Mn oxide/PAN) composite spheres and the investigation of Sr(II) sorption by experimental design, *Chem. Eng. J.* **168** (2011) 1263–1271.
- [10] S.H. Hasana, P. Srivastava, M. Talat, Biosorption of lead using immobilized *Aeromonas hydrophila* biomass in up flow column system: Factorial design for process optimization, *J. Hazard. Mater.* **177** (2010) 312–322.
- [11] M. Šljivić, I. Smičiklas, S. Pejanović, I. Plećaš, Comparative study of Cu²⁺ adsorption on a zeolite, a clay and a diatomite from Serbia, *Appl. Clay Sci.* **43** (2009) 33–40.
- [12] M. Šljivić, I. Smičiklas, I. Plećaš, S. Pejanović, The role of external and internal mass transfer in the process of Cu²⁺ removal by natural mineral sorbents, *Environ. Technol.* **32** (2011) 933–943.
- [13] G.P. Rao, C. Lu, F. Su, Sorption of divalent metal ions from aqueous solution by carbon nanotubes: A review, *Sep. Purif. Technol.* **58** (2007) 224–231.
- [14] S. Meski, S. Ziani, H. Khireddine, S. Boudboub, S. Zaidi, Factorial design analysis for sorption of zinc on hydroxyapatite, *J. Hazard.Mater.* **186** (2011) 1007–1017.
- [15] H.K. Beyer, in H. G. Karge, J. Weitkamp (Eds.), *Molecular Sieves*, Vol. 3, Springer-Verlag, Berlin, 2002, pp. 203–255.
- [16] N. G.Turan, S. Elevli, B. Mesci, Adsorption of copper and zinc ions on illite: Determination of the optimal conditions by the statistical design of experiments, *Appl. Clay Sci.* **52** (2011) 392–399.
- [17] E. Dana, A. Sayari, Optimization of copper removal efficiency by adsorption on amine-modified SBA-15: Experimental design methodology, *Chem. Eng. J.* **167** (2011) 91–98.
- [18] O. Freitas, C. Delerue-Matosb, R. Boaventura, Optimization of Cu(II) biosorption onto *Ascophyllum nodosum* by factorial design methodology, *J. Hazard. Mater.* **167** (2009) 449–454.
- [19] B. Wopenka, J.D. Pasteris, A mineralogical perspective on the apatite in bone, *Mater. Sci. Eng., C* **25** (2005) 131–143.
- [20] F. Yates, *The design and analysis of factorial experiments*, Imperial Bureau of Soil Science, Harpenden, 1937.

SUMMARY**ANALYSIS OF FACTORS INFLUENCING Cu(II) SORPTION BY CLINOPTIOLITE**

Marija Z. Šljivić-Ivanović, Ivana D. Smičiklas, Jelena P. Marković, Aleksandra S. Milenković

University of Belgrade, Vinča Institute of Nuclear Sciences, P.O. Box 522, Belgrade Serbia

(Scientific paper)

Experimental design methodology represents a powerful tool for the analysis and optimization of various processes. Immobilization of toxic substances by sorption onto low-cost materials has gained a lot of attention in the last decade. Fundamental knowledge about sorption processes and their practical use can be improved by experimental planning and statistical analysis. In this study, the effects of initial metal concentration and pH, as well as the sorbent mass and particle size, on Cu(II) sorption by natural clinoptilolite were evaluated and compared. Full factorial experimental design at two levels was applied. Statistically significant factors were determined considering residual Cu(II) concentrations as a system response. The Pareto graphs of standardized effects, Main effect plots and Interaction plots were created using statistical software. Initial sorbate concentration, sorbent mass and their interaction were recognized as statistically significant, at 95% confidence level. Main effect plot approved that sorbent mass increase and initial Cu(II) concentration decrease caused reduction of residual Cu(II) concentration in solution. On the other hand, the change of initial solution pH and sorbent particle size didn't provoke significant response changes. Bearing in mind that pH is a factor with high effect on heavy metal sorption, the insignificant influence of initial pH detected in this study can be explained by buffering properties of the applied clinoptilolite and relatively narrow pH range chosen in order to prevent sorbent dissolution on one side and sorbate precipitation on the other. By regression analysis, the mathematical model for process description was derived. The correlation between predicted and experimental values was high ($R^2 > 0.99$). In the investigated ranges of parameters, the obtained empirical equation can be applied for the prediction of system response.

Keywords: Clinoptilolite • Cu(II) • Sorption • Experimental design

The effect of processing parameters on energy consumption of ball mill refiner for chocolate

Aleksandar Z. Fišteš, Dušan Z. Rakić, Biljana S. Pajin, Ljubica P. Dokić, Ivana R. Nikolić

Department of Food Engineering, Faculty of Technology, University of Novi Sad, Serbia

Abstract

A laboratory ball mill consisting of a vertical cylinder, equipped with a rotating shaft with arms, and filled with steel balls as a grinding medium has been used in the experiments. The aim of the study was to examine the effect of agitator shaft speed and amount of grinding media (steel balls) on power requirements and energy consumption of a ball mill. With constant mass of the steel balls (20, 30 and 40 kg), the agitator shaft speed was increased from 10 to 100% of the maximum speed, which corresponds to a speed of 50 rpm. The power consumption (W) was recorded upon which milling energy consumption (J/kg) has been calculated. The results were statistically analyzed using ANOVA. The increase of the agitator shaft speed, in steps of 10% to the maximum speed of 50 rpm, led to a statistically significant increase in milling energy consumption. At low agitator shaft speed (10%), increase in the mass of the steel balls had no influence on the power requirements. Power requirements for the grinding runs using 30 and 40 kg are similar and higher compared to power requirement in trial with 20 kg, as agitator shaft speed increases from 20 to 70%. At high agitator shaft speeds ($\geq 80\%$), increase in steel balls mass led to a significant increase in power requirements of the ball mill.

Keywords: ball mill refiner, processing parameters, power requirements, energy consumption.

Available online at the Journal website: <http://www.ache.org.rs/HI/>

Size reduction of cocoa solids is an important unit operation in the production of chocolate. During this operation, called refining, cocoa solids and sugar crystals are reduced to a size that makes them small enough that they cannot be detected on the tongue [1]. It is followed by the phase of conching in which chocolate aroma is fully developed, and the newly created surface during the size reduction of cocoa solids is covered with fat, improving the flow properties [2]. During any comminution operation, both material properties and milling methods affect particle breakage [3]. The factors affecting particle size reduction can be classified into those arising from the physicochemical properties of the material and those related to the design and operation of the milling equipment [4]. Comminution equipment can be classified according to the process or the maximum size of product [5], while comminution as an industrial process is evaluated upon investment and energy costs and the characteristics that they provide to the product. In traditional chocolate production line, grinding is carried out using a five roll mill (four vertically aligned grinding rolls and the feed roll), with feed roll gap and roll speed as adjust-

able parameters [6]. However, the equipment used in traditional production lines is relatively expensive with regards to investment and energy consumption and the process is time consuming (up to 48 h) [3,7]. Over the years, possibilities and solutions have been sought out in order to find the alternative to traditional process and make it more efficient especially for the medium-small size companies. The most common ones are based on using a ball mill [2], in which both grinding (refining) and conching is carried out simultaneously. Surprisingly, over the years only a few papers have been published dealing with the issue of using the ball for these purposes [1,7–9,11].

Ball mills are vertical or horizontal cylinders (stationary tank), equipped with a rotating shaft with arms, filled to as much as 70% of the available volume with grinding media (usually steel balls) [8]. The mass and the balls are agitated by a shaft with arms, rotating at a variable speed [1]. Generally, size reduction in any practical machine is achieved by mechanical forces (compression, impact or shear) that cause rupture while one of the forces is usually predominant [10]. In the ball mill refiner the feed material is comminuted between the grinding media, the stirrer and the cylinder wall by compression and shear [7,8]. The factors affecting the grinding action of the ball mill are the mill speed and quantity, type and size of grinding media.

The aim of this study was to examine the effect of agitator shaft speed and amount of grinding media (steel balls) on energy consumption of a laboratory ball mill.

SCIENTIFIC PAPER

UDC 663.91.05:66.03

Hem. Ind. **67** (5) 747–751 (2013)

doi: 10.2298/HEMIND121025122F

Correspondence: I.R. Nikolić, Department of Food Engineering, Faculty of Technology, University of Novi Sad, Bulevar cara Lazara 1, 21000 Novi Sad, Serbia.

E-mail: ivananikolic@tf.uns.ac.rs

Paper received: 25 October, 2012

Paper accepted: 26 December, 2012

MATERIALS AND METHODS

Experiments were conducted using a laboratory ball mill constituted of a double-jacket cylinder, 0.25 m in diameter and 0.31 m in height (0.0152 m³ in volume), containing 9.1 mm diameter water resistant steel balls and a stirring group. The vertical shaft with horizontal arms, while rotating, puts the steel balls in movement. A little of vegetable fat was added to minimize undesirable friction between the steel balls. The ball mill is equipped with a temperature control system made up of a water jacket equipped with temperature sensor and thermo-regulators controlled by electric board. The experiments were carried out at 35 °C. The agitator shaft speed was increased from 10 to 100% (in steps of 10%) of the maximum speed, which corresponds to a speed of 50 rpm. The experiments were carried out without the material flow.

The milling energy consumption, E (J/kg), was calculated by Eq. (1):

$$E = \frac{Pt}{m} \quad (1)$$

Here, m is the mass of the steel balls (20, 30 and 40 kg) and t is the time of the grinding run (180 s) determined by the chronometer. The milling energy consumption during grinding runs was determined using a Network recorder MC750/UMC750 (Iskra MIS, Slovenia). Power readings, P (W), were recorded every 15 s, giving a total of 13 power readings during the 3 min interval of the grinding run. The results are expressed as mean ± standard deviation, as coefficient of variation, and as 95%

confidence interval for mean values given by Student's *t*-distribution. The mean values of corresponding data (P) are used to calculate the milling energy consumption according to Eq. (1). The significance of the differences between power readings obtained at different agitator shaft speeds and steel balls mass were statistically analyzed using ANOVA (analysis of variance). All statistical analyses were performed using Statistica 10 software.

RESULTS AND DISCUSSION

The mean value (MV), standard deviation (SD), coefficient of variation (CV) and 95% confidence interval for the power readings given by Student's *t*-distribution (CI), as well as energy consumption, E (J/kg), calculated according to Eq. (1), are given in Table 1.

Basic statistical parameters show that at same agitator shaft speed power readings are highly reproducible, with CV below 0.4% and CI less than ±1 W. Since the time of the grinding run ($t = 180$ s) was kept constant through the experiment, with constant mass of the steel balls, the power and energy consumption are directly correlated according to Eq. (1). Practically, the values of the basic statistic parameters determined for the power readings can be directly transferred to energy consumption. The correlation between the agitator shaft speed and power, as well as the correlation between agitator shaft speed and energy consumption, is very high ($r = 0.997$). They both exhibited similar relationship as the agitator shaft speed was altered, giving an almost linear response, as can be seen from Figures 1 and 2.

Table 1. Power readings, energy consumption and basic statistical parameters

Steel balls mass, kg	Power reading [W]	Agitator shaft speed (% of the maximum speed of 50 rpm)									
		10	20	30	40	50	60	70	80	90	100
20	Mean value	165.65	178.55	213.18	248.10	282.46	316.65	353.02	376.11	417.88	464.22
	±SD	±0.45	±0.32	±0.33	±0.37	±0.50	±1.06	±1.26	±1.15	±1.49	±1.18
	CV / %	0.273	0.181	0.153	0.149	0.177	0.334	0.356	0.305	0.357	0.254
	±CI	±0.27	±0.20	±0.20	±0.22	±0.30	±0.64	±0.76	±0.69	±0.90	±0.71
	Energy consumption E / J kg ⁻¹	1490.9	1607.0	1918.7	2232.9	2542.2	2849.9	3177.2	3385.0	3760.9	4177.9
30	Mean value	167.81	186.71	221.34	262.05	298.27	336.61	366.01	406.84	457.41	510.39
	±SD	±0.43	±0.54	±0.41	±0.45	±0.68	±0.82	±0.82	±0.97	±1.03	±1.13
	CV / %	0.254	0.288	0.185	0.172	0.229	0.245	0.223	0.239	0.225	0.221
	±CI	±0.25	±0.33	±0.25	±0.27	±0.41	±0.50	±0.49	±0.59	±0.62	±0.68
	Energy consumption E / J kg ⁻¹	1006.8	1120.2	1328.0	1572.3	1789.6	2019.7	2196.1	2441.0	2744.4	3062.3
40	Mean value	168.95	189.46	226.89	263.19	300.28	338.96	371.91	426.09	492.13	554.57
	±SD	±0.35	±0.69	±0.84	±0.55	±1.05	±1.20	±0.86	±0.91	±1.34	±2.36
	CV / %	0.207	0.366	0.370	0.207	0.350	0.354	0.231	0.215	0.272	0.426
	±CI	±0.21	±0.42	±0.51	±0.33	±0.64	±0.72	±0.52	±0.55	±0.81	±1.43
	Energy consumption E / J kg ⁻¹	760.3	852.6	1021.0	1184.4	1351.2	1525.3	1673.6	1917.4	2214.6	2495.6

Analysis of variance provides a statistical test of whether or not the means of several groups are all equal. The basic hypothesis that had been set was that there was no statistically significant difference between the power requirements at different agitator shaft speed. The hypothesis has been rejected and results showed that, with constant mass of the steel balls, every increase of 10% of the agitator shaft speed led to a statistically significant ($p < 0.05$) increase in power requirements and milling energy consumption. The dynamic of the increase in grinding runs with different mass of the steel balls had a similar trend (Figures 1 and 2). Beside energy consumption, the agitator speed

also influences the magnitude of the stress and the relative contributions of compressive and shearing forces. The magnitude and the nature of the forces acting on particles will determine the degree of particle size reduction and energy required for grinding. In practice, the agitator should be run at the lowest possible speed to meet the requirements of the process. However, in some cases, with slow agitator the particle size of the product and demands for increased capacity could not be met.

Comparing the power requirements, recorded at the same agitator speed but with different steel ball mass, a certain pattern can be noticed (Figure 1). At

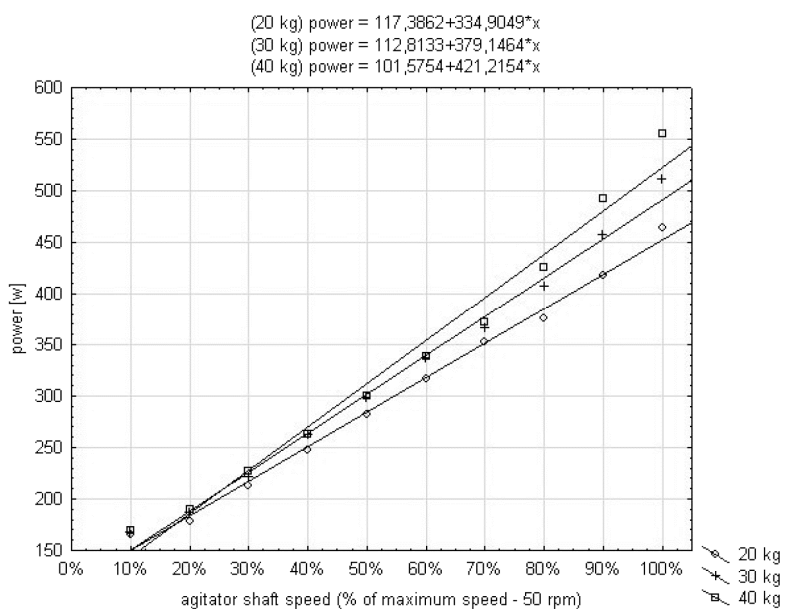


Figure 1. Effect of agitator shaft speed and steel balls mass on power requirements.

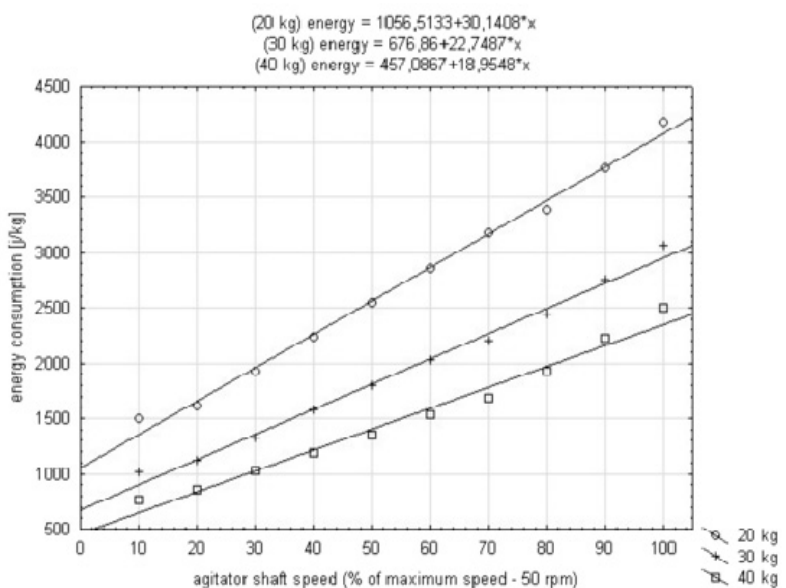


Figure 2. Effect of agitator shaft speed and steel balls mass on milling energy consumption.

low agitator shaft speed (10%), there was practically no difference in power readings between the grinding runs with different amount of grinding media. At agitator speed in the range of 20–70%, the power readings recorded with $m = 30$ kg and $m = 40$ kg were similar and relatively higher compared to the grinding run with $m = 20$ kg. At high agitator shaft speeds ($\geq 80\%$), the difference in power requirements became noticeable between the grindings run with 30 and 40 kg as well. However, it is interesting to point out the hypothesis that there is no statistically significant difference between the power requirements in the grindings runs with different steel balls mass has been rejected even at 10% agitator speed, there the difference between the grinding runs is only 1–2 W. The fact that the power readings within the individual grinding runs were highly reproducible (extremely small SD, CV and CI) causes statistically significant difference even in the cases of small difference between power readings of individual grinding runs, such as 1–2 W, which from the practical side of view can be considered negligible.

Increasing the mass of the steel balls at same agitator speed led to a significant decrease in energy consumption (Figure 2). It needs to be pointed out that the power readings were recorded without material flow and the energy consumption calculated using Eq. (1) is relative to the mass of steel balls. Usually, the energy required for grinding is given as energy consumption per unit mass of grounded material. Therefore, a more realistic view on influence of the mass of the balls on energy consumption can be obtained only with the grinding runs with material flow, because this processing parameter also influences the magnitude of the forces acting on particles and the degree of particle size reduction.

CONCLUSION

The consumption of energy in the process, especially in the process where the large part of it is energy required for grinding, should be kept at the lowest possible level. The agitator shaft speed significantly influences the energy consumption of the ball mill. Therefore, the agitator should be run at lowest possible speed to meet the degree of particle size reduction

that is needed (or any other product quality parameter), and handle the capacity of the process.

Acknowledgments

The authors highly appreciate financial support of the Provincial Secretariat for Science and Technological Development of the Government of Autonomous Province of Vojvodina, Republic of Serbia, project: Cookies and crackers with functional characteristics aimed for consumers with special dietary needs.

REFERENCES

- [1] M. Lucisano, E. Casiraghi, M. Mariotti, Influence of formulation and processing variables on ball mill refining of milk chocolate, *Eur. Food Res. Technol.* **223** (2006) 797–802.
- [2] S.T. Becket, in: S.T. Becket (Eds.), *Conching: Industrial chocolate manufacture and use*, 3rd ed., Blackwell Science, Oxford, 1999, pp. 153–181.
- [3] M.G. Scanlon, J. Lamb, Fracture mechanism and particle shape formation during size reduction of a model food material, *J Mater Sci.* **30** (1995) 2577–2583.
- [4] G.M. Campbell, P.J. Bunn, C. C. Webb, S.C.W. Hook, On predicting roller milling performance Part II: The breakage function, *Powder Technol.* **115** (2001) 243–255.
- [5] E. Haque, Application of Size Reduction Theory to Roller Mill Design and Operation, *Cereal Foods World* **36** (1991) 368–374.
- [6] G.R. Ziegler, R. Hogg, in S.T. Becket (Eds.), *Particle size reduction: Industrial chocolate manufacture and use*, 3rd ed., Blackwell Science, Oxford, 1999, pp. 115–136.
- [7] D. Zarić, B. Pajin, M. Rakin, Z. Šereš, Lj. Dokić, J. Tomić, Effect of soya milk on nutritive, antioxidative, rheological and textural properties of chocolate in a ball mill, *Hem. Ind.* **65** (2011) 563–573.
- [8] C. Alamprese, L. Datei, Q. Semeraro, Optimization of processing parameters of a ball mill refiner for chocolate, *J. Food Eng.* **83** (2007) 629–636.
- [9] K. Franke, E. Scheruhn, H.D. Tscheuschner, Influence of milk powder properties on flow behaviour of milk chocolate, *Milchwissenschaft* **57** (2002) 535–539.
- [10] P. Fellows, *Food Processing Technology: Principles and Practice*, Ellis Horwood Ltd., Chichester, 1988.
- [11] B. Pajin, Lj. Dokić, D. Zarić, D. Šoronta-Simović, I. Lončarević, I. Nikolić, Crystallization and rheological properties of soya milk chocolate produced in a ball mill, *J. Food Eng.* **114** (2013) 70–74.

IZVOD

UTICAJ PROCESNIH PARAMETARA NA POTROŠNJU ENERGIJE U KUGLIČNOM MLINU ZA PROIZVODNJU ČOKOLADE

Aleksandar Z. Fišteš, Dušan Z. Rakić, Biljana S. Pajin, Ljubica P. Dokić, Ivana R. Nikolić

Tehnološki fakultet, Univerzitet u Novom Sadu, Srbija

(Naučni rad)

U ovom radu primenjen je i ispitani laboratorijski kuglični mlin koji se sastoji od vertikalnog cilindra, opremljenog rotirajućim vratilom sa mešaćima i napunjenoj čeličnim kuglicama kao medijumom za mlevenje. U kugličnom mlinu proces mlevenja se ostvaruje usitnjavanjem materijala između čeličnih kuglica, mešača i zida cilindra silama kompresije i smicanja. Faktori koji utiču na proces mlevenja su brzina mešanja, kao i količina, vrsta i veličina medijuma za usitnjavanje. Primenom kugličnog mlina u proizvodnji čokolade objedinjuju se dve procesne faze istovremeno, faza mlevenja i faza končiranja. Cilj istraživanja je bio da se ispita uticaj brzine mešača i udela medijuma za usitnjavanje (čeličnih kuglica) na iznos potrebne snage i potrošnju energije u kugličnom mlinu. Pri konstantnoj masi čeličnih kuglica (20, 30 i 40 kg), brzina obrtanja vratila sa mešaćima je povećavana od 10 do 100% od maksimalne brzine (koja odgovara brzini od 50 o/min). Potrebna snaga (W) je registrovana, a energetska potrošnja (J/kg) je izračunata. Dobijeni rezultati su statistički obrađeni pomoću statističke metode analize varijanse (ANOVA). Povećanje brzine vratila sa mešaćima, u iznosima od po 10% do maksimalne brzine obrtanja od 50 o/min, dovelo je do statistički značajnog povećanja potrošnje energije za mlevenje. Pri malim brzinama vratila (10%), povećanje mase čeličnih kuglica nije imalo nikakav uticaj na potrebnu snagu, odnosno potrošnju energije. Prilikom porasta brzine obrtanja vratila od 20 do 70%, energetski zahtevi pri količini medijuma za usitnjavanje, čeličnih kuglica od 30 i 40 kg, su slični i veći u odnosu na energetske zahteve pri primeni 20 kg čeličnih kuglica. Pri velikim brzinama obrtanja vratila sa mešaćima ($\geq 80\%$), povećanje mase čeličnih kuglica doveđe do značajnog povećanja potrošnje energije u kugličnom mlinu.

Ključne reči: Kuglični mlin • Procesni parametri • Potrebna snaga • Potrošnja energije

Mogućnosti primene atmosferskog plazma-sprej postupka za dobijanje prevlaka hidroksiapatita na uzorcima od nerđajućeg čelika

Marija D. Mihailović, Aleksandra S. Patarić, Zvonko P. Gulišija, Zoran V. Janjušević, Miroslav D. Sokić

Institut za tehnologiju nuklearnih i drugih mineralnih sirovina, Beograd, Srbija

Izvod

Hidroksiapatitna (HAp) prevlaka je atmosferskim (APS) plazma-sprej postupkom naneta na metalne uzorke napravljene od 316LVM čelika, namenjenog za izradu implantata u ortopedskoj hirurgiji. Razvoj savremenih ortopedskih implantata podrazumeva da se na podlogu od bioinertnih legura nanosi bioaktivna HApl prevlaka. Sintetički HApl je hemijski sličan onom koji čini mineralnu građu kostiju i zuba. Zahvaljujući dobrim bioaktivnim svojstvima hidroksiapatitnih prevlaka moguće je obrazovanje stabilne veze između koštanog tkiva i implantata. U radu je prikazana mogućnost primene APS postupka za dobijanje stabilnih HApl prevlaka na uzorcima od nerđajućeg čelika 316LVM. Praćena je mikrostruktura i poroznost prevlake metodom optičke mikroskopije i skenirajuće elektronske mikroskopije. Ca/P odnos je određen EDS analizom.

Ključne reči: atmosferski plazma-sprej postupak, hidroksiapatit, nerđajući čelik 316LVM.

Dostupno na Internetu sa adresu časopisa: <http://www.ache.org.rs/HI/>

Bescementni implantati pripadaju novoj generaciji ortopedskih proteza kuka kod kojih se veza sa kosti ne ostvaruje preko polimernog koštanog cementa, već preko tankog, stabilnog bioaktivnog hidroksiapatitnog (HApl) sloja koji je deo samog implantata. Ugradnja implantata uz korišćenje biokompatibilnog polimernog koštanog cementa garantuje trenutno vezivanje i rano postizanje potpune nosivosti. Osnovni nedostatak ovakvog načina fiksiranja implantata predstavlja topota koja se oslobađa tokom polimerizacije cementa, što može dovesti do uništenja vitalnih ćelija kostiju. Osim toga, metakrilatni monomer deluje citotoksično na okolno tkivo [1]. Kod bescementnih proteza se, međutim, srastanje ostvaruje preko HApl sloja debeline do nekoliko stotina mikrona, koji svojim sastavom i strukturom omogućava specifičan biološki odgovor organizma na međupovršini materijala implantata i same kosti.

Sam hidroksiapatitni sloj nastaje prevlačenjem metalnog stema proteze hidroksiapatitom, primenom nekog od sledećih postupaka: atmosferski plazma-sprej postupak, plazma-sprej postupak u vakuumu, termalni-sprej postupak, nanošenje elektronskim ili jonskim snopom, nanošenje laserskim impulsima, elektroforetsko taloženje, ili primenom kombinovanih tehnika [2–13].

Veoma bitna osobina HApl prevlake je čvrstoća veze prevlake sa metalnim supstratom jer otkinute čestice takođe mogu imati veoma štetne efekte na okolna tkiva u organizmu. Osim toga, prevlaka treba da je slabo rasztorna u telesnoj tečnosti. Bioaktivnost prevlake obez-

NAUČNI RAD

UDK 615.477::617.3–089:66

Hem. Ind. 67 (5) 753–757 (2013)

doi: 10.2298/HEMIND120910001M

beđuje osteointegraciju, odnosno srastanje kosti sa optimalno poroznom prevlakom. Brzina rastvaranja ne sme da bude veća od brzine srastanja, a stabilnost HApl prevlake obezbeđuje se povoljnim odnosom kristalne i amorfne faze u strukturi nanete prevlake. Na ove osobine utiče se izborom tehnike nanošenja prevlake, a suštinski kontrolom parametara samog postupka nanošenja. Atmosferski plazma-sprej postupak (APS) se najčešće primenjuje zbog svoje relativne jednostavnosti, dostupnosti, kao i zbog mogućnosti promene parametara u širokim granicama.

U toku ovih eksperimenata na uzorke od nerđajućeg čelika 316LVM nanete su stabilne hidroksiapatitne prevlake atmosferskim plazma-sprej postupkom. Na osnovu mikrostrukture prevlake praćene optičkom mikroskopijom određena je poroznost prevlake kao bitan parametar za srastanje sa kostima. Snimanjem na skenirajućem elektronском mikroskopu utvrđena je morfologija prevlake. Praćena je brzina rastvaranja prevlake u vodenim rastvorima i na osnovu nje je utvrđeno da je postignuta zavodoljavajuća stabilnost prevlake.

EKSPERIMENTALNI DEO

APS je u osnovi postupak nanošenja sprejem istoplijenih ili toplotom omešalih čestica materijala na površinu supstrata. Čestice HApl praha dimenzija 50–100 µm ubrizgavaju se u visokotemperaturni plamen plazme, gde se brzo zagrevaju i ubrzavaju. Zagrejane čestice velikom brzinom udaraju o hladnu podlogu supstrata i hlađe se formirajući prevlaku. Povoljno je što se tokom ovog postupka metalni materijal supstrata ne zagreva, čime se izbegavaju bilo kakve strukturne promene u njemu, koje bi uticale na promenu mehaničkih osobina.

Prepiska: M.D. Mihailović, Institut za tehnologiju nuklearnih i drugih mineralnih sirovina, Franše d'Eperea 86, 11 000 Beograd, Srbija.

E-pošta: m.mihailovic@itnms.ac.rs

Rad primljen: 10. septembar, 2012

Rad prihvaćen: 24. oktobar, 2012

Brizgaljka za APS se sastoji od vodom hlađenih anode i katode, a noseći gas (argon, azot, vodonik i helijum) teče oko katode i kroz anodu koja se sužava u mlaznicu (slika 1). Plazmu stvara visokonaponsko pražnjenje koje dovodi do lokalne ionizacije i stvaranja provodnog luka između anode i katode. Elektrootporno zagrevanje usled luka izaziva zagrevanje gasa do veoma visokih temperatura, njegovu disocijaciju i ionizaciju i stvaranje plazme. Plazma koja izlazi iz anodne malznicice je slobodna, odnosno neutralna (ne prenosi električnu struju). Prah se dovodi spolja u plamen plazme, gde se zagreva i ubrzava do te mere da se može brizgati sa udaljenosti od 25 do 200 mm. Korišćen je komercijalno dostupan HAp prah Amdry 60, kompanije Metco, USA, namenjen za medicinsku upotrebu. Plazma-sprej postupak je izведен pod atmosferskim uslovima (APS), mada se može izvoditi i u vakuum komorama koje su prethodno bile napunjene zaštitnim gasom pod niskim pritiskom.

Plazma-sprej postupak ima tu prednost što se pomoću njega mogu nanositi prevlake od materijala sa visokom tačkom topljenja, kao što su vatrostalni materijali i keramika. Prevlake nanete ovim postupkom su generalno kompaktnije, čvršće i čistije u odnosu na prevlake dobijene korišćenjem postupaka termalnog nanošenja. Mogućnost variranja parametara, kojima se utiče na strukturu, bioaktivne i mehaničke osobine veoma je raznovrsna.

Izrađeni su uzorci (metalni supstrati od legure AISI316 LVM) za nanošenje plazma-sprej prevlake i to pločice (50 mm×25 mm×2mm) i epruvete ($2r = 25,4$ mm).

Eksperimenti nanošenja hidroksiapatitnih prevlaka APS postupkom rađeni su sa ciljem da se odredе parametri deponovanja HAp praha radi dobijanja prevlake na metalnom materijalu koja ima prihvatljive mikrostrukturne karakteristike i fazni sastav. Prevlake su nanete variranjem sledećih parametara: sastav plazmene gasne smeše, snage plazme, rastojanja mlaznice i metalnog supstrata, kao i masenog unosa praha.

U toku ovih istraživanja praćena je mikrostruktura prevlake optičkom mikroskopijom, kao i snimanjem na skenirajućem elektronskom mikroskopu (SEM) – koje je iskorišćeno i za određivanje odnosa Ca/P pomoću EDX sonde. Ovaj odnos je bitan za praćenje kinetike rastvaranja u vodenim rastvorima (i rastvorima simuliране telesne tečnosti). Kinetika desorpcije/adsorpcije određivana je praćenjem rastvorljivosti Ca i P na telesnoj temperaturi i na povišenim temperaturama.

Poroznost prevlake određena je na mikrofotografijama pomoću softverske aplikacije Quick Photo Industrial 2.2. Rezultati poroznosti treba da budu optimalni kako bi prevlaka zadržala svoju konzistenciju i omogućila srastanje okolnog tkiva sa prevlakom.

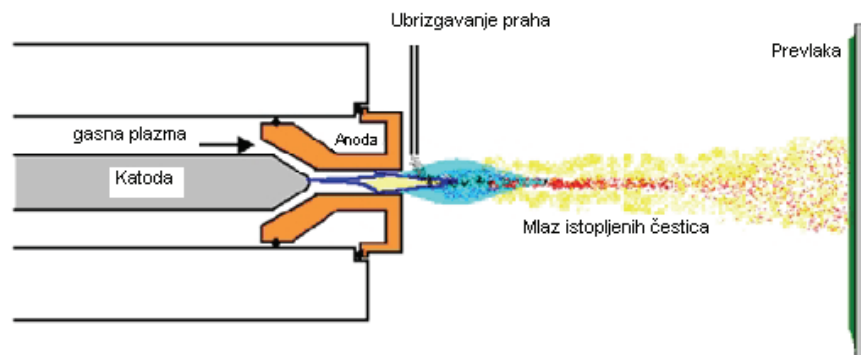
HAp prah je nanošen uz korišćenje dve različite plazmene gasne smeše Ar/H₂ i N₂/H₂, sa promenljivim udelenjem vodonika. Varirani su parametri deponovanja: snaga plazme (25–75 kW), ideo sekundarnog gasea, koncentracija vodonika, distanca nanošenja (100–250 mm) i maseni unos praha (1.5–5 g/s).

Athezija je određivana na epruvetama po standardu ASTM C633, tako što je na čeone delove kružnog poprečnog preseka epuveta nanet HAp prah, a oni su potom spojeni autopolimerizujućim akrilatom SIMGAL nakon čega je određivan Jangov modul elastičnosti.

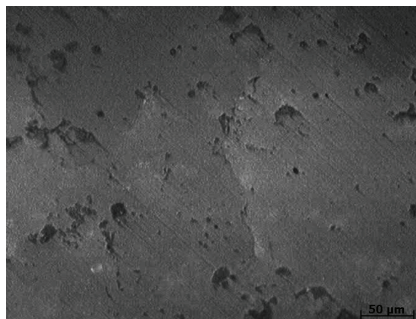
REZULTATI I DISKUSIJA

Karakteristični izgledi mikrostrukture prevlaka dobijenih plazma-sprej postupkom snimljeni optičkim mikroskopom Carl Zeiss Axovert CA 25 pri uvećanju od 200× i 500× prikazani su na slikama 2 i 3.

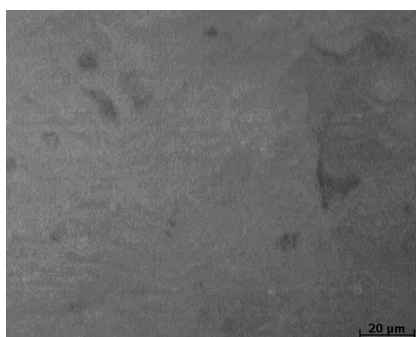
Osim zapreminske udeline pora, određen je i zapreminski ideo nestopljenih čestica, koje su ovde označene kao uključci u strukturi prevlake. U tabeli 1 dati su rezultati dobijeni poluautomatskom analizom slike. Rezultati ispitivanja poroznosti zadovoljavaju optimalan kvalitet koji prevlaka treba da ima kako bi sa jedne strane bilo obezbeđeno srastanje sa kostima, a sa druge strane dugotrajna stabilnost.



Slika 1. Shematski prikaz atmosferskog plazma-sprej postupka.
Figure 1. Schematic overview of the atmospheric plasma-spraying.



Slika 2. Izgled hidroksiapatitne plazma prevlake (uključci).
Figure 2. The appearance of the HAp coating (inclusions).



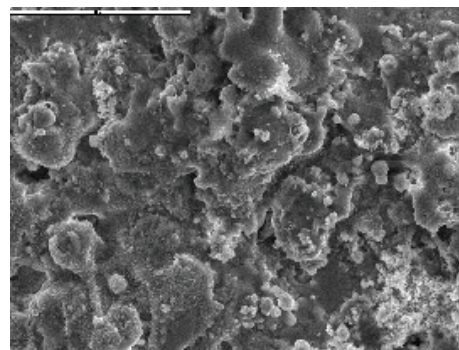
Slika 3. Izgled hidroksiapatitne plazma prevlake (pore).
Figure 3. The appearance of the HAp coating (pores).

Mikrostruktura, ali i odnos Ca/P praćeni su na skeirajućem elektronskom mikroskopu JEOL JSM 5800 opremljenim EDX uređajem. Na slici 4 prikazana je mikrostruktura HAp prevlake. Prevlaka je kompaktna sa morfologijom tipičnom za navedene uslove nanošenja praha.

Dobijene prevlake su kompaktne, sa morfologijom tipičnom za HAp prevlaku tražene kristaličnosti i odnosa Ca/P od približno 2. Izmerene vrednostni odnosa Ca/P predstavljaju srednju vrednost merenja na više različitim mesta i u su skladu sa literaturnim navodima [6,9]. Athezija je određivana na epruvetama po standardu ASTM C633, a vrednosti Jangovog modula elastičnosti kreću se od 23 do 42 GPa. Dobijeni rezultati poroznosti su na donjoj granici saopštenih vrednosti [7–9], ali je ostvarena zadovoljavajuća athezija [13].

Kristaličnost se određuje po posebnom obrascu kao odnos udela kristalne i amorfne faze u uzorku [4,11].

Analiza je pokazala da je na kontaktu samog metala i nanete prevlake veće prisustvo amorfne faze, koja ima veću rastvorljivost u telesnoj tečnosti od kristalnog oblika. Pojava amorfne faze na granici metal/hidroksiapatit je uobičajena zbog velike razlike u temperaturi metalnog supstrata i same plazme [2,10], ali je kontrolom parametara APS postupka moguće održati debjinu ovog sloja takvom da se u kontaktu sa telesnim tečnostima nalazi samo stabilniji, kristalni oblik.



Slika 4. Morfologija HAp prevlake; razmernik: 50 μm.
Figure 4 Morphology of the HAp coating; bar size: 50 μm.

Rastvorljivost prevlake određivana je u destilovanoj vodi na temperaturi bliskoj telesnoj temperaturi, na 37 °C, kao i na 100 °C, kako bi se proverila stabilnost nanete HAp prevlake, slike 5 i 6. Ova istpitivanja treba ponoviti u simuliranoj telesnoj tečnosti (SBF) kako bi bila potpuno uporediva sa literaturnim navodima. Pojavu amorfne faze treba izbeći na površini, a ispitivanjima je pokazano da je u toj oblasti preovlađujući sadržaj kristalne faze koja prevlaci daje zahtevanu stabilnost.

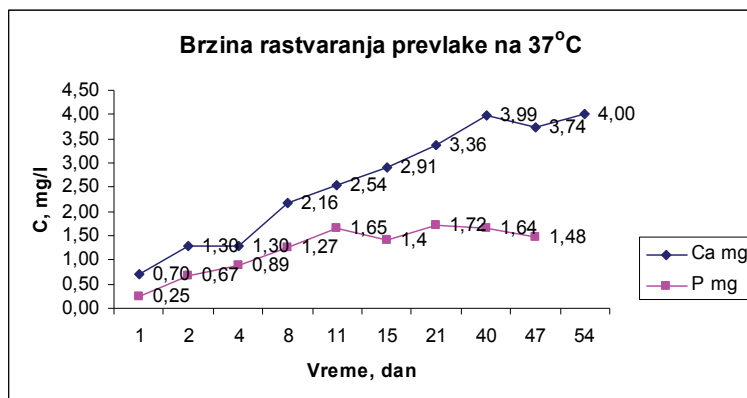
Plazma-sprej postupak nanošenja hidroksiapatitnih prevlaka na metalnu osnovu otropedskog implantata pokazao se kao povoljan zbog velike primenljivosti i mogućnosti variranja samog praha koji se nanosi, ali još više zbog mogućnosti variranja velikog broja parametara kojima se utiče na buduću strukturu prevlake, a time i na njene mehaničke osobine i bioaktivnost.

Nanošenjem prevlake sprečava se direktni kontakt metalnog dela implantata sa okolnim tkivom, a hidroksiapatit zbog svoje biokompatibilnosti sa ljudskim organizmom, bioaktivnosti koja omogućava brže sras-

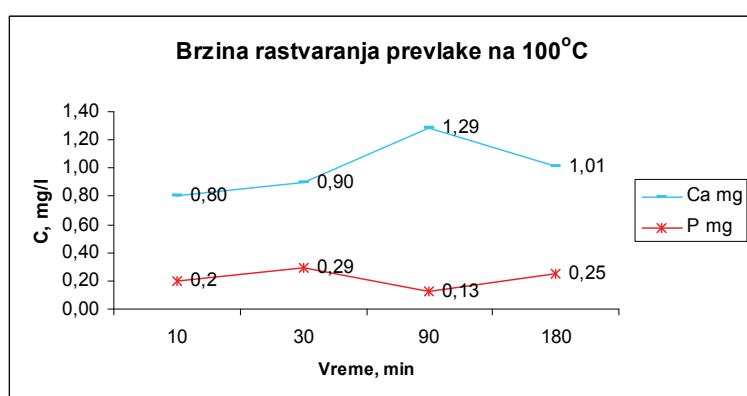
Tabela 1. Rezultati analize poroznosti prevlake sa fotografija mikrostrukture

Table 1 The results of the coating porosity analysis obtained from the microstructure photographs

Oznaka uzorka	Sadržaj uključaka u prevlaci, %	Oznaka uzorka	Sadržaj pora u prevlaci, %
U 1	9,62	E 1	3,00
U 2	11,93	E 2	1,20
U 3	7,03	E 3	1,10
U 4	4,51	E 4	1,30
U 5	6,36	E 5	0,85
Srednja vrednost	7,89		1,49



Slika 5. Brzina rastvaranja prevlake na 37 °C.
Figure 5. Coating dissolution rate at 37 °C.



Slika 5. Brzina rastvaranja prevlake na 100 °C.
Figure 5. Coating dissolution rate at 100 °C.

tanje i bolju mehaničku fiksaciju omogućava manje hranjenje i veću trajnost implantata.

Fazne i mikrostruktturne karakteristike veoma zavise od uslova nanošenja prevlaka na suprstrat, a osobine se mogu poboljšati dodavanjem vezivnog međusloja koji će uticati na strukturu i smanjiti količinu amorfne faze na međufaznoj granici metal-hidroksiapatit.

ZAKLJUČCI

Plazma-sprej postupak ima tu prednost što se pomoću njega mogu nanositi prevlake od materijala sa visokom tačkom topanja, kao što su vlastostalni materijali i keramika. Prevlake nanete ovim postupkom su generalno kompaktnej, čvršće i čistije u odnosu na prevlake nanete drugim postupcima termalnog nanošenja. Mogućnost variranja parametara, a time uticaj na strukturu, bioaktivne i mehaničke osobine veoma je raznovrsna.

Dobijene prevlake su kompaktne, sa morfolojijom tipičnom za HAp prevlaku tražene kristaličnosti i odnosa Ca/P od približno 2. Dobijeni rezultati poroznosti su u intervalu saopštenih literaturnih vrednosti, a ostvarena je zadovoljavajuća athezija.

Zahvalnost

Ovaj rad je rezultat rada na projektu TR 34002 koji finansira Ministarstvo prosvete, nauke i tehnološkog razvoja Republike Srbije.

LITERATURA

- [1] T. Atsumi, S. Fujisawa, K. Tonosaki, (Meth)acrylate monomer-induced cytotoxicity and intracellular Ca^{2+} mobilization in human salivary gland carcinoma cells and human gingival fibroblast cells related to monomer hydrophobicity, *Biomater.* **27** (2006) 5794–5800.
- [2] R.B. Heimann, H. Kurzweg, D.G. Ivey, M.L. Wayman, Microstructural and *in vitro* chemical investigations into plasma-sprayed bioceramic coatings, Inc. J. Biomed. Mater. Res. (Appl. Biomater.) **43** (1998) 441–450.
- [3] J.M. Choi, H.E. Kim, I.S. Lee, Ion-beam-assisted deposition (IBAD) of hydroxyapatite coating layer on Ti-based metal substrate, *Biomater.* **21** (2000) 469–473.
- [4] M. Mihailović, A. Patarić, Z. Gulišija, Dj. Veljović, Dj. Janačković, Electrophoretically deposited nanosized hydroxyapatite coatings on 316Lvm stainless steel for orthopaedic implants, *Chem. Ind. Chem. Eng. Q.* **17** 1 (2011) 45–52.

- [5] M. Mihailović, A. Patarić, Z. Gulišija, Z. Janjušević, M. Sokić, Č. Lačnjevac, The possibility of bioactive coatings obtaining by electrophoretic deposition of HAp on the steel implants, *Zaštita materijala* **53** (2012) 62–67.
- [6] N. Eliaz, T.M. Sridhar, U.K. Kamachi Mudali, B. Raj, Electrochemical and electrophoretic deposition of hydroxyapatite for orthopaedic applications, *Surf. Eng.* **21** (2005) 1–5.
- [7] L. Sun, C.C. Berndt, C.P. Grey, Phase, structural and microstructural investigations of plasma sprayed hydroxyapatite coatings, *Mater. Sci. Eng., A* **360** (2003) 70–84.
- [8] P. Sakar, P.S. Nicholson, Electrophoretic deposition (EPD): mechanisms, kinetics, and application to ceramics, *J. Am. Ceram. Soc.* **79** (1996), 1987–2002.
- [9] L. Sun, C. Brendt, K.A. Gross, A. Kuchuk, Material fundamental and clinical performance of plasma-sprayed Hap coatings: A Review, *J. Biomed. Mater. Res.* **58** (2001) 570–572.
- [10] L. Chou, B. Marek, W.R. Wagner, Effects of hydroxyapatite coating crystallinity on biosolubility, cell attachment efficiency and proliferation *in vitro*, *Biomater.* **20** (1999) 977–985.
- [11] E. Landi, A. Tampieri, G. Celotti, S. Sprio, Densification behaviour and mechanisms of synthetic hydroxyapatites, *J. Eur. Ceram. Soc.* **20** (2000), 2377–2387.
- [12] Z. Gulišija, A. Patarić, M. Mihailović, M. Sokić, Zaštite prevlake na bazi hidroksiapatita na implantatima za ortopedsku hirurgiju, Monografija: Korozija i zaštita materijala, Z. Gulišija, Č. Lačnjevac (Eds.), ITNMS I IDK, Beograd, 2012, str. 715–739.
- [13] M.R. Mucalo, D.L. Foster, B. Wielage, S. Steinhaeuser, H. Mucha, D. Knighton, J. Kirby, The novel use of waste animal bone from New Zealand agricultural sources as a feedstock for forming plasma sprayed hydroxyapatite coatings on biomedical implant materials, *J. Appl. Biomater. Biomech.* **2** (2004) 96–104.

SUMMARY

THE POSSIBILITIES OF ATMOSPHERIC PLASMA-SPRAYING APPLICATION TO OBTAIN HYDROXYAPATITE COATINGS ON THE STAINLESS STEEL SAMPLES

Marija D. Mihailović, Aleksandra S. Patarić, Zvonko P. Gulišija, Zoran V. Janjušević, Miroslav D. Sokić

Institute for Technology of Nuclear and other Mineral Raw Materials, Franchet d'Esperey St 86, 11 000 Belgrade, Serbia

(Scientific paper)

For decades, the standard metallic materials for hip implants, besides the 316LVM stainless steel, were titanium- and cobalt/chromium-based alloys. Although bioinert, due to their corrosion resistance, they are not biocompatible. Contemporary surgical implants are no longer made solely from bioinert metals anymore, but with deposited bioactive hydroxyapatite (HAp) coatings. Hydroxyapatite is chemically identical with the mineral constituent of bones and teeth, which, besides its biocompatibility, provides bioactivity as well. The HAp limitations are, however, weak tensile strength and low fatigue resistance for long term loadings, if used alone. This is the reason for HAp to be deposited onto the surgical implant, and to enable its bioactivity, which means intergrowth with bones, and therefore the long-lasting and mechanical stable non-cemented prosthesis. This is important predominantly because of the need for such prostheses for younger population and a better life quality. There are several contemporary techniques that have been used for deposition of these coatings onto the metal implant. The possibilities of atmospheric plasma-spraying for obtaining stable HAp coatings on 316LVM stainless steel, ordinarily used as a standard material for hip implants production, are presented in this paper. The coatings of a commercially available hydroxyapatite powder were plasma-sprayed onto specimens of medical grade 316LVM stainless steel under various operating conditions. Optical microscopy was used for microstructure and porosity characterization, while the coating morphology and Ca/P ratio were analyzed using an SEM equipped with EDX. The coating microstructure varied from a porous to a glassy structure, depending on the operating conditions and coating thickness. Coating porosity was determined to be at the lower required limit requested for the bone-coating intergrowth possibility, but nevertheless adhesion measurements showed good results. The Ca/P ratio was determined for both as-deposited coatings and after ageing in distilled water for various time and temperature combination.

Keywords: Atmospheric plasma-spraying

- Hydroxyapatite • Stainless steel
- 316LVM

Integration of system design and production processes in robust mechatronic product architectures development – extended M-FBFP framework

Krešimir Osman¹, Dragi Stamenković², Mihailo Lazarević³

¹Faculty of Mechanical Engineering and Naval Architecture, University of Zagreb, Croatia

²Termoelektra Ltd., Belgrade, Serbia

³Faculty of Mechanical Engineering, University of Belgrade, Serbia

Abstract

The complexity of mechatronic products, such as climate chamber subsystems, results in enormous difficulties in understanding where the main design process inefficiencies are. It is therefore extremely difficult to determine which improvements will have the most significant impact on a company or on a specific project. Mechatronic products are characterized by a high level of interdisciplinarity and complexity in the technical system and the relevant development processes. The main challenge in this respect is how to deal with the high complexity of and a variety of interdependencies in such products. We are therefore presenting a framework for integrated mechatronic product and process modelling – extended M-FBFP framework. This framework provides different independent perspectives of the overall product to improve their architecture. As a result of the proposed framework, risk analysis through subsystems in the components domain and through processes in the technical processes domain is enabled and it is now possible to provide feedback on product architecture. To obtain optimally robust product architectures from available alternative solutions, an evaluation analysis was performed across all stages, including the initialization and subsequent refinements with several evaluation criteria: complexity, interdependency and process duration. To test the validity of the proposed framework, we are presenting a case study involving a climate chamber with heat regeneration.

Keywords: complexity, mechatronic product design, product architecture, extended M-FBFP framework, technical process, risk analysis, evaluation.

Available online at the Journal website: <http://www.ache.org.rs/HI/>

The design issues and decisions encountered in the early stages of product design relate to certain information, including requirements, functions, components and engineering characteristics, which capture the performance measures of the system [1]. As such, several design tools have been developed to structure this conceptual design information using matrices. However, these existing tools do not provide algorithms for evaluating this conceptual design information [2]. Numerous system analysis methods have been developed in order to identify potential areas of design improvement in terms of requirements, functionality, and components. Many risks inherent in a product and/or development process are defined within the product architecture. Such product information and specifications, as well as the development of certain criteria, are considered to be important for product

SCIENTIFIC PAPER

UDC 62–52:621:004

Hem. Ind. **67** (5) 759–771 (2013)

doi: 10.2298/HEMIND121109003O

robustness. Product robustness therefore includes a combination of both product and production engineering [3].

Successful product development is determined by the fulfilment of customer needs using a product under constraints of time, cost, and quality [4,5]. Risk or uncertainty adds a new dimension that is very difficult to address [6]. Effective risk management in new product development can reduce the likelihood of cost, schedule, and performance deviations during the execution. Risk management is therefore closely related to the success of a product development process. It offers promising approaches to dealing with uncertainties in early product development phases. Uncertainty in customer requirements and input data results in an uncertain number of design iterations in parallel with the specification's evolution.

This paper presents the integration of certain matrix methods (extended matrix – function-based failure propagation method framework) aimed to provide a designer with feedback about expected behaviour (properties) of predefined subsystem architecture and technical processes. In product modelling, it focuses on the relationship between functions using the function

Correspondence: K. Osman, Chair of Design and Product Development, Department of Design, Faculty of Mechanical Engineering and Naval Architecture, University of Zagreb, Ivana Lučića 5, 10000 Zagreb, Croatia.

E-mail: kresimir.osman@fsb.hr

Paper received: 9 November, 2012

Paper accepted: 18 December, 2012

based failure propagation method [7] and extends their impact on the Quality Function Deployment (QFD) method [8] and other domains (requirements, technical processes and components) in a Multiple-Domain Matrix (MDM) [9]. In regards to process modelling, on the other hand, it deals with modelling of risk interactions based on their identification and evaluation and risk propagation and re-evaluation [10–12]. Based on the result derived from process modelling, improvements are made to the QFD and technical process domain in the MDM matrix. All of this is carried out in the early design phase (conceptual design) by presenting a mapping as an iteration process to improve product architecture. The feedback generated by the product design and production process phases should highlight the elements within the system architecture that are unable to operate within the given parameters, thus resulting in unstable system behaviour. To obtain optimally robust product architectures from available alternative solutions, an evaluation analysis was performed across all stages, including the initialization and subsequent refinements with several evaluation criteria: complexity, interdependency and process duration [13,14].

The section below presents research motivation and the background for this research. The fourth section will provide a more detailed description of the proposed framework. The fifth section will evaluate and test the validity of the proposed framework. An actual case study will be presented here. Discussions on obtained results and a conclusion with regard to future research close this paper.

Motivation

Mechatronic products, in particular, have become significantly complex because of technological competition and reduced product development cycles [15]. They are characterized by a high level of interdisciplinarity and complexity in the technical system and the belonging development processes. As a result, achieving high quality has gradually become more difficult. At the same time, as a product becomes more complex, the corresponding development project also becomes more complex. A need for early estimations development processes arises, especially in the early stages of product development. In system design, an interdisciplinary design team needs to decide very early on which product concept they will implement and which they will abandon. This decision needs to be taken on the basis of limited information, but should consider the different costs amongst competing product design concepts [16]. To focus on product design and development, most project budgets are defined during the design phase before any actual work is done. Adequate planning is one of the key elements required to meet project quality, reduce financial and schedule risks, and help a project achieve success [17]. As a result, a sys-

tematic approach to robust product architecture development and evaluation, including integration of system design and the production process with mutual impacts, is needed.

Background

Product and process modelling techniques currently developed and applied to industry do not sufficiently enhance the overall system understanding and fail to create sufficient awareness of the importance of discipline-integrating milestones. This is due to a distinct decoupling of the representations of the technical system itself on the one hand and the relevant development processes on the other.

The Characteristics-Properties Modelling / Property-Driven Development (CPM/PDD) approach [18] can be used in product development to model products and product development processes. The essence of the CPM/PDD theory is clear distinction between characteristics and properties. The CPM/PDD approach defines product development as a sequence of synthesis, analysis and evaluation steps. In each evaluation step, one or several property value(s) (it is not always possible to measure a property using a countable value, e.g., the haptic of a surface) is (are) compared with the required properties. The difference between the existing and required properties indicates which properties need to be customized by modifying the related characteristics.

Change Prediction Method (CPM) tool, a software tool for predicting change propagation. It was developed at the Engineering Design Centre in Cambridge [19,20]. The CPM tool supports the design change process in two different ways. First, it supports abstract product-model building [21]. It helps both individual designers and team leaders understand how components in their area of responsibility are connected to other product parts and where any interfaces with other teams may exist. Another benefit provided by the CPM tool is a platform to analyse change propagation data based on combined component interrelations. For that purpose, algorithms for calculating combined risk based on direct impact and likelihood values were developed and integrated into the tool [22]. This allows designers to quickly assess the probability of change propagation from one component to others, as well as the overall risk associated with a change to a component.

The signposting framework was also developed at the Engineering Design Centre in Cambridge [23,24]. It is a dynamic framework describing design tasks in terms of input and output parameters, where the term "parameter" may be used to refer to a description of any aspect of a product or process that change over time [25]. Designing is characterized as identification and iterative refinement of parameters. Design pro-

cesses are represented as a set of parameters and tasks, each defined in terms of one input state and one or several output state(s). An input state describes the parameters used for a task, including a numerical description of the minimum level of confidence in each that is deemed appropriate to initiating the task. Similarly, output states describe the parameters produced after a task is completed, including the level of confidence the task provides to each parameter. At any time, the state of a process may be represented by a vector describing the level of confidence in each parameter.

Pedersen *et al.* [26] have presented a design method that can help design aligned modular product and production architectures. The idea behind the method is to modularize a concept process similar to how products are modularized, which means that the process would be divided into two phases: a preparatory phase and an executive phase. The product concept consists of several sub-solutions or technical solutions. Each of these solutions corresponds to a transformation that needs be carried out in the manufacturing set-up. The process chosen corresponds to the overall set-up, so the production layout depends on the product concept and this dependency is modelled and visualized instantly. Once the dependency is optimized in accordance with the best possible product concept and the best possible production set-up, we might say the product and production architectures are aligned.

Multiple-Domain Matrix (MDM) [9] is one of the most commonly used matrix approaches. It is described in detailed in the paper background [17], so only the most important aspects will be addressed here. When applying MDM to a complex system, the classification of implied domains and dependency types can help users keep track of the relevant system aspects and linkages. Users are then able to specify the most important domains. The alignment of MDM automatically indicates all possible combinations of domains for subsequent specification of dependency types. Conversely, users can start with familiar dependency types and subsequently derive the corresponding domains of the complex system in question. In either case, the system of MDM supports the complete capturing of all basic aspects of a complex system.

3D-MDM [27] is an interactive 3D visualization, generation of a transparent view of dependencies between different domains of interest. It uses the open source scene graph library “Open Scene Graph” and is linked to the software tool LOOME [28] *via* an XML interface. It allows for an intuitive and transparent view of complex mechatronic products. By increasing the transparency and with it the understanding of the system, this representation assists engineers within the mechatronic development process.

The Integrated PKT approach [29,30] was developed at the Institute for the Product Development and mechanical engineering design in hamburg. This approach adapts product architecture to offer high external variety on the market without increasing the internal diversity in the company to the same extent. The elements of the approach are the Design for Variety and Life Phases Modularization modules.

A methodological approach to assessing product robustness [3,31] was developed at TU Munich, Institute for Product Development. It begins with a discussion on the focus and the requirements for the tool, both areas are modelled, a measure is generated, and documents are prepared for the implementation. In addition, the modelling phase in this project is extended to different companies to obtain more feedback regarding the practicability. The stepwise evaluation focuses on the modelling part. This enables us to understand the industrial need more clearly and to derive as early as possible such types of models that can be applied to industry after the project is completed. In contrast to the DFX shell, we focus more on the interdependence analysis on different levels and on the issue of which abstraction levels in the design process with regard to certain production aspects are best implemented.

The framework for integrated modelling and planning of mechatronic processes [32] combines different views of complex systems and provides an overall model to combine and analyse relations within the system. The various elements of such system are referred to as domains (*e.g.*, functions, persons and milestones) that interact in different ways and on different levels. The main idea behind the approach is to use functional validation of high level mechatronic functions during the integration and testing phase as a basis for the structuring and planning of the development process.

The MDM-based approach to the interrelation of lifecycle phases based on their association with DFX-guidelines [33] is a procedure to process generic information by using non-company-specific design guidelines and a set of lifecycle phases, which can be recognized in many products and has helped understand which lifecycle phases and which DFX-guidelines play more central roles in their respective networks than others. This information can be valuable to a product planner; it may help involve respective stakeholders throughout the lifecycle and provide support to consider and prioritize certain DFX-guidelines already included in the planning phase.

Autogenetic Design Theory (ADT) [34], developed at Otto-von-Guericke-Universität Magdeburg, Chair for Information Technologies in Mechanical Engineering, Germany is the genesis of a product during the development process is viewed as an analogy to the evo-

lution of living creatures. With ADT, this process is described as an evolutionary development process of technique and technology in a turbulent environment, which consists of requirements, starting conditions, boundary conditions, and constraints, which all may change dynamically along the process. Finally, ADT provides a better understanding of the nature of the development process.

EXTENDED M-FBFP FRAMEWORK – DESCRIPTION

The extended M-FBFP framework (Figure 1) presented in this paper is based on the Theory of Technical Systems (TTS) [35,36] and the VDI 2206 standard [37]. It focuses on making system performance immune to variations under uncertain operating conditions. Variations are everywhere, both wanted and unwanted, but unwanted variations can impair the quality of the resulting products. A robust design does not aim to attempt to eliminate such variations, but rather to

make the product insensitive to them. Feedback to the structural design is clearly only based on the results from the product and process modelling phases. In addition to the above disadvantages pertaining to this link only, a long period will elapse between structural changing iterations. The steps in the framework are presented as follows:

Forecast the overall customer requirements

Mapping of the overall design requirements [38] regarding the market segmentation grid is the first step. The market segmentation grid is an attention-directing tool providing a link between management, marketing and engineering designers to help identify potential opportunities. Thus, the overall design requirement could be generated by integrating all such market segmentation. During the product definition phase, marketing and data collection efforts should be completed before the beginning of procedure modelling.

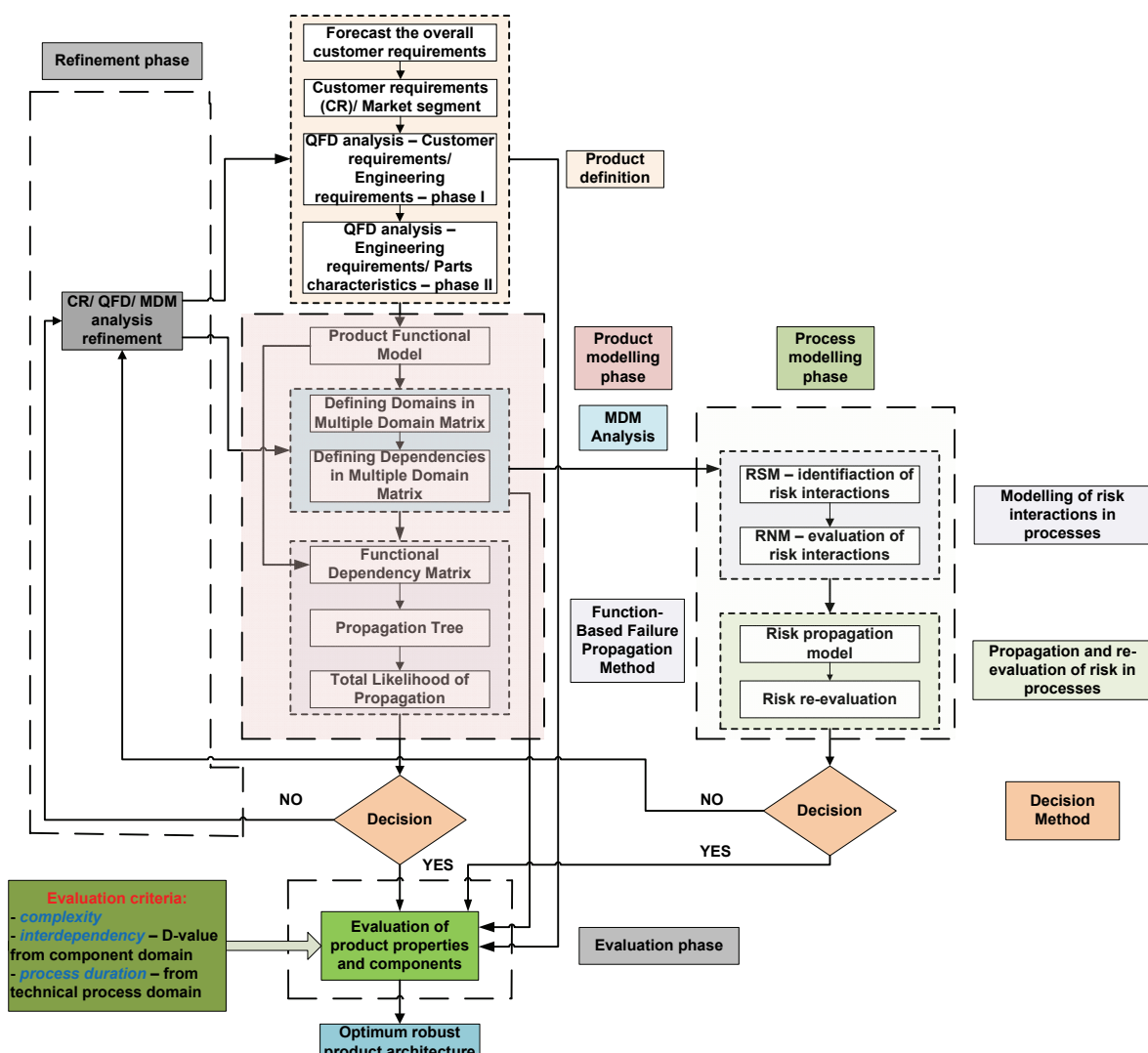


Figure 1. Schema of extended M-FBFP framework.

Customer requirements/market segment

This is where we will try to determine the overall customer requirements [38] for each group within the customer base. This includes different requirements from different market segment grids. The customer base is provided on the basis of a list generated in the first step. The market segmentation grid is created based on the size of the product family. Importance data is provided to match the customer requirements and market segment (importance is set to zero in certain cases to imply that there is no requirement).

QFD Analysis – Phase I

This step imports the overall customer requirements (CRs) rating and customer requirement to House of Quality (HoQ) [8] to obtain the engineering characteristics. On the left side of the QFD matrix, the importance value is presented by the overall rating from the preceding step. The engineering requirements (ERs), which can satisfy customer requirements, are determined as shown on the top and the relationships between them are provided.

QFD Analysis – Phase II

Following the QFD procedure [8], the engineering requirements (ERs) are input with weighting to the left side of QFD phase II, and the parts characteristics and relationships between engineering requirements and parts characteristics (PCs) are also obtained. Furthermore, the interdependencies between parts characteristics are presented on the roof of QFD phase II.

Product modelling phase – with several intermediate steps:

a) Product functional modelling

Functional modelling is a design tool that describes a product or system in terms of the functions it performs [38]. Our model is based on the function of a product.

b) Multiple Domain Matrix (MDM) analysis

According to the procedure of structural complexity management [9], we first defined the system using the Multiple-Domain Matrix (MDM). The key domains that can be found here are: requirements, technical processes, functions and components (according to the Theory of Technical Systems – TTS [35,36]). In the next step, the types of dependencies between domains (inter-domain) were defined. As we can see in Figure 5 later on, the dependency meanings were not indicated for all possible domain combinations represented by the matrix subsets. Those not shaded indicate dependency information that is available, but not required for further system investigation (architecting and refinement). Finally, we defined the meanings for the intra-domain dependencies of components, functions, technical processes and requirements.

c) Functional dependency matrix

To perform the function-based failure propagation method [10], a functional dependency matrix was generated on the basis of the system's functional model using the flows as the common interface. Functions are directly dependent on the functions connected to them by one or more flows. The functional dependency matrix is then populated with the likelihoods failure propagation to a particular function from the one it is dependent on. The initiating functions are the functions that fail initially, and the dependent functions are those that failure propagates to. For this method, the likelihood values are decimal values between zero and one, zero denoting no likelihood of propagation, and one representing certain propagation of failure. This is done to allow the use of Boolean operators [39] in the calculation of the total likelihood of propagation. Where there is no dependency, there is no likelihood of propagation, and thus place is completed with a zero or left blank (see Table 3 later on).

d) Propagation tree

Next, using the functional dependency matrix [7], propagation trees are built for each function in the model. These trees trace the path of potential failure to each possible function that can propagate its failure to the end function. Each branch represents a different starting function, travelling to the same “root”.

e) Total likelihood of risk propagation

Finally, we calculated the total likelihood of risk propagation. Using the direct likelihoods generated from the functional dependency matrix and the propagation trees, the total propagation likelihood is calculated using the Boolean operators “AND” and “OR” [39]. Wherever there are multiple functions that failures can propagate from, the “OR” calculation is used. If a branch can only propagate failure to a single function, the “AND” calculation is used. In order to properly use this method, historical data pertaining to failure propagation must exist. Finally, these failures were then tabulated into a matrix showing the number of times each function pair had appeared. These numbers were then normalized using the most frequently occurring failure propagation pair as the normalizing factor. In this way, each value collected becomes a decimal value between zero and one. It is unlikely for each possible failure mode that a function might fail because it has the same likelihood of propagation. Some failure modes may have higher or lower likelihoods of propagation than others. However, to facilitate the calculation of those likelihoods, each failure mode for a function is assumed to have the same likelihood. Using a modified form of the likelihood mapping form [40], the likelihood of each function pair was then calculated (Table 1).

Table 1. Collected failure propagation data for final concept of climate chamber

Branch	Total likelihood
F0 – F1	0.1
F0 – F1 – F6 – F7 – F8 – F13 – F14	0.000054
F0 – F5 – F6 – F7 – F8 – F13 – F14	0.000108
Full tree	0.100162

Process modelling phase – with several intermediate steps:

a) Modelling of risk interactions in processes

– Identification of risk interactions in processes –

Risk Structure Matrix (RSM)

Using identification, we are able detect and establish cause-effect relationships between risks. For this purpose, we defined the Risk Structure Matrix (RSM) [10–12], a binary and square matrix where the value $RSM_{ij} = 1$ if there is an interaction between the two risks R_i and R_j .

– An evaluation of risk interactions is provided using the Risk Numerical Matrix (RNM) [10–12] based on AHP-based principles [41]. The numerical values in the matrix were obtained from a Saaty scale for both the causes (inputs) and effects (outputs) to provide a risk pair wise comparison [41,42]. Using a combination of eigenvalues from two square matrices, the Numerical Effect Matrix (NEM) and the Numerical Cause Matrix (NCM), we can define the Risk Numerical Matrix (RNM) using a global weighting operation:

$$RNM(i, j) = \sqrt{NCM(i, j) \times NEM(i, j)}, \quad (1)$$

$$\forall(i, j), 0 \leq RNM(i, j) \leq 1$$

b) Propagation and re-evaluation of risk in processes

We used an approach where risks are propagated and re-evaluated by taking into account their propagation behaviour in the network. This approach is referred to as the Risk propagation model [43]. After such risk re-evaluation, we can see the result of the probabilities of the respective risks using a re-evaluated risk probability vector and a re-evaluated risk critical vector between elements in network (technical processes) [44]. Based on this result (high probability of risk in interactions), we are able determine whether there is a need make certain refinements in product architecture. This can help designers make improvements in product architectures in the evaluation phase.

Refinement phase

The refinement phase can be conducted after the product and process modelling phase through changes in a CR/QFD/MDM analysis. According to the feedbacks received in the refinement phase, we are able to evaluate product parts and properties.

Evaluation of product parts and properties

Such evaluation is based on three pieces of information (evaluation criteria) obtained from the QFD and MDM analyses: complexity, interdependency and process duration [13] (Table 2). We choose these criteria for an early evaluation of product properties. The degrees of complexity are determined based on the designer's experience. On the other hand, process duration data is adopted from an activity-based DSM (technical process domain in MDM), while interdependency is adopted from the D-value (sum of columns) from a component-based DSM (component domain in MDM) (see Figure 4 later on).

Each data is converted to the level of importance (Table 2). We then input the importance data to the upper side of QFD phase II, the rating corresponding to each part's characteristics obtained by summing up the values in the column. The lowest row and the rightmost column are calculated using the level of importance, the ratings for evaluation criteria, and the relationship between engineering requirements and parts characteristics, after which the summed up ratings of all engineering requirements and parts characteristics are obtained (based on which we are able to see the critical components and critical properties).

CASE STUDY

The objective of the case study is to demonstrate how the proposed matrix approach can support mechanical designers during conceptual designing. For this purpose, we used the example of a climate chamber, which is very often an integral part of HVAC systems for large facilities (e.g., office buildings). We started with the initial climate chamber concept with operating conditions based on designer experience (Figure 2a). Our goal in the case study was to propose architecture for such operating conditions using the procedure concerned.

In OFD Phase I, customer requirements are input in relation to the engineering requirements that can meet them. According to the calculation of the importance of customer requirements, the engineering requirements that can meet them were determined and presented on the top, including their mutual relationships. Phase I of the QFD procedure contains a roof, which represents the correlations between engineering requirements. This data is not relevant to this research, so the roof part has been removed. During phase II of the QFD procedure, the engineering requirements with a weighting factor are put to the left side and the part characteristics are then determined. This was followed by determining the relationships between engineering requirements and parts characteristics. Furthermore, the interdependencies between part characteristics are

Table 2. Importance level for criteria information (for final concept of climate chamber); importance: high, 9, medium, 3, low, 1

Components	Process duration		Interdependency		Complexity	
	Day	Importance	Degree	Importance	Degree	Importance
12	5	3	1	1	Medium	3
44	1	1	10	9	Low	1
10	10	9	3	1	High	9
42	4	3	0	1	Medium	3
16	15	9	1	1	High	9
14	5	3	1	1	Medium	3
45	1	1	13	9	Low	1
13	14	9	18	9	High	9
51	4	3	1	1	Medium	3
19	5	3	1	1	Medium	3
46	1	1	10	9	Low	1
18	10	9	10	9	High	9
29	15	9	0	1	High	9
22	15	9	0	1	High	9
25	5	3	1	1	Medium	3
47	1	1	19	9	Low	1
24	10	9	2	1	High	9
48	4	3	10	9	Medium	3
5	4	3	3	1	Medium	3
41	2	1	13	9	Low	1
37	2	1	20	9	Low	1
2	12	9	1	1	High	9
50	4	3	1	1	Low	1
39	2	1	3	1	Medium	3
49	4	3	1	1	Medium	3
52	4	3	1	1	Medium	3
40	2	1	5	3	Low	1
43	2	1	4	3	Low	1
31	4	3	4	3	Medium	3

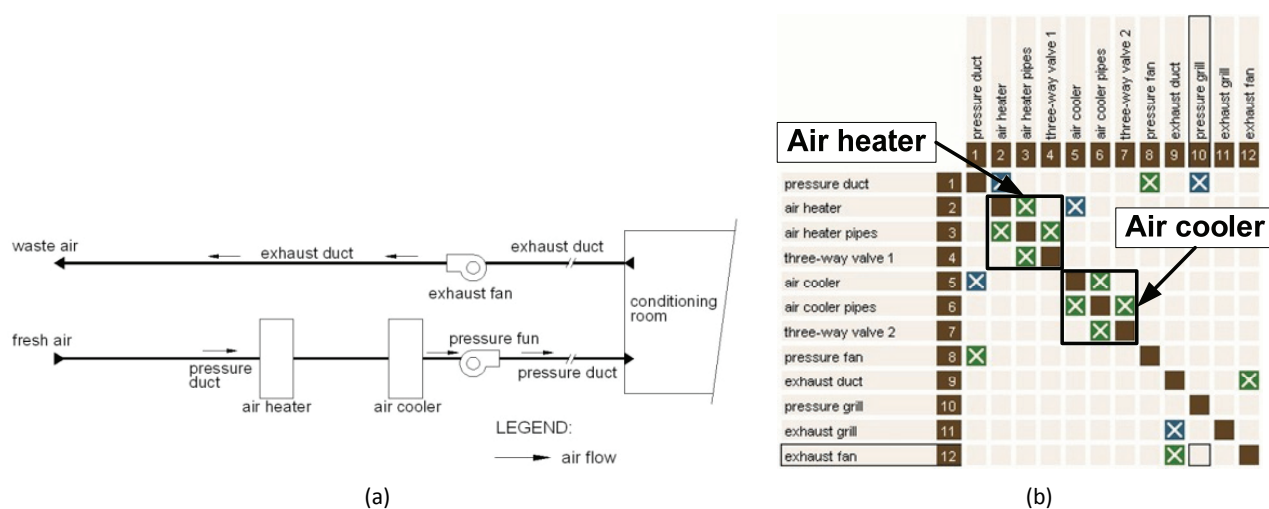


Figure 2. a) Simplified schema of initial concept of climate chamber; b) Component domain representation in MDM with possible modules (subsystems) identified in proposed product architecture for initial concept of climate chamber (screenshots from LOOME® software).

represented on the roof of phase II of the QFD procedure. After presenting the functional model of the system, an MDM analysis was provided (using LOOME® software [28]). It starts with domains for our initial climate chamber concept (Figure 3). This case study presents a component-based DSM (component domain) for the initial (Figure 2b) and final climate chamber concepts (Figure 4), after a few steps of refinement. After determining the dependencies between domains (inter and intra), we can proceed to build a functional dependency matrix for our product's functional model of the initial climate chamber concept. Figure 6 shows the functional dependency matrix for final climate chamber based on the product's functional model, Figure 5. We can see that the initiating functions are shown across the top of the matrix and the dependent functions are listed alongside. Next, based on the propagation tree created and starting from the "top" function and linking it to each function, we are able to calculate the total likelihood for each system. Each of these chains (branches) is linear because they only have one path from the initiator to

the top function. Table 1 presents the failure propagation data collected for the final climate chamber concept, after a few steps of refinement. As we can see in Table 1, if we follow this procedure (as a Function-Based Failure Propagation Method), we can see for the entire tree (our proposed system with subsystems) the individual likelihoods of each branch and determine which branch of the tree has the highest likelihood. Based on this, we can add some new elements within our refinement phase (Figure 1).

We obtained an improved model after several feedback loops within the proposed framework to reduce risk likelihood and build our system that will fulfil our initial operating conditions (see the matrix representation of the system with its subsystems after clustering [45] – Figure 4).

The problem was solved by adding some new elements: a heat regenerator, a bypass duct, a recirculation duct, a humidifier and an air warm-up heater.

As we can see, each data element (Table 2) is converted to a value to represent a level of importance (9 stands for strong, 3 stands for medium and 1 stands for

Product family	Requirements (R)	Technical Processes (TP)	Functions (C)	Components (C)
Requirements (R)	Requirements - requirements domain	R has influence on TP		
Technical Processes (TP)		Technical processes - technical processes domain	TP has influence on F	
Functions (F)		F has influence on C	Functions - functions domain	F has influence on C
Components (C)			C has influence on F	Components - components domain

Figure 3. Domains in Multiple-Domain Matrix (MDM).

pressure grill	38
hygrometer	36
three way valve 1	12
air heater pipes	44
air heater	10
filter 1	42
circulation pump	16
three way valve 2	14
humidifier pipes	45
humidifier	13
silencer 1	51
three way valve 3	19
air cooler pipes	46
air cooler	18
exhaust fan	29
pressure fan	22
three way valve 4	25
air warm-up heater pipes	47
air warm-up heater	24
filter 2	48
motor blinds 1	5
by-pass duct	41
pressure duct	37
plate heat recuperator	2
filter 4	50
exhaust grill	39
filter 3	49
silencer 2	52
exhaust duct	40
recirculating duct	43
motor blinds 3	31

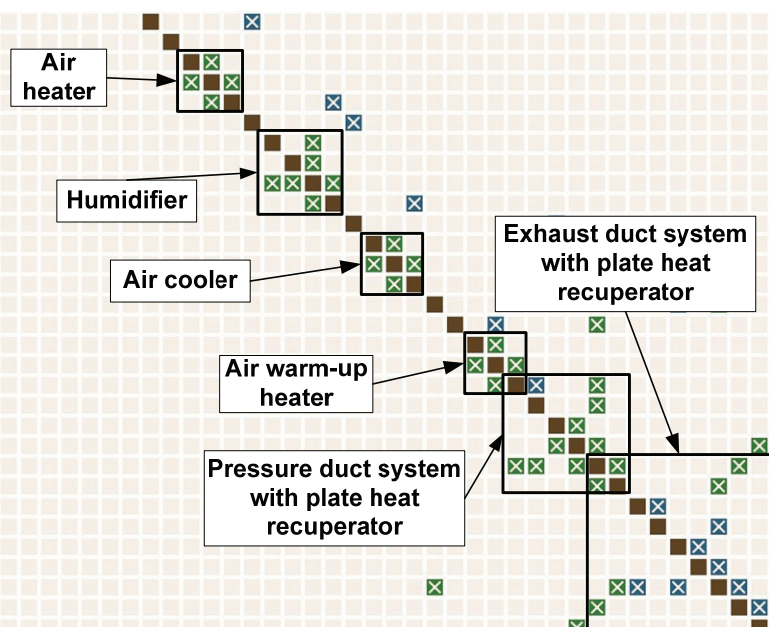


Figure 4. Component domain representation in MDM with possible modules (subsystems) identified in proposed product architecture for final concept of climate chamber (screenshots from LOOME® software).

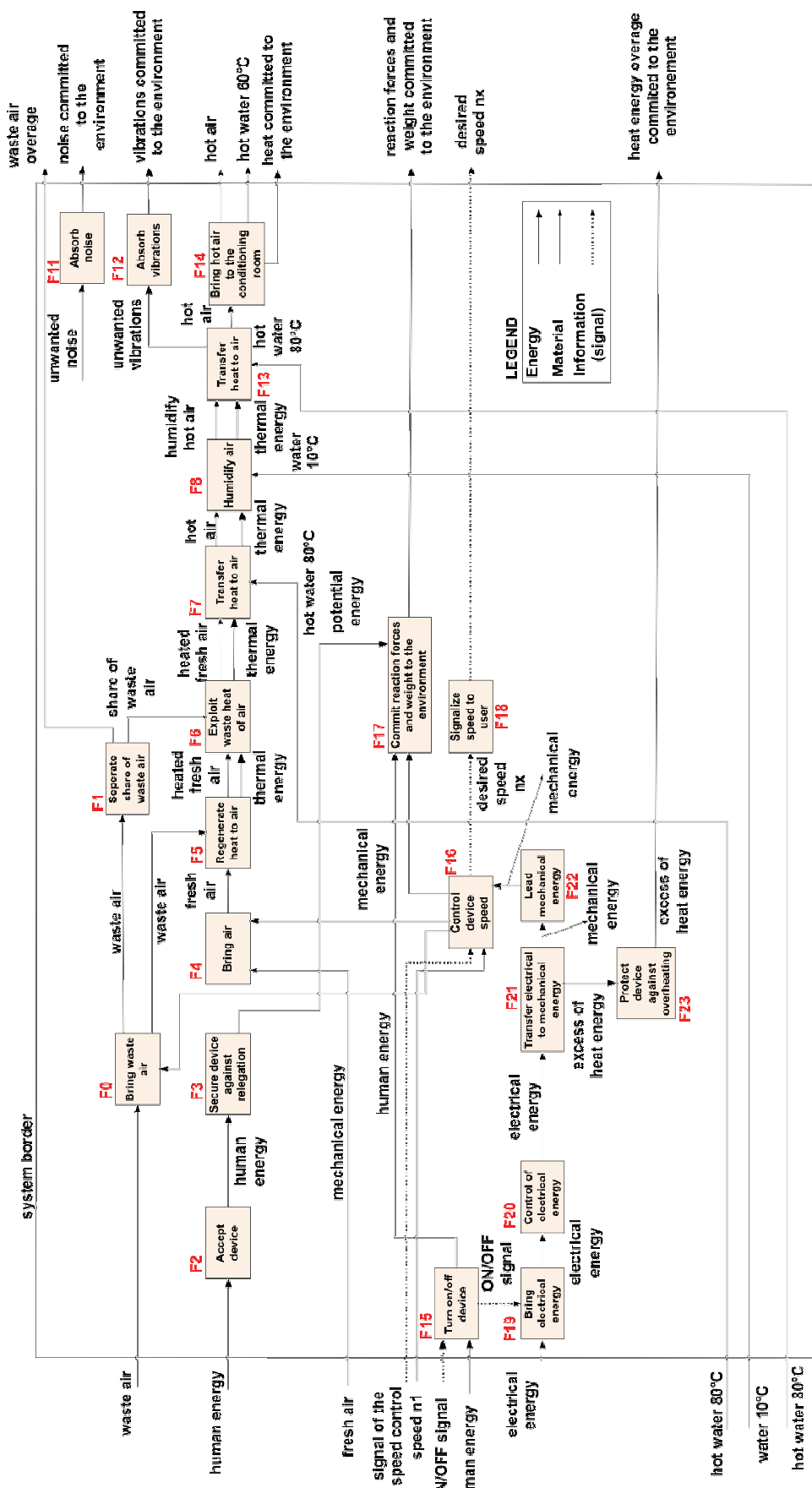


Figure 5. Product functional model for final concept of climate chamber.

		Likelihood <i>I</i>													
		Initiating function													
Dependent function	F0 - bring waste air	F0	F1	F2	F3	F4	F5	F6	F7	F8	F9	F10	F11	F12	F13
	F1 – separate share of waste air	0,1													
	F2 - accept device														
	F3 – secure device against relegation														
	F4 – bring air														
	F5 – regenerate heat to air	0,3				0,3									
	F6 – exploit waste heat to air		0,3				0,2								
	F7 – transfer heat to air							0,3							
	F8 – humidify air								0,1						
	F9 – absorb noise														
	F10 – absorb vibrations														
	F11 – absorb noise														
	F12 – absorb vibrations														
	F13 – transfer heat to air									0,2					
	F14 – bring hot air to the conditioning room												0,3		

Figure 6. Functional dependency matrix for final concept of climate chamber.

weak). Using the information provided in Table 2, we can determine the critical properties and critical parts of our proposed product architecture within QFD Phase II.

Putting the given criteria information on the upper side of QFD Phase II, we can recalculate the ratings for all engineering requirements, as well as the ratings for all part characteristics.

In the process modelling phase, we first provided a modelling of risk interactions through technical processes (using the technical processes domain in MDM). We thus created the Risk Structure Matrix (RSM) (Figure 7a) to identify risk interactions and the Risk

Numerical Matrix (RNM) (Figure 7b) to evaluate risk interactions.

Now we can use the approach based on the Risk Propagation Model (Table 3) for risk propagation and re-evaluation. Based on such results, we are able to decide whether we need to make any improvements in product architectures within the refinement phase (see Figure 1). As we can see, we need to provide a few feedbacks to make improvements in product architecture.

The final climate chamber concept following a few feedback loops in the refinement phase is presented in

	0	1	2	3	4	5	6	7	8	9	10	11	12	13	14
0															
1	1														
2															
3															
4															
5	1														
6	1	1													
7															
8															
9															
10															
11															
12															
13															
14															

(a)

$$A = \begin{bmatrix} 0 & 0 & 0 & 0 & 0 & 0 & 0 & 0 & 0 \\ 0,1 & 0 & 0 & 0 & 0 & 0 & 0 & 0,25 & 0 \\ 0 & 0 & 0 & 0 & 0 & 0 & 0 & 0 & 0 \\ 0 & 0 & 0 & 0 & 0 & 0 & 0 & 0 & 0 \\ 0 & 0 & 0 & 0 & 0 & 0 & 0,35 & 0 & 0 \\ 0,25 & 0 & 0 & 0 & 0,2 & 0 & 0 & 0 & 0 \\ 0,15 & 0,1 & 0 & 0 & 0 & 0,2 & 0 & 0 & 0 \\ 0 & 0 & 0 & 0 & 0 & 0 & 0,15 & 0 & 0 \\ 0 & 0 & 0 & 0 & 0 & 0 & 0 & 0 & 0,1 \end{bmatrix}$$

(b)

Figure 7. a) Risk Structure Matrix for final concept of climate chamber; b) Risk Numerical Matrix for final concept of climate chamber.

Table 3. Risk Propagation Model for final concept of climate chamber

Spontaneous probability		Re-evaluated probability	
Risk ID	Value	Risk ID	Value
R1	0.1	R1	0.087
R2	0.25	R2	0.311
R3	0.35	R3	0.288
R4	0.25	R4	0.265
R5	0.2	R5	0.225
R6	0.15	R6	0.186
R7	0.1	R7	0.119
R8	0.2	R8	0.224
R9	0.15	R9	0.157
R10	0.1	R10	0.119
R11	0.1	R11	0.122
R12	0.25	R12	0.283
R13	0.25	R13	0.278
R14	0.2	R14	0.186
R15	0.2	R15	0.177
R16	0.2	R16	0.177
R17	0.2	R17	0.133

Figure 8. In this current research stage, the feedback loop is performed manually based on the results provided by the Total Likelihoods in Function-Based Failure Propagation Method from the product modelling phase and the Risk Propagation Model from the process modelling phase.

CONCLUSION AND FUTURE RESEARCH

This paper proposes an extended M-FBFP framework, which combines a number of different methods to deal with complex mechatronic systems. It could help designers obtain optimally robust product architectures using continuous risk analysis throughout all

stages from initialization to subsequent refinements within the product and process modelling phase using several evaluation criteria: complexity, interdependency and process duration in early design stages. It enables analysing different product architecture arrangements of function interactions against changes in product architecture and production processes. Designers could make refinements to existing subsystem structures by adding new features to them. They could also see the impact of the whole analysis on other domains (requirements, technical processes and components) to enable their refinement and changes. The framework also enables designers to evaluate robust design alternatives using the evaluation phase. The

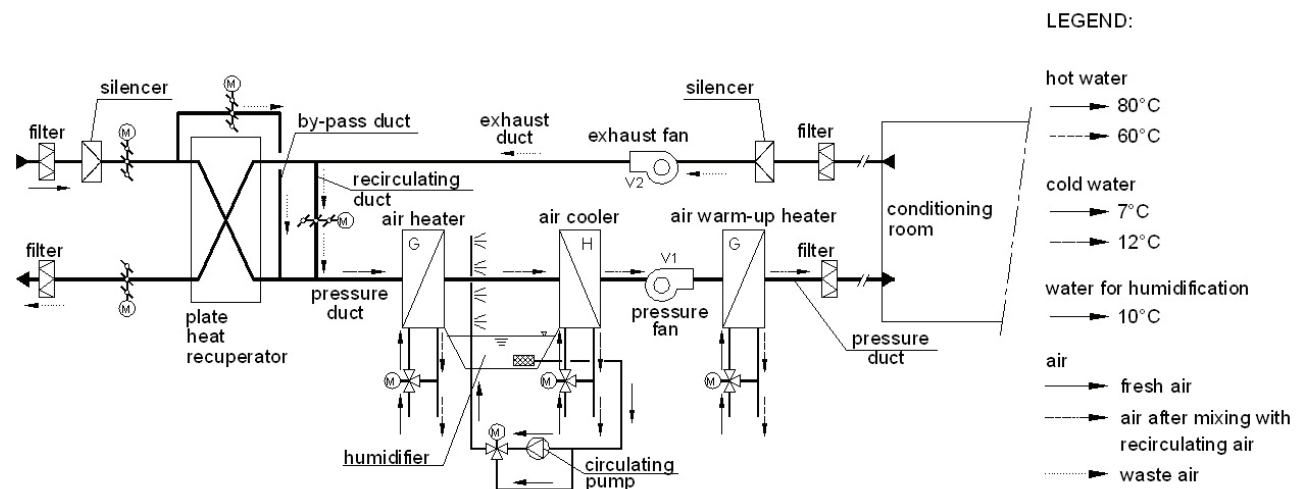


Figure 8. Simplified schema of final concept of climate chamber.

evaluation phase shows us that the framework and its methods are applicable in practical applications and that the results are meaningful and useful to the designers involved.

Future research could be continued through several options. One of them could extend the approach to all types of product development rather than just the modular or the present one. The second option could involve the elaboration and implementation of a decision-making method in the approach on which it will be based if it is necessary to make refinements in the QFD and MDM methods. Finally, the overall framework needs to be implemented in a software prototype as computational support is essential.

REFERENCES

- [1] G.M. Mocko, J.D. Summers, G.M. Fadel, S. Teegavarapu, R.A. Jonathan, J.R.A. Maier, T. Ezhilan, A Modelling Scheme for Capturing and Analysing Multi-Domain Design Information: A Hair Dryer Design Example, International Conference of Engineering Design – ICED 2007, Paris, 2007.
- [2] C. Pepe, D. Whitney, E. Henrique, R. Fardon, M. Moss, Development of a Framework for Improving Engineering Processes, International Conference of Engineering Design – ICED 2011, Copenhagen, 2011.
- [3] K. Helten, D. Hellenbrand, U. Lindemann, A Procedural Model to Assess Main of Production on Product Design, International Design Conference - DESIGN 2010, Cavtat-Dubrovnik, Croatia, 2010, pp. 789–798.
- [4] U. Lindemann, Methodische Entwicklung Technischer Produkte, 2nd ed., Springer, Berlin, 2006.
- [5] K. Ulrich, S. Eppinger, Product Design and Development, 3rd ed., Irwin McGraw-Hill, New York, 2003.
- [6] E. Crawley, O. de Weck, S. Eppinger, C. Magee, J. Moses, W. Seering, J. Schindall, D. Wallace, D. Whitney, The Influence of Architecture in Engineering Systems, Engineering Systems Monograph, 2004.
- [7] D. Krus, K. Grantham Lough, Risk due to function failure propagation, International Conference of Engineering Design - ICED 2007, Paris, 2007.
- [8] Y. Akao, QFD – Quality Function Deployment, Verlag Modernel Industrie, Landsberg, 1992.
- [9] U. Lindemann, M. Maurer, T. Braun, Structural Complexity Management: An Approach for the Field of Product Design, Springer-Verlag, Berlin, 2009.
- [10] F. Marle, L.-A. Vidal, Potential applications of DSM principles in project risk management, 10th International DSM Conference, Stockholm, Sweden, 2008, pp. 157–168.
- [11] F. Marle, Using DSM Approach to manage interactions between projects risks, 12th International DSM Conference, Cambridge, United Kingdom, 2010, pp. 17–29.
- [12] F. Marle, L.-A. Vidal, Project risk management processes: improving coordination using a clustering approach, R. Eng. Des. **22** (2011) 189–206.
- [13] U. Lindemann, M. Maurer, Early evaluation of product properties for individualized products, Int. J. Mass Cust. 1(2–3) (2006) 299–314.
- [14] K. Osman, D. Marjanović, Matrix based approach in assessing optimum robust product architectures, Design for X - Beiträge zum 23. DfX-Symposium, Bamberg, Germany, 2012, pp. 249–261.
- [15] K. Oizumi, K. Kitajima, N. Yoshie, T. Koga, K. Aoyama, Management of Product Development Projects Through Integrated Modelling of Product and Process Information, International Conference of Engineering Design – ICED 2011, Copenhagen, Denmark, 2011.
- [16] S.C. Braun, U. Lindemann, A Multilayer Approach for Early Cost Estimation of Mechatronical Products, International Conference of Engineering Design – ICED 2007, Paris, France, 2007.
- [17] K. Osman, D. Stamenković, M. Lazarević, Robust Product Architecture Development Combining Matrix-Based Approaches and Function-Based Failure Propagation Method – M-FBFP Framework, FME Trans. **39** (4) (2011) 145–156.
- [18] C. Weber, CPM/PDD – An Extended Theoretical Approach to Modelling Products and Product Development Processes, 2. German-Israeli Symposium on Advances in Methods and Systems for Development of Products and Processes, Fraunhofer-IRB-Verlag, Stuttgart, 2005, pp. 159–179.
- [19] P.J. Clarkson, C. Simons, C.M. Eckert, Predicting Change Propagation in Complex Design, DETC '01, USA, 2001.
- [20] T. Jarratt, C.M. Eckert, P.J. Clarkson, Development of a Product Model to Support Engineering Change Management, TCME conference 2004, Lausanne, Switzerland, 2004.
- [21] R. Keller, T. Eger, C.M. Eckert, P.J. Clarkson, Visualizing Change Propagation, In: International Conference of Engineering Design - ICED 2005, Melbourne, Australia, 2005.
- [22] P.J. Clarkson, C. Simons, C.M. Eckert, Predicting Change Propagation in Complex Design, ASME J. Mech. Des. **126**(5) (2004) 765–797.
- [23] B.D.O. O'Donovan, Modelling and Simulating Design Processes, PhD thesis, University of Cambridge, Cambridge, United Kingdom, 2004.
- [24] P.J. Clarkson, J.R. Hamilton, Signposting: a parameter-driven task-based model of the design process, R. Eng. Des. **12**(1) (2000) 18–38.
- [25] D.C. Wynn, C.M. Eckert, P.J. Clarkson, Modelling and Simulating Iterative Development Processes, International Conference of Engineering Design – ICED 2005, Melbourne, Australia, 2005.
- [26] R. Pedersen, M. Kvist, N.H. Mortensen, Method for Alignment of Product and Production Concepts, International Conference of Engineering Design - ICED 2005, Melbourne, Australia, 2005.
- [27] H. Diehl, D. Hellenbrand, U. Lindemann, Transparent 3D Visualization of Mechatronic System Structures, International Design Conference – DESIGN 2008, Cavtat-Dubrovnik, Croatia, 2008, pp. 1255–1262.

- [28] TESEON, LOOMEQ complexity software, <http://www.teseon.de/loomeo> (accessed in Nov, 2013).
- [29] D. Krause, S. Eilmus, A Methodical Approach for Developing Modular Product Families, International Conference on Engineering Design-ICED 2011, Copenhagen, Denmark, 2011, pp. 299–308.
- [30] M. Brosch, G. Beckmann, D. Krause, Towards an Integration of Supply Chain Requirements into the Product Development Process, International Design Conference - DESIGN 2012, Cavtat-Dubrovnik, Croatia, 2012, pp. 23–32.
- [31] K. Helten, D. Hellenbrand, U. Lindemann, Product Robustness as a basis for the Improvement of production Planning Processes – Key factors in Early Design Phases, International Conference of Engineering Design - ICED 2009, Stanford, CA, USA, 2009.
- [32] D. Hellenbrand, U. Lindemann, A Framework for Integrated Process Modelling and Planning of Mechatronic Products, International Conference of Engineering Design – ICED 2011, Copenhagen, Denmark, 2011.
- [33] C. Hepperle, W. Biedermann, A. Böcker, U. Lindemann, Design for X-Guidelines and Lifecycle Phases with Relevance for Product Planning – An MDM-Approach, International Conference of Engineering Design – ICED 2011, Copenhagen, Denmark, 2011.
- [34] S. Vajna, S. Clement, A. Jordan, T. Bercsey, The Autogenetic Design Theory: An Evolutionary View of the Design Process, *J. Eng. Des.* **16**(4) (2005) 425–440.
- [35] V. Hubka, W.E. Eder, Engineering Design: General Procedural Model of Engineering Design, Springer-Verlag Berlin, 1992.
- [36] V. Hubka, W.E. Eder, *Theory of Technical Systems: A Total Concept Theory for Engineering Design*, Springer-Verlag, Berlin, 1988.
- [37] VDI 2206 – Design methodology for mechatronic systems, Verein Deutscher Ingenieure, Dusseldorf, 2004.
- [38] K. Otto, K. Wood, *Product Design: Techniques in Reverse Engineering and New Product Development*, Prentice Hall, Upper Saddle River, NJ, 2001.
- [39] U. Peruško, *Digital Logic – Logic and Electric Design*, Školska knjiga, Zagreb, 1996.
- [40] K. Grantham Lough, R.B. Stone, I. Turner, The risk in early design (RED) method: Likelihood and consequence formulations, ASME 2006 International Design Engineering Technical Conferences and Computers and Information in Engineering Conference, IDETC/CIE 2006, Philadelphia, PA, 2006, pp. 1119–1129.
- [41] T.L. Saaty, *Decision Making for Leaders: The Analytic Hierarchy Process for Decisions in a Complex World*, RWS Publications, Pittsburgh, PA, 1994.
- [42] T.L. Saaty, Decision-making with the AHP: Why is the principal eigenvector necessary?, *Eur. J. Oper. Res.* **145**(1) (2003) 85–91.
- [43] C. Fang, F. Marle, L-A. Vidal, Modelling risk interactions to re-evaluate risks in project management, 12th International DSM Conference, Cambridge, United Kingdom, 2010, pp. 31–44.
- [44] S. Kirin, A. Sedmak, L. Grubić Nešić, I. Čosić, Upravljanje rizikom projekata u kompleksnom petrohemijском систему, *Hem. Ind.* **66**(1) (2012) 135–148 (in Serbian).
- [45] D. Steward, The Design Structure Matrix: A Method for Managing the Design of Complex Systems, *IEEE Trans. Eng. Man.* **28**(3) (1981) 321–342.

IZVOD

POVEZIVANJE SUSTAVA I PROIZVODNIH PROCESA U RAZVOJU ARHITEKTURA ROBUSNIH MEHATRONIČKIH SUSTAVA – PROŠIRENO M-FBFP OKRUŽENJE

Krešimir Osman¹, Dragi Stamenković², Mihailo Lazarević³

¹*Fakultet strojarstva i brodogradnje, Sveučilište u Zagrebu, Hrvatska*

²*Termoelektr d.o.o, Srbija*

³*Mašinski fakultet, Univerzitet u Beogradu, Srbija*

(Naučni rad)

Složenost mehatroničkih proizvoda, kao što su sustavi klima komora, dovodi do ogromnih poteškoća u sagledavanju gdje su glavne neučinkovitosti u procesu. Dakle, vrlo je teško odlučiti koja će poboljšanja imati najznačajniji utjecaj na tvrtku ili za određeni projekt. Mehatronički proizvodi se odlikuju visokim stupnjem interdisciplinarnosti i složenosti u tehničkom sustavu i pripadajućem razvojnog procesu. Ovdje nam kao glavni izazov predstavlja kako se nositi s visokom složenošću i raznolikošću međuvisnosti u takvim proizvodima. Stoga je ovdje predstavljeno okruženje za integraciju modeliranja mehatroničkih proizvoda i proizvodnih procesa – prošireno M-FBFP okruženje. Ono nam nudi različite nezavisne poglede na cijeli proizvod kako bi se poboljšala njegova arhitektura. Kao rezultat predloženog okruženja, analize rizika u podsustavima kroz domenu komponenata i u procesima kroz domenu tehničkih procesa postaje moguća, te putem dobivenih povratnih informacija mogu se raditi izmjene u arhitekturi proizvoda. Da bi se testirala valjanost predloženog okruženja, ovdje je predstavljen primjer s klima komorom s regeneracijom topline.

Ključne reči: Složenost • Konstruiranje mehatroničkih proizvoda • Arhitektura proizvoda • Prošireno M-FBFP okruženje • Tehnički proces • Analiza rizika

Comparative study of binding strengths of heavy metals with humic acid

Ivana S. Kostić¹, Tatjana D. Andelković¹, Ružica S. Nikolić¹, Tatjana P. Cvetković², Dušica D. Pavlović², Aleksandar Lj. Bojić¹

¹University of Niš, Faculty of Science and Mathematics, Višegradska 33, 18000 Niš, Serbia

²University of Niš, Faculty of Medicine, Bul. Zorana Đindjića 81, 18000 Niš, Serbia

Abstract

The complexation of humic acid with certain heavy metal ions (Co(II), Ni(II), Cu(II), Zn(II) and Pb(II)) was investigated. The stability constants of humate complexes were determined by a method based on the distribution of metal ions between solution and resin in the presence and the absence of ligand, known as Schubert's ion exchange method. Experiments were performed at 25 °C, pH 4.0 and ionic strength of 0.01 mol dm⁻³. It was found that the 1:1 complexes were formed between metal ions and humic acid. Obtained results of the stability constants, $\log \beta_{mn}$, of complexes formed between the metal ions and humic acid follow the order Co(II) < Ni(II) < Cu(II) > Zn(II), which is the same as in the Irving–Williams series for the binding strength of divalent metal ion complexes. The stability constant of complex between Pb(II) ions and humic acid is greater than the stability constants of other investigated metal–humate complexes. The investigation of interaction between heavy metal ions and humics is important for the prediction of the distribution and control of the migration of heavy metals in natural environment.

Keywords: heavy metal pollution, humic acid, stability constant.

Available online at the Journal website: <http://www.ache.org.rs/HI/>

Heavy metals contamination of the environment is a threat to all living organisms. Since the metals are not biodegraded and that many of them are soluble in water, they can become more available for living systems and can accumulate in the environment [1]. Defining the factors that affect their bioavailability, leaching and toxicity in soil/water systems is of crucial importance.

Industrial discharge to the atmosphere, soil and water is the most important source that contributes to increased concentrations of heavy metals in the environment. The greatest heavy metal dispersion is observed in areas with metallurgy industries. During the processing of ore, the heavy metals, which occur in nature at very low concentrations, are released into the environment in high concentrations [2]. Around 100 times more lead (Pb), 13 times more copper (Cu) and 21 times more zinc (Zn) is emitted to the atmosphere by human activities than by natural processes. These industrial areas can be considered as risk areas with regard to trace metals and need to have discharge control or in some cases remediation strategy. These metal ions under certain conditions favor the interaction with functional groups such as carboxylic, phenolic, alcoholic, enolic –OH and amino groups. All this shows the necessity for improving the knowledge

SCIENTIFIC PAPER

UDC 502/504:504.5:547.992

Hem. Ind. **67** (5) 773–779 (2013)

doi: 10.2298/HEMIND121107002K

about heavy metals behavior in soils and waters in order to make accurate risk assessments for human health, define long-term ecological effects, set limit values and identify priorities in remediation of contaminated sites [3].

Heavy metals can be involved in a series of complex chemical and biological interactions. Factors that affect their mobility through the soil/water system are pH, redox status of the environment, sorbent nature, presence and amount of organic and inorganic ligands, including humic and fulvic acids, root exudates and nutrients [4].

Humic acids have natural and powerful adsorbent properties and are deeply related to the transportation and accumulation of heavy metals [5,6]. They are widely distributed in soils/waters and the type and structure of their functional groups depend on their genesis, but also on the method of their isolation and purification [7,8]. They control the behavior of heavy metals in the environment and their interactions with metals are complex, depending on the characteristics of humic acid, concentration of metal ions, pH value, etc.[9]. The complexation of humic acid with metals can affect the fate of metals in soils and waters, thus speciation of metals is affected by these complexes as well as oxidation-reduction reactions. Humic acid can serve as carrier of toxic metals, forming complexes that are stable and enhance transport of toxic metals in waters [10–12].

Environmental implication of humic-metal binding depends on the possibility whether metal ions form soluble humic complexes that can potentially conta-

Correspondence: I. Kostić, Faculty of Science and Mathematics, Višegradska 33, 18000 Niš, Serbia.

E-mail: ivana.kostic83@gmail.com

Paper received: 7 November, 2012

Paper accepted: 19 December, 2012

minate groundwater and retain the metal in soil solution or metal ions form insoluble humic complexes that will result in a reduction of bioavailability and ecotoxicity of the metals [12,13]. Studies of interactions between humic substances and heavy metals are mainly focused on estimating stability constants at a specific pH and ionic strength [8,9]. Thus, complexation of heavy metals in the environment is usually assumed or extrapolated for the complex natural system that involve a large number of different parameters (presence of competition ions, dissolved and particular organic matter, etc.). Therefore, investigation of the mechanism of interaction between heavy metal ions and humics is very important for the prediction of the distribution and control of the migration of heavy metals in natural environment [12–14].

Humic matter–metal ion stability constants are determined by a variety of different analytical techniques such as: centrifugation–depletion, equilibrium dialysis, ultrafiltration, chromatography, diffusive gradients in thin films, etc. Competitive methods are Schubert's method, competing dissolved ligand and kinetic discrimination [15].

The aim of this paper is to predict the behavior of heavy metals regarding the presence of humic acid in the environment, based on the strength of formed complexes. We have determined stability constants of five transition metals by using Schubert's cation exchange equilibrium method. The results confirm that Schubert's method can be used not only for stoichiometrically defined ligands but also for complexes of polyfunctional and stoichiometrically undefined ligands, such humic ligands are. Finding the relative order of metal–humic complexes stabilities can help in estimation of the fate transport and distribution of heavy metals through different compartments of the environment [16–18].

EXPERIMENTAL

Chemical reagents and instrumentation

Stock solutions of each metal were prepared from metal salts ($\text{Pb}(\text{NO}_3)_2$, $\text{CuCl}_2 \cdot 2\text{H}_2\text{O}$, $\text{Zn}(\text{NO}_3)_2 \cdot 6\text{H}_2\text{O}$, $\text{Co}(\text{NO}_3)_2 \cdot 6\text{H}_2\text{O}$ and $\text{Ni}(\text{SO}_4)_2 \cdot 6\text{H}_2\text{O}$). All metal salts were of analytical grade purity (purchased from Merck, Germany). Humic acid was purchased from Aldrich (HA, catalog H1, 675-2 lot No. S15539-264). All solutions were prepared using deionized water (conductivity less than $0.1 \mu\text{S cm}^{-1}$). Measurements of pH were made with a sensION MM 374 (precision 0.01 units of pH) using a HACH gel-filled glass electrode (LZW 5010 t.97.002). The pH electrode was standardized using commercially prepared pH 4.1, 7.0 and 10.0 buffers. The prepared solutions were analyzed by flame atomic

absorption spectroscopy (FAAS) using an AAnalyst 300 (Perkin Elmer) instrument.

Experimental procedure of resin preparation

The cation-exchange resin used in determination of stability constants was Dowex 50WX8, 100–200 mesh, Na-form, with an exchange capacity of 1.7 meq cm^{-3} . About 30 g of the resin was prepared by transferring to a glass column, and sequentially rinsing with 2 dm^3 of deionized water, 2 dm^3 of 2 mol dm^{-3} HCl, 2 dm^3 of 2 mol dm^{-3} NaOH and finally with 2 dm^3 of deionized water. The resin was changed in Na-form by passing 2 dm^3 of 2 mol dm^{-3} NaCl, followed by rinsing with 2 dm^3 deionized water. The resin was then air-dried for 24 h and stored in an air-tight polyethylene container.

Experimental procedure for establishing metal(II) ion-exchange isotherms (D_0) and determination of conditional stability constant of metal–ligand complexes

Ion-exchange isotherm was measured at pH 4.0 for each metal ($\text{Cu}(\text{II})$, $\text{Pb}(\text{II})$, $\text{Ni}(\text{II})$, $\text{Zn}(\text{II})$ and $\text{Co}(\text{II})$). Metal concentration solutions ranged from 5 to 20 mg dm^{-3} . For each measurement, metal solutions were prepared by adding different volumes of metal stock solutions to 50.0 cm^3 volumetric flask along with 0.01 mol dm^{-3} NaCl, and adjustment of pH with the addition of 0.1 mol dm^{-3} NaOH and/or 0.1 mol dm^{-3} HCl. Accurately weighed 0.100 g of cleaned, Na-saturated cation exchange resin Dowex 50WX8 (100–200 mesh) was added to 50.0 cm^3 of the prepared metal solutions. All samples were shaken for 2 h, at constant temperature of 25°C .

The ion-exchange procedure used to determine stability constants for ligands and divalent metal ion was similar to the procedure used to establish the distribution coefficient, D_0 , with difference that the solution contained ligand. Each solution contained variable concentration of metal ions, from 5 to 20 mg dm^{-3} for each metal, and concentration of humic acid, from 0.005 to $0.015 \text{ mol dm}^{-3}$. The solution was adjusted to pH 4.0, 0.100 g of resin in the Na-form was added and solutions were equilibrated under the same conditions as previous. Each determination was carried out in triplicate.

RESULTS AND DISCUSSION

The ion-exchange equilibrium method originally developed by Schubert, and first applied to water soluble organic matter complexes by Miller and Ohlrogge, is the most attractive procedure for the determination of stability constants [19,20]. The equilibrium reaction for chelate or complex formation can be written as:



$$K = \frac{[M][L]^n}{[ML_n]} \quad (2)$$

The distribution coefficient, D_0 , between the resin and solution phase for metal ion in the absence of ligand and the distribution coefficient, D , between the resin and solution phase for metal ion in the presence of ligand was calculated by equilibrium ratio:

$$D_0 = \frac{\alpha_0 V}{(100 - \alpha_0)m_r} \quad (3)$$

where α_0 is the percentage of total metal bound to exchange resin; $(100 - \alpha_0)$ is the percentage of total metal remaining in solution; V is the volume of solution (cm^3) and m_r is the weight of exchange resin (g).

The number of equivalents of the complexing agent, n , combined with a particular metal ion was found from the slope of the linear function:

$$\log\left(\frac{D_0}{D} - 1\right) = \log \beta_{mn} + n \log c_L \quad (4)$$

where c_L is the concentration of ligand (mol dm^{-3}).

Equation (4) is used to determine conditional stab-

ility constants for mononuclear complexes. Possible problems with the Schubert's method occur when the complex, M_mL_n , is not mononuclear ($m \neq 1$). The following equation of the modified Schubert's method is used to eliminate this source of errors and presents the modified method of data treatment and analysis:

$$\begin{aligned} \log M_c &= \log\left(\frac{D_0}{D} - 1\right) = \\ &= \log m + \log \beta_{mn} + (m-1)\log M + n \log c_L \end{aligned} \quad (5)$$

Equation (5) is used to calculate the $\log \beta_{mn}$ for polynuclear complexes. Equation (4) is a reduced form of Eq. (5) for the case when $m = 1$, when a mononuclear complex is present [21–23].

The isotherms for each metal ion were investigated at 25 °C temperature and pH 4.0 in order to avoid hydrolysis of metal ions and carbonate formation. Humic acid was characterized in detail previously [24].

The isotherm linear range was obtained for each metal, in order to estimate D_0 and choose the appropriate concentrations for preventing the effect of metal loading [21–24].

Table 1 gives a summary of the percentage of total metal bound to exchange resin, α_0 , distribution coefficient between the resin and solution phase for metal ion in the absence (D_0) and presence (D) of ligand for

Table 1. Experimentally determined percentage of total metal bound to exchange resin, α_0 , distribution coefficients, D_0 , metal-ligand ratio and logarithm of conditional stability constant, $\log \beta_{mn}$, for complexes Pb(II), Cu(II), Zn(II), Ni(II) and Co(II) (5 mg dm⁻³) with humic acid, at pH 4.0 and ionic strength of $I = 0.01$; M:L = 1:1

Metal ion	$c_{HA} \times 10^3 / \text{mol dm}^{-3}$	α_0	D_0	D	$\log(D_0/(D-1))$	Log β_{mn}	
						Determined	Mean
Co(II)	0	61.14	786.67	—	—	—	1.95
	5	50.36			507.25	-0.259	2.04
	10	46.46			433.88	-0.090	1.91
	20	41.78			358.81	0.076	1.89
Ni(II)	0	12.48	71.30	—	—	—	2.24
	5	6.94			37.29	-0.040	2.26
	10	4.84			25.43	0.256	2.26
	20	4.10			21.37	0.368	2.19
Cu(II) ^a	0	58.52	705.4	—	—	—	2.33
	5	49.28			485.80	-0.347	2.25
	10	27.00			184.93	0.449	2.45
	20	20.84			131.63	0.639	2.29
Zn(II)	0	31.04	225.06	—	—	—	2.25
	5	18.74			115.31	-0.021	2.28
	10	14.46			84.522	0.221	2.22
	20	11.02			61.924	0.421	2.24
Pb(II) ^a	0	52.56	553.96	—	—	—	2.50
	5	29.40			208.21	0.220	2.52
	10	24.20			159.63	0.393	2.39
	20	14.00			81.39	0.764	2.59

^a Results for Cu(II) and Pb(II) are previously reported and are taken from reference [24]

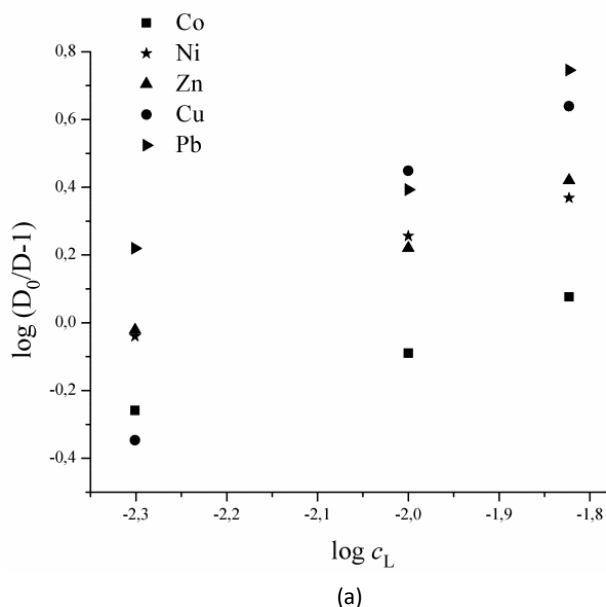
each of five metals, and values of stability constants, $\log \beta_{mn}$. The presented results show the obtained parameters only for 5 mg dm⁻³ metal ions concentration, while the investigations were done at 10, 15 and 20 mg dm⁻³ metal ions concentrations as well.

The results in Table 1 show that the percentage of total metal bound to exchange resin, α_0 , for Co(II) was 61.14% and was the highest comparing to other metal ions Cu(II) (58.52%), Pb(II) (52.56%), Zn(II)(31.04%) and Ni(II) (12.48%). For each metal ion, the percentage of total metal bound to the exchange resin, α_0 , decreased with increase of humic acid concentration. This trend was expected because by increasing humic acid concentration, the number of binding sites increases and

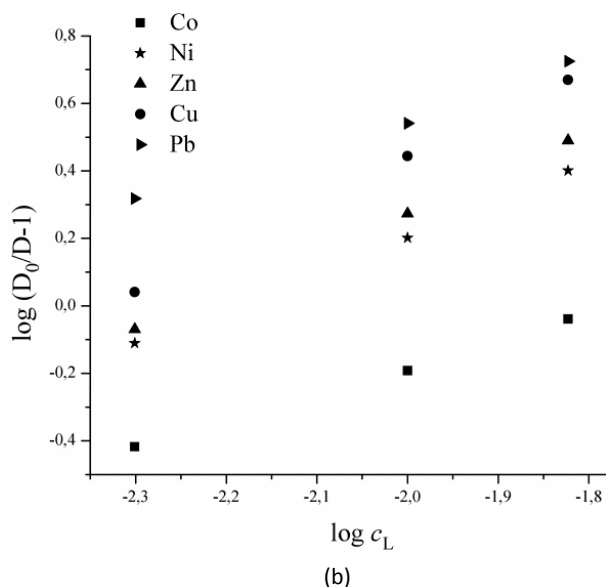
therefore, the amount of metal absorbed on the resin is reduced.

Figure 1 presents plots of $\log(D_0/(D-1))$ vs. $\log c_L$ for each metal ion at four concentrations.

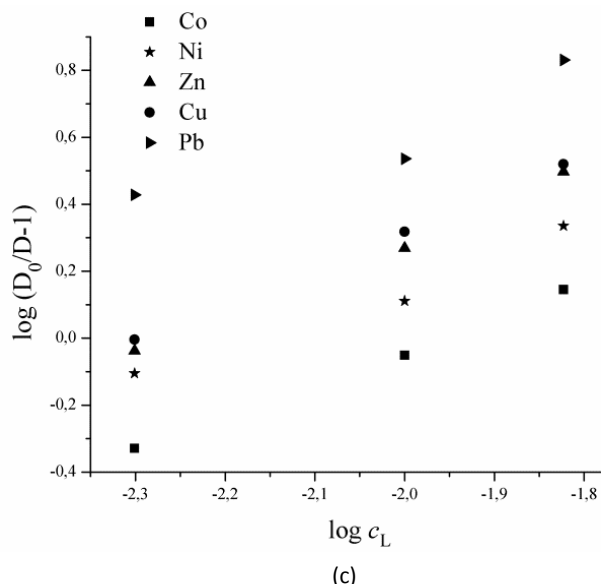
The slopes of the plots presented in Figure 1 give the composition of complexes. Values of n close to unity indicate that the metal ligand ratio in these complexes is 1:1. Also, Figure 1 shows that the stability sequence of the metal ions under the given conditions is: Co(II) < Ni(II) < Zn(II) < Cu(II) < Pb(II). All these transition metals tend to favor formation of a covalent or coordination bond with the humic ligand with partial or total breakdown of the hydration sphere of the metal. Thus, the investigated metals are more tightly held pre-



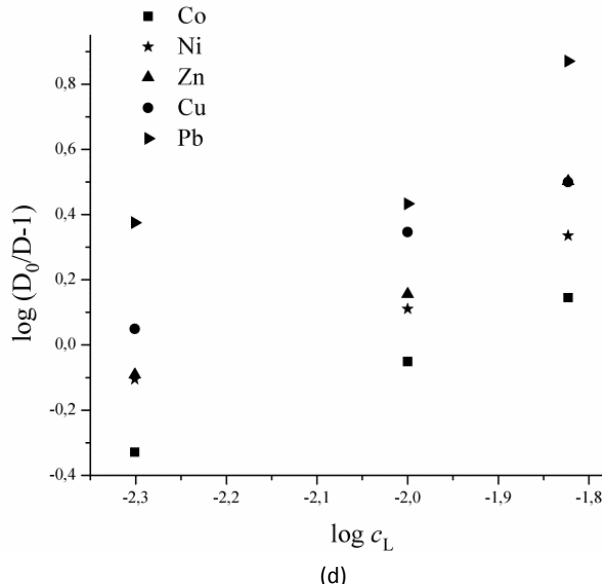
(a)



(b)



(c)



(d)

Figure 1. Schubert's plots of the ratio of complexed metal to free metal ($\log(D_0/(D-1))$) versus $\log c_{HA}$ for Pb(II), Cu(II), Zn(II), Ni(II) and Co(II) ions with humic acid and concentration of metal ion: a) 5; b) 10; c) 15; d) 20 mg dm⁻³.

ferably creating inner sphere complexes than for example, alkali and alkaline earth metals which tend to favor creation of outer sphere complexes, with bonds of purely electrostatic nature, where metal retain their hydration spheres [20].

The stability constants, $\log \beta_{mn}$, and metal-ligand ratios for complexes between each concentration of Pb(II), Cu(II), Zn(II), Ni(II) and Co(II) ions with humic acid are summarized in Table 2.

The obtained stability constants, $\log \beta_{mn}$, show that the investigated divalent ions follow the Irving-Williams series type: Co(II) < Ni(II) < Cu(II) > Zn(II) for the binding strength of divalent metal ion complexes in complexation with humic acid, therefore to interact according to the basic principles of the formation of the complex. The Irving-Williams order is based on empirical observation and related to both the increase of effective nuclear charge and increase of atomic number. The position of Cu(II) in the Irving-Williams order is considered out-of-line (Mn(II) < Fe(II) < Co(II) < Ni(II) < Cu(II) > Zn(II)), probably as a consequence of the fact that Cu(II) often forms distorted octahedral complexes. The different affinity of Pb(II), Cu(II), Zn(II), Ni(II) and Co(II) can be explained by their chemical properties such as the size of ion radius (r_M^{2+}), charge (z) of the metal ion, that is ionic potential, $I_p = z/r$, the electronegativity of the element, ligand field stabilization energy effects and classification, which is based on the electron configuration of the cations and the concept of hard/soft acids and bases (HSAB theory) [23,24].

Stability constants obtained for complexes between Cu(II), Zn(II), Ni(II) and Co(II) and humic acid were founded to be smaller than stability constant obtained for Pb(II) humate complex, which can be explained with HSAB theory. Humic acids behave as weak acid polyelectrolytes with a variety of oxygen containing functional groups such as carboxylic, hydroxyl, phenolic and carbonyl, with oxygen as a donor atom show hard base properties (high electronegative atom) and make strong bonds with hard acids. According to the HSAB theory, cations Pb(II) and Cu(II) form stronger complexes with humic acids than with Co(II) and Zn(II). The affinity of the metals to humic acid can also be expected

to increase in line with increasing electronegativity. This seems to be true for Cu(II), Ni(II), Zn(II) and Co(II), but not for Pb(II). The tendency of cations to form inner-sphere complexes with humic acid increases with increasing ionic potential (I_p). For the group of divalent metal ions this means that the smaller the radius of the ion is, the more likely it is to be found in an inner-sphere complex. Inner-sphere complexes are usually much stronger than outer-sphere complexes associated with a hydrated cation and an anion held by long-range electrostatic forces [23,25].

Despite its low I_p , the Pb(II)-ion's great affinity to humic acid may be explained by its borderline acid properties. The electronic configuration of the Pb(II) ion is $(n-1) 18e^- + n2e^-$, which classifies it as a borderline metal acid and results in greater stability of the Pb(II)-humate complex comparing to other complexes. On the other hand, Cu(II) and Zn(II) are classified as soft acids and do not form stable complexes with O-donor ligands, although should have high ability to coordinate with bases which contain N and/or S as donor ligands. According to this rule, the stability constant of complexes between these ions and humic acid is lower than the stability constant of Pb(II)-humate complex. Due to the large ion size of Pb(II), the electrons are easily polarized and to a lesser degree retained by the nucleus [25].

Comparison of the obtained results for stability constants and stoichiometry of complexes Pb(II), Cu(II), Zn(II), Ni(II) and Co(II) with humic acid with literature data, indicate that the values are approximately equal. Variation of stability constants values in humic complexation studies is not uncommon due to differences in humic's elemental composition, their chemical structure and period of genesis during the humification process [20–22,26].

The established trend of metal-humate complexes stabilities can be used for predicting the strength of interaction between the humics and metal ions, as well as to predict their competition in binding to humate ligand. The obtained results indicate that there may be competition between these metal ions in the binding for humate macromolecules. Therefore, in conditions

Table 2. Stability constants, $\log \beta_{mn}$, and metal-ligand ratio for complexes of Pb(II), Cu(II), Zn(II), Ni(II) and Co(II) with humic acid, at pH 4.0 and ionic strength of $I = 0.01$; M:L = 1:1

Metal ion	Log β_{mn}			Mean value	Literature values [22,23,26–30]		
	$c_{HA} \times 10^3 / \text{mol dm}^{-3}$						
	5	10	15				
Co(II)	1.96	1.91	1.93	1.93	2.82–6.05		
Ni(II)	2.21	2.17	2.18	2.19	1.56–3.20		
Cu(II) ^a	2.31	2.39	2.36	2.35	1.95–5.28		
Zn(II)	2.24	2.23	2.30	2.26	2.74–4.70		
Pb(II) ^a	2.64	2.47	2.62	2.58	2.76–5.32		

^a Results for Cu(II) and Pb(II) are previously reported and are taken from reference [24]

of increased concentrations of metal ion in the natural environment, the metal ion may displace other ions, which can lead to increasing mobility and bioavailability of other metal ions.

The investigation reveals that humic acid can effectively bind heavy metals and due to this has potential to be used in remediation methods. For example, it can be used in wastewater treatment for heavy metal removal, as a metal detoxification agent for industrial and domestic effluents, which contain high levels of such heavy metals. Due to the ability to form complexes, humic acid also promotes retention and accumulation of heavy metals and thus, can be used in remediation processes.

CONCLUSION

Our results provide information on the interaction of Pb(II), Cu(II), Zn(II), Ni(II) and Co(II) with humic acid and distribution of those heavy metals through soil-/water natural systems. Schubert's method can be used not only for stoichiometrically defined ligands but also for complexes of polyfunctional and stoichiometrically undefined ligands, such humic ligands are. The obtained results derived using Schubert's method indicate that the stability constant, $\log \beta_{mn}$, for the Pb(II)-humate complex was greater than that of other investigated humate complexes at pH 4.0. All investigated humic complexes showed 1:1 stoichiometry.

The established trend of metal-humate complexes stabilities, which follows the Irving-Williams series, can be used for predicting the strength of interaction between the humics and metal ions, thus for predicting mobility and bioavailability of metal ions.

Acknowledgement

This study was supported by the Ministry of Education, Science and Technological Development of the Republic of Serbia and was performed as a part of Project III41018.

REFERENCES

- [1] A. Dube, R. Zbytniewski, T. Kowalkowski, E. Cukrowska, B. Buszewski, *Pol. J. Environ. Stud.* **10** (2001) 1–10.
- [2] J.M. Garcia-Mina, *Org. Geochem.* **37** (2006) 1960–1972.
- [3] S. Ross (ed.), *Toxic Metals in Soil–Plant Systems*, Wiley, New York, 1994.
- [4] I. Christl, R. Kretzschmar, *Environ. Sci. Technol.* **35** (2001) 2505–2511.
- [5] R. Sutton, G. Sposito, *Environ. Sci. Technol.* **23** (2005) 9009–9015.
- [6] J.P. Gustafsson, P. Pechova, *Environ. Sci. Technol.* **37** (2003) 2767–2774.
- [7] C.A. Coles, R. Yong, *Eng. Geol.* **85** (2006) 26–32.
- [8] I.I. Lishtvan, F.N. Kaputskiy, Y.G. Yanuta, A.M. Abramets, V.P. Strigutskiy, E.V. Kachanova, *Chem. Sustain. Dev.* **14** (2006) 267–373.
- [9] I. Christl, C. Milne, D. Kinniburgh, R. Kretzschmar, *Environ. Sci. Technol.* **35** (2001) 2512–2517.
- [10] D. Sparks, *Environmental soil chemistry*, 2nd ed., Academic press, San Diego, CA, 1995.
- [11] C. Rey-Castro, P. Lodeiro, R. Herrero, M. Sastre de Vicente, *Environ. Sci. Technol.* **37** (2003) 5159–5167.
- [12] L.J. Evans, B. Sengdy, D.G. Lumsdon, D.A. Stanbury, *Chem. Speciation Bioavail.* **15** (2003) 93–100.
- [13] T. Andjelković, J. Perović, M. Purenović, D. Andjelković, *Facta Universitatis*, **3** (2004) 79–85.
- [14] E. Tipping, *Cation binding of humic substances*, 1st ed., Cambridge University Press, Cambridge, 2002.
- [15] M. Schizer, S.U. Kahn, *Humic substances in the Environment*, Dekker, New York, 1972.
- [16] J.M. de la Rosa, M. Santos, M.F. Araujo, *Estuarine Coastal Shelf Sci.* **93** (2011) 478–485.
- [17] K. Furukawa, Y. Takahashi, *Chemosphere* **73** (2008) 1272–1278.
- [18] [18] S. Wang, C. N. Mulligan, *Chemosphere* **74** (2009) 274–279.
- [19] J. Schubert, *Theoret. J. Phys. Colloid Chem.* **52** (1947) 340–350.
- [20] J. Schubert, J. W. Richter, *Theoret. J. Phys. Colloid Chem.* **52** (1947) 350–357.
- [21] H. Baker, F. Khalili, *Anal. Chim. Acta* **497** (2003) 235–248.
- [22] H. Baker, F. Khalili, *Anal. Chim. Acta* **542** (2005) 240–248.
- [23] H. Baker, F. Khalili, *Ann. Environ. Sci.* **1** (2007) 35–44.
- [24] I. Kostić, T. Andjelković, R. Nikolić, A. Bojić, M. Purenović, S. Blagojević, D. Andjelković, *J. Serb. Chem. Soc.* **76** (2011) 1–12.
- [25] F.A. Cotton, G. Wilkinson, C.A. Murillo, M. Bochmann, *Advanced Inorganic Chemistry*, 6th ed., Wiley, New York, 1999.
- [26] E. Giannakopoulos, K.C. Christoforidis, A. Tsipis, M. Jerzykiewicz, Y. Deligiannakis, *J. Phys. Chem., A* **109** (2005) 2223–2232.
- [27] K. Gao, J. Pearce, J. Jones, C. Taylor, *Environ. Geochem. Health* **21** (1999) 13–26.
- [28] K. Pandey, S.D. Pandey, V. Misra, *Ecotoxicol. Environ. Saf.* **47** (2000) 195–200.
- [29] T.I. Nifant'eva, P. Burba, O. Fedorova, V.M. Shkinev, B. YaSpivakov, *Talanta* **53** (2001) 1127–1131.
- [30] J.Z. Du, W.J. Li, H.Q. Zhang, X.D. Wang, Z.J. You, C.Y. Zhou, W.M. Dong, Z.Y. Tao, *J. Radioanal. Nucl. Chem.* **241** (1999) 651–654.

IZVOD**UPOREDNA ISPITIVANJA JAČINE VEZIVANJA JONA TEŠKIH METALA SA HUMINSKOM KISELINOM**

Ivana S. Kostić¹, Tatjana D. Andđelković¹, Ružica S. Nikolić¹, Tatjana P. Cvetković², Dušica D. Pavlović², Aleksandar Lj. Bojić¹

¹Univerzitet u Nišu, Prirodno-matematički fakultet, Višegradska 33, 18000 Niš

²Univerzitet u Nišu, Medicinski fakultet, Bul. Zorana Đindjića 81, 18000 Niš

(Naučni rad)

Kontaminacija životne sredine teškim metalima predstavlja opasnost za žive organizme. Pošto metali nisu biorazgradivi, ali su rastvorljivi u vodi, oni mogu postati dostupni živim organizmima i može doći do njihove akumulacije u životnoj sredini. Najveća kontaminacija životne sredine teškim metalima javlja se u blizini industrije metala. Teški metali mogu učestvovati u složenim hemijskim i biološkim procesima. Faktori koji utiču na njihovu pokretljivost kroz zemljišne i vodene sisteme su pH, redoks potencijal, priroda sistema, prisustvo različitih materija koje mogu imati ulogu sorbenta, prisustvo i količina organskih liganda, uključujući huminske i fulvo kiseline i prisustvo neorganskih liganda. Procesi vezivanja, transporta, biodostupnosti i mobilnosti jona metala u zemljištu i vodenim sistemima u velikoj meri zavise od interakcije sa huminskim supstancama. Joni metala mogu nagraditi rastvorne komplekse sa huminskim supstancama i tako prouzrokovati kontaminaciju površinskih i podzemnih voda, usled zadržavanja metala u zemljišnom rastvoru. Takođe, može doći i do stvaranja nerastvornih kompleksa, i akumulacije metala u zemljištu i sedimentima. U ovom radu vršena su uporedna ispitivanja kompleksa jona teških metala (Co(II), Ni(II), Cu(II), Zn(II) i Pb(II)) sa huminskom kiselinom. Vrednosti konstanti stabilnosti formiranih kompleksa određene su pomoću Šubertove jonoizmenjivačke metode, koja se zasniva na raspodeli količine metala između smole i vodene faze u sistemima sa i bez prisustva liganda. Ispitivanja su vršena na pH 4,0, temperatura od 25 °C i pri jonskoj jačini od 0,01 mol dm⁻³. Utvrđeno je da joni ispitivanih metala sa huminskom kiselinom grade mononuklearne komplekse, 1:1. Dobijene vrednosti konstante stabilnosti formiranih kompleksa prate redosled Co(II) < Ni(II) < Cu(II) > Zn(II), koji odgovara raspolisu u Irving-Vilijamsovoj seriji jačine vezivanja, koja je određena za dvovalentne jone. Vrednost konstante stabilnosti dobijene za kompleks formiran između Pb(II) jona i huminske kiseline veća je u odnosu na vrednosti konstanti stabilnosti ostalih ispitivnih kompleksa. Rezultati dobijeni ispitivanjem interakcije jona teških metala sa huminskom kiselinom mogu se koristiti za predviđanje distribucije i kontrolu migracije teških metala u prirodnom okruženju.

Ključne reči: Zagađenje teškim metalima

- Huminska kiselina • Konstanta stabilnosti

Change of sensory characteristics and some quality parameters of mixed milk and cocoa spreads during storage up to 180 days

Jovanka V. Popov-Raljić¹, Jovanka G. Laličić-Petronijević², Etelka B. Dimić³, Vladimir S. Popov⁴, Vesna B. Vučasinović⁵, Ivana V. Blešić¹, Milijanko J. Portić¹

¹University of Novi Sad, Faculty of Science, Trg Dositeja Obradovića 3, 21000 Novi Sad, Serbia

²University of Belgrade, Faculty of Agriculture, Nemanjina 6, 11080 Belgrade – Zemun, Serbia

³University of Novi Sad, Faculty of Technology, Bulevar Cara Lazara 1, 21000 Novi Sad, Serbia

⁴University of Novi Sad, Faculty of Agriculture, Trg Dositeja Obradovića 8, 21000 Novi Sad, Serbia

⁵College of Professional Studies in Management and Business Communication, Mitropolita Stratimirovića 110, Sremski Karlovci, Serbia

Abstract

The main role of milk and milk products in the technology of confectionery products (chocolates, caramels-candy products, dairy products, spreads, etc.) is to increase the nutritional value of the final product and to influence some sensory characteristics of quality (appearance, consistence/texture, flavor). In this study, mixtures of milk and cocoa spreads of a new composition with increased content of milk components were produced, and then assessed for sensory quality traits, peroxide value, free fatty acid content and the content of heavy metals (lead, cadmium and copper) during storage from 30 to 180 days at room temperature (18–20 °C). The samples were evaluated using the analytical-descriptive sensory analysis (point system) with description of the dominant properties (appearance-color, surface gloss, consistence-spreadability, dynamic property of melting, the consistence in the oral cavity–oiliness and flavor–odor and taste). The results of sensory analysis were statistically analyzed using two-way analysis of variance MANOVA, LSD and Levene's test. Based on the obtained results, it can be concluded that the composition of mixtures of milk and cocoa spreads significantly affects all characteristics, whereas the storage time significantly affects the appearance, consistence, i.e., spreadability, and taste of the product.

Keywords: sensory analysis, spreads, peroxide value, free fatty acid, heavy metals, storage.

Available online at the Journal website: <http://www.ache.org.rs/HI/>

According to the rulebook on quality and other demands for cocoa products, chocolate products, products similar to chocolate and confectionery spreads [1], spreads are obtained by processing sugar, milk and dairy products, vegetable fats and other food products. Regarding the consistence, they are produced as: spreadable, bars, granules or "crispy" spread-cream products [2]. At the market they can be found as dairy cream-products, containing at least 12% of non-fat dry matter of milk (calculated on the whole product), mixtures of milk-spreads products, cacao-spreads products and others. Spreads are concentrated food with high energetic (about 2.272 kJ/100g) and nutritive value, and are favourite in the nutrition of children and sportists, but also of healthy grown-ups [3]. Condensed milk, milk powder, partially skimmed and skimmed milk powder are mostly used in the confectionery industry. Besides, milk crumb, "block milk", anhydrated milk fat,

whey powder, cheese powder, whey powder and serum proteins are also used [4–6].

The main physical and functional characteristics that affect the quality of milk powder are: powder structure, distribution of powder particles dimensions, density of particles, air incorporated in and between the particles, burnt particles, reconstruction ability, hygroscopy, heat-stability and emulsification stability. The reconstruction stability includes several characteristics of powder: solubility and moistening ability [7]. Milk powder used in the confectionery industry contributes to the nutritive value of the product, and improves the consistence (texture), odor taste and stability [6,8]. Whey powder contains proteins with high-valueable amino acids, milk sugar – lactose, vitamins and mineral components from the milk. Besides the improvement of flavor, whey powder also affects better texture, better stability of the product. The main role of milk products is to increase the nutritive value of confectionery products, and to influence some sensory characteristics – flavor, color, texture and others [5,6]. Condensed whey, i.e., syrup-like product with 80 to 85% of dry matter, can be also used in the confectio-

Correspondence: J.G. Laličić-Petronijević, University of Belgrade, Faculty of Agriculture, Nemanjina 6, 11080 Belgrade – Zemun, Serbia.

E-mail: jovankal@agrif.bg.ac.rs

Paper received: 3 September, 2012

Paper accepted: 9 January, 2013

SCIENTIFIC PAPER

UDC 663.914/.916:66

Hem. Ind. **67** (5) 781–793 (2013)

doi: 10.2298/HEMIND120903004P

nery industry. When condensed whey is used, the colour of the final products (caramele) is darker [9]. Serum proteins are mainly used to achieve the appropriate nutritive value of the final product, and to improve some functional characteristics: foam or gel formation, production and stabilization of emulsion [4,10]. A number of authors [2,11,12] cite that sugar can be completely or partially replaced with sweeteners (fructose, maltitol, lactitol and xylitol) in accordance with the rulebook on quality and conditions of use of additives in food products and other demands for additives and their mixtures [1].

As one of the main constituents of chocolate products, with content in spreads between 25 and 40%, fats are an important raw material that affect the behaviour of spreads during the processing, and a number of quality characteristics of the final product – taste, melting, mouth-feel, consistence/texture, other physical characteristics of these products, as well as their nutritive value [13,14]. Due to economic reasons, cocoa butter is often replaced with special vegetable fats, *i.e.*, cocoa butter substitutes and/or replacers. These fats are obtained by different technological processes from natural oils and fats and oils like palm oil [15], cocoa-fat, rapeseed oil, palm seed oil, etc. [13], and can completely or partially replace the traditional chocolate fat – cocoa butter. These fats can be found at the market, with different names, kind of raw material, way of processing and recommended use.

The tempering of products is not necessary when cocoa butter substitutes and replacers are used [16]. Nowadays, the opinion of the consumers is that hydrogenated oils and fats, containing saturated or *trans* isomers of unsaturated fatty acids, are undesirable in the nutrition [16]. Besides having a negative effect on the cardio-vascular system [17], the *trans* fatty acids are also related to the development of some types of carcinomas, type 2-diabetes, allergies and asthma in children and thrombosis [13]. Therefore, hydrogenated fats are partially replaced with vegetable oils in the formula of nutritively high-valuable products. The use of cocoa powder results in lower energetic value of the product, however, this ingredient is a source of fiber and mineral components. Cocoa powder resembles chocolate, due to specific cocoa flavor and therefore is an ingredient in a number of products. Non-fat cocoa products, with fat content < 8%, enables better mixing with special fats [3]. Spreadable cream products should have certain sensory quality characteristics, *i.e.*, smooth and shiny surface, soft consistence, *i.e.*, spreadability, and characteristic flavor. Spreadable consistence should remain in the temperature interval from 8 to 20–22 °C. Investigation of rheological characteristics of domestic commercial spreads has shown that they express pseudo-plastic behaviour [14]. The mentioned products

are characterized by rich creamy, milky-chocolate taste, with a light flavor of roasted hazelnut [12,14,18] or added peanut [19]. Petkovic *et al.* [12] dealt with sensory analysis of cocoa spreads with sucrose, as well as those with full or partial replacement of sucrose with maltitol, in which they have evaluated the following sensory properties: shape, color, surface, texture, chewiness, taste and odor.

The main goal of this paper was to produce new products – spreads, under semi-industrial conditions, of appropriate composition and stability, without antioxidants and preservation agents, from mixtures of: defatted (skimmed) milk powder, whey powder and their combinations, hydrogenated vegetable fat (*trans* fatty acids < 10%) and refined sunflower oil, cocoa-powder and hazelnut. The other aspect was the sensory evaluation of the obtained spread *i.e.* acceptability (appearance, texture/consistence, flavor) and investigation of some quality parameters important for safety of the products.

MATERIALS AND METHODS

In this study, correction of the standard industrial recipe for mixtures of milk and cocoa spreads was performed in order to obtain better sensory acceptability of the final products, as well as improved composition (increased content of dairy products, the use of cocoa powder with reduced amount of fat).

Preparation of samples

The basic raw materials for the production of milk and cocoa-cream products were skimmed powdered milk and whey powder (obtained from Mlekara Subotica, Subotica); hydrogenated vegetable fat (*trans* fatty acids < 10%) and refined sunflower oil (Dijamant, Zrenjanin); cocoa powder (Centroproizvod, Belgrade); roasted dehulled hazelnut (Florida Bel, Belgrade-Zemun); powdered sugar and vanilla sugar (Centroproizvod, Belgrade); defatted soybean flour and soy lecithin (Sojaprotein, Bečej). All raw materials were produced in Serbia. The roasted and dehulled hazelnut was ground to obtain hazelnut pasta. With the addition of skimmed milk powder, whey powder, powdered sugar, a part of vegetable fat/oil, cocoa-powder, soybean flour, a pastose cream mass was obtained. At the end, the remaining fat/oil, lecithin and vanilla sugar were added. The prepared cream-mass was milled and homogenized in the colloid mill (Frima-Rheinfelden, Germany).

The size of the largest particles in the final product was from 30–50 µm. The samples were packed in appropriate glass packagings (200 ml glass jars) and stored at room temperature up to 180 days.

Sample 1. Sugar, 20% skimmed milk powder (min 8.5% non-fat dry matter of milk), hydrogenated vege-

table fat, refined sunflower oil, cocoa powder with reduced cocoa-butter content (min. 2.5% dry non-fat cocoa solids), soybean flour, emulsifier – lecithin, vanilla sugar.

Sample 2. Sugar, 15% skimmed milk powder (min. 8.5% non-fat dry matter of milk), hydrogenated vegetable fat, cocoa powder with reduced content of cocoa-butter (min. 2.5% dry non-fat cocoa solids), hazelnut paste, soybean flour, emulsifier – lecithin, vanilla sugar.

Sample 3. Sugar, 10% skimmed milk powder, 5% whey powder, refined sunflower oil, hydrogenated vegetable fat, cocoa powder with reduced cocoa-butter content (min. 2.5% dry non-fat cocoa solids), hazelnut paste, emulsifier – lecithin, vanilla sugar.

Sample 4. sugar, 12% skimmed milk powder, refined sunflower oil, hydrogenated vegetable fat, cocoa powder with reduced content of cocoa-butter (min. 2.5% dry non-fat cocoa solids), emulsifier – lecithin, hazelnut paste, vanilla sugar.

Sample 5. Sugar, 20% whey powder, hydrogenated vegetable fat, refined sunflower oil, emulsifier – lecithin, hazelnut paste, cocoa powder with reduced cocoa-butter content (min. 2.5% dry non-fat cocoa solids), vanilla sugar.

Sensory analysis of quality

Ten experienced assessors evaluated the sensory quality of mixtures of milk and cocoa spreads [20,21]. The appearance (colour, surface gloss), consistence/texture (spreadability, dynamic melting property and oiliness), flavor (odor and taste) and overall sensory quality of mixed milk and cocoa spreads were evaluated (Table 1).

Twenty individual samples were evaluated from every group of samples, 1, 2, 3, 4 and 5 ($n = 100$). The sensory evaluation was performed in a laboratory [22] at room temperature 18–20 °C. The scoring system (from 1.00 to 5.00) was applied for the sensory eva-

Table 1. Sensory evaluation of spreads quality

Property	Characteristic	Coefficient of significance	Description	Score
Appearance	Visually evaluated characteristic of: - colour - surface shine	2.00	Excellent colour, smooth shiny (bright) surface Unexceptionable color, surface smooth and shiny Poorer color, unsufficiently shiny surface, inside air-bubbles Partially uniform of shade and gloss of surface color Nonuniform shade and gloss of surface color	5.00 4.00 3.00 2.00 1.00
Texture	Visually evaluated characteristic of: - consistence - spreadability	4.00	Characteristic consistence and spreadability Very good consistence and spreadability Good consistence and spreadability Inappropriate consistence and spreadability Unsatisfactory consistence and spreadability	5.00 4.00 3.00 2.00 1.00
	Orally evaluated dynamic characteristic of melting ^a , - oiliness	6.00	Characteristic melting and characteristic oily coating of oral cavity Very good melting and oily coating of oral cavity Good melting and good oily coating of oral cavity Inappropriate melting and insufficient oily coating of oral cavity Unsatisfactory melting and insufficient oily coating of oral cavity	5.00 4.00 3.00 2.00 1.00
Flavor	Olfactorily evaluated characteristic of: - odor	2.00	Characteristic, pleasant odor of certain (distinct) note that can be identified Characteristic, pleasant odor Bland pleasant but unsufficiently intensive odor Unsufficiently intensive, undefined odor Without odor, atypical odor note	5.00 4.00 3.00 2.00 1.00
	Orally evaluated dynamic characteristic of: - taste	6.00	Characteristic, pleasant archaic taste Characteristic pleasant taste Bland pleasant but unsufficiently intensive taste Unsufficiently expressed taste or tasteless No taste or distasteful	5.00 4.00 3.00 2.00 1.00

^aDynamic melting characteristic – contact with skin or in the mouth, and the term time/intensity refers to time necessary for the change of state and feeling in the mouth (melting in the mouth – without chewing)

luation, with possibility of use half or a quarter point. A weight coefficient (WC) was determined for each quality characteristic (appearance, texture/consistence and flavor) in order to correct (by multiplying) the obtained score. The coefficients depend on the influence of certain characteristics on the overall quality and are balanced in such a manner that their sum is 20. The sum of individual scores (points) is a complex parameter representing the total sensory quality, and is expressed as the % of maximal possible quality. Dividing this value with the total sum of weight coefficient (WC = 20), the weighted mean score is obtained, representing the total sensory quality of the assessed spreads.

The quality category was determined depending on the range of marks: products which were evaluated with less than 2.5 points, were considered as unsatisfactory, *i.e.*, as unacceptable; scores within limits 2.5–3.5 characterized good quality products, 3.5–4.5 very good quality and 4.5–5 – excellent products [5,23].

The data obtained in the investigations performed in this study were analyzed by descriptive and analytical statistics. Basic parameters of the descriptive statistics included calculations of the arithmetic mean values, and variability parameters of the investigated properties included determinations of standard deviations (S_d) and variation coefficients (C_v) expressed in percents.

For analytical statistics (for evaluation of sensory determinations) the two factorial analysis of variance MANOVA was applied, with the first factor being the storage time, and the second one – the composition of the evaluated samples of mixtures of milk and cocoa spreads, as well as the LSD test (test of the least significant differences of pairs). For finding out if the prerequisites for variance analysis methods are justified, homogeneities of variances were determined using Levene's test [24].

Determination of peroxide value – PV

The PV of the fat phase was determined by standard iodometric method [25], used for the determination of oxidation products of oils and fats. The method is based on the reaction between the hydroperoxides and peroxides with HI acid, which is formed from KI in acidic media. The amount of separated I_2 is determined by titration with $Na_2S_2O_3$. The peroxide value is expressed as milimoles per kg.

Determination of free fatty acids content – FFA

The acidity of fat phase was determined by alkalometric titration method [26]. The chloroform solution of fat, obtained by cold extraction [27], was titrated with standard KOH solution till the change of indicator color. The used alkali amount is directly proportional to the amount of free fatty acids. The acidity is expressed

as the content of free fatty acids calculated on % of oleic acid.

Determination of heavy metals content by atomic absorption spectrometry

The content of bioresidues, *i.e.* lead, cadmium and copper in the investigated spread samples, was determined by atomic absorption spectrometry (AAS) on Spektrolab AA 202 (England). The heavy metals were determined at different wavelengths, lead – 217 nm, cadmium – 228.8 nm and copper – 324.26 nm.

The determinations are in accordance with the rule-book on amount of pesticides, metals and metalloids and other toxic substances, hemiotherapeutics, anabolics and other substances that can be present in food products [28].

RESULTS AND DISCUSSION

The changes of individual sensory properties (appearance: color, surface shine; texture: consistence, spreadability, melting and oiliness; flavour: odor and taste) of mixtures of milk and cocoa spreads during 180 days of storage are shown in Figures 1–5. The overall sensory quality during 180 days of storage is presented in Figure 6.

The mixture of milk and cocoa spread – sample 1 was of excellent sensory quality, during the first month after the production ($X_m = 4.59$, or 91.80% of the maximal possible quality). The appearance – color, surface gloss of sample 1 got somewhat lower mark, $X_m = 4.15$, since the dark (cocoa) and light (milk) phase were mixed (Figure 1). During the storage period of up to 180 days at room temperature, the overall sensory quality of sample 1 decreased by one quality category, *i.e.*, to very good, $X_m = 4.28$, or 85.70% (Figure 6) primarily due to moderate spreadability (Figure 2) and dynamic melting characteristics, as well as noticeable oiliness and sandiness (Figure 3). According to data presented earlier [11], sandiness may appear when lactitol (a substitute for saccharose) is used, since the proper granulation of this sweetener is somewhat hard to achieve.

The total sensory quality of fresh sample 2 was excellent, $X_m = 4.81$, or 96.3% of the maximal possible quality (Figure 1). On the basis of sensory evaluation for the 0–30 days period, the score for sensory characteristic – appearance of sample 2 was the highest of all examined samples – $X_m = 4.95$ (Figure 2). Furthermore, the dynamic characteristic of melting in the mouth was excellent and without oiliness (Figure 3). The visually evaluated consistence/textural and spreadability are also characteristic for spreadable cream products. The surface of this product was firm, smooth and moderately shiny. No sandiness was detected. The sample 2 was characterized by a distinct, pleasant milky flavor.

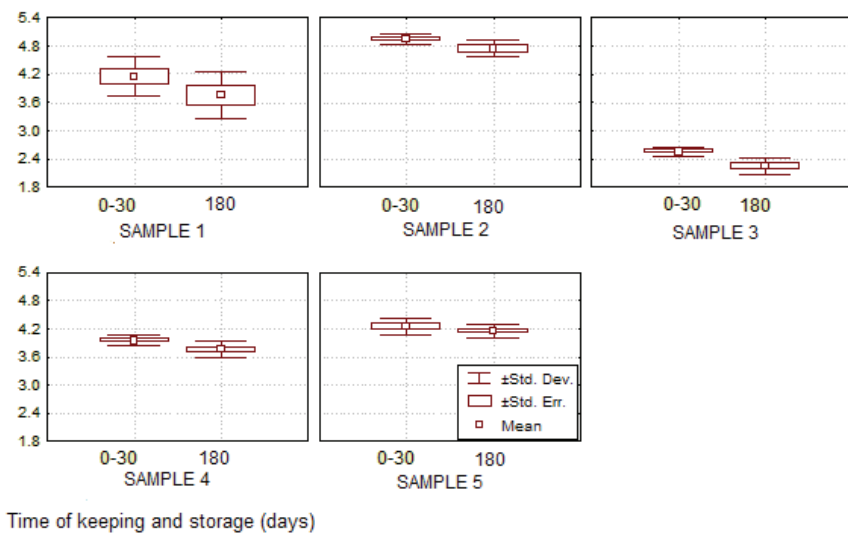


Figure 1. Box-plots for sensory characteristic – appearance.

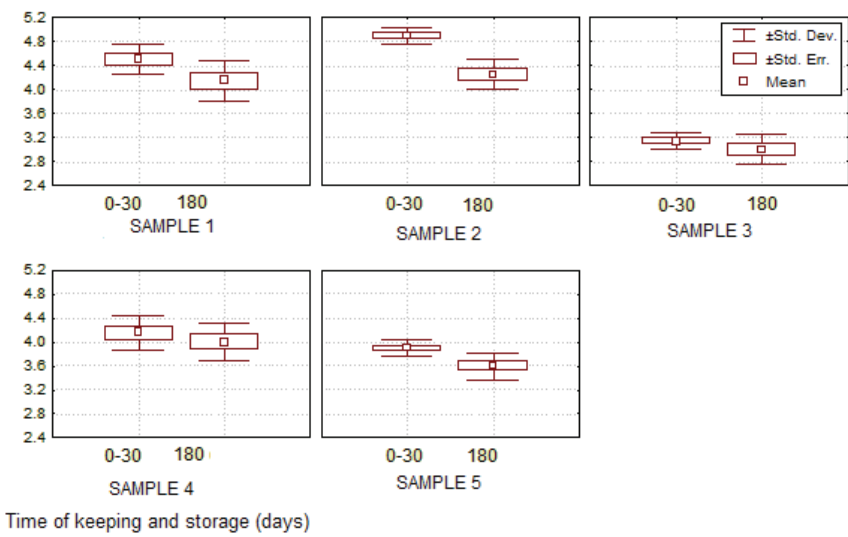


Figure 2. Box-plots for sensory characteristic consistence/texture, i.e., spreadability.

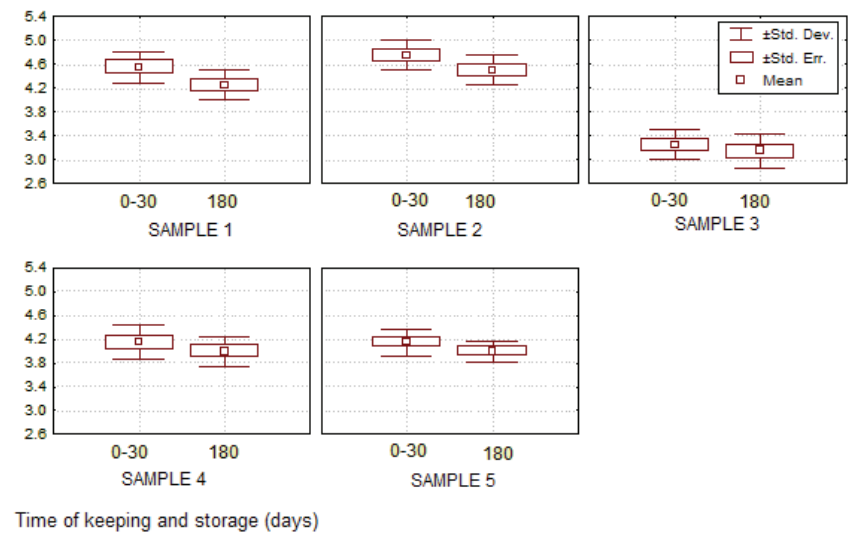


Figure 3. Box-plots for sensory property consistence/texture – as dynamic property melting and oiliness.

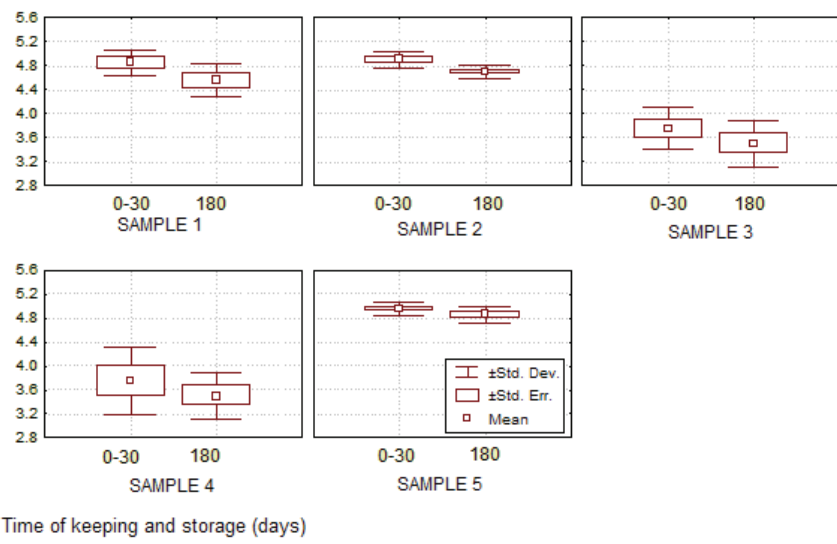


Figure 4. Box-plots for sensory property – flavor-odor.

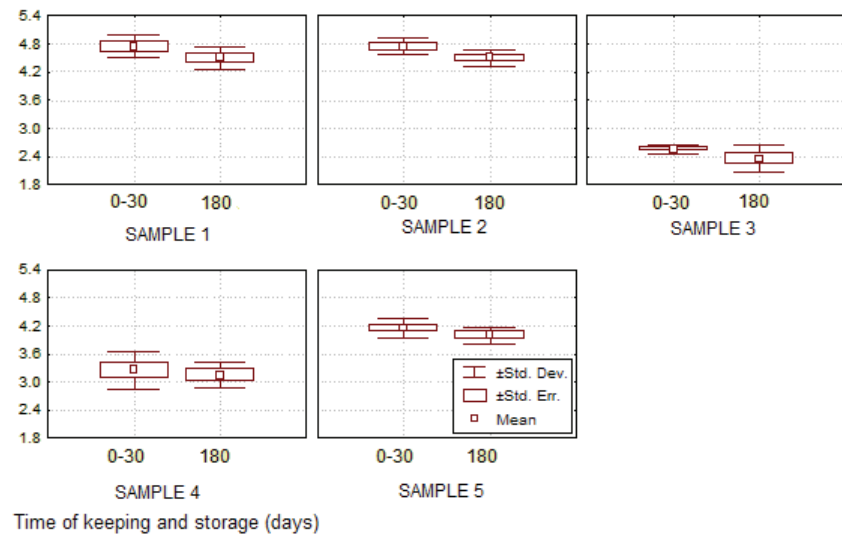


Figure 5. Box-plots for sensory property – flavor-taste.

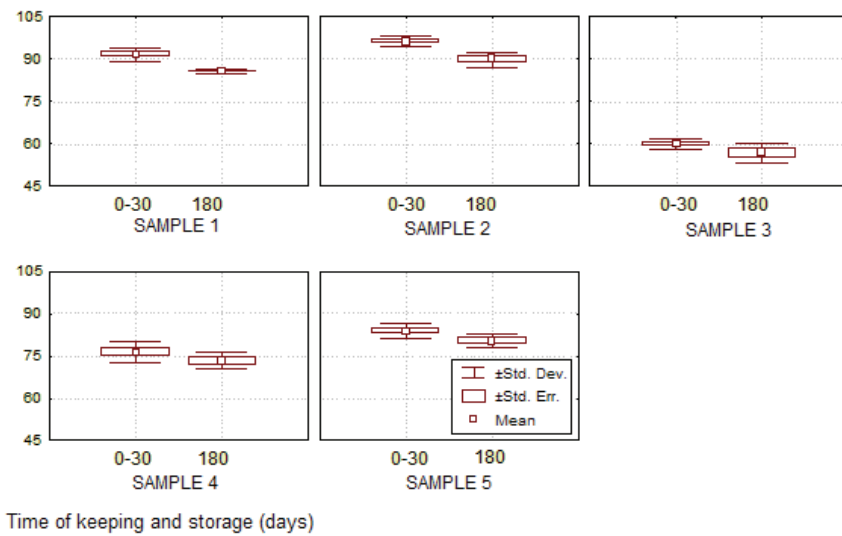


Figure 6. Box-plots for weighted mean value.

During the storage the sensory quality of sample 2 remained in the excellent quality category with average score $X_m = 4.50$, or 90.00% of the maximum possible quality (Figure 6), however, very near to very good quality due to slight decrease of milky note of odor intensity (Figure 4).

The sensory quality of cocoa-milk spread (sample 3) was the lowest compared to other samples, with total score $X_m = 3.00$, or 60% of the maximum possible quality at the first investigating period (0 to 30 days). Expressive surface oiliness and surface moisture was observed. Graining was also noticed. The sensory taste property score was significantly lower compared to other investigated samples, $X_m = 2.55$, due to slight rancidity (Figure 5). This sensation was more expressed after 180 days of storage. The changes of sample 3 were visible during the oral evaluation of texture, expressed in poorer dynamic property of melting and oiliness, *i.e.*, consistency. During storage, the sensory quality progressively deteriorated and after 180 days it was in the range of good quality category, $X_m = 2.83$, or 56.50% (Figure 6). Certain rancidity was estimated by olfactory evaluation of flavor-odor.

Immediately after production (0 to 30 days), sample 4 was of very good sensory quality, and remained in the same category throughout the whole storage period. The flavor-taste was scored $X_m = 3.25$ (Figure 5), due to certain change of taste (loss of milky flavor). By visual evaluation it could be noted that two phases (milk and cocoa) were not distributed equally. Minor changes of sensory characteristic – dynamic characteristic of melting and oiliness were observed orally.

The total sensory quality of sample 5, mixture of milk and cocoa spread, after production was $X_m = 4.19$, or 83.80% of the max possible quality (Figure 6). During storage up to 180 days, the sensory quality was very good $X_m = 4.02$, or 80.40%. This sample gained the highest score for olfactory characteristic flavor-odor, compared to all other samples: $X_m = 4.85$ (Figure 4), due to expressed pleasant characteristic hazelnut-like odor. Hazelnut paste contributes to pleasant taste and odor (flavor) and also improves the product nutritive value. Namely, hazelnut paste is rich in natural antioxidants and phytochemicals (phenolic compounds), with expressed antioxidative properties [29].

The orally estimated characteristic flavor-taste of sample 5 was scored somewhat lower, as the taste is pronouncedly sweet. Appearance of grainy structure was also observed, and by visual estimation it was found that the color of the milk phase was darker compared to other evaluated samples.

The results of Levene's test (Table 2) indicated that the data are homogenous for properties of consistency/texture, spreadability, melting-oiliness, further for flavor-taste and weighted average scores. For the properties of flavor-odor the data are non-homogenous at the level of significance $p < 0.05$, and for the sensory characteristic-appearance non-homogenous at the level of significance $p < 0.01$.

The results of two-factorial analysis of variance (Table 3) show that time of storage, as first observed factor, affect highly significantly ($p < 0.01$) the investigated sensory characteristics of appearance, consistency/texture-spreadability, flavor-taste and weighted mean value of scores; while significantly ($p < 0.05$)

Table 2. Results of Levene's test of homogeneity of variances of samples – mixtures of milk and cocoa spreads

Sensory quality characteristic	Levene's test	
	F	p
Appearance	3.488	0.003
Consistence/texture	Spreadability	1.033
	Dynamic melting characteristic – oiliness	0.519
Flavor	Odor	2.645
	Taste	1.434
Weighted mean value of score	1.725	0.115

Table 3. Analysis of variance of sensory properties of samples - mixtures of milk and cocoa spreads

Sensory quality characteristic	Time		Composition		Interaction		
	F	p	F	p	F	p	
Appearance	11.876	0.001	133.402	0.000	0.536	0.709	
Consistence/texture	Spreadability	22.021	0.000	58.150	0.000	1.806	0.146
	Dynamic melting characteristic – oiliness	7.148	0.011	46.485	0.000	0.267	0.897
Flavor	Odor	6.453	0.015	44.713	0.000	0.153	0.960
	Taste	7.521	0.009	150.802	0.000	0.177	0.948
Weighted mean value of score	34.793	0.000	263.235	0.000	0.975	0.432	

affects the investigated sensory characteristic of consistence/texture – dynamic melting property, oiliness and flavor-odor. The second observed factor – product composition, affects highly significantly ($p < 0.01$) all the investigated sensory characteristics.

The results of LSD test for sensory characteristics of appearance for samples 1–5, mixtures of milk and cocoa spreads show that the investigated factor-time of storage up to 180 days significantly affects the mentioned characteristics ($p < 0.01$) (Table 4).

Table 4. Comparison of changes of sensory property – appearance over storage time for samples 1–5 of mixture of milk and cocoa spreads (LSD test)

Time of storage, days	Time of storage, days		Means
	0–30	180	
	3.970	3.730	
0–30	–	0.001	
180	–	–	

Differences in appearance exist ($p < 0.01$) between all the samples 1–5; however, between samples 1 and 5 the differences are at level $p < 0.05$ and between samples 1 and 4 the differences are not significant (Table 5).

Table 5. Comparison of changes of sensory property – appearance depending on the composition for samples 1–5 of mixture of milk and cocoa spreads (LSD test)

Sample	Sample				
	1	2	3	4	5
	3.950	4.850	2.400	3.850	4.200
1	–	0.000	0.000	0.369	0.028
2	–	–	0.000	0.000	0.000
3	–	–	–	0.000	0.000
4	–	–	–	–	0.003
5	–	–	–	–	–

According to the results of the LSD test for sensory characteristics – consistence/texture, spreadability, for mixtures of milk and cocoa-cream spreads, the investigated factor time of storage affects the mentioned characteristics of the samples at the level of $p < 0.01$ (Table 6). The differences between the visually evaluated consistence-texture, *i.e.*, spreadability are significant for all samples ($p < 0.01$), except between samples 1 and 2, and 1 and 4, where the mentioned differences are significant at the level of $p < 0.05$ (Table 7).

The consistence of spreads of exquisite sensory characteristics should be creamy, light and with no separation, *i.e.*, migration of oil to the surface [12] during the storage, *i.e.*, on the shelves of the super-

markets during the period of 6 months. Sufficient amount of hard fat in the total fat-phase contributes to the product stability. The spread should have a firm structure, however, it should also be spreadable at room temperature. Likewise, it should not be oily, not even after keeping for a certain time at 30 °C [3,18].

Table 6. Comparison of changes of sensory property – consistence/texture – spreadability over storage time for samples 1–5 of mixture of milk and cocoa spreads (LSD test)

Time of storage, days	Time of storage, days		Means
	0–30	180	
	4.120	3.800	
0–30	–	0.000	
180	–	–	

Table 7. Comparison of changes of sensory property – consistence/texture – spreadability depending on the composition for samples 1–5 of mixture of milk and cocoa spreads (LSD test)

Sample	Sample				
	1	2	3	4	5
	4.325	4.575	3.075	4.075	3.750
1	–	0.025	0.000	0.025	0.000
2	–	–	0.000	0.000	0.000
3	–	–	–	0.000	0.000
4	–	–	–	–	0.000
5	–	–	–	–	–

The characteristic consistence/texture, including the orally evaluated dynamic melting property and oiliness of mixtures of milk and cocoa spreads for the observed factor – storage time, affects significantly ($p < 0.05$) the analyzed property (Table 8). The differences in texture/melting and oiliness between samples 1 and 2, and 4 and 5, are not significant, however, between other samples the differences are (statistically) highly significant ($p < 0.01$) (Table 9). Having in mind that different physical sensations form the consistence/texture of food products, this characteristic is referred by some authors as “textural properties” [30]. The texture as a sensory attribute depends on the food structure (molecular, microscopic and macroscopic), and human senses are irreplaceable in perceiving of this multiparametric attribute [31]. So, the textural characteristics are determined as: mechanical characteristics – connected with the reaction of food product on the pressure geometrical characteristics – depending on size, shape; and particles orientation in the food; other characteristics – connected with water and fat content in the food [32].

Table 8. Comparison of changes of sensory property – consistency/texture – dynamic characteristic of melting, oiliness over storage time for samples 1–5 of mixture of milk and cocoa spreads (LSD test)

Time of storage, days	Time of storage, days	
	0–30	180
	Means	
	4.170	3.980
0–30	–	0.011
180	–	–

Table 9. Comparison of changes of sensory property – consistency/texture – dynamic characteristic of melting, oiliness depending on the composition for samples 1–5 of mixture of milk and cocoa spreads (LSD test)

Sample	Sample				
	1	2	3	4	5
	Means				
	4.400	4.625	3.200	4.075	4.075
1	–	0.052	0.000	0.006	0.006
2	–	–	0.000	0.000	0.000
3	–	–	–	0.000	0.000
4	–	–	–	–	1.000
5	–	–	–	–	–

The sensory property flavor-odor of investigated samples – mixtures of milk and cocoa spreads changes at the level of $p < 0.05$ during the storage period (Table 10). Regarding flavor-odor for the evaluated factor-composition, on the basis of LSD test results, the differences are not significant for samples 1 and 2, 3 and 4, 1 and 5, 2 and 5; however, the differences regarding the odor, are significant at the level of $p < 0.01$ for samples 1 and 3, 2 and 3, 1 and 4, 2 and 4, and for 3 and 5, and 4 and 5 (Table 11).

Table 10. Comparison of changes of sensory property – flavor-odor over storage time for samples 1–5 of mixture of milk and cocoa spreads (LSD test)

Time of storage, days	Time of storage, days	
	0–30	180
	Means	
	4.440	4.220
0–30	–	0.015
180	–	–

The results of LSD test show that the factor – storage time affects highly significantly ($p < 0.01$) the sensory property flavor-taste of mixtures of milk and cocoa-cream spreads (Table 12). The difference in flavor-taste between all samples are at significance level of $p < 0.01$, with the exception for samples 1 and

2, where the differences for taste are not significant (Table 13).

Table 11. Comparison of changes of sensory property – flavor-odor depending on the composition for samples 1–5 of mixture of milk and cocoa spreads (LSD test)

Sample	Sample				
	1	2	3	4	5
	Means				
	4.700	4.800	3.625	3.625	4.900
1	–	0.469	0.000	0.000	0.152
2	–	–	0.000	0.000	0.469
3	–	–	–	1.000	0.000
4	–	–	–	–	0.000
5	–	–	–	–	–

Table 12. Comparison of changes of sensory property – flavor-taste over storage time for samples 1–5 of mixture of milk and cocoa spreads (LSD test)

Time of storage, days	Time of storage, days	
	0–30	180
	Means	
	3.890	3.700
0–30	–	0.009
180	–	–

Table 13. Comparison of changes of sensory property – flavor-taste depending on the composition for samples 1–5 of mixture of milk and cocoa spreads (LSD test)

Sample	Sample				
	1	2	3	4	5
	Means				
	4.625	4.625	2.450	3.200	4.075
1	–	1.000	0.000	0.000	0.000
2	–	–	0.000	0.000	0.000
3	–	–	–	0.000	0.000
4	–	–	–	–	0.000
5	–	–	–	–	–

The weighted mean value of the scores for mixtures of milk and cocoa spreads changes significantly during storage (Table 14). The results of LSD test show that the differences between all samples are at significance level $p < 0.01$ (Table 15).

The noticed changes of sensory properties of mixtures of milk and cocoa spreads are supported by the results of peroxide value (Figure 7) and of FFA content (Figure 8). The sources of contamination with heavy metals, in the confectionery products, are mostly the main ingredients [33] that are used for the production.

Besides achieving the appropriate sensory properties (appearance, colour, surface, shine, consistence and flavor), as very important parameters for the con-

sumers, a considerable task for the confectionery industry is to obtain a healthy-sound final product. The content of lead, cadmium and copper in prepared samples of mixtures of milk and cocoa spreads is presented in Table 16.

Table 14. Comparison of changes of the weighted mean value of the scores over storage time for samples 1–5 of mixture of milk and cocoa spreads (LSD test)

Time of storage, days	Time of storage, days		Means				
	0–30 180		81.660 77.220				
	Means		1	2	3	4	5
0–30	—	0.000	—	—	—	—	—
180	—	—	—	—	—	—	—

It can be noted that all analysed samples had very equable content of lead and cadmium, while the copper content varied in the broader range (from 2.168 mg/kg for sample 2, up to 9.899 mg/kg for sample 3). However, the content of heavy metals in all investigated samples of mixtures of milk and cocoa spreads (Table 16) is acceptably low and fulfills the demands given in the Rulebook [28] in the period up to 180 days.

Table 15. Comparison of changes the weighted mean value of the scores depending on the composition for samples 1–5 of mixture of milk and cocoa spreads (LSD test)

Sample	Sample				
	1	2	3	4	5
	Means	88.750	93.100	58.350	74.900
1	—	0.000	0.000	0.000	0.000
2	—	—	0.000	0.000	0.000
3	—	—	—	0.000	0.000
4	—	—	—	—	0.000
5	—	—	—	—	—

Table 16. Content of heavy metals in the mixtures of milk and cocoa spreads

Sample	Content of heavy metals, mg/kg		
	Lead	Cadmium	Copper
1	0.103–0.105	0.010–0.011	2.258–2.285
2	0.104–0.107	0.011–0.010	2.168–2.200
3	0.090–0.099	0.008–0.009	9.886–9.899
4	0.101–0.108	0.010–0.010	5.258–5.288
5	0.090–0.096	0.009–0.010	4.479–4.496

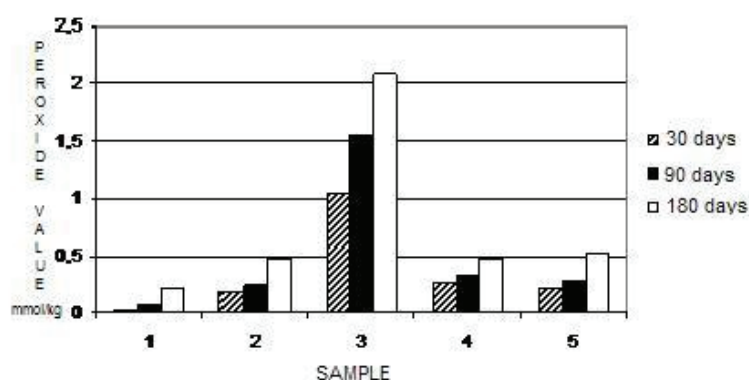


Figure 7. Change of peroxide value (mmol/kg) of mixtures of milk and cocoa-spreads during 180 days of storage.

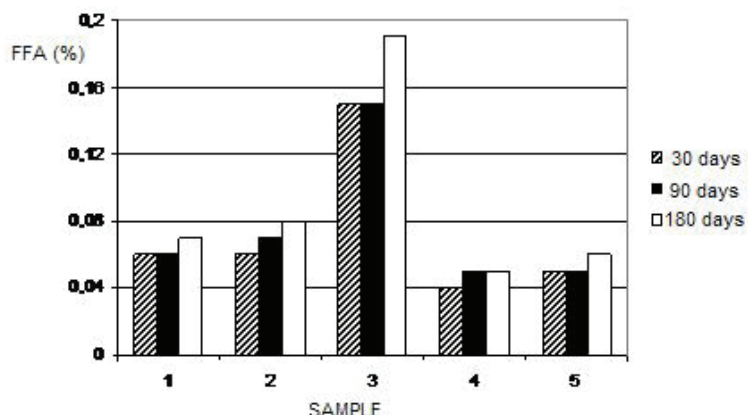


Figure 8. Change of FFA content (% of oleic acid) of mixtures of milk and cocoa spreads during 180 days of storage.

CONCLUSION

Based on the obtained results, the following can be concluded:

1. In semi-industrial conditions, a new quality spread product was produced, with increased content of dairy products intended firstly for children, composed of skimmed milk powder, whey powder and their combination, hydrogenated vegetable fat ($\text{FFA} < 10\%$) and refined sunflower oil, with the addition of cocoa powder with reduced cocoa butter content and hazelnut, without antioxidants and preservers, with shelf-life up to 180 days.

2. 30 days after the production, spread samples 1 and 2 were of excellent, samples 4 and 5 of very good, and sample 3 of good total sensory quality.

3. After 180 days of storage, at $18\text{--}20^\circ\text{C}$, all investigated spread samples remained in the initial quality category, with the exception of sample 1, where the total sensory quality decreased by one category, due to slightly sensory texture changes.

4. According to results of two-factorial analyses of variance, it was found that the factor-storage time significantly affects the appearance, consistence/texture, spreadability, flavor-taste, while the factor-composition greatly affects all investigated quality characteristics of spreads.

5. The results of descriptive statistics show that the mean value of scores regarding the quality characteristics: appearance, consistence/texture, spreadability and dynamic melting characteristics-oiliness, was the highest for spread 2. The highest mean value for evaluated characteristic flavor-odor was for spread 5, primarily due to a hazelnut-like odor. Further, the results show the highest mean scores for flavor-dominant milky taste was gained by spreads 1 and 2. The sensory characteristic of spread 3 were evaluated with the lowest scores, thereby causing the lowest mean scores (appearance, consistence/texture and flavor).

6. Finally, the conclusion is that the overall quality (appearance, texture/consistence and flavor) and stability of spreads depend on the choice of the main raw materials (skimmed powdered milk, whey powder and their combination) and also of their percentage ratio.

Acknowledgement

This study was funded by the Ministry of Education, Science and Technological Development of the Republic of Serbia – Project No.: 46009. The authors are sincerely grateful to the Ministry for financing and understanding.

REFERENCES

- [1] Rules on quality and other requests concerning cocoa-products, chocolate products, chocolate-alike products and creamy products (FRY Official Gazette 1/2005) (in Serbian).
- [2] L. Goldoni, Cocoa-products and chocolate-alike products, Kugler, Zagreb, 2004.
- [3] M. Gavrilović, The Technology of the Confectionery Products, University of Novi Sad, Faculty of Technology, Novi Sad, 2003 (in Serbian)
- [4] D. Maćejić, S. Jovanović, M. Barać, Milk proteins, Monograph, University of Belgrade, Faculty of Agriculture, Belgrade-Zemun, 2007 (in Serbian).
- [5] J. Popov-Raljić, Lj. Stojšin, The Technology of the Confectionery Products, University of Belgrade, Faculty of Agriculture, Belgrade, 2007, pp. 49–54 (in Serbian)
- [6] A. Belčak-Cvitanović, D. Komes, R. Božanić, Milk powder as raw material for the production of milk chocolate, Hrvat. čas. prehrambenu tehnol. biotehnol. i nutr. **4**(3-4) (2009) 109–115.
- [7] M. Carić, S. Milanović, Dried dairy products: physical and functional characteristics, Symposium "Milk and dairy products", Tara, 2005 (in Serbian).
- [8] J. Laličić, Influence of the composition and time of storage on the chosen properties of quality of various types of chocolate, Ms. Thesis, University of Belgrade, Faculty of Agriculture, Belgrade-Zemun, 2007 (in Serbian).
- [9] J. Popov-Raljić, V. Sikimić, Possibility of use of milk and dairy products in confectionery, Proceedings of Technical College in Pozarevac, 2007, pp. 41–49 (in Serbian).
- [10] S. Jovanović, M. Barać, D. Maćejić, T. Vučić, Serum proteins-technological and functional properties and possibility of use, Savremena poljoprivreda **56** (2007) 114–125 (in Serbian).
- [11] T. Topalović, S. Damjanović, G. Janković, Z. Marković, Dietary Cocoa Cream Production, Acta Agric. Serb. **XII**(24) (2007) 77–83.
- [12] M.M. Petković, B.S. Pajin, J.M. Tomić, A.M. Torbica, Z.I. Šereš, D.B. Zarić, D.M. Šoronta-Simović, Textural and sensory properties of spreads with sucrose and maltitol, Hem. Ind. **66** (2012) 385–394 (in Serbian).
- [13] S. Kravić, N. Marjanović, Z. Suturović, J. Švarc-Gajić, Z. Stojanović, M. Pučarević, Determination of trans-fatty acids in chocolate products by method of gas chromatography-mass-spectrometry, Glasnik hemičara tehnologa i ekologa Republike Srpske **2** (2009) 79–83 (in Serbian).
- [14] B. Pajin, Đ. Karlović, Lj. Dokić, M. Hadnađev, Characterization of creamy-spread products, Uljarstvo **37**(1–2) (2006) 13–16 (in Serbian).
- [15] J. Laličić, B. Rabrenović, J. Popov-Raljić, K. Pičurić-Jovanović, Possibilities of use of palm-kernel oil in confectionery, Uljarstvo **36**(3–4) (2005) 35–40 (in Serbian).
- [16] E. Hartig, V. Stajić, Lj. Stojšin, Use of special-purpose lipids in confectionery, 46th conference-production and processing of oilseeds, with international participation, Petrovac, 2005, pp. 157–163 (in Serbian).
- [17] M.D. Laryea, B. Biggemann, M. Funke, I. Lombeck, H.J. Bremer, Trans fatty acid content of selected brands of West German nut-nougat cream, Z. Ernährungswiss. **27**(4) (1988) 266–271.

- [18] J. Popov-Raljić, J. Laličić, R. Gorjanović, R. Romanić, Texture properties of quality of creamy products and greasy spreads, 48th conference-production and processing of oilseeds, with international participation, Herceg Novi, 2007, pp. 213–217 (in Serbian).
- [19] C.A. Chu, A.V.A. Resurrección, Sensory profiling and characterization of chocolate peanut spread using response surface methodology, *J. Sens. Stud.* **20** (2005) 243–274.
- [20] ISO 8586-1, Sensory Analysis-General guidance for selection, training and monitoring of assessors-Part 1: Selected assessors, 1993.
- [21] ISO 8586-2, Sensory Analysis-General guidance for selection, training and monitoring of assessors-Part 2: Experts, 1994.
- [22] ISO 8589, Sensory Analysis – General guidance for the design of test rooms, 1988.
- [23] R. Radovanović, J. Popov-Raljić, Sensory analysis of foodstuffs, University of Belgrade, Faculty of Agriculture, Belgrade-Novi Sad, 2000/2001, CIP 641:658.526 641:001.893 (in Serbian)
- [24] J. Stanković, N. Ralević, I. Ralević, Statistics with application in agriculture, Faculty of Agriculture, Belgrade, 2002, ISBN 86-387-0317-1 (in Serbian).
- [25] ISO 3960, Animal and vegetable fats and oils – Determination of peroxide value, International Organization for Standardization, Geneva, 2001.
- [26] ISO 660, Animal and vegetable fats and oils – Determination of acidity, International Organization for Standardization, Geneva, 2000.
- [27] E. Dimić, J. Turkulov, Quality control in the technology of edible oils, University of Novi Sad, Faculty of Technology, Novi Sad, 2000, (in Serbian).
- [28] Rules on quantity of pesticides, metals and metalloids and other toxic substances, chemotherapeutics, anabolic steroids and other substances that may be found in foodstuffs, FRY Official Gazette 5/1992, 11/1992 and 32/2002 (in Serbian).
- [29] C. Alasavar, F. Shahidi, Natural antioxidants in tree nuts, *Eur. J. Lipid Sci. Technol.* **111** (2009) 1056–1062.
- [30] M.C. Bourne, Texture and Viscosity of Foods, 2nd ed., Academic Press, London, 2002.
- [31] A.S. Szczesniak, Texture is a Sensory Property, *Food Qual. Prefer.* **13** (2002) 215–225.
- [32] ISO 11036, Sensory Analysis-Methodology-Texture profile, 1994.
- [33] D. Sudhir, K. Rupali, A.G. Hegde, R.M. Sharma, Lead, cadmium and nickel in chocolates and candies from suburban areas of Mumbai, India, *J. Food Compost. Anal.* **6** (2005) 517–522.

IZVOD**PROMENE SENZORNIH KARAKTERISTIKA I POJEDINI PARAMETRI KVALITETA MEŠAVINE MLEČNOG I KAKAO-KREM NAMAZA TOKOM SKLADIŠTENJA DO 180 DANA**

Jovanka V. Popov-Raljić¹, Jovanka G. Laličić-Petronijević², Etelka B. Dimić³, Vladimir S. Popov⁴, Vesna B. Vujsinović⁵, Ivana V. Blešić¹, Milijanko J. Portić¹

¹Univerzitet u Novom Sadu, Prirodno-matematički fakultet, Trg D. Obradovića 3, 21000, Novi Sad, Srbija

²Univerzitet u Beogradu, Poljoprivredni fakultet, Nemanjina 6, 11080, Beograd – Zemun, Srbija

³Univerzitet u Novom Sadu, Tehnološki fakultet, Bulevar Cara Lazara 1, 21000, Novi Sad, Srbija

⁴Univerzitet u Novom Sadu, Poljoprivredni fakultet, Trg D. Obradovića 8, 21000, Novi Sad, Srbija

⁵Visoka škola strukovnih studija za menadžment i poslovne komunikacije, Mitropolita Stratimirovića 110, Sremski Karlovci, Srbija

(Naučni rad)

Primena mleka i proizvoda od mleka u tehnologiji konditorskih proizvoda (čokolada, bombonski proizvodi-karamele, mlečni krem namazi i dr.) ima za cilj povećanje hranljive vrednosti finalnog proizvoda i uticaj na pojedina senzorna svojstva kvaliteta (izgled, konzistencija/tekstura i aroma). U radu su proizvedeni uzorci mešavine mlečnog i kakao krema, novog sastava, sa povećanim udelom mlečnih delova, na kojima su, potom, ocenjene promene senzornih svojstava, određen peroksidni broj, sadržaj slobodnih masnih kiselina i sadržaj teških metala (olova, kadmijuma i bakra), tokom skladištenja do 180 dana, pri sobnoj temperaturi od (18–20 °C). Primanjena je analitička-deskriptivna senzorna analiza (bod sistem), uz opisivanje dominantnih svojstava (izgled-boja, oblik, sjaj površine, konzistencija-mazivost, dinamičko svojstvo topljenja, konzistentnost usne duplje- uljavost i aroma-miris i ukus). Rezultati su statistički obrađeni primenom dvofaktorijske analize varianse MANOVA, LSD i Levene's testa. Na osnovu dobijenih rezultata može se konstatovati da sastav namaza (obrano mleko u prahu, surutka u prahu i njihova kombinacija, hidrogenizovana biljna mast (trans masne kiseline ispod 10%) i rafinisano suncokretovo ulje, kakao-prah sa redukovanim sadržajem kakao maslaca i lešnik) statistički vrlo značajno utiče na sva ocenjivana svojstva, dok vreme skladištenja, statistički vrlo značajno utiče na izgled, konzistenciju tj. mazivost i na ukus.

Ključne reči: Senzorna analiza • Krem proizvod • Peroksidni broj • Slobodne masne kiseline • Teški metali • Skladištenje

Nanoemulzije dobijene variranjem tipa emulgatora i udela masne faze: Uticaj formulacije i procesnih parametara na karakteristike i fizičku stabilnost

Sanela M. Đorđević¹, Nebojša D. Cekić², Tanja M. Isailović¹, Jela R. Milić¹, Gordana M. Vučeta¹,
Miodrag L. Lazić², Snežana D. Savić¹

¹Katedra za farmaceutsku tehnologiju i kozmetologiju, Farmaceutski fakultet, Univerzitet u Beogradu, Beograd, Srbija

²Tehnološki fakultet, Univerzitet u Nišu, Leskovac, Srbija

Izvod

Cilj ovog istraživanja bio je da se homogenizacijom pod visokim pritiskom izrade nanoemulzije stabilizovane alkil poliglukozidnim (APG) emulgatorom i da se njihove karakteristike i fizička stabilnost uporede sa nanoemulzijama stabilizovanim standardnom kombinacijom lecitina (L) i polisorbata 80 (P80). U istraživanju je praćen uticaj parametara formulacije, i to vrste i koncentracije emulgatora (smeša L/P80 vs. APG, u koncentraciji od 4, 6 i 8%) i koncentracije uljane faze (20, 30 i 40% trigliceridi srednje dužine lanca) na veličinu i raspodelu veličina kapi, zeta potencijal (ζ) i fizičku stabilnost nanoemulzija. Takođe je praćen uticaj procesnih parametara (postupak, pritisak i broj ciklusa homogenizacije) na veličinu kapi i indeks polidisperznosti (Pdl), u cilju identifikovanja optimalnih uslova za izradu nanoemulzija. Dobijeni rezultati pokazuju da postoji uticaj sastava formulacije na karakteristike (L/P80 nanoemulzije: veličina kapi 147–156 nm, ζ oko –20 mV; APG nanoemulzije: veličina kapi 165–228 nm, ζ oko –50 mV) i fizičku stabilnost ispitivanih nanoemulzija, i da se diskontinualnim postupkom homogenizacije (9 ciklusa, 500 bar) mogu dobiti nanoemulzije optimalnih svojstava (veličina kapi, Pdl).

Ključne reči: nanoemulzija, kapril/kapril glukozid, lecitin, polisorbat 80, homogenizacija pod visokim pritiskom, fizička stabilnost.

Dostupno na Internetu sa adresu časopisa: <http://www.ache.org.rs/HI/>

Nanoemulzije su nosači sa dugom i uspešnom istorijom primene u parenteralnoj ishrani, a od nedavno su počele da se intenzivno istražuju i kao nosači lekova za različite puteve primene, kao što su intravenska, oralna, rektalna, dermalna i primena u oku [1–5]. Prednosti nanoemulzija kao terapijskih sistema su kontrolisana veličina kapi, niska koncentracija emulgatora, visok solubilizacioni kapacitet za lipofilne lekove [6,7] i mogućnost povećanja njihove biološke raspoloživosti [4]. Pored toga, nanoemulzije se obično sastoje od visoko biokompatibilnih i biodegradabilnih sastojaka, što ih čini pogodnim sistemima za osetljive puteve primene (intravenska, primena u oku), kao i za primenu u kozmetičke svrhe [6]. Primeri formulacija koje su odobrene za terapijsku primenu su intravenske nanoemulzije diazepama, propofola, liposolubilnih vitamina i amfotericina B [5,8].

U fizičkom smislu, nanoemulzije su emulzije sa veličinom kapi ispod 100 nm, analogno nanočesticama iste veličine [9,10]. Danas se, međutim, ovaj termin koristi

NAUČNI RAD

UDK 66.063.61:544.7:615

Hem. Ind. 67 (5) 795–809 (2013)

doi: 10.2298/HEMIND120905005D

za sve metastabilne emulzije sa veličinom kapi ispod jednog mikrona, koje se generalno nazivaju submikronskim emulzijama [6]. U principu, nanoemulzije (poznate i kao miniemulzije, ultrafine emulzije, submikronske emulzije) uglavnom se opisuju kao ulje/voda (U/V) emulzije sa veličinom kapi ispod 1000 nm, najčešće u rasponu 100–500 nm [6,8,11], mada se navodi i opseg veličina 50–200 nm [12]. Zavisno od veličine kapi, nanoemulzije mogu biti translucentne ili transparentne (veličina ispod 100 nm) i neprovidne ili mlečne (veličina iznad 100 nm), a plavkasta nijansa ukazuje na pojavu Rejljevog (Rayleigh) rasipanja svetlosti od malih kapi nanoemulzije [6,9].

Za razliku od mikroemulzija, nanoemulzije su termo-dinamički nestabilne – slobodna energija koloidne disperzije (uljane kapi u vodi) je veća od slobodne energije odvojenih faza (ulje i voda). Međutim, ako se obezbedi dovoljna energetska barijera između ove dve faze, nanoemulzije će biti kinetički stabilne [13]. Dobra dugo-ročna fizička stabilnost čini ove sisteme jedinstvenim [12], a proističe iz činjenice da su konvencionalni destabilizacioni fenomeni, poput kriminga (eng. creaming, raslojavanje) i koalescencije, uveliko sprečeni ili usporeni, usled Braunovog kretanja malih kapi, koje se suprotstavlja gravitaciji [11,12]. Glavni izvor nestabilnosti je Ostvaldovo sazrevanje koje predstavlja tendenciju malih kapi da se sjedine u veće, usled razlika u

Prepiska: S. Savić, Katedra za farmaceutsku tehnologiju i kozmetologiju, Farmaceutski fakultet, Vojvode Stepe 450, 11000 Beograd, Srbija.

E-pošta: snexs@pharmacy.bg.ac.rs

Rad primljen: 5. septembar, 2012

Rad prihvaćen: 13. decembar, 2012

njihovoj rastvorljivosti [6,9]. Ovo sporo povećanje veličine kapića će konačno, tokom vremena, dovesti do separacije (odvajanja) faza nanoemulzije [14]. Pored toga, mogu da se javi i reverzibilni destabilizacioni fenomeni kao što su flokulacija, razdvajanje uslovljeno gravitacijom (kriming/sedimentacija) [15]. Odgovarajućim izborom vrste ulja, vrste emulgatora, njihovih koncentracija i uslova izrade, mogu da se dobiju nanoemulzije zadovoljavajuće kinetičke stabilnosti (meseci i godine) [13].

Nanoemulzije se izrađuju iz ulja, vode, emulgatora i, često, koemulgatora, i pošto su termodinamički nestabilni sistemi, uvek zahtevaju dovođenje neke spoljašnje energije sistemima. Metode za izradu nanoemulzija mogu se podeliti u dve grupe: visoko-energetske (koriste se mehanički uređaji—homogenizator pod visokim pritiskom, mikrofluidizer, ultrazvuk) i nisko-energetske (zasnivaju se na fizičko–hemijskim svojstvima sistema – fazno-inverzni i spontani emulgajući metod) [3,6,12].

Emulgatori imaju važnu ulogu u formiranju nanoemulzija: smanjenjem međupovršinskog napona smanjuje se Laplasov pritisak (razlika pritiska između unutrašnjosti i spoljašnjosti kapića), a otuda je i stres potreban za lomljenje kapića smanjen. Emulgatori takođe sprečavaju koalescenciju novonastalih kapića [12]. Generalno, za izradu nanoemulzija mogu da se koriste različiti površinski aktivni agensi: konvencionalne površinske aktivne materije (PAM), proteini i polisaharidi [13]. Lecitini su još uvek emulgatori izbora u smislu biokompatibilnosti. Nalaze se među najbezbednijim emulgatorima (GRAS status) i stoga se tradicionalno primenjuju u razvoju parenteralnih nanoemulzija. Lecitin stabilizuje nanoemulzije formiranjem višeslojnog omotača oko kapića, koji deluje kao efektivna strukturno-mehanička barijera. U cilju poboljšanja fizičke stabilnosti sistema dodaju se sterni stabilizatori, kao što su emulgajući agensi sa sternim voluminoznim grupama poput polisorbata. Dodatak pogodnog koemulgatora može da pobolji fleksibilnost međupovršinskog filma što se značajno reflektuje na stabilnost ovih emulzija [6].

Problemi vezani za upotrebu klasičnih PAM (lecitina) u nanoemulzijama potiču od toga što su fosfolipidi podložni oksidativnoj i hidrolitičkoj degradaciji, koja ima za posledicu nepovoljne promene u izgledu i mirisu nanoemulzija nakon određenog perioda čuvanja. Osim toga, smeše lecitina imaju visok potencijal za stvaranje agregata, što dovodi do formiranja vezikularnih i multilamelarnih struktura u toku izrade nanoemulzija. Uprkos decenijama istraživanja na ovom polju, još uvek nije u potpunosti razjašnjeno mogu li se ove strukture izbeći i da li njihovo prisustvo ima negativni efekat na dugoročnu stabilnost nanoemulzija [16]. Iako je uloga lecitina kao emulgatora davno utvrđena, kompleksno ponašanje fosfolipida u nanoemulzijama, još uvek nije u potpunosti predvidivo [6].

Tokom proteklih godina, brzo povećanje ekološke svesti o održivim PAM, pokrenulo je upotrebu prirodnih PAM koje se mogu dobiti iz obnovljivih izvora. U tom smislu, postoji sve veće interesovanje za alkil poliglukozide (APG), novu klasu nejonskih PAM koji se dobijaju iz obnovljivih sirovina kao što su glukoza i masni alkoholi. APG pokazuju izuzetnu biorazgradivost, odlična dermatološka svojstva i dobru površinsku aktivnost [17]. Dodatni razlozi za povećanu upotrebu ovih molekula, posebno u formulacijama za primenu na kožu, jesu minimalna osetljivost na promene pH i prisustvo elektrolita u poređenju sa etoksilovanim PAM [18].

Budući da upotreba APG kao potencijalnih stabilizatora nanoemulzija još uvek nije detaljno ispitana, jedan od ciljeva sprovedenog istraživanja bio je da se utvrdi da li su emulgatorom ovog tipa mogu da se dobiju stabilne nanoemulzije sa malom veličinom kapića i uskom raspodelom veličina kapića (indeks polidisperznosti, eng. *polydispersity index, Pdi*). U tu svrhu izrađena je serija model nanoemulzija sa APG emulgatorom srednje dužine alkil lanca (kaprilil/kapril glukozid) metodom homogenizacije pod visokim pritiskom i izvršena njihova karakterizacija, a dobijeni rezultati upoređeni su sa rezultatima dobijenim za nanoemulzije stabilizovane standardnom kombinacijom lecitina i polisorbata 80.

Dobro je poznato da parametri formulacije (tip i koncentracija emulgatora, ideo masne faze), kao i parametri procesa (temperatura, pritisak i broj ciklusa homogenizacije), utiču na fizičko–hemijska svojstva i stabilnost nanoemulzija [19]. S tim u vezi, u sprovedenom istraživanju dodatno je praćen uticaj vrste emulgatora (smeša lecitina i polisorbata 80 vs. kaprilil/kapril glukozid), kao i rastućih koncentracija uljane faze (20, 30 i 40 mas.%) i emulgatora (4, 6 i 8 mas.%) na veličinu kapića, površinsko nanelektrisanje i fizičku stabilnost izrađenih nanoemulzija.

Drugi važan cilj istraživanja bio je da se utvrde optimalni procesni parametri za izradu nanoemulzija, variranjem postupka (kontinualan vs. diskontinualan), pritisaka i broja ciklusa homogenizacije.

EKSPERIMENTALNI DEO

Materijal

Za izradu nanoemulzija korišćeni su: trigliceridi srednje dužine lanca (MCT) odnosno kaprilino/kaprinski trigliceridi (Miglyol® 812, SB Trade, Srbija), lecitin iz jajeta (Lipoid® E80, Lipoid GmbH, Nemačka), polisorbat 80 (Tween® 80, Croda Chemicals, Engleska), APG emulgator kaprilil/kapril glukozid (Plantacare® 810, Cognis, Nemačka) i sveže dobijena prečišćena voda naknadno propuštena kroz membranski bakteriološki filter (visokoprečišćena voda) (Milli-Q, Millipore GmbH, Nemačka).

Metode

Izrada nanoemulzija

U skladu sa standardnom procedurom opisanom u literaturi [3,20–22], izrađeno je šest različitih formulacija U/V nanoemulzija metodom homogenizacije pod visokim pritiskom. Komponente koje su ušle u sastav nanoemulzija, izabrane su na osnovu njihove stabilnosti i biokompatibilnosti. Sve nanoemulzije su izrađene sa MCT kao masnom fazom, visokoprečišćenom vodom kao vodenom fazom, dok su lecitin iz jajeta, polisorbat 80 i APG (kaprilil/kapril glukozid) upotrebljeni kao emulgatori. Prvi set formulacija izrađen je sa smešom lecitin/polisorbat 80 (1/1); analogno je izrađen i drugi set formulacija sa APG emulgatorom. Koncentracija MCT varirana je na 20, 30 i 40 mas.%, a koncentracija emulgatora na 4, 6 i 8 mas.%, pri čemu je maseni odnos masne faze i emulgatora držan konstantnim i bio je 5:1. Sastav formulacija i njihove oznake prikazani su u Tabeli 1.

Masna i vodena faza su pripremljene odvojeno. Masna faza se sastojala od MCT i u njoj je rastvoren lecitin zagrevanjem na 70 °C na magnetnoj mešalici (IKA Mag, IKA Staufen, Nemačka). U vodenu fazu, koju je činila visokoprečišćena voda, dodat je polisorbat 80, odnosno APG emulgator kaprilil/kapril glukozid. Obe faze su zagrejane na 50 °C, na magnetnoj mešalici. Zatim je vodena faza dodata u masnu fazu i izrađena preemulzija mešanjem na rotor-stator homogenizatoru (Ultra-Turrax®, IKA Staufen, Nemačka) 3 min, brzinom od 8000 obrtaja/min, na 50 °C. Da bi se dobila finalna emulzija, ovako izrađena homogena preemulzija (veličina kapi oko 2 μm, Pdl oko 0,6) propuštena je kroz homogenizator pod visokim pritiskom (EmulsiFlex-C3, Avestin, Kanada), diskontinualnim postupkom, 9 puta, pri pritisku od 300 bar i temperaturi od 50 °C [21]. Nakon hlađenja na sobnu temperaturu, svaka nanoemulzija podeljena je u dva dela, koji su čuvani u dobro zatvorenim staklenim bočicama na 25 °C tokom 180 dana i na 40 °C tokom 30 dana, u cilju ispitivanja njihove fizičke stabilnosti.

U cilju procene da li i kako postupak homogenizacije i procesni parametri utiču na karakteristike nanoemulzija, dodatno su izrađena četiri uzorka F1L/P80 preemulzije koje su homogenizovane pod visokim pri-

tiskom u toku 10 ciklusa pod različitim uslovima. Variiran je postupak homogenizacije (kontinualan vs. diskontinualan) i pritisak (300 vs. 500 bar). Pre homogenizacije i nakon svakog drugog ciklusa homogenizacije uzimani su uzorci za analizu veličine i raspodele veličina kapi.

Analiza veličine čestica

Prosečna veličina kapi (hidrodinamički prosečan prečnik, eng. *intensity-weighted mean diameter, z-average – z-ave*) i raspodela veličina kapi (Pdl) merene su na uređaju Zetasizer Nano ZS90 (Malvern Instruments, Velika Britanija) primenom tehnike dinamičkog rasipanja svetlosti (eng. *Dynamic Light Scattering, DLS*, tzv. foton korelaciona spektroskopija, eng. *Photon Correlation Spectroscopy, PCS*). Ovom tehnikom meri se stepen fluktuacije intenziteta rasute svetlosti usled Braunovog kretanja čestica/kapi u uzorku i prevodi u veličinu kapi pomoću Stokes-Einstein-ove jednačine [23]. Pdl je mera za raspodelu veličina kapi i ukazuje na kvalitet ili homogenost disperzije [24]. Kreće se od 0 (monodisperzna) do 0,5 (relativno široka raspodela). Na primer, za parenteralne nanoemulzije vrednosti Pdl do 0,25 smatraju se prihvatljivim [25].

Da bi se umanjio uticaj gustine i viskoziteta nanoemulzija na rezultate merenja, uzorci nanoemulzija su pre merenja 500 puta razblaženi visokoprečišćenom vodom. Merenje je izvedeno u polistirenskim kivetama za jednokratnu upotrebu na temperaturi od 25 °C pod uglom rasipanja svetlosti od 90°. Svaki uzorak je meren tri puta.

Pošto je opseg merenja Zetasizer Nano ZS90 uređaja 2 nm do 3 μm, za utvrđivanje mogućeg prisustva većih kapi, kao dodatna metoda karakterizacije primenjena je tehnika statičkog rasipanja svetlosti (eng. *Static Light Scattering, SLS*), poznata i kao laserska difracija (eng. *Laser Diffraction, LD*). Da bi se izbegli efekti višestrukog rasipanja svetlosti, nanoemulzije su razblažene visokoprečišćenom vodom i nakon 5 min stabilizacije uzorka, merena je veličina kapi na uređaju Malvern Mastersizer (Malvern Instruments, Velika Britanija) na 25 °C, pri čemu je svaki uzorak meren tri puta. Uredaj je podržan softverom koji analizira zavisnost između ugla rasipanja svetlosti i veličine kapi (što je kap

Tabela 1 Sastav izrađenih nanoemulzija (mas.%); ostatak do 100 mas.% čini visokoprečišćena voda
Table 1 Composition of prepared nanoemulsions (mass%)

Formulacija	Komponenta			
	Mygliol® 812	Lipoid® E80	Tween® 80	Plantacare® 810
F1L/P80	20	2	2	–
F2L/P80	30	3	3	–
F3L/P80	40	4	4	–
F1APG	20	–	–	4
F2APG	30	–	–	6
F3APG	40	–	–	8

veća, manji je ugao pod kojim se svetlost rasipa), i, primenom Mie teorijskog modela rasipanja svetlosti, daje zapreminsku raspodelu veličina kapi u nanoemulziji. Najčešći način izražavanja rezultata dobijenih LD metodom je prikazivanje LD prečnika kapi (eng. *volume-weighted mean diameters*) $d10\%$, $d50\%$ i $d90\%$, koji se označavaju i kao $d(v,0.1)$, $d(v,0.5)$ i $d(v,0.9)$. Prečnik $d(v,0.1)$ je veličina kapi na kojoj 10% zapremine uzorka čine kapi čija je veličina manja od „ $d(v,0.1)$ “ vrednosti. Prečnik $d(v,0.5)$ (eng. *median volume particle size*) znači da 50% zapremine uzorka sadrži kapi manje od „ $d(v,0.5)$ “ vrednosti, a 50% uzorka čine kapi veće od ove vrednosti. Prečnik $d(v,0.9)$ znači da 90% zapremine uzorka ima veličinu kapi manju od „ $d(v,0.9)$ “ vrednosti, i predstavlja osetljiv parametar za utvrđivanje prisustva većih kapi, kao i agregata kapi.

Svetlosna mikroskopija

U cilju detekcije eventualnog prisustva većih mikrometarskih kapi i pojave agregacije u izrađenim formulacijama u toku čuvanja, nerazblaženi uzorci nanoemulzija posmatrani su pod svetlosnim mikroskopom Motic digital microscope DMB3-223ASC, koji je podržan softverom Motic Images Plus v.2.0 (Motic GmbH, Nemačka), na uvećanju od 1000 puta.

Merenje zeta potencijala

Zeta potencijal, koji karakteriše nanelektrisanje na površini emulgovanih kapi ulja, meren je na već spomenutom uređaju Zetasizer Nano ZS90 (Malvern Instruments, Velika Britanija). Pre merenja, uzorci nanoemulzija su razblaženi visokoprečišćenom vodom (10 μL uzorka je razblaženo sa 4990 μL visokoprečišćene vode). Merenje je vršeno na 25 °C u savijenoj (eng. *folded*) kapilarnoj ćeliji (DTS 1060) za jednokratnu upotrebu. Izmerena elektroforetska pokretljivost kapi u električnom polju prevedena je u zeta potencijal primenom Helmholz-Smoluchowski jednačine:

$$\zeta [\text{mV}] = EM \frac{4\pi\eta}{\epsilon} \quad (1)$$

gde je ζ zeta potencijal, EM elektroforetska pokretljivost, η viskozitet disperzionog sredstva, a ϵ dielektrična konstanta disperzionog sredstva [26]. Dobijeni rezultati za zeta potencijal izraženi su kao srednja vrednost tri merenja.

Ispitivanje stabilnosti

U cilju ispitivanja fizičke stabilnosti izrađenih nanoemulzija sprovedene su ubrzana i dugotrajna studija stabilnosti. Sve nanoemulzije su nakon izrade podeljene u dve grupe. Prva grupa uzorka čuvana je na 25 °C u toku 6 meseci (dugotrajna studija stabilnosti), a druga na 40 °C tokom mesec dana (ubrzana studija stabilnosti). Uzorci su čuvani u dobro zatvorenim staklenim bočicama sa aluminijumskom krimp kapicom. Pored

praćenja fizičkog izgleda nanoemulzija, u fiksnim vremenskim intervalima mereni su veličina kapi, Pdl , zeta potencijal, pH vrednost i provodljivost. Uzroci su analizirani na dan izrade i nakon 14 i 30 dana za procenu kratkoročne, odnosno 30 i 180 dana za procenu dugoročne stabilnosti sistema.

Merenje pH vrednosti

pH vrednost izrađenih nanoemulzija merena je jednostavnim uranjanjem elektrode pH metra (pH meter HI9321, Hanna Instruments, Portugalija) u uzorak, na temperaturi od 25 °C. Merenje je izvedeno tri puta za svaki uzorak i izračunata srednja vrednost.

Merenje provodljivosti

Električna provodljivost nanoemulzija merena je konduktometrijskom metodom (CDM230 MeterLab, Radiometer, Danska) direktnim uranjanjem elektrode u ispitivane uzorce, na 25 °C. Prikazane vrednosti za provodljivost predstavljaju srednju vrednost tri merenja.

Statistička analiza

Statistička analiza podataka izvršena je pomoću programa SPSS (verzija 18.0) primenom jednofaktorske ili dvofaktorske analize varianse (ANOVA), kao i Student *t*-testa, gde je to bilo potrebno. Za poređenje srednjih vrednosti veličine kapi, Pdl , zeta potencijala, provodljivosti i pH vrednosti nanoemulzija tokom ispitivanja njihove dugoročne i kratkoročne stabilnosti, korišćeni su jednofaktorska ANOVA (za tri grupe podataka) i *t*-test (za dve grupe podataka). Jednofaktorska ANOVA je korišćena i za ispitivanje uticaja broja ciklusa homogenizacije (nezavisno promenljiva) na veličinu kapi i Pdl nanoemulzije (zavisno promenljive), dok je za ispitivanje uticaja dva faktora (pritisak i postupak homogenizacije) na jednu zavisno promenljivu (veličina kapi, Pdl) korišćena dvofaktorska ANOVA. P vrednost manja od 0,05 smatrana je statistički značajnom.

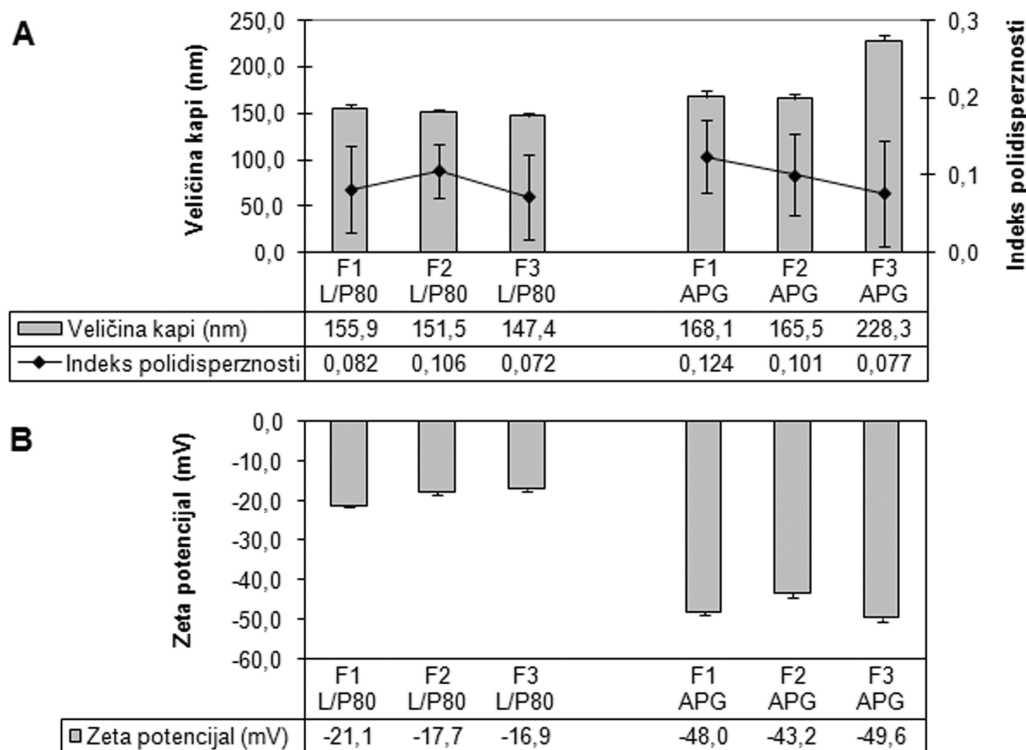
REZULTATI I DISKUSIJA

Uticaj sastava formulacije na karakteristike nanoemulzija

Sve izrađene nanoemulzije bile su tečne, mlečno bele (usled višestrukog rasipanja svetlosti) sa plavičastim odsjajem. Ovakva vizuelna pojava je inače karakteristična za nanoemulzije čija veličina kapi prelazi 100 nm [6].

Naime, analiza veličine kapi (slika 1A) pokazuje da su na dan izrade sve formulacije nanoemulzija imale prosečnu veličinu kapi, merenu PCS metodom, u opsegu od 147 do 228 nm, sa veoma uskom raspodelom veličine kapi (Pdl u opsegu 0,072–0,124).

Vrednosti Pdl manje od 0,1 ili 0,2 ukazuju na dobar kvalitet sistema i na relativno usku raspodelu veličina kapi, odnosno na unimodalnu raspodelu. Vrednosti Pdl



Slika 1. Prosečna veličina kapi (z-average \pm SD), raspodela veličine kapi (Pdl \pm SD) i zeta potencijal (\pm SD) nanoemulzija koje sadrže rastuće koncentracije MCT (20, 30 i 40%) i emulgatora (4, 6 i 8%) na dan izrade.

Figure 1. Mean droplet size (z-average \pm SD), particle size distribution (Pdl \pm SD) and zeta potential (\pm SD) of nanoemulsions containing increasing concentrations of MCT (20, 30 i 40%) and emulsifiers (4, 6 i 8%) on day of preparation.

blizu 1 (najviša vrednost) imaju sistemi lošeg kvaliteta čija veličina kapi više nije u nanometarskom opsegu [24].

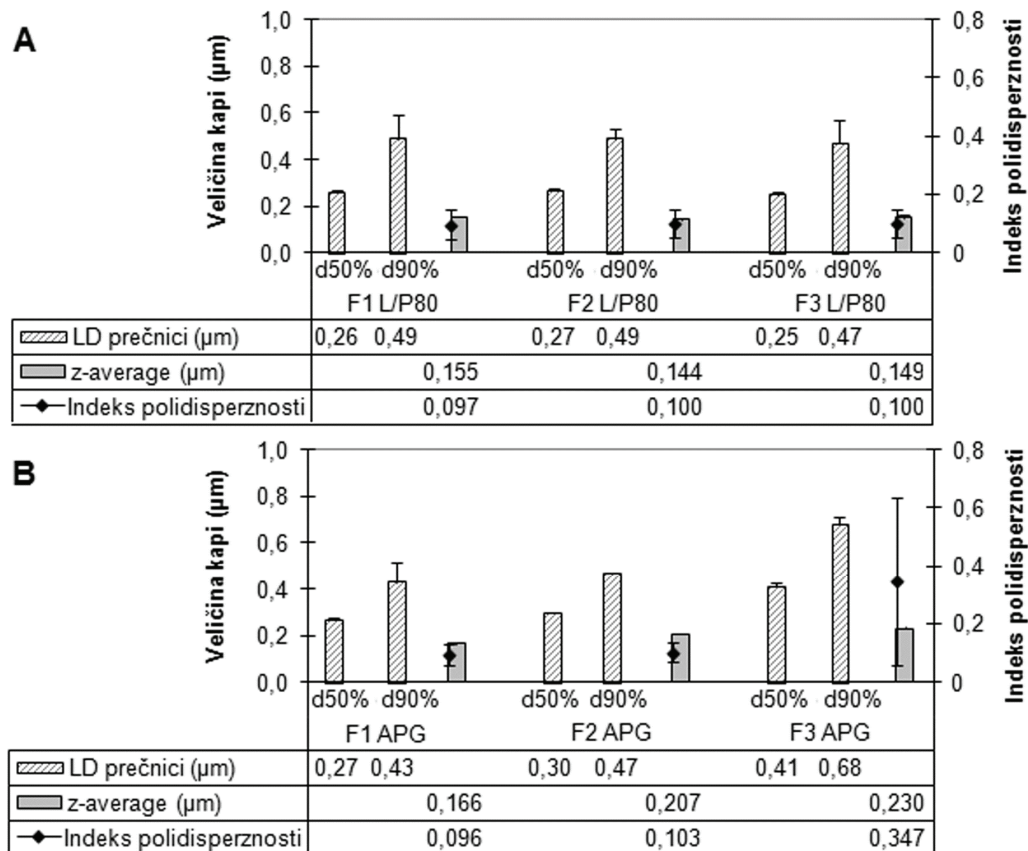
Dobijeni rezultati (slika 1A) jasno ukazuju da postoji uticaj sastava nanoemulzija na veličinu kapi. Kod nanoemulzija izrađenih sa smešom PAM lecitin/polisorbat 80 veličina kapi je bila manja (147–156 nm) u poređenju sa nanoemulzijama na bazi APG. Ovi nalazi mogu se objasniti različitom hidrofilnošću upotrebljenih emulgatora. Naime, Tan i Nakajima [27] su pokazali da emulgatori sa većom hidrofilnošću mogu efikasnije da obuhvate i stabilizuju kapi u U/V nanoemulzijama, što za posledicu ima formiranje manjih kapi. APG su u osnovi lipofilniji, imaju niže HLB vrednosti [28], pa bi veća hidrofilnost polisorbata 80, između ostalog, mogla biti odgovorna za manju veličinu kapi nanoemulzija izrađenih sa smešom lecitin/polisorbat 80.

Poznato je da postoji uticaj koncentracije emulgatora i udela uljane faze na finalnu veličinu kapi nanoemulzija [12,19,21]. Ispitivanja su pokazala da je sa povećanjem udela uljane faze i koncentracije emulgatora došlo do smanjenja veličine kapi kod svih ispitivanih formulacija nanoemulzija, sem F3APG, gde je došlo do povećanja veličine kapi (slika 1A).

Povećanje koncentracije emulgatora ima za posledicu nastanak manjih kapi [5,7]. Nasuprot tome, povećanje količine dispergovane (uljane) faze dovodi do

povećanja kolizije kapi i otuda do koalescencije u toku samog procesa emulgovanja [12]. Veća veličina kapi je nepovoljnija u pogledu stabilnosti, ali je, s druge strane, potencijalni solubilizacioni kapacitet za lipofilne lekove veći [29]. Međutim, u sprovedenom istraživanju istovremeno su povećavani udeo masne faze i koncentracija emulgatora, tako da je njihov maseni odnos u svim formulacijama bio konstantan (5:1). Pokazano je da ako se maseni odnos emulgatora i dispergovane faze drži konstantnim, tj. ako se sa povećanjem udela masne faze povećava i koncentracija emulgatora, u sistemu dolazi do smanjenja međupovršinskog napona i nastanka manjih kapi [12]. Ovo zapažanje je, kao što je već navedeno, sa izuzetkom formulacije F3APG sastavljene od MCT, APG i vode u odnosu 40:8:52, potvrđeno u sprovedenom istraživanju. Dodatno, smatra se da bi odnos uljane faze i emulgatora od 5:3 doveo do najmanje veličine kapi [30].

Da bi se isključilo prisustvo većih kapi u ispitivanim nanoemulzijama, kao dodatne metode za procenu veličine kapi u sistemu, primenjene su LD i svetlosna mikroskopija. Slika 2 daje uporedni pregled veličine kapi merene PCS metodom i LD metodom 7 dana nakon izrade nanoemulzija. Kod nanoemulzija izrađenih sa smešom lecitin/polisorbat 80, 50% kapi bilo je manje od 270 nm, dok je veličina 90% kapi bila ispod 490 nm.



Slika 2. Prosečna veličina kapi merena foton korelacionom spektroskopijom (z-average), LD prečnici mereni laserskom difrakcijom (d50% i d90%) i indeks polidisperznosti (Pdl) različitih formulacija nanoemulzija 7 dana nakon izrade (srednja vrednost ± SD, n = 3).
Figure 2. Mean particle size measured by photon correlation spectroscopy (z-average), LD diameters measured by laser diffraction (d50% and d90%) and polydispersity index (Pdl) of various nanoemulsion formulations after 7 days of preparation (mean ± SD, n = 3).

Kod nanoemulzija stabilizovanih kaprilil/kapril glukozidom, $d(v,0.5)$ vrednosti su bile između 270 i 410 nm, dok su se vrednosti za $d(v,0.9)$ kretale od 430 do 680 nm. U svim ispitivanim formulacijama najveće kapi bile su manje od 1 μm. Kada se uporede veličine kapi dobijene PCS metodom i LD metodom, vidi se da su vrednosti LD prečnika veće. Razlog za to je što LD daje zapreminsku raspodelu veličine kapi, dok je kod PCS merenje zasnovano na intenzitetu svetlosti [25]. Svetlosna mikroskopija je dodatno potvrdila da nije bilo većih kapi, ili agregata kapi, ni u jednoj od izrađenih formulacija (slika 3).

Merenjem zeta potencijala uzorka nanoemulzija stabilizovanih sa oba tipa emulgatora dobijeni su delom neočekivani rezultati.

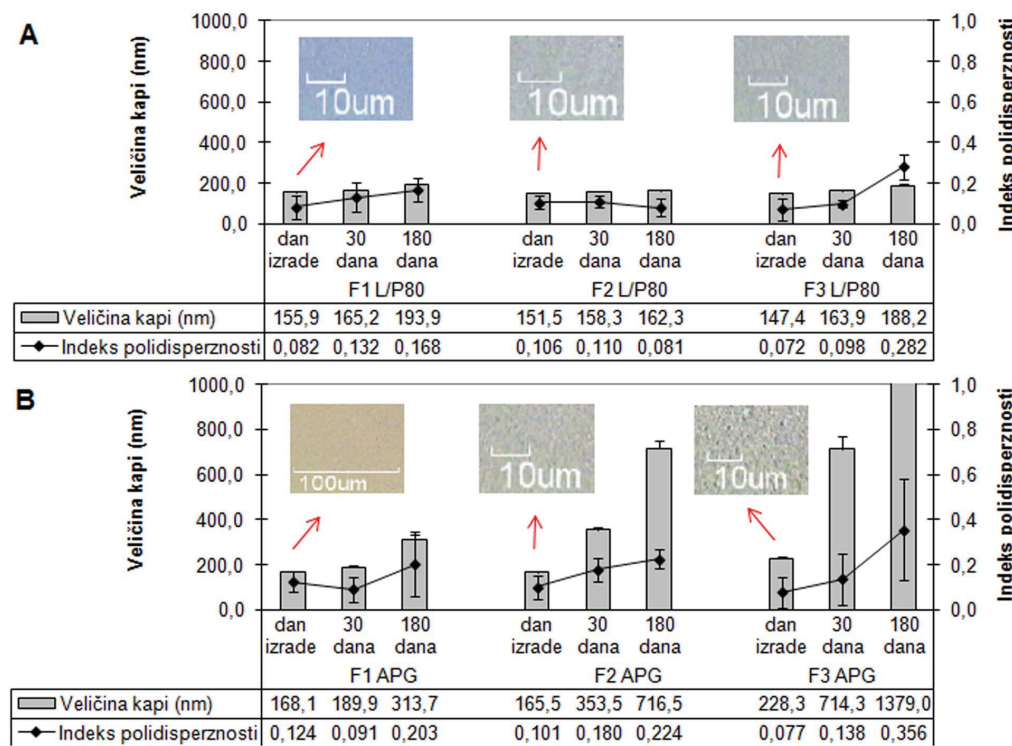
Poznato je da zeta potencijal približno karakteriše površinsko nanelektrisanje kapi u emulzijama i jedan je od faktora koji određuje njihovu fizičku stabilnost. Ako sve čestice/kapi u disperziji imaju visok pozitivni ili visok negativni zeta potencijal, doći će do njihovog međusobnog odbijanja što sprečava koalescenciju i povećava stabilnost sistema [31,32]. Veličina zeta potencijala, dakle, ukazuje na potencijalnu stabilnost nanodisperznog koloidnog sistema.

Zeta potencijali ispitivanih formulacija nanoemulzija, mereni odmah nakon izrade, bili su u opsegu od -17 do -50 mV (slika 1B). Nanoemulzije izrađene sa smešom lecitin/polisorbat 80 imale su zeta potencijal oko -20 mV, dok je zeta potencijal nanoemulzija izrađenih sa kaprilil/kapril glukozidom bio značajno veći (*t*-test, $p < 0,05$) i iznosio je oko -50 mV. Ove razlike u vrednostima zeta potencijala su očigledno posledica upotrebe različitog tipa emulgatora.

Kaprilil/kapril glukozid je nejonski sterni stabilizator, pa bi se na prvi pogled moglo očekivati niže vrednosti zeta potencijala. Međutim, ovaj polihidroksilni emulgator u svojoj strukturi ima hidrofobni deo, koji se smešta na površinu emulgovanih kapi ulja, i dug hidrofilni rep koji penetrira u vodenu fazu. Hidrofilni deo sadrži molekule glukoze koji mogu privući potencijalno negativno nanelektrisane hidroksilne jone, čime bi se mogla objasniti dobijena visoka negativna vrednost zeta potencijala [26].

Fizička stabilnost nanoemulzija stabilizovanih različitim tipom emulgatora

Stabilnost nanoemulzija je složeno pitanje i zavisi od brojnih faktora kao što su sastav, veličina kapi, vis-



Slika 3. Prosečna veličina kapi ($\pm SD$) i indeks polidisperznosti ($\pm SD$) formulacija stabilizovanih smešom lecitin/polisorbat 80 (A) i kaprilil/kapril glukozidom (B) na dan izrade (sa fotomikrografijama) i nakon 30 i 180 dana čuvanja na 25 °C.

Figure 3. Mean droplet size ($\pm SD$) and polydispersity index ($\pm SD$) of formulations stabilized with lecithin and polysorbate 80 mixture (A) and caprylyl/capryl glucoside (B) on day of preparation (with photomicrographs) and after 30 and 180 days of storage at 25 °C.

kozitet nanoemulzija i uslovi sredine (temperatura čuvanja, sile smicanja) [6,19].

Fizička stabilnost izrađenih nanoemulzija ispitivana je podvrgavanjem uzoraka čuvanju na dve različite temperature: 25 °C u toku 6 meseci i 40 °C u toku mesec dana. U definisanim vremenskim intervalima praćeni su veličina kapi, Pdl , zeta potencijal, pH i provodljivost ispitivanih formulacija.

U toku dugotrajnog čuvanja na sobnoj temperaturi, nanoemulzije stabilizovane APG emulgatorom nisu promenile svoje organoleptičke osobine. Zadržale su mlečno-beli izgled, bez pojave znakova kriminga ili flokulacije u toku čuvanja. Nanoemulzije stabilizovane smešom lecitin/polisorbat 80 su pak imale blago žutu boju i uočene su dve faze: gornja, koncentrovana emulzija i gotovo čist, viskozni rastvor. Opisana pojava se pripisuje fenomenu kriminga u toku koga se faza manje gustine izdvaja na površini emulzije [33,34]. Međutim, nakon laganog protresanja (u skladu sa zahtevima Ph. Eur. 7.0) došlo je do redispersovanja i dobijene su homogene nanoemulzije.

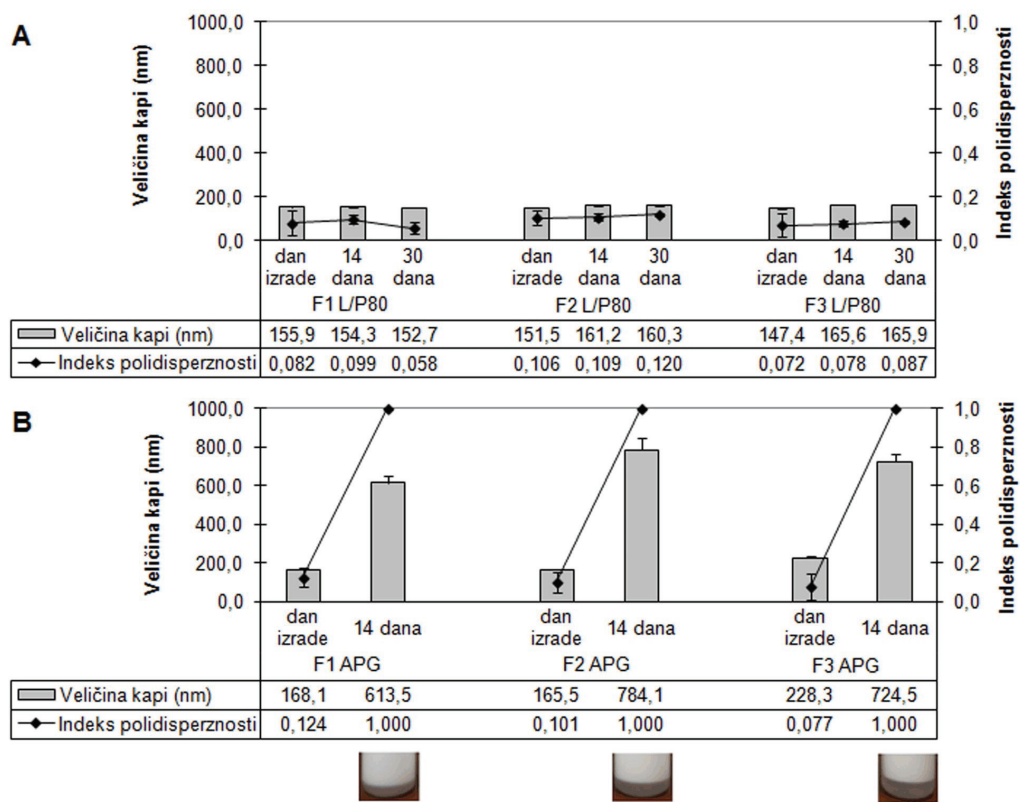
Nakon mesec dana čuvanja na povišenoj temperaturi, lecitin/polisorbat 80 nanoemulzije su bile slabo žute i neprijatnog mirisa, a na površini formulacije sa 40% masne faze bila je prisutna tanka skrama od uljanih kapi. APG nanoemulzije su pokazale nestabilnost,

odnosno došlo je do ireverzibilnog razdvajanja faza (gornji, mlečno beli i donji, bistri sloj).

Veličina kapi je upotrebljena kao jedan od reprezentativnih indikatora stabilnosti za sve formulacije nanoemulzija čuvanih na 25 (slika 3), odnosno 40 °C (slika 4).

Slika 3 pokazuje promene u veličini kapi i Pdl ispitivanih uzoraka nanoemulzija u toku čuvanja od 180 dana na 25 °C. Kod nanoemulzija stabilizovanih kombinacijom lecitina i polisorbata 80 zabeleženo je povećanje veličine kapi, koje je kod formulacija sa 20 i 40% MCT iznosilo oko 40 nm, a kod formulacije sa 30% MCT oko 10 nm. Pdl , koji daje informaciju o odstupanju od prosečne veličine kapi, bio je manji od 0,2 što odslikava relativno homogene kapi. Jedino je kod F3L/P80 Pdl bio veći (oko 0,3). Kod ove nanoemulzije je povećanje i veličine kapi i Pdl tokom vremena bilo statistički značajno (ANOVA, Tukey test, $p < 0,05$).

Posle istog perioda čuvanja, formulacije sa kaprilil/kapril glukozidom pokazale su značajno povećanje prosečne veličine kapi (ANOVA, Tukey test, $p < 0,05$). Najmanje i najsporije povećanje veličine kapi (od 168 na 314 nm) i Pdl manji od 0,2 imala je formulacija sa 20% MCT i ona se može smatrati fizički stabilnom. Kod APG formulacija sa 30 i 40% MCT, veličina kapi je bila daleko veća (716 nm i preko 1 µm) sa Pdl preko 0,2 odnosno 0,4, respektivno. Dobijeni rezultati upućuju na



Slika 4. Veličina kapi ($\pm SD$) i indeks polidisperznosti ($\pm SD$) formulacija stabilizovanih smešom lecitin/polisorbat 80 (A) i kaprilil/kapril glukozidom (B) na dan izrade i nakon 14 i 30 dana čuvanja na 40 °C.

Figure 4. Mean droplet size ($\pm SD$) and polydispersity index ($\pm SD$) of formulations stabilized with lecithin and polysorbate 80 mixture (A) and caprylyl/capryl glucoside (B) on day of preparation and after 14 and 30 days of storage at 40 °C.

širu raspodelu veličina kapi koja je indikator manje otpornosti nanoemulzije na Ostvaldovo sazrevanje u poređenju sa sistemima koji imaju uže raspodele, odnosno niži Pdl .

Brzo povećanje veličine kapi ukazuje na lošu stabilnost sistema [35]. U principu, manje kapi imaju manju tendenciju ka krimingu, a veću ka agregacijom, jer su brojnije u datom odnosu faza i podložnije uticaju Braunovog kretanja, pri čemu i jedno i drugo vodi ka koliziji kapi i nestabilnosti sistema [15].

Prisustvo agregata kapi u uzorcima nanoemulzija posle 180 dana dodatno je potvrđeno svetlosnom mikroskopijom (mikrografije nisu prikazane).

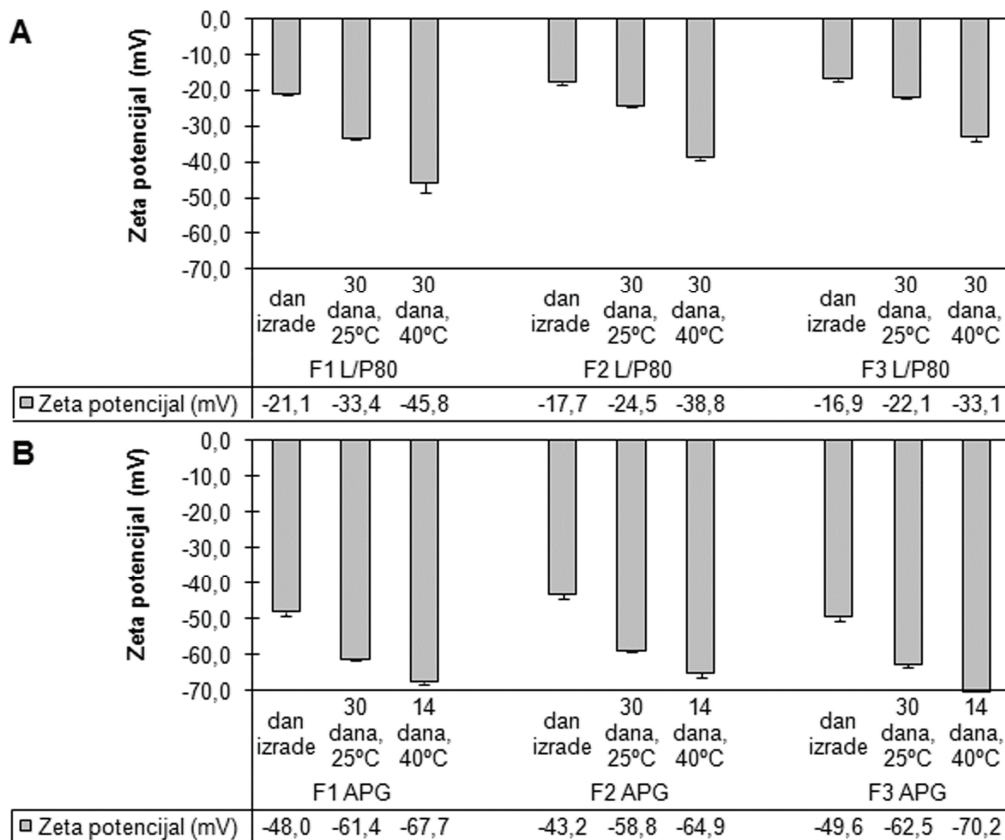
Slika 4 pokazuje veličinu kapi i Pdl ispitivanih formulacija nanoemulzija u toku čuvanja na 40 °C. Na osnovu veličine i raspodele veličina kapi može se zaključiti da su nanoemulzije stabilizovane standardnom kombinacijom emulgatora (lecitin/polisorbat 80) bile fizički stabilne u toku mesec dana čuvanja na povišenoj temperaturi. Najstabilnija je bila formulacija sa najmanjim sadržajem uljane faze (F1L/P80), kod koje se vrednosti za veličinu kapi i Pdl gotovo nisu promenile (ANOVA, post hoc Tukey test, $p > 0,05$). Sa povećanjem udela uljane faze (formulacije F2L/P80 i F3L/P80) došlo je do porasta veličine kapi za 10–20 nm, što se pokazalo sta-

tistički značajnim (ANOVA, Tukey test, $p < 0,05$). Povećanje veličine kapi bilo je izraženije kod formulacije sa 40% uljane faze (F3L/P80). Sve formulacije su, međutim, zadržale usku raspodelu veličine kapi, odnosno Pdl je bio oko 0,1, što može da ukaže na veću otpornost sistema na Ostvaldovo sazrevanje.

Za razliku od nanoemulzija sa lecitinom i polisorbatom 80, sve formulacije nanoemulzija stabilizovane APG emulgatorom bile su nestabilne na 40 °C, što se pokazalo već nakon dve nedelje. Došlo je do značajnog povećanja veličine kapi (Paired-Samples t-test, $p < 0,05$), i svi uzorci su bili jako polidisperzni (Pdl jednak 1) usled prisustva većih agregata kapi. Razlog za ovu nestabilnost može biti neadekvatan ideo emulgatora u datim formulacijama [36].

U prilog prethodnim nalazima idu i rezultati merenja zeta potencijala ispitivanih nanoemulzija. Slika 5 daje uporedni prikaz promena vrednosti zeta potencijala kod nanoemulzija nakon mesec dana čuvanja na sobnoj i temperaturi od 40 °C.

Kao što je već objašnjeno, veliko površinsko nanelektrisanje kapi smatra se jednim od ključnih faktora u održavanju stabilnosti nanoemulzija. Apsolutne vrednosti zeta potencijala veće od 30 mV uglavnom ukazuju na dobru fizičku stabilnost, dok vrednosti iznad 60 mV



Slika 5. Zeta potencijali nanoemulzija stabilizovanih smešom lecitin/polisorbat 80 (A) i kaprilil/kapril glukozidom (B) nakon čuvanja na 25 i 40 °C.

Figure 5. Zeta potentials of nanoemulsions stabilized with lecithin and polysorbate 80 mixture (A) and caprylyl/capryl glucoside (B) after storage at 25 and 40 °C.

ukazuju na odličnu dugoročnu stabilnost [31,37]. Za vrednost zeta potencijala oko -20 mV smatra se da obezbeđuje kratkoročnu stabilnost [38]. Ovo se, međutim, odnosi na sisteme koji su isključivo elektrostatički stabilizovani. U slučaju dodatne sterne stabilizacije (kao sa polisorbatom 80) vrednosti zeta potencijala oko ±20 mV su, takođe, dovoljne za postizanje zadovoljavajuće stabilnosti nanoemulzije [39].

Nakon mesec dana čuvanja na sobnoj temperaturi, kod svih nanoemulzija su dobijene značajno negativnije vrednosti zeta potencijala u odnosu na dan izrade (*Paired-Samples t-test*, $p < 0,05$). Od nanoemulzija stabilizovanih lecitinom i polisorbatom 80, najveći zeta potencijal imala je formulacija sa 20% masne faze (oko -33 mV), dok je zeta potencijal formulacija sa 30 i 40% masne faze bio manji (oko -25 mV) (slika 5A). Na osnovu dobijenih rezultata može se zaključiti da lecitin sa svojim negativno nanelektrisanim fosfolipidima, u prisustvu polisorbata 80 kao dodatnog sredstva za stabilizaciju, može da proizvede zadovoljavajući negativni potencijal površine kapi kod svih formulacija nanoemulzija.

Kod nanoemulzija stabilizovanih APG emulgatorom absolutne vrednosti zeta potencijala bile su 10–15 mV

veće u odnosu na inicijalne vrednosti (slika 5B). Ovako visoke negativne vrednosti zeta potencijala ukazuju na poboljšanu fizičku stabilnost, što se, međutim, za formulacije sa 30 i 40% uljane faze ne može reći na osnovu analize veličina kapi. Kod ovih sistema uočeno je veliko povećanje veličine kapi uprkos zadovoljavajućoj inicijalnoj raspodeli veličina kapi (slika 3B). Međutim, izgled ovih nanoemulzija nije ukazivao na destabilizaciju.

U toku čuvanja na 40 °C, nanoemulzije stabilizovane smešom lecitin/polisorbat 80 pokazale su značajno povećanje apsolutne vrednosti zeta potencijala, sa oko -20 na -40 mV (*Paired-Samples t-test*, $p < 0,05$, slika 5A). Ovo povećanje najčešće je uzrokovano hidrolizom molekula lecitina [16]. Hemiska degradacija ove PAM dovodi do povećanja koncentracije lizolecitina i slobodnih masnih kiselina, koji doprinose većem negativnom nanelektrisanju površina kapi [1]. Ovaj fenomen se prema tome smatra znakom fizičkohemijske destabilizacije sistema i može se preduprediti stabilizacijom lecitina, na primer primenom antioksidanasa [16].

Nanoemulzije stabilizovane APG emulgatorom su nakon 14 dana čuvanja na 40 °C imale vrednosti zeta potencijala u opsegu od -65 do -70 mV (slika 5B). Na osnovu ovih vrednosti reklo bi se da je njihova stabil-

nost odlična, što zapravo nije slučaj. Ovo pokazuje da zeta potencijal ne treba posmatrati kao garanciju za stabilnost, jer drugi relevantni faktori nisu obuhvaćeni ovim parametrom [40]. S druge strane, treba imati u vidu da je zeta potencijal inherentna karakteristika sistema, i da se njegove značajnije promene najčešće ne odigravaju kod fizički stabilnih sistema. Nestabilnost APG nanoemulzija pod stresnim uslovima (40°C) može se objasniti time da se na višim temperaturama pojavljuju dodatni faktori koji imaju destabilizući efekat [26].

U prilog prethodnim nalazima mogu ići i rezultati praćenja pH vrednosti i električne provodljivosti ispitivanih nanoemulzija. Praćenje pH važno je za procenu stabilnosti nanoemulzija zato što promene pH ukazuju na pojavu hemijskih reakcija koje mogu kompromitovati kvalitet finalnog proizvoda [35].

Slika 6 pokazuje promene pH vrednosti ispitivanih nanoemulzija u toku čuvanja na 25°C . Kod svih formulacija došlo je do značajnog opadanja pH vrednosti u funkciji vremena čuvanja (ANOVA, Tukey test, $p < 0,05$), koje je manje izraženo kod nanoemulzija stabilizovanih lecitinom i polisorbatom 80 u odnosu na one stabilizovane kaprilil/kapril glukozidom. Takođe se može primetiti da je do najvećeg pada pH došlo u toku prvih mesec dana čuvanja, dok je kasnije pH sporije opadao.

U toku čuvanja na 40°C , nanoemulzije su takođe pokazale promene pH vrednosti (slika 7). Došlo je do

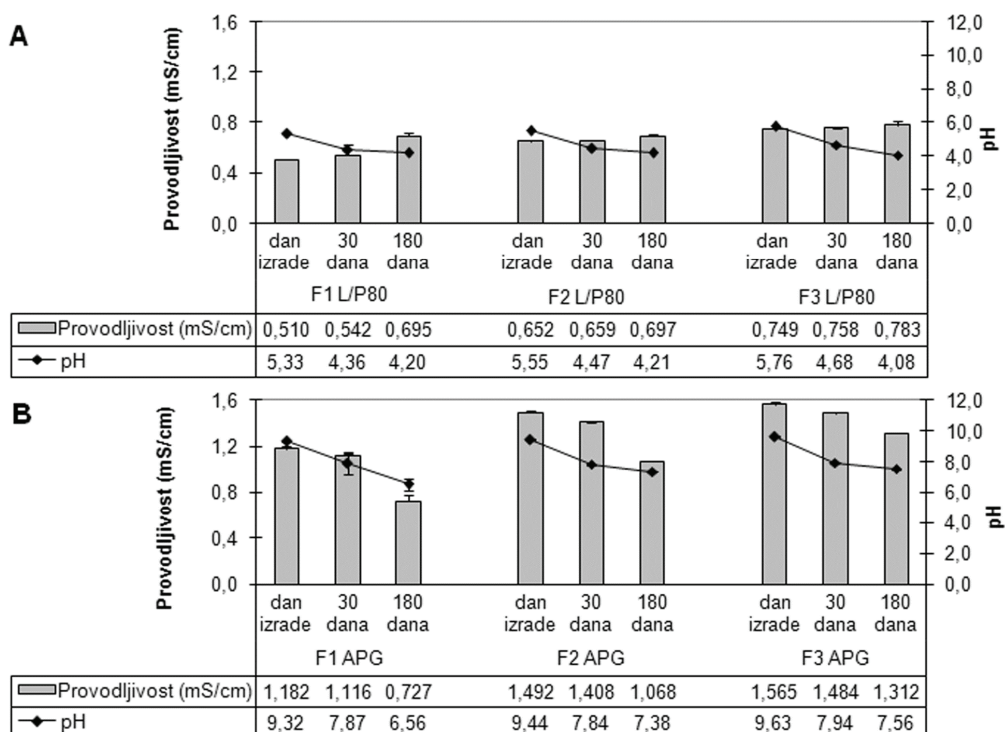
statistički značajnog pada pH nanoemulzija stabilizovanih i kombinacijom lecitin/polisorbat 80 (ANOVA, Tukey test, $p < 0,05$) i kaprilil/kapril glukozidom (*Paired-Samples t-test*, $p < 0,05$).

Opadanje pH vrednosti nanoemulzija dovodi se u vezu sa hidrolizom triglicerida iz uljane faze i fosfolipida iz lecitina, što dovodi do formiranja slobodnih masnih kiselina, lizofosfolipida i glicerofosfolipida [6,34]. Formiranje slobodnih masnih kiselina je odgovorno za kontradiktorno povećanje negativnih vrednosti zeta potencijala koje je napred opisano [6].

Baker i saradnici su pokazali da oslobađanje malih količina slobodnih masnih kiselina u toku čuvanja nanoemulzija, usled hidrolize fosfolipida i ulja, dovodi do povećanja negativnih vrednosti zeta potencijala, čime se povećava stabilnost ovih formulacija. Međutim, povećanje zeta potencijala može se smatrati samo delimično korisnim jer je formiranje slobodnih masnih kiselina udruženo sa smanjenjem pH vrednosti. Ovo promoviše dalju degradaciju kroz hidrolizu triglicerida i fosfolipida i destabilizuje nanoemulzije [1].

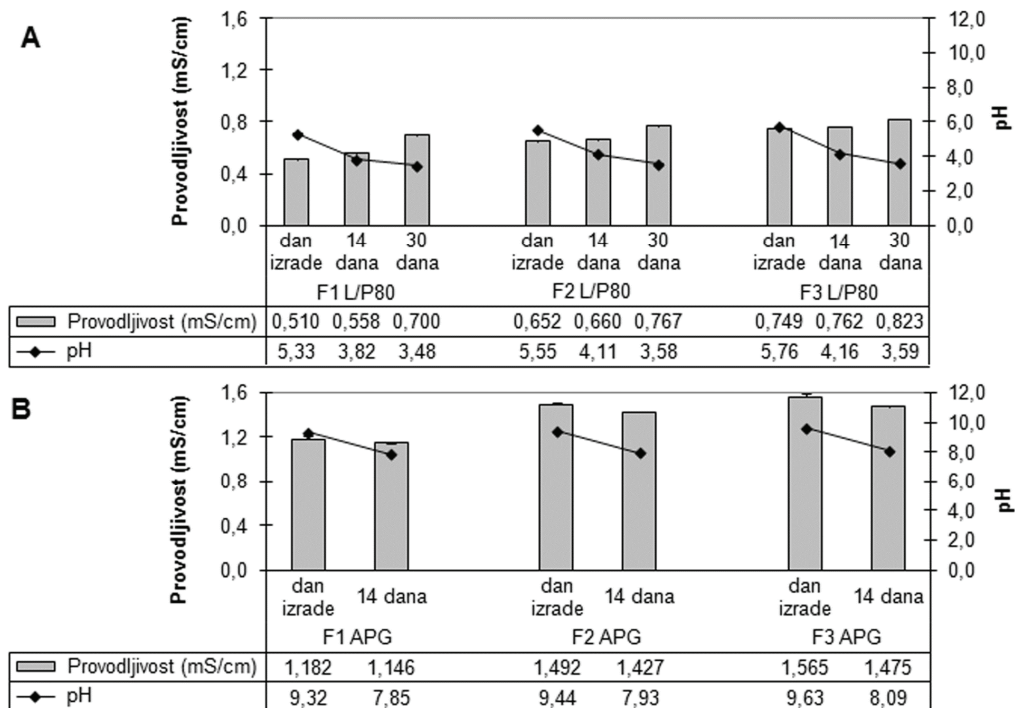
Iako se smanjenje pH vrednosti nanoemulzija u toku studija dugotrajne stabilnosti odvija sporo, preporučuje se podešavanje pH neposredno nakon izrade, kao i primena antioksidanasa [6].

Rezultati dobijeni merenjem električne provodljivosti pokazuju da je kod svih ispitivanih formulacija



Slika 6. pH vrednost ($\pm SD$) i električna provodljivost ($\pm SD$) nanoemulzija stabilizovanih sмеšom lecitin/polisorbat 80 (A) i kaprilil/kapril glukozidom (B) na dan izrade i nakon 30 i 180 dana čuvanja na 25°C .

Figure 6. pH value ($\pm SD$) and electrical conductivity ($\pm SD$) of nanoemulsions stabilized with lecithin and polysorbate 80 mixture (A) and caprylyl/capryl glucoside (B) on day of preparation and after 30 and 180 days of storage at 25°C .



Slika 7. pH vrednost ($\pm SD$) i električna provodljivost ($\pm SD$) nanoemulzija stabilizovanih smešom lecitin/polisorbat 80 (A) i kaprilil/kapril glukozidom (B) na dan izrade i nakon 14 i 30 dana čuvanja na 40 °C.

Figure 7. pH value ($\pm SD$) and electrical conductivity ($\pm SD$) of nanoemulsions stabilized with lecithin and polysorbate 80 mixture (A) and caprylyl/capryl glucoside (B) on day of preparation and after 14 and 30 days of storage at 40 °C.

nanoemulzija, u svim uslovima čuvanja, došlo do značajnih promena ovog parametra (slike 6 i 7).

Tokom 6 meseci čuvanja na 25 °C, nanoemulzije stabilizovane kombinacijom lecitin/polisorbat 80 pokazale su porast u električnoj provodljivosti, dok se kod nanoemulzija stabilizovanih kaprilil/kapril glukozidom električna provodljivost smanjila (ANOVA, Tukey test, $p < 0,05$) (slika 6). Tokom čuvanja na 40 °C, takođe je kod nanoemulzija sa lecitinom i polisorbatom 80 došlo do povećanja (ANOVA, Tukey test, $p < 0,05$), a kod APG nanoemulzija do smanjenja električne provodljivosti (Paired-Samples t-test, $p < 0,05$, slika 7).

Promene u električnoj provodljivosti mogu ukazati na nestabilnost i mogu da utiču na veličinu kapi nanoemulzija [35]. Generalno, kada je emulzija stabilna, ne zapažaju se promene u provodljivosti. Povećanje provodljivosti se može smatrati znakom destabilizacije nanoemulzije koja će se ispoljiti pre ili kasnije. Međutim, teško je samo na osnovu provodljivosti proceniti stabilnost nanoemulzije [41].

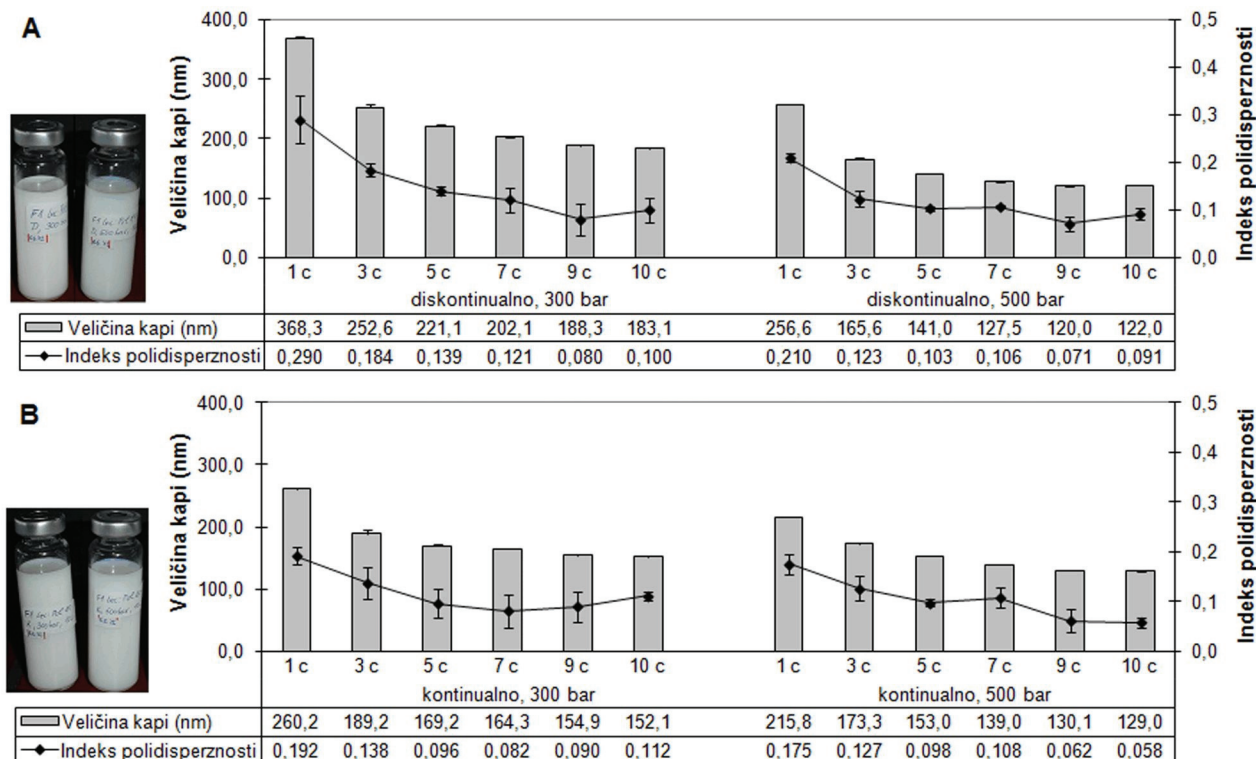
Merenje provodljivosti takođe omogućava da se utvrdi da li je kontinualna faza nanoemulzije vodena ili masna, kao i da se prati pojava inverzije faza [42]. Rezultati za provodljivost dobijeni u ovom istraživanju pokazuju da su u toku praćenja sve nanoemulzije imale vodenu fazu kao kontinualnu, odnosno nisu pokazale inverziju faza.

Uticaj procesnih parametara na karakteristike nanoemulzija

U ovom delu ispitivan je uticaj parametara procesa homogenizacije na veličinu i raspodelu veličina kapi nanoemulzija, u cilju pronalaženja optimalnih uslova izrade nanoemulzija. Na osnovu rezultata eksperimenta sprovedenih u prvom delu istraživanja, za radnu formulaciju odabrana je nanoemulzija sa najmanjom koncentracijom emulgatora, koja je imala malu veličinu kapi i bila stabilna u svim uslovima čuvanja. Ova formulacija, sastavljena od 20% MCT i po 2% lecitina i polisorbata 80, homogenizovana je na 50 °C variranjem broja ciklusa (do 10), pritiska (300 i 500 bar) i postupka homogenizacije (kontinualan i diskontinualan). Slika 8 prikazuje efekat pomenutih procesnih parametara na velećinu kapi i Pdl model nanoemulzije.

Veličina kapi nanoemulzije obično može da se smanji povećanjem unosa energije usled dužeg vremena homogenizacije (tj. povećanja broja prolazaka kroz homogenizator) ili većeg pritiska [43].

Kao što se i očekivalo, povećanje broja ciklusa homogenizacije dovelo je do značajnog smanjenja veličine kapi (ANOVA, Tukey test, $p < 0,05$), pri čemu se prosečna veličina kapi nakon devetog i desetog ciklusa homogenizacije nije značajno razlikovala. Takođe, sa povećanjem broja ciklusa homogenizacije, dobijena je i značajno uža raspodela veličine kapi (ANOVA, Tukey test, $p < 0,05$), mada razlike u vrednostima Pdl nakon



Slika 8. Uticaj variranja procesnih parametara na veličinu i raspodelu veličina kapi izrađenih uzoraka nanoemulzije.

Figure 8. Influence of variation of the production parameters on particle size and particle size distribution of prepared nanoemulsion samples.

petog ciklusa nisu bile statistički značajne. Osim toga, može se primetiti da sa desetim prolaskom kroz homogenizator nije došlo do poboljšanja u vrednosti Pdl (slika 8). Na osnovu dobijenih rezultata može se zaključiti da je za dobijanje optimalne veličine kapi sa uskom raspodelom dovoljno 9 ciklusa homogenizacije pod povišenim pritiskom.

Pritisak homogenizacije značajno utiče na svojstva emulzija, jer sile smicanja i turbulencije, koje zavise od pritiska, a nastaju u toku homogenizacije, mogu da utiču na veličinu kapi i raspodelu veličine [19]. Rezultati dobijeni u ovom istraživanju pokazuju da su veličina kapi i Pdl bili manji pri višem pritisku (slika 8).

Statistički je pokazano (dvofaktorska analiza varianse) da na veličinu kapi uzorka nanoemulzije nakon devetog ciklusa homogenizacije značajno utiče pritisak, ali i da postoji značajan uticaj postupka homogenizacije, kao i značajne interakcije ovih promenljivih. Pošto su oba faktora (pritisak i postupak homogenizacije) imala po dva nivoa (300/500 bar i kontinualan/diskontinualan, raspektivno) ne radi se post hoc test, ali je sproveden post hoc test za interakcije ova dva faktora. Razmatranjem efekta postupka izrade u zavisnosti od pritiska (kontinualno, 300 bar vs. kontinualno, 500 bar; diskontinualno, 300 bar vs. diskontinualno, 500 bar) dobijeno je da je veličina kapi u oba slučaja, pri kontinualnom i diskontinualnom postupku, značajno manja

($p < 0,05$) na višem pritisku (500 bar). Kada je, pak, posmatran efekat pritiska u zavisnosti od postupka izrade (300 bar, kontinualno vs. 300 bar, diskontinualno; 500 bar, kontinualno vs. 500 bar, diskontinualno) zaključeno je da se na nižem pritisku (300 bar) dobija značajno manja ($p < 0,05$) veličina kapi kada se homogenizacija odvija kontinualno; dok se na višem pritisku (500 bar) značajno manja ($p < 0,05$) veličina kapi dobija kada je postupak homogenizacije diskontinualan. Ovo zapažanje, međutim, nije lako objasniti.

Poznato je da tokom procesa emulgovanja, koji se odvija u homogenizatoru pod visokim pritiskom, dolazi do deformacije i lomljenja (usitnjavanja) kapi, adsorpcije emulgatora na novoformiranu međupovršinu, kolizijske i, verovatno, rekoalescencije novonastalih kapi. Ravnoteža između lomljenja i rekoalescencije kapi određuje finalnu veličinu kapi nanoemulzije, a ova ravnoteža, između ostalog, zavisi i od pritiska homogenizacije. Naime, sa povećanjem pritiska homogenizacije povećava se brzina i stepen rekoalescencije, čime se objašnjava zašto povećanje pritiska ne dovodi uvek do smanjenja veličina kapi [44,45].

Moguće je da je pri kontinualnom procesu homogenizacije koji se odvija na višem pritisku (500 bar) pojava rekoalescencije kapi izraženija nego kod diskontinualnog procesa, pri čemu nije sasvim jasno šta je

tačno do ovoga dovelo, što svakako otvara puteve za dalja istraživanja.

Kada je kao zavisno promenljiva posmatran *Pdl* dobijen nakon devetog ciklusa homogenizacije, dvofaktorskom analizom varijanse nije utvrđen značajan uticaj ni pritiska, ni postupka homogenizacije, kao ni značajnost interakcija ovih parametara ($p > 0,05$).

Dobijeni rezultati jasno upućuju da se diskontinualnom homogenizacijom pod pritiskom od 500 bar može dobiti nanoemulzija optimalnih karakteristika (veličina kapi, *Pdl*).

Dalji korak u istraživanju bio bi procena uticaja procesnih parametara na fizičku stabilnost nanoemulzija i razmatranje uticaja dodatnih stabilizatora, kao i različitih model lekovitih supstanci na karakteristike i stabilnost nanoemulzija.

ZAKLJUČAK

Homogenizacijom pod visokim pritiskom uspešno su izrađene nanoemulzije sastavljene od visokoprečišćene vode i rastućih koncentracija MCT i emulgatora- kapril/lipil/kapril glukozida ili kombinacije lecitina i polisorbata 80. Vrsta emulgatora je uticala na veličinu kapi, ali je ona kod svih izrađenih nanoemulzija bila između 145 i 230 nm, sa *Pdl* ispod 0,2.

Tokom čuvanja na 25 i 40 °C, kod svih nanoemulzija došlo je do porasta veličine i raspodele veličina kapi, povećanja negativne vrednosti zeta potencijala i opadanja pH vrednosti, dok se električna provodljivost povećala kod nanoemulzija sa lecitinom i polisorbatom 80, a smanjila kod APG nanoemulzija. Tokom 6 meseci čuvanja na 25 °C, veličina kapi nanoemulzija stabilizovanih smešom lecitin/polisorbat 80 povećala se za 10–40 nm, dok je kod APG nanoemulzija povećanje veličine kapi, zavisno od udela masne faze, bilo 140–1000 nm. Na osnovu analize veličine i raspodele veličina kapi, može se reći da su nanoemulzije izrađene sa 20% MCT i 4% emulgatora (smeša lecitin/polisorbat 80 (1/1) odnosno APG) bile stabilne pod ovim uslovima čuvanja. Ekstremni porast veličine kapi od oko 1000 nm, zabeležen kod APG nanoemulzije sa 40% MCT, može biti posledica neadekvatnog udela APG emulgatora u formulaciji ili njegove nemogućnosti da sam, bez prisustva koemulgatora, stabilizuje nanoemulzije sa ovakom visokim udelom ulja. U toku mesec dana čuvanja na 40 °C, nanoemulzije stabilizovane smešom lecitin/polisorbat 80 bile su fizički stabilne, dok su sve nanoemulzije stabilizovane APG emulgatorom bile nestabilne.

Procenom uticaja procesnih parametara na veličinu kapi i *Pdl* nanoemulzije, mogu se odabrati optimalni procesni parametri: 9 ciklusa homogenizacije, pritisak od 500 bar i diskontinualan postupak homogenizacije.

Zahvalnica

Ovaj rad urađen je u okviru projekta tehnološkog razvoja TR34031 koji finansira Ministarstvo prosvete i nauke Republike Srbije.

LITERATURA

- [1] M.T. Baker, M. Naguib, Propofol: the challenges of formulation, *Anesthesiology* **103** (2005) 860–876.
- [2] S. Tamilvanan, S. Benita, The potential of lipid emulsion for ocular delivery of lipophilic drugs, *Eur. J. Pharm. Biopharm.* **58** (2004) 357–368.
- [3] E. Yilmaz, H.H. Borchert, Design of a phytosphingosine-containing, positively-charged nanoemulsion as a colloidal carrier system for dermal application of ceramides, *Eur. J. Pharm. Biopharm.* **60** (2005) 91–98.
- [4] M. Sznitowska, M. Gajewska, S. Janicki, A. Radwanska, G. Lukowski, Bioavailability of diazepam from aqueous-organic solution, submicron emulsion and solid lipid nanoparticles after rectal administration in rabbits, *Eur. J. Pharm. Biopharm.* **52** (2001) 159–163.
- [5] M. Sznitowska, S. Janicki, E. Dabrowska, K. Zurowska-Pryczkowska, Submicron emulsions as drug carriers; Studies on destabilization potential of various drugs, *Eur. J. Pharm. Sci.* **12** (2001) 175–179.
- [6] V. Klang, C. Valenta, Lecithin-based nanoemulsions, *J. Drug Del. Sci. Tech.* **21** (2011) 55–76.
- [7] H. Zhou, Y. Yue, G. Liu, Y. Li, J. Zhang, Q. Gong, Z. Yan, M. Duan, Preparation and characterization of a lecithin nanoemulsion as a topical delivery system, *Nanoscale Res. Lett.* **5** (2010) 224–230.
- [8] X. Li, L. Du, C. Wang, Y. Liu, X. Mei, Y. Jin, Highly efficient and lowly toxic docetaxel nanoemulsions for intravenous injection to animals, *Pharmazie* **66** (2011) 479–483.
- [9] T.G. Mason, J.N. Wilking, K. Meleson, C.B. Chang, S.M. Graves, Nanoemulsions: formation, structure, and physical properties, *J. Phys. Condens. Matter* **18** (2006) R635–R666.
- [10] J.V.L. Henry, P.J. Fryer, W.J. Frith, I.T. Norton, Emulsification mechanism and storage instabilities of hydrocarbon-in-water sub-micron emulsions stabilised with Tweens (20 and 80), Brij 96v and sucrose monoesters, *J. Colloid Interface Sci.* **338** (2009) 201–206.
- [11] V. Klang, N.B. Matsko, C. Valenta, F. Hofer, Electron microscopy of nanoemulsions: An essential tool for characterisation and stability assessment, *Micron* **43** (2012) 85–103.
- [12] T. Tadros, P. Izquierdo, J. Esquena, C. Solans, Formation and stability of nano-emulsions, *Adv. Colloid Interface Sci.* **108–109** (2004) 303–318.
- [13] D.J. McClements, Nanoemulsions versus microemulsions: terminology, differences, and similarities, *Soft Matter* **8** (2012) 1719–1729.
- [14] K. Welin-Berger, B. Bergenstahl, Inhibition of Ostwald ripening in local anesthetic emulsions by using hydrophobic excipients in the disperse phase, *Int. J. Pharm.* **200** (2000) 249–260.

- [15] D.J. McClements, Food emulsions: Principles, practices and techniques, 2nd ed., CRC Press, Boca Raton, FL, 2005.
- [16] V. Klang, N. Matsko, K. Raupach, N. El-Hagin, C. Valenta, Development of sucrose stearate-based nanoemulsions and optimisation through γ -cyclodextrin, *Eur. J. Pharm. Biopharm.* **79** (2011) 58–67.
- [17] W. von Rybinski, B. Guckenbiehl, H. Tesmann, Influence of co-surfactants on microemulsions with alkyl polyglycosides, *Colloids Surfaces, A* **142** (1998) 333–342.
- [18] O. Söderman, I. Johansson, Polyhydroxyl-based surfactants and their physico-chemical properties and applications, *Curr. Opin. Colloid Interface Sci.* **4** (1999) 391–401.
- [19] Y. Yuan, Y. Gao, J. Zhao, L. Mao, Characterization and stability evaluation of b-carotene nanoemulsions prepared by high pressure homogenization under various emulsifying conditions, *Food Res. Int.* **41** (2008) 61–68.
- [20] S. Hoeller, A. Sperger, C. Valenta, Lecithin based nanoemulsions: A comparative study of the influence of non-ionic surfactants and the cationic phytosphingosine on physicochemical behaviour and skin permeation, *Int. J. Pharm.* **370** (2009) 181–186.
- [21] Y. Baspinar, C.M. Keck, H.H. Borcher, Development of a positively charged prednicarbate nanoemulsion, *Int. J. Pharm.* **383** (2010) 201–208.
- [22] V. Klang, N. Matsko, A.M. Zimmermann, E. Vojnikovic, C. Valenta, Enhancement of stability and skin permeation by sucrose stearate and cyclodextrins in progesterone nanoemulsions, *Int. J. Pharm.* **393** (2010) 152–160.
- [23] C. Rupp, H. Steckel, B.W. Müller, Mixed micelle formation with phosphatidylcholines: The influence of surfactants with different molecule structures, *Int. J. Pharm.* **387** (2010) 120–128.
- [24] N. Anton, P. Gayet, J.P. Benoit, P. Saulnier, Nano-emulsions and nanocapsules by the PIT method: an investigation on the role of the temperature cycling on the emulsion phase inversion, *Int. J. Pharm.* **344** (2007) 44–52.
- [25] R.H. Müller, S. Schmidt, I. Buttle, A. Akkar, J. Schmitt, S. Brömer, SolEmuls® – novel technology for the formulation of i.v. emulsions with poorly soluble drugs, *Int. J. Pharm.* **269** (2004) 293–302.
- [26] A. Kovacevic, S. Savic, G. Vuleta, R.H. Müller, C.M. Kreck, Polyhydroxy surfactants for the formulation of lipid nanoparticles (SLN and NLC): Effects on size, physical stability and particle matrix structure, *Int. J. Pharm.* **406** (2011) 163–172.
- [27] C.P. Tan, M. Nakajima, β -Carotene nanodispersions: preparation, characterization and stability evaluation, *Food Chem.* **92** (2005) 661–671.
- [28] H. Tesmann, J. Kahre, H. Hensen, B.A. Salka, in: K. Hill, W. von Rybinski, G. Stoll (Eds.), Alkyl Polyglycosides: Technology, Properties and Applications, Wiley-VCH Verlag GmbH, Weinheim, 2008, pp. 71–98.
- [29] M. Jumaa, B.W. Müller, The effect of oil components and homogenization conditions on the physicochemical properties and stability of parenteral fat emulsions, *Int. J. Pharm.* **163** (1998) 81–89.
- [30] S. Jahnke, in: R.H. Müller, B.H.L. Böhm (Eds.), Dispersion Techniques for Laboratory and Industrial Scale Processing, Wissenschaftliche Verlagsgesellschaft mbH, Stuttgart, 2001, pp. 7–30.
- [31] R.H. Müller, Zetapotential und Partikelladung in der Laborpraxis, Band 37, Wissenschaftliche Verlagsgesellschaft mbH, Stuttgart, 1996.
- [32] S.A. Wissing, R.H. Müller, Solid lipid nanoparticles as carrier for sunscreens: in vitro release and in vivo skin penetration, *J. Control. Release* **81** (2002) 225–233.
- [33] M. Trotta, F. Pattarino, T. Ignoni, Stability of drug-carrier emulsions containing phosphatidylcholine mixtures, *Eur. J. Pharm. Biopharm.* **53** (2002) 203–208.
- [34] K. Zurowska-Pryczkowska, M. Sznitowska, S. Janicki, Studies on the effect of pilocarpine incorporation into a submicron emulsion on the stability of the drug and the vehicle, *Eur. J. Pharm. Biopharm.* **47** (1999) 255–260.
- [35] D.S. Bernardi, T.A. Pereira, N.R. Maciel, J. Bortoloto, G.S. Viera, G.C. Oliveira, P.A. Rocha-Filho, Formation and stability of oil-in-water nanoemulsions containing rice bran oil: in vitro and in vivo assessments, *J. Nanobiotechnology* **9** (2011) 44.
- [36] S. Feng, G. Huang, Effects of emulsifiers on the controlled release of paclitaxel (Taxol) from nanospheres of biodegradable polymers, *J. Control. Release* **71** (2001) 53–69.
- [37] T.M. Riddick, Control of Colloid Stability through Zeta Potential, Zeta-Meter Inc. via Livingston Publishing Company, Wynnewood, 1968.
- [38] P.R. Mishra, L. Al Shaal, R.H. Müller, C.M. Keck, Production and characterization of Hesperetin nanosuspensions for dermal delivery, *Int. J. Pharm.* **371** (2009) 182–189.
- [39] K. Mitri, R. Shegokar, S. Gohla, C. Anselmi, R.H. Müller, Lipid nanocarriers for dermal delivery of lutein: Preparation, characterization, stability and performance, *Int. J. Pharm.* **414** (2011) 267–275.
- [40] A. Akkar, R.H. Müller, Formulation of intravenous carbamazepine emulsions by SolEmuls technology, *Eur. J. Pharm. Biopharm.* **55** (2003) 305–312.
- [41] H. Masmoudi, Y.L. Dréau, P. Piccerelle, J. Kister, The evaluation of cosmetic and pharmaceutical emulsions aging process using classical techniques and a new method: FTIR, *Int. J. Pharm.* **289** (2005) 117–131.
- [42] M.J. Lawrence, G.D. Rees, Microemulsion-based media as novel drug delivery systems, *Adv. Drug Deliv. Rev.* **45** (2000) 89–121.
- [43] W. van Nieuwenhuyzen, B.F. Szuhaj, Effects of lecithins and proteins on the stability of emulsions, *Fett/Lipid* **100** (1998) 282–291.
- [44] J. Flouri, J. Bellette, J. Legrand, A. Desrumaux, Analysis of a new type of high pressure homogeniser. A. Study of the Flow Pattern, *Chem. Eng. Sci.* **59** (2004) 843–853.
- [45] J. Flouri, J. Legrand, A. Desrumaux, Analysis of a new type of high pressure homogeniser. Part B. study of droplet break-up and reconnection phenomena, *Chem. Eng. Sci.* **59** (2004) 1285–1294.

SUMMARY**NANOEMULSIONS PRODUCED BY VARYING THE TYPE OF EMULSIFIER AND OIL CONTENT: EFFECT OF FORMULATION AND PROCESS PARAMETERS ON THE CHARACTERISTICS AND PHYSICAL STABILITY**

Sanela M. Đorđević¹, Nebojša D. Cekić², Tanja M. Isailović¹, Jela R. Milić¹, Gordana M. Vučeta¹, Miodrag L. Lazić², Snežana D. Savić¹

¹*Department of Pharmaceutical Technology and Cosmetology, Faculty of Pharmacy, University of Belgrade, Belgrade, Serbia*

²*Faculty of Technology, University of Niš, Leskovac, Serbia*

(Scientific paper)

The aim of the present study was to prepare oil-in-water nanoemulsions stabilized with a novel natural alkyl polyglucoside surfactant and to compare them with corresponding lecithin/polysorbate 80-based nanoemulsions in terms of physicochemical properties and physical stability. Nanoemulsions were prepared by high pressure homogenization, using 20, 30 and 40 mass% medium chain triglyceride as oil phase, and 4, 6 and 8 mass% lecithin/polysorbate 80 mixture (1/1) or caprylyl/capryl glucoside as emulsifiers. The effects of emulsifier type, emulsifier concentration and oil content were investigated with respect to changes in particle size, particle size distribution, surface charge and physical stability. The influence of production parameters (number of homogenization cycles, type of homogenization process, homogenization pressure) on particle size was also investigated. Analysis was performed by photon correlation spectroscopy, laser diffraction, zeta potential, pH and electrical conductivity measurements. All the produced formulations revealed a small droplet size ranging from 147 to 228 nm and a very narrow size distribution (polydispersity index range 0.072–0.124). Zeta potentials were found to be about –20 and –50 mV for nanoemulsions stabilized with lecithin/polysorbate 80 and caprylyl/capryl glucoside, respectively. The results obtained from the stability studies (6 months at 25 °C and 1 month at 40 °C) indicated that nanoemulsion stability was influenced by their composition. The results also suggested the most appropriate production parameters: 9 homogenization cycles, homogenization pressure of 500 bar and discontinuous process of homogenization.

Keywords: Nanoemulsion • Caprylyl/capryl glucoside • Lecithin • Polysorbate 80 • High pressure homogenization • Physical stability

Serbian heavy clays behavior: Application in rough ceramics

Milica V. Arsenović¹, Lato L. Pezo², Zagorka M. Radojević¹, Slavka M. Stanković³

¹Institute for testing of materials IMS, Bulevar vojvode Mišića 43, 11000 Belgrade, Serbia

²University of Belgrade, Institute of general and physical chemistry, Studentski trg 12, 11000 Belgrade, Serbia

³Faculty of Technology and Metallurgy, University of Belgrade, Kneževićevo 4, 11000 Belgrade, Serbia

Abstract

This study is focused on the behavior of five new deposits of heavy clays from Serbia, with the aim to evaluate their potential suitability as raw materials in rough ceramic applications. The Pfefferkorn plasticity coefficient (PC) and drying susceptibility using Bigot's curve were measured for each raw sample. Thermoanalytical analysis (TDA) showed the behavior of dry products during firing. Samples groups were fired in the range of 850–1000 °C. Water absorption capacity (WAC) and compressive strength (CS) measurements were done in order to characterize the clays after firing. Linear regression models were used to fit the results. Mathematical tools were used to determine statistical difference of major oxides content, shaping moist and compressive strength of dry laboratory products, using post-hoc Tukey's HSD test. The chemical and mineralogical compositions of samples do not differ considerably, but their possible application does. All studied clays seem to be easily adaptable to a correct brick making process.

Keywords: heavy clay, technological characteristics, application.

Available online at the Journal website: <http://www.ache.org.rs/HI/>

Clays and clay minerals have been widely used as the main raw materials in the fabrication of rough ceramic products for construction materials due to many specific properties before and after firing. The study of mineral phases present in the raw material is rather difficult, because industrial clays have a very complex mineralogical composition. During the firing process, a series of transformations occur, which affect the final properties of the ceramic products. Plasticity, chemistry, color, mechanical strength after firing, water absorption capacity etc. are the important properties of clay that are of interest to the ceramics industry [1]. The knowledge of these characteristics leads to optimization of the use of new clay deposits in local or regional ceramic industries.

During the ceramic process, once the crystalline structures of minerals exceed their stability limits, they are partially decomposed while others are simultaneously formed. The high temperature, low-pressure mineral transformations are mainly influenced by the chemical and mineralogical compositions of the original clay, its grain-size distribution, the maximum heating temperature, heating rate, duration of firing and kiln atmosphere. The knowledge of the physicochemical behavior of the clays is essential when exploring suitable compositions required for rough ceramics production. Common components that play fundamental roles

SCIENTIFIC PAPER

UDC 553.6(497.11):666.3

Hem. Ind. **67** (5) 811–822 (2013)

doi: 10.2298/HEMIND121123006A

for optimum processing and performance of the final products are kaolins for plasticity, silica as filler, and feldspar as fluxing agent to lower the temperature required for formation of a vitreous phase that promotes densification [2,3].

The masonry industry in Serbia was founded in 1866. According to the Association of Clay Products industry data, until recently there were about 90 brick factories, of which more than a half used primitive production technology, which had been for two decades completely abandoned in Europe. Nowadays, with more foreign investors and major manufacturers, the situation has changed significantly. The number of facilities is reduced and product quality requirements are increased in coordination with the European Norms.

Loess (both onshore and swamp) in north Serbia is mostly used in the brick industry, and therefore belongs to the brick raw materials. Almost the entire production of solid bricks is based on loess, mostly in small factories at a low level of technology and equipment. Favorable particle size distribution, low shrinkage and sensitivity to drying and firing lead to much easier production. The presence of carbonates in loess in the form of large concretions and "loess dolls" is common. Such material is not suitable for the application, or requires special processing line with a cleaner and multiple grinding in degrees of granularity below 0.5 mm [4,5].

One of the main factors currently preventing realization of the potential of local materials in Serbia is insufficient scientific analyses. Serbian clays have been often characterized, but in the literature there are very few presented studies on the quality and potential use,

Correspondence: M.V. Arsenović, Institute for testing of materials IMS, Bulevar vojvode Mišića 43, 11000 Belgrade, Serbia.

E-mail: milica.arsenovic@institutims.rs

Paper received: 23 November, 2012

Paper accepted: 10 January, 2013

although clay is a primary material for local ceramic manufacturers [3–8]. For this reason, particular attention should be paid to the investigation of clay deposits in Serbia for ceramic applications. The raw clay materials from non-exploited deposits presented in this paper were neither tested for masonry production, nor characterized. This is the first detailed, multi-level analysis of interest from an academic and technological viewpoint. The main objective of this work is determination of chemical and mineralogical compositions, as well as technological behavior that altogether allows the evaluation of the applicability of the clay deposits studied, while giving a picture on the quality of the clay from Serbia from different localities.

EXPERIMENTAL

This paper presents the ceramic and technological behavior of five new opened clay deposits in Serbia, which can be used in the formulation of masonry raw materials mix. The clays originate from Svilajnac (SV), Jagrjevo (JG), Mala Plana (MP), Leskovac (LE) and Novi Pazar (NP). These clays are representative raw materials that reflect the similarities and differences in the quality and possible application.

After collecting, the samples were dried in the oven at 105 ± 5 °C until constant mass and then milled following the usual practice in ceramic laboratories. The clays were moistened and mixed with about 24–26% of water. They were left to rest for 24 h in sealed nylon bags to obtain homogenous moist distribution. The shaping process was done following the usual procedure [8] using a laboratory extruder (Händle). Laboratory samples are produced in the form of tiles (120 mm×50 mm×14mm), hollow blocks with vertical voids (55.3 mm×36 mm×36 mm) and cubes (30 mm×30 mm×30 mm).

Firing was done in the oxygen atmosphere kiln, with average heating speed of 1.4 °C/min until 610 °C, and later with the rate of 2.5 °C/min until the final given temperature was reached, at which the samples were treated for 2 h. Firing was conducted at 850, 900, 950 and 1000 °C. Properties of dry and fired samples are presented, with the suggested ways of applying the tested materials for certain products.

In order to precisely define the technological characteristics of brick raw materials from new locations in Serbia, it is necessary to determine their chemical, mineralogical and granulometric composition. Three samples for each deposit were analyzed to obtain the mineralogical and chemical compositions (average values are shown and discussed).

Granulometry analysis was done by the sieve and pipette method, after drying at room temperature. The sample was dipped in distilled water for 24 h, and then gently boiled for 1 h. The cooled suspension was sieved

on the 0.063 mm sieve, the fraction was dried and measured, and later the filtrate was treated in an ultrasonic bath for 30 min. Samples were taken by pipette at appropriate intervals. Due to the size of particles in the sample NP, it was necessary to do sedimentation analysis (fractions under 0.063 mm).

The mineralogical analysis was carried out by X-ray diffraction (XRD) using a powder diffractometer (Philips PW-1050) with $\lambda_{\text{Cu-K}\alpha}$ radiation and scanning speed 0.05°/s, both on powder (bulk samples) and oriented aggregates (treated with ethylene glycol and heated to 450 °C for 2 h) of the clay fraction obtained, following the criteria described in the literature [9].

The chemical analysis was performed by classical silicate, gravimetric analysis [3,10]. Loss on ignition (LOI) was determined by standard procedure [11].

The Pfefferkon method was used to determine the plasticity coefficient (PC) as described in the literature [12]. After moistening and shaping of tiles, the mass is used to obtain the drying capacity of the clays by using a barelattograph to trace Bigot's curve.

The water absorption capacity (WAC) was determined in fired clay pieces by soaking in distilled water for 24 h, according to standard EN 771-1 [13]. The laboratory hollow blocks compressive strength was tested in a laboratory hydraulic press, according to standard EN 772-1 [14].

Thermodilatometric analysis (TDA) was carried out using a Linseis dilatometer with a rhodium oven and thermopar platina – rhodium (L76). Firing conditions were such that the temperature increment was 10 °C/min, and the sample was held up at the final temperature of 1000 °C for 1 h. This technique consists in measuring the length of a sample as a function of the temperature, allowing the study of the sintering process. The extruded sample was dried overnight at 105 °C and then heated in the dilatometer. Length changes were recorded every minute during the heating stage. Descriptive statistical analyses for calculating the means and the standard error of the mean were performed using Microsoft Excel 2007 software. All obtained results were expressed as the mean \pm standard deviation (SD). Regression analysis and the evaluation of one-way analysis of variance (ANOVA) of obtained results were performed for comparison of means, and significant differences are calculated according to post-hoc Tukey's HSD test at the $p < 0.05$ level, using StatSoft Statistica 10 software.

RESULTS AND DISCUSSION

Granulometry and mineralogy

Granulometry analysis gave the information about particle size and their quantity (in %), as presented in Figure 1. Based on these results, Figure 2 is obtained,

where clay (< 2 µm) and sand sized particles (> 50 µm) are observed. The rest of the material (until 100%) presented allevrite (2–50 µm) [15].

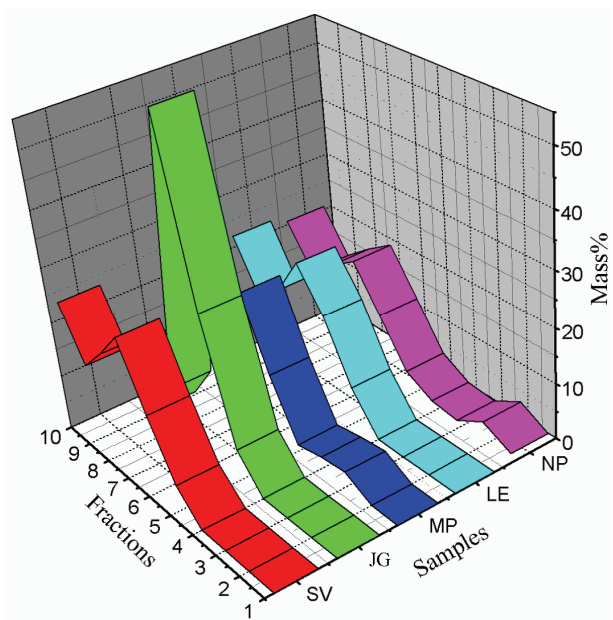


Figure 1. The particle size distribution (in mm): 1 – 2.0, 2 – 1.0, 3 – 0.5, 4 – 0.125, 5 – 0.063, 6 – 0.032, 7 – 0.016, 8 – 0.008, 9 – 0.004, 10 – 0.001.

Soil texture is presented according to Unified Soil Classification System (Figure 2). All the samples belong to allevrite type sediments (silt fraction), where NP showed the highest level of sand (19.42±0.99%), JG of allevrite (87.53±4.19%) and MP of clay (28.85±1.73%). The samples SV and MP belong to silty clay loam, LE and NP are defined as silty loam, while JG represents silt.

The particle size distribution could have an effect on the bulk density and compressive strength of the green body, which should be dependent on the way in which the particles are packed. Better particle packing is obtained when finer particles fill the void space between the larger particles.

Characteristics of good plasticity and high levels of water absorption are linked to the fraction of the particles less than 2 µm in size, which represents the clay fraction. A high content of this fraction gives plasticity in conjunction with high initial water content and drying problems due to the high drying shrinkage. Higher proportions of finer particles in the raw material favour vitrification due to the good compaction of samples during moulding, and this has a positive influence on resistance of fired samples [16]. The content of fraction below 2 µm is similar in SV, MP, LE and NP and ranges between 23.89–28.85%, while sample JG contains only 0.69±0.03% of clay, which remarkably affects its ceramic and technological properties.

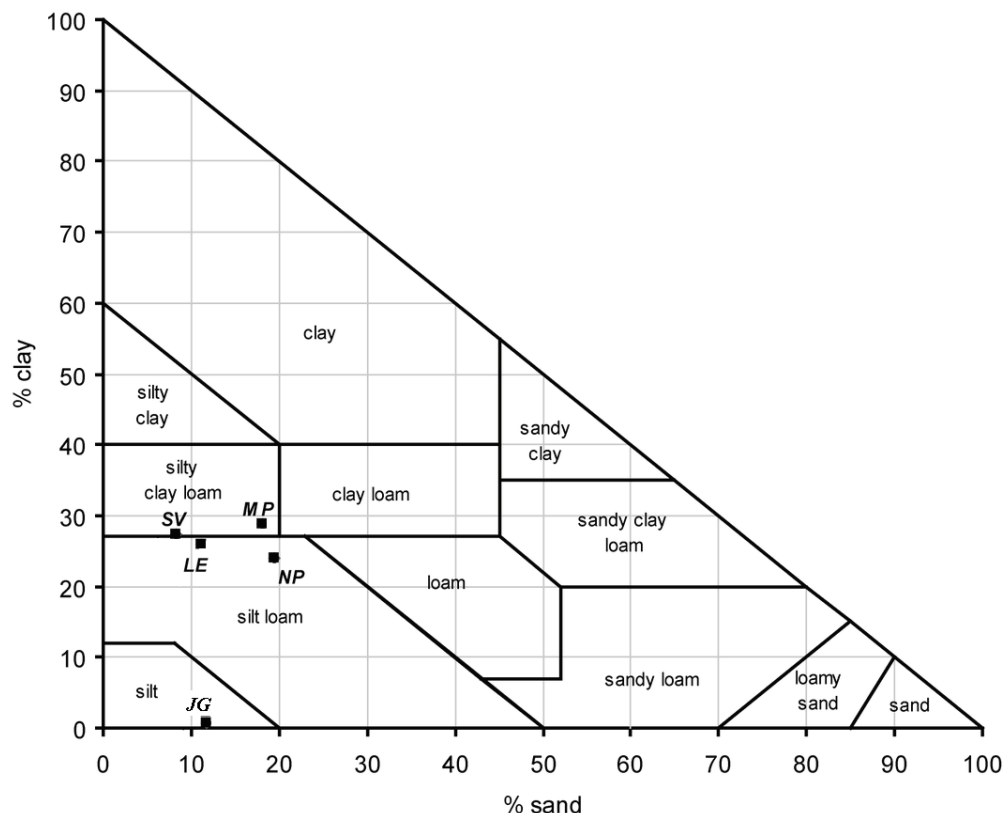


Figure 2. Samples texture diagram.

Optimal compositions of material mixtures can be based on the granulometric composition of soil using the Winkler diagram [17], the traditional way to roughly determine the possible usage of raw materials in certain brick products (for example solid bricks, hollow blocks and roofing tiles). The samples tested did not belong to any group, according to Winkler's diagram. Particle size distribution (Figure 1) showed that all the samples mostly contained particles between 8 and 32 µm, and JG even 58.5±2.37% of 16–32 µm particles. The largest particles were observed in NP, which had 1.68±0.05% of > 2.0 mm and 4.36±0.05% of > 1.0 mm particles. The problem that can arise from the presence of coarser particles can be solved by simply crushing and sifting. Generally, particles below 53 µm are called the "plasticity fraction" because they provide the necessary plasticity for shaping, combined with strength for handling wet products. The particle size distribution in moistened raw material also depends on the water content [12]. This means that the Winkler diagram cannot be taken literally.

The mineralogical composition of all the samples was dominated by quartz and layered silicates (Table 1). All the samples showed very similar clay composition: mica, chlorite and smectite were found. Low detected amounts of layered silicates were in JG in the case of smectite, and in LE chlorite. The sample SV also contained a low amount of kaolinite.

It is known that red-firing clays are rich in mica [18]. Decomposition of unstable illite leads to formation of mica by isostructural replacement. Micas belong to primary minerals, which have larger particles than clay minerals (fractions usually greater than 10 µm [19]. Because of the possibility of isostructural substitution of aluminum in octahedron and silicon cations in the

tetrahedral configuration with the other cations, there are many minerals that are montmorillonite-like, with a common name smectites [12,20]. Smectite shows a good plasticity behavior, it is an expanding clay mineral that dries hard [21]. The absence of a significant amount of smectitic minerals will ensure a ceramic body against possible difficulties during drying [22]. In principle, the illite and smectite are clay brick essential ingredients because they sinter at relatively low temperatures [18].

Calcite was found in most of the samples (SV, MP and LE) in low proportions. Samples JG and NP showed larger contents of calcite, while JG also showed presence of dolomite. Feldspars are mainly present in low rates in the form of plagioclase (JG, LE, NP and MP). Other feldspar minerals – amphiboles, are also detected in low rate in the sample MP. These different types of clay raw materials do not present great differences in mineralogical composition.

Chemical composition

The five clays present the expected typical compositions (Table 2), rich in silica and alumina, with satisfying content of potash, minor contents of titan, phosphorus and sulfur, accompanied by a significant amount of iron oxides. The post-hoc Tukey's HSD tests were evaluated for comparison between oxides content in samples, and statistically significant differences were found between all samples, significant at $p < 0.05$ level.

In the chemical compositions of heavy clay, high quartz content is mainly related to SiO₂ percentages. The Al₂O₃ content is correlated to clay minerals. K₂O and Na₂O, first of all, presume the presence of mica, then K feldspar and Na feldspar contents. High MgO content indicates dolomite [3,5]. By viewing the con-

Table 1. Mineralogical composition of the studied clays; Q – quartz; layered silicates (M – mica, Ch – chlorite, Sm – smectite, K – kaolinite), carbonates (C – calcite, D - dolomite), F – feldspars (P – plagioclase, A – amphiboles), + – present, +l – present in low rate

Sample	Q	Layered silicates				Carbonates		F ^a	
		M	Ch	Sm	K	C	D	P	A
SV	+	+	+	+	+l	+l			
JG	+	+	+	+l		+	+	+l	
MP	+	+	+	+		+l		+l	+l
LE	+	+	+l	+		+l		+l	
NP	+	+	+	+		+		+l	

Table 2. Macroelements content (mass%); values with the same letter, written in superscript are not statistically different at the p < 0.05 level, 95% confidence limit, according to post-hoc Tukey's HSD test

Sample	SiO ₂	Al ₂ O ₃	Fe ₂ O ₃	CaO	MgO	Na ₂ O	K ₂ O	TiO ₂	P ₂ O ₅	SO ₃	LOI
SV	62.60±1.40 ^c	14.00±0.05 ^a	6.76±0.29 ^b	2.56±0.10 ^b	1.46±0.07 ^a	1.02±0.05 ^a	3.14±0.13 ^a	0.75±0.04 ^a	0.24±0.01 ^b	0.00±0.00 ^a	7.45±0.24 ^a
JG	47.10±1.63 ^a	10.50±0.39 ^c	4.00±0.23 ^c	11.50±0.25 ^e	5.98±0.24 ^e	1.58±0.07 ^b	3.07±0.12 ^{ab}	0.55±0.01 ^b	0.15±0.01 ^a	0.04±0.00 ^b	15.39±0.66 ^d
MP	55.37±3.32 ^b	15.05±0.96 ^{ab}	7.86±0.60 ^a	3.46±0.12 ^c	3.43±0.13 ^d	1.50±0.01 ^b	3.20±0.15 ^a	1.15±0.06 ^c	0.09±0.00 ^c	0.00±0.00 ^a	9.14±0.37 ^b
LE	60.13±2.13 ^{bc}	15.54±0.25 ^b	8.07±0.20 ^a	1.50±0.11 ^a	1.92±0.10 ^b	0.81±0.02 ^c	2.75±0.11 ^b	0.74±0.03 ^a	0.25±0.01 ^b	0.00±0.00 ^a	8.00±0.38 ^{ab}
NP	49.42±0.67 ^a	17.87±0.48 ^c	7.51±0.33 ^{ab}	7.25±0.44 ^d	2.37±0.12 ^c	1.12±0.03 ^a	3.14±0.09 ^a	0.75±0.03 ^a	0.15±0.01 ^a	0.07±0.00 ^c	10.60±0.12 ^c

tent of major oxides in clay minerals given in literature [19], it can be observed that the highest content of aluminum is in kaolinite, potassium in illite and sodium in montmorillonite. These results confirm the mineralogical content as described previously.

The amount of silica (49.42 ± 0.67 to $62.60 \pm 1.40\%$) was relatively high in all the samples. The Al_2O_3 content varied between 10.50 ± 0.39 and 17.87 ± 0.48 mass%, depending on the content of clay minerals. Actually, these clays consist mainly of SiO_2 and Al_2O_3 (overall 57.60–76.60%) showing the dominant presence of quartz and clay minerals. Relatively high amount of Fe_2O_3 (4 ± 0.23 to $8.07 \pm 0.20\%$) regards these samples as acceptable for use in rough ceramics. The amount of the earth-alkaline oxides (CaO and MgO) is low, indicating that the studied red clay is not so rich in carbonates. JG showed the highest CaO content ($11.50 \pm 0.25\%$) and loss on ignition ($15.39 \pm 0.66\%$) due to the decomposition of calcium carbonates, and probably the content of organic carbon in allevrite. This result agreed with that of calcimetry tests (not shown in this work). After microscopic identification of 0.063 mm sieve residue, it is determined that sample JG had shells remains and loess fragments.

Most of the samples (SV, JG, MP and NP) showed high relative amounts of alkaline oxides ($\text{Na}_2\text{O} + \text{K}_2\text{O}$), which, in reaction with silica and alumina, promote liquid phase formations that facilitate densification, explaining why samples sinter at relatively low temperatures [23]. The loss on ignition was in the range of 7.45 ± 0.24 to $15.39 \pm 0.66\%$, and can be, besides carbonates, attributed to the presence of clay minerals, hydroxides and organic matter [16].

Some harmful constituents such as sulfur compounds, which can cause efflorescence [21], were not detected in some of the samples (SV, MP and LE), and were found in low quantities ($0.08 \pm 0.001\%$) in JG and NP samples.

Color

The color of clay bricks generally depends on the mineralogical composition of raw materials, temperature and firing conditions. Aluminum oxide (Al_2O_3), iron oxide (Fe_2O_3) and calcium oxide (CaO) are responsible for the final product color. The dominant influence belongs to iron (III). The color of natural iron oxides and hydroxides varies from orange to red, depending on the type and degree of crystallinity and therefore influences soil color. Brick raw materials contain iron mainly in the form of minerals from the hydroxide group (goethite, limonite). In the process of burning, iron hydroxide is transformed into hematite, which gives the ceramic body characteristic color. The transformation of hydroxide into oxide by dehydroxylation begins at a temperature of about 300°C , and with the achievement of 400°C , the oxide is formed. The degree

of oxidation greatly depends on the heating regime and the atmosphere in the furnace [6,18]. The yellow color of a fired product may come from calcium or aluminum oxide if the iron content is low, when iron (III) oxide associates with silicates [24]. For raw clay brick samples, the contents of oxides that affect the color are given in Table 2. After calculation of oxides important for color to 100%, Figure 3 can be constructed. The ternary diagram shows the color differences between the samples according to Piltz [25].

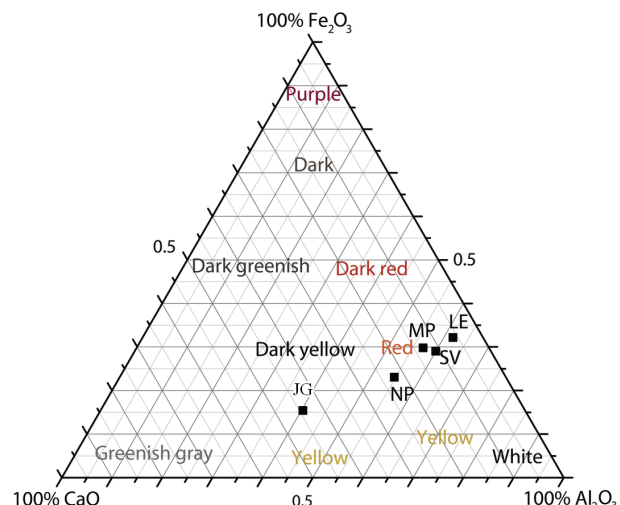


Figure 3. Three-component diagram showing fired brick color differences.

From the results shown in Table 2 and the diagram shown in Figure 3, the color of all fired samples is red with some hue differences. LE, MP and SV were of the most intensive red color, while firing at the higher temperatures (950 and 1000°C) gave a darker hue. Similar behavior was observed with NP samples, bearing in mind that they were of brighter red color. The JG sample was of reddish yellow color at all firing temperatures.

Ceramic and technological tests

In order to define the behavior of raw clay materials from Serbia in the technological process of brick production, it is important to define their technological and ceramic characteristics. Test results are shown in tables and graphs, and include: properties of materials after processing, homogenization and shaping, the behavior of raw materials in the process of drying and dry product characteristics and technological features of fired products.

Raw material and green samples

Table 3 shows important parameters concerning raw materials and dry samples. The post-hoc Tukey's HSD tests were evaluated for comparison between the molding moisture and dry compressive strength, and

Table 3. Properties of materials after processing and drying; values with the same letter, written in superscript are not statistically different at the $p < 0.05$ level, 95% confidence limit, according to post-hoc Tukey's HSD test

Parameter	SV	JG	MP	LE	NP
Molding moisture (%)	24.23 ± 0.07^a	24.71 ± 1.06^a	24.34 ± 0.25^a	25.56 ± 0.80^a	24.52 ± 1.64^a
Dry compressive strength (MPa)	16.30 ± 0.28^c	10.76 ± 0.19^a	11.98 ± 0.48^a	19.22 ± 0.88^b	19.25 ± 0.59^b

statistically significant differences were found between all samples, significant at $p < 0.05$ level (Table 3).

The quantity of water used to make plastic mass was similar for all the samples and in the range of 24.23 ± 0.07 to $25.56 \pm 0.80\%$. The compressive strength of dry samples indicates the transport possibility of the products from the kiln to the dryer, so it is desirable to be as high as possible. A higher compressive strength will show samples with better packing and higher content of clay minerals, which are subjected to an appropriate drying regime. In our case the samples LE and NP behaved the best.

Plasticity is one of the most important rheological properties of raw materials for traditional ceramics, because it points to the possibility of forming clay bodies by application of pressure, and the mechanical properties of the product [26,27]. The mineralogical composition of the clays and the particle size distribution influence plasticity. The plasticity of clays is related to the morphology of the plate-like clay mineral particles that slide over the others when water is added, which acts as a lubricant. As the water content of clay is increased, the plasticity increases up to a maximum, depending on the nature of the clay [12]. The materials

with the highest content of clay particles (SV, LE and MP) showed the most plastic features (Figure 4). The differences in the plasticities of the samples were almost understandable from the particle size distribution data (Figure 2). Varying amounts of quartz also influenced the plasticity and drying behavior of the clays [22].

The Pfefferkorn diagram is presented as a link between water content and material stiffness (Figure 4). Most of the samples (SV, MP, LE and NP) showed very high plastic behavior ($PC > 30$), explaining their excellent aptitude for pressing; only the JG sample had moderately plastic properties ($PC = 24.5$).

The experimental data obtained were fitted to linear regression models ($y = a + bx$) solved by a Levenberg–Marguardt numerical method, and the results were examined using standard statistical error tests, *i.e.*, coefficient of determination (r^2), the mean relative percent error (MPE), the root mean square error ($RMSE$) and the reduced chi-square (χ^2). The higher the values of r^2 and the lower the values of MPE , $RMSE$ and χ^2 , the better is the goodness of fit (Table 4). These parameters were calculated as follows:

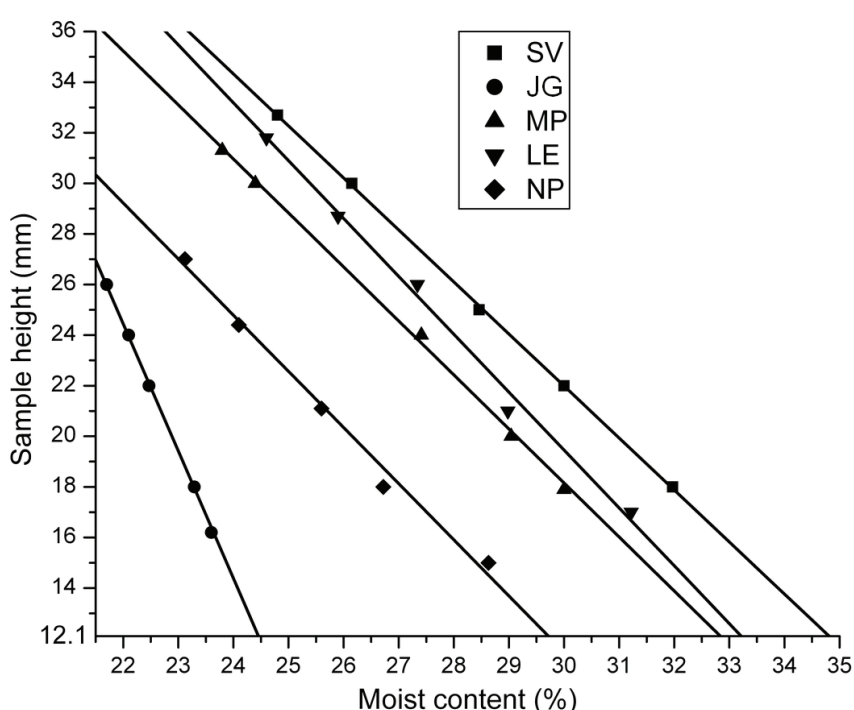


Figure 4. Plasticity determination of materials.

Table 4. Linear regression model constants for plasticity determination by Pfefferkorn method; All constants were significant at $p<0.05$ level, 95% confidence limit, according to ANOVA calculation

Constant	SV	JG	MP	LE	NP
a	83.72 ± 0.55	137.06 ± 1.42	82.57 ± 1.25	87.79 ± 3.01	77.65 ± 3.23
b	-2.06 ± 0.02	-5.12 ± 0.06	-2.15 ± 0.05	-2.28 ± 0.11	-2.21 ± 0.13
r^2	0.999	0.999	0.999	0.993	0.990
$\chi^2 \times 10^2$	1.24	0.997	6.50	31.9	31.9
$MPE \times 10^{12}$	-1.49	-5.32	0.308	0.662	0.66
$RMSE \times 10^{12}$	3.33	1.19	0.688	1.48	1.48

$$MPE = \frac{100}{N} \sum_{i=1}^n \frac{|y_{\text{exp},i} - y_{\text{pre},i}|}{y_{\text{exp},i}},$$

$$RMSE = \left[\frac{1}{N} \sum_{i=1}^n (y_{\text{exp},i} - y_{\text{pre},i})^2 \right]^{1/2},$$

$$\chi^2 = \frac{\sum_{i=1}^n (y_{\text{exp},i} - y_{\text{pre},i})^2}{N-n},$$

where $y_{\text{exp},i}$ is the i -th experimentally observed value, $y_{\text{pre},i}$ is the i -th mathematical model predicted value, N is the number of observations and n is the number model constants ($n = 2$, for linear model).

Bigot's curves with critical points (K_t) coordinates are given in Figure 5. ΔG_k is mass loss, and ΔS_k presents shrinkage in critical point. The drying capacities for the studied clay deposits were done in laboratory conditions, by drying in air for 24 h [28]. These curves were used as preliminary indicators in the choice of raw materials [27] for the ceramic industry.

According to the results, the behavior of SV, MP, LE and NP were somewhat similar, although they have different values of shrinkage and moisture at critical points. SV and LE clays showed the highest shrinkage, 8.02 and 7.99% respectively, due to their high plasticity coefficient and clay content, while consequently they have more problematic drying behavior and susceptibility. The sample MP shrunk by 3.58%, and by contrast, JG and NP showed more suitable behavior, with respectively 3.57 and 5.37% shrinkage during air drying. Most of the tested samples are highly susceptible in drying process (mass loss during drying in the air at critical point, $\Delta G_k > 10$), where SV should be the most carefully dried ($\Delta G_k = 13.77\%$); followed by MP ($\Delta G_k = 12.44\%$), LE ($\Delta G_k = 11.80\%$) and NP ($\Delta G_k = 10.35\%$). The sample JG belonged to the susceptible clays group because of smectite absence ($\Delta G_k = 8.40\%$). It is known that with higher sand content, the clay is less sensitive to drying [23].

In summary, increased dispersion of raw clay material together with the content of fine particles caused more shrinkage, greater plasticity, increased mecha-

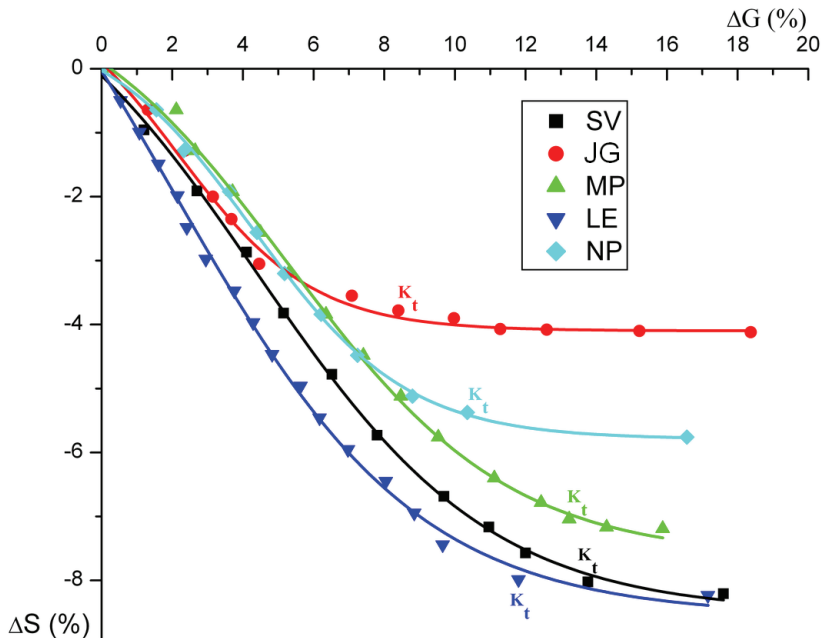


Figure 5. Bigot's curves of analyzed clay samples: K_t – critical point, ΔS_k – critical point shrinkage, ΔG_k – critical point mass loss.

nical strength in the dry state and susceptibility during drying [12].

Fired samples

Raw materials characteristics and processing parameters affect the microstructure and final properties of ceramics, so it is necessary to test the behavior of samples as a function of the firing temperature [8]. The presence of minerals in different amounts influences the behavior of fired products. Depending on the characteristics of raw materials, the recommended firing regimes differ. Some researchers [29,30] in the first part of the process, until a temperature of 600 °C, practiced slow warming (2–5 °C/min) to avoid the appearance of cracks during the phase transformation of quartz at 573 °C, with later increasing of heating rate to 5–10 °C/min. The firing regime used in this research

(1.4 °C/min until 610 °C, 2.5 °C/min until the final temperature) was very slow and enough for all reactions to take place. All the tested samples were fired under the same regime in order to have comparable results. In order to optimize the mechanical properties of laboratory heavy clay products, water absorption is also a phenomenon that must be controlled [31].

Figure 6 shows the firing temperature dependence of compressive strength of the laboratory blocks and average water absorption capacity (WAC) of all extruded samples.

Compressive strength and water absorption results are fitted in the linear regression models, as already described in this paper, and presented in Table 5.

The samples SV, MP and LE showed similar behaviour, where at the higher temperature sample LE had the lowest water absorption value (and consequently

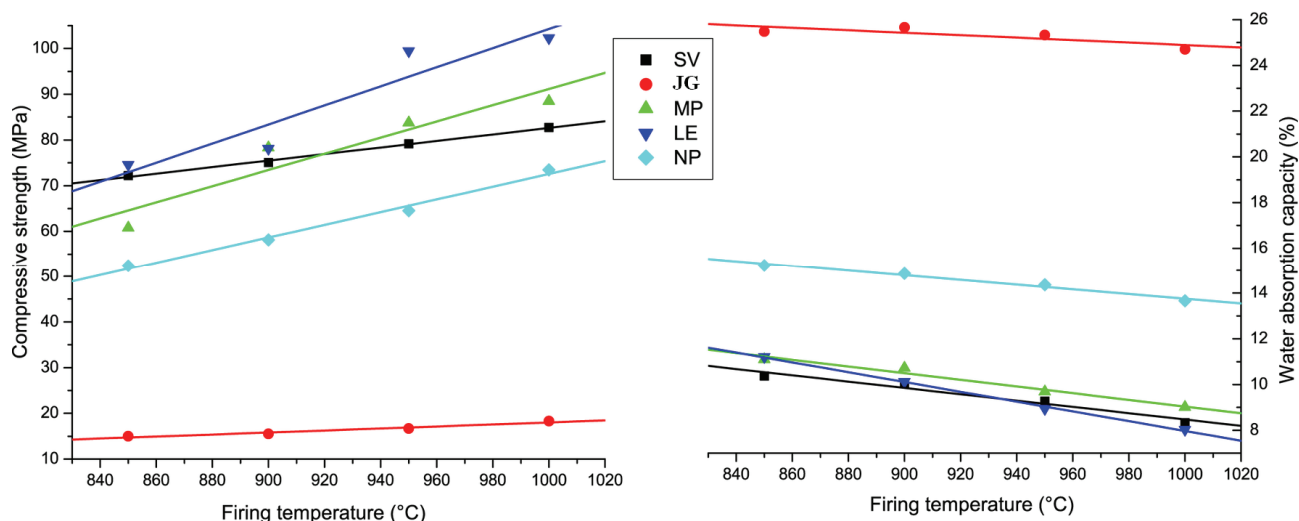


Figure 6. Compressive strength and water absorption depending on the firing temperature applied.

Table 5. Linear regression model constants for compressive strength and water absorption;

Constant	SV	JG	MP	LE	NP
CS					
<i>a</i>	11.20±3.13 ^a	-3.99±3.00 ^a	-86.05±40.38 ^a	-104.61±47.64 ^a	-66.61±9.48 ^b
<i>b</i>	0.07±0.00 ^b	0.02±0.00 ^b	0.18±0.04 ^a	0.21±0.05 ^a	0.14±0.01 ^b
<i>r</i> ²	0.998	0.946	0.892	0.892	0.989
<i>χ</i> ²	0.425	0.174	0.237	0.330	1.31
MPE×10 ¹²	-8.19	74.9	0.725	-0.188	-0.712
RMSE×10 ¹²	16.4	1.50	1.45	0.377	1.42
WA					
<i>a</i>	22.27±1.86 ^b	30.27±2.38 ^b	23.66±1.63 ^b	29.41±0.71 ^b	24.17±1.03 ^b
<i>b</i>	-0.01±0.00 ^b	-0.01±0.00 ^a	-0.01±0.00 ^b	-0.02±0.00 ^b	-0.01±0.00 ^b
<i>r</i> ²	0.959	0.886	0.972	0.997	0.978
<i>χ</i> ² ×10 ²	5.03	8.27	3.85	0.729	1.54
MPE×10 ¹²	-0.327	449	0.427	0.167	0.00222
RMSE×10 ¹²	0.655	898	0.854	0.335	0.00444

^aSignificant at *p* < 0.10 level; ^bSignificant at *p* < 0.05 level

the highest compressive strength). NP showed moderately high WAC level, and JG very high. The characteristics of the JG raw sample are responsible for the high values of water absorption and low compressive strength, due to the amount of carbonates (and the highest loss on ignition values). High porosity and water absorption observed in JG sample can be explained by its loess origin, meaning higher calcite content [4].

Thermodilatometric analysis

Dilatometric curves are used to determine the occurrence of densification in temperate regions as a function of the clay minerals content [30]. The dimensional change during firing of the 20 mm samples is shown in Figure 7.

The majority of raw materials, except JG, had no dimensional changes up to 97 °C. Then, SV and NP began to shrink with the same intensity up to about 124 °C, and then the collection ended with the NP already at about 146 °C for 6.8 µm (0.034%), and with SV even at 245 °C for 26.5 µm (0.13%). A slight expansion followed by shrinkage between room temperature and 120 °C can be attributed to the loss of the adsorbed water. In some cases, adsorbed water removal can last even until 650 °C [16]. LE mainly did not change the dimensions until the temperature of 220 °C, after which it began to slightly shrink for about 24 µm (0.12%), with the end at 374 °C. MP did not change the dimensions up to 338 °C, when spreading occurred. Between 450 and 650 °C, all the samples shrank due to

the dehydroxylation of clay minerals. Singer and Singer [32] pointed out that the transformation of quartz α to quartz β occurs at 573 °C with a volume increase of 2%, and by further slow heating β -quartz changes to β_2 -tridymite at 870 °C with a volume increase of 12%. JG spreaded constantly until 579 °C, when all the samples started with the moderate expansion, with maxima from 678.5 (MP) to 834 °C (LE). The greatest expansion occurred in JG (205 µm, 1.02%) and the lowest in MP (55 µm, 0.28%), due to different quartz contents. Further shrinkage can be attributed to sintering, formation of vitreous phase, decarbonization and recrystallization of new ceramic phases [16]. After this period, most of the samples rapidly shrank until 1000 °C. Vitrification occurred at temperatures above 900 °C due to the significant presence of illite [33]. The sample JG began to spread rapidly at 927 °C for 166 µm (0.83%). It can be explained by the presence of dolomite (Table 1). Only this sample contained dolomite from the all five investigated samples, and it is known that dolomite decomposes completely above 900 °C. The product resulting from this relatively low-temperature calcination is highly porous and reactive and is known as "calcinated dolomite".

Possible applications of tested clays in rough ceramics

Each ceramic product requires clays with particular and appropriate characteristics [16]. Based on chemical and mineralogical composition, as well as particle size distribution, analyzed deposits could be considered as

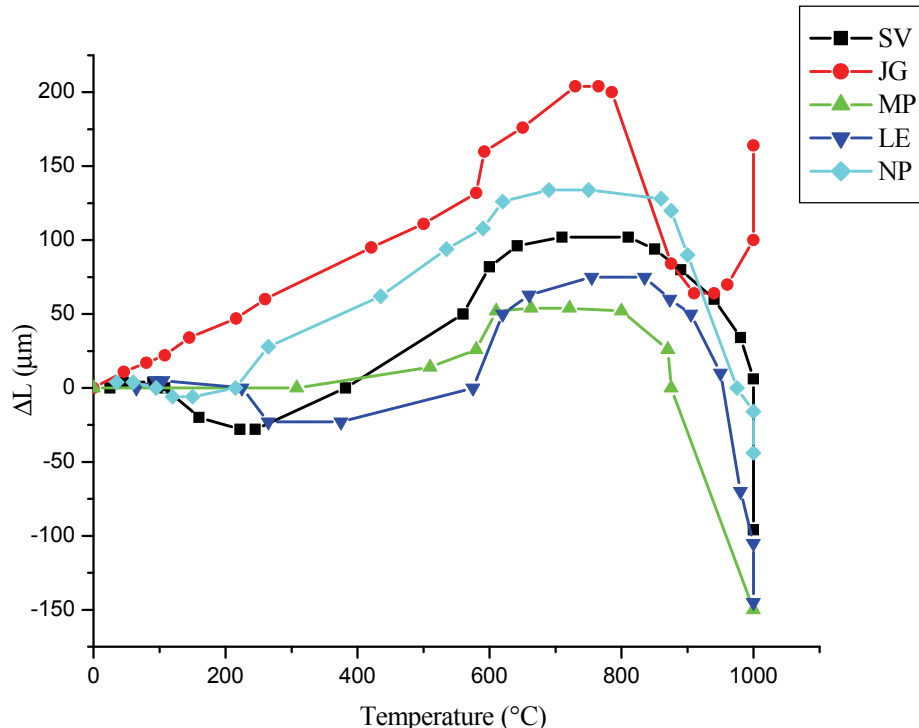


Figure 7. Dimensional change (ΔL) during heating up to 1000 °C (thermodilatometric curves).

raw materials for use in rough ceramic products. All the studied clays seem to be easily adaptable to a correct ceramic process. It is recommendable to add sand for plasticity correction and reduction of susceptibility in drying in the samples SV, MP, LE and NP. Grinding below 1 mm is preferred because of the appearance of limestone concretions, and subsequent aging for equalization of rheological properties.

The tested SV, MP and NP samples had the highest clay sized particles content (24 ± 1.12 to $29\pm1.61\%$), so they can be used in the production of hollow bricks and blocks, as well as ceiling elements. As a primary raw material, these samples can be used in light-weighted bricks. In contrast, the JG sample is more suitable for the production of solid bricks, due to the low clay and high carbonates content, as well as the loess raw material nature, which causes low plasticity. In order to improve the product quality, more plastic clay should be added in the mixture for hollow blocks production. The JG sample can also be used to produce facade bricks, usually yellow colored, but firing must be carried out at relatively high temperatures ($1100\text{--}1150\text{ }^{\circ}\text{C}$). The LE sample, after grinding below 0.5 mm to avoid the appearance of lime corns, can be used in roof tiles and facade elements production.

CONCLUSIONS

Clays from different parts of Serbia were characterized by chemical, mineralogical, ceramic and technological analysis. All the samples contained mostly sand and clay minerals (mica, chlorite and smectite), with particles between 8 and 32 μm . Different mineralogical composition has a strong effect on the behavior of fired samples; consequently that is of decisive importance for the final quality of the end products.

The color of fired samples was red with some shade differences. All the samples except JG showed high plasticity and drying susceptibility. The possible usability of these raw materials in the manufacture of various rough masonry products, such as solid bricks, hollow bricks and blocks, ceiling elements and roof tiles depends on major differences in water absorption and compressive strength. All the studied clays seem to be easily adaptable to a correct brick making process. Most of the tested clays can be used as a primary raw material in the light-weighted brikcs production.

Acknowledgement

The authors are grateful for the financial support of the Scientific Research Projects of Serbian Ministry of Education, Science and Technological Development, Contract No. III450080.

REFERENCES

- [1] B.K. Ngun, H. Mohamada, S.K. Sulaiman, K. Okadac, Z.A. Ahmada, Some ceramic properties of clays from central Cambodia, *Appl. Clay. Sci.* **53** (2011) 33–41.
- [2] B.R. Ilić, A.A. Mitrović, Lj.R. Miličić, Thermal treatment of kaolin clay to obtain metakaolin, *Hem. Ind.* **64**(4) (2010) 351–356.
- [3] M. Arsenović, Z. Radojević, S. Stanković, Ž. Lalić, L. Pezo, What to expect from heavy clay?, *Ceram. Int.* **39** (2013) 1667–1675.
- [4] Z. Radojević, Ž. Lalić, R. Vasić, A. Mitrović, Brick raw materials quality in Serbia and the influence for the products quality and to the production technology - loess sediments, *Izgradnja* **59** (2005) 45–49.
- [5] M. Arsenović, S. Stanković, L. Pezo, L. Mančić, Z. Radojević, Optimization of the production process through response surface method: Bricks made of loess, *Ceram. Int.* **39** (2013) 2013–2022.
- [6] Z. Radojevic, M. Arsenovic, M. Vasic, Quality evaluation of south Serbia raw clay materials, *Izgradnja* **62** (2008) 157–161.
- [7] M. Arsenović, S. Stanković, Z. Radojević, L. Pezo, Prediction and fuzzy synthetic optimization of process parameters in heavy clay brick production, *Ceram. Int.* (2013), doi: 10.1016/j.ceramint.2012.08.053.
- [8] C.M.F Veira, R. Sanchez, S.N. Monteiro, Characteristics of clays and properties of building ceramics in the state of Rio de Janeiro, Brazil, *Constr. Build. Mater.* **22** (2008) 781–787.
- [9] D.M. Moore, Jr., R.C. Reynolds, *X-ray diffraction and the identification and analysis of clay minerals*, Oxford University Press, Oxford, 1997.
- [10] M.S. Randelović, M.M. Purenović, A.R. Zarubica, I.D. Mladenović, J.M. Purenović, M.Z. Momčilović, Fizičko-hemijska karakterizacija bentonita i njegova primena u uklanjanju Mn^{2+} iz vode, *Hem. Ind.* **65**(4) (2012) 381–387.
- [11] M.B. Dalmacija, M.D. Dalmacija, D.M. Krčmar, M.Đ. Prica, Lj.M. Rajić, S.D. Rončević, O. Gavrilović, Solidifikacija/stabilizacija sedimenta vodotoka Krivaja zagađenog metalima, *Hem. Ind.* **66**(4) (2012) 469–478 (in Serbian).
- [12] M. Tecilazić – Stevanović, *Osnovi tehnologije keramike*, Faculty of Technology and Metallurgy, Belgrade, 1990 (in Serbian).
- [13] EN 771-1:2010, Specification for masonry units - Part 1: Clay masonry units.
- [14] EN 772-1:2010, Methods of test for masonry units – Part 1: Determination of compressive strength.
- [15] J. Qian, X. Shan, Z. Wang, Q. Tu, Distribution and plant availability of heavy metals in different particle-size fractions of soil, *Sci. Total. Environ.* **187** (1996) 131–141.
- [16] H. Baccour, M. Medhioub, F. Jamoussi, T. Mhiri, Influence of firing temperature on the ceramic properties of Triassic clays from Tunisia, *J. Mater. Process. Tech.* **209** (2009) 2812–2817.
- [17] H.G.F. Winkler, Bedeutung der Korngrößen-verteilung und Mineral-bestandess von tonnen für die Herstellung

- grobkeramischer Erzeugnisse, Ber. Der DKG **31** (1954) 337–343.
- [18] M. Arsenović, Z. Radojević, S. Stanković, Removal of toxic metals from industrial sludge by fixing in brick structure, *Constr. Build. Mat.* **37** (2012) 7–14.
- [19] R.F. Lopez, Calcined Clayey Soils as a Potential Replacement for Cement in Developing Countries, , PhD Thesis, École Polytechnique Fédérale de Lausanne, Lausanne 2009 (http://biblion.epfl.ch/EPFL/theses/2009/4302/EPFL_TH4302.pdf).
- [20] T.B. Novaković, Lj.S. Rožić, Z.M. Vuković, S.P. Petrović, Uticaj dodatka polietilen-glikola u lantana na mehanizam sinterovanja aluminijum-oksida dobijenog sol-gel postupkom, *Hem. Ind.* **65**(4) (2011) 355–362 (in Serbian).
- [21] A. Tretau, E. Rimpel, Ullmann's Encyclopedia of Industrial Chemistry, Construction Ceramics, Wiley Online Library, DOI:10.1002/14356007.a07_425.pub2, 2011.
- [22] G.W.A. Nyakairu, H. Kurzweil, C. Koeberl, Mineralogical, geochemical, and sedimentological characteristics of clay deposits from central Uganda and their applications, *J. Afr. Earth. Sci.* **35** (2002) 123–134.
- [23] K. Jeridi, M. Hachani, W. Hajjaji, B. Moussi, M. Medhioub, A. López-Galindo, F. Kooli, F. Zargouni, J. Labrincha, F. Jamoussi, Technological behaviour of some Tunisian clays prepared by dry ceramic processing, *Clay Miner.* **43** (2008) 339–350.
- [24] V. Valanciene, R. Siauciunas, J. Baltusnikaite, The influence of mineralogical composition on the colour of clay body, *J. Eur. Ceram. Soc.* **30** (2010) 1609–1617.
- [25] G. Piltz, Untersuchung der Möglichkeiten der Aufhellung der Brennfarben von Ziegelrohstoffen, Westdt. Verl., Köln, 44 S.m.Abb. Nordrhein-Westfalen: Forschungsberichte, 1964.
- [26] P. Bormans, Ceramics are more than clay alone, Cambridge International Science Publishing, 2003.
- [27] S. Meseguer, F. Pardo, M.M. Jordan, T. Sanfelix, I. González, Ceramic behaviour of five Chilean clays which can be used in the manufacture of ceramic tile bodies, *Appl. Clay Sci.* **47** (2010) 372–377.
- [28] Ž. Lalic, M. Arsenovic, Đ. Janackovic, M. Vasic, Z. Radojevic, Influence of increased temperature on clay fast drying process. *Rev. Rom. Mat.* **39** (2009) 175–179.
- [29] K.Y. Chiang, P.H. Chou, C.R. Hua, K.L. Chien, C. Cheeseman, Lightweight bricks manufactured from water treatment sludge and rice husks, *J. Hazard. Mater.* **171** (2009) 76–82.
- [30] M. Sutcu, S. Akkurt, The use of recycled paper processing residues in making porous brick with reduced thermal conductivity, *Ceram. Int.* **35** (2009) 2625–2631.
- [31] M. Raimondo, M. Dondi, G. Davide, G. Guarini, F. Mazzanti, Predicting the initial rate of water absorption in clay bricks, *Constr. Build. Mater.* **23** (2009) 2623–2630.
- [32] F. Singer, S.S. Singer, Industrial Ceramics, Chapman and Hall Ltd., London, 1963.
- [33] J.A. de la Casa, M. Lorite, J. Jiménez, E. Castro, Valorization of wastewater from two-phase olive oil extraction in fired clay brick production, *J. Hazard. Mater.* **169** (2009) 271–278.

IZVOD

OPEKARSKE GLINE IZ SRBIJE: PRIMENA U PROIZVODNJI GRUBE KERAMIKE

Milica V. Arsenović¹, Lato L. Pezo², Zagorka M. Radojević¹, Slavka M. Stanković³

¹*Institut za ispitivanje materijala IMS, Bulevar vojvode Mišića 43, 11000 Beograd, Srbija*

²*Univerzitet u Beogradu, Institut za opštu i fizičku hemiju, Studentski trg 12, 11000 Beograd, Srbija*

³*Univerzitet u Beogradu, Tehnološko–metalurški fakultet, Karnegijeva 4, 11000 Beograd, Srbija*

(Naučni rad)

Gline i glineni minerali se, usled mnogih specifičnih osobina pre i nakon pečenja, decenijama koriste kao osnovni materijali za proizvodnju grube keramike. Proučavanje i utvrđivanje mineralnih faza koje su prisutne u materijalu je komplikovano zato što prirodne gline imaju veoma heterogen mineralni sastav. Tokom processa pečenja dolazi do mnogobrojnih transformacija, koje mogu imati ključni uticaj na osobine gotovih opekarskih proizvoda. Osim sastava važni parametri koji opisuju gline su plastičnost, mehanička čvrstoća nakon pečenja, kapacitet upijanja vode, itd. Poznavanje ovih karakteristika pomaže da se optimizuje korišćenje novootvorenih ležišta gline u lokalnoj ili regionalnoj opekarskoj industriji. Istraživanje prikazano u ovom radu je bazirano na ponašanju opekarskih gline iz Srbije, u kojoj postoji važna lokalna opekarska industrija. Otvoreno je pet novih ležišta, uzorci prikupljeni, a zatim su ispitane njihove fizičke, hemijske, mineraloške i tehničke karakteristike, da bi se ocenila njihova eventualna pogodnost kao sirovina za različite opekarske proizvode. Koeficijent plastičnosti prema Feferkornu i osetljivost u sušenju na osnovu Bigo krive su određeni za svaki uzorak. Nakon što su uzorci oblikovani ekstruzijom i adekvatno osušeni, određene su mehaničke karakteristike proizvoda u suvom stanju i urađena je termodilatometrijska analiza. Uzorci oblika pločica, blokčića i kockica su pečeni na temperaturama od 850–1000 °C u oksidacionoj atmosferi i pri sporom režimu. Kapacitet upijanja vode i pritisna čvrstoća su određeni da bi se uzorci okarakterisali nakon pečenja, pri čemu su korišćeni linearni regresioni modeli. Matematički alati su korišćeni da se odredi statistički značaj sadržaja makroelemenata, vlage oblikovanja i pritisne čvrstoće suvih uzoraka, prema HSD testu. Iako se hemijski i mineraloški sastav uzoraka značajno ne razlikuje, ali sasvim je suprotno što se tiče moguće primene ovih sirovina. Zaključeno je da sve ispitivane opekarske sirovine mogu jednostavno da se uklope u proces proizvodnje grube keramike.

Ključne reči: Opekarska gлина • Tehnološke karakteristike • Primena

Procena kvaliteta vode značajno izmenjenih vodnih tela na teritoriji Vojvodine primenom multivarijacionih statističkih metoda

Svetlana Vujović¹, Srđan Kolaković¹, Milena Bečelić-Tomin²

¹Fakultet tehničkih nauka, Departman za građevinarstvo, Univerzitet u Novom Sadu, Novi Sad, Srbija

²Prirodno-matematički fakultet, Departman za hemiju, biohemiju i zaštitu životne sredine, Univerzitet u Novom Sadu, Novi Sad, Srbija

Izvod

Multivarijacione statističke metode, faktorska analiza/analiza glavnih komponenti i klaster analiza, primenjene su za obradu dela podataka kvaliteta vode značajno izmenjenih vodnih tela na teritoriji Vojvodine. U radu su korišćeni podaci Republičkog Hidrometeorološkog zavoda (RHMZ) za 2010. godinu. Faktorska analiza je primenjena za objašnjenje korelacije između parametara kvaliteta vode (varijabli). Primenom faktorske analize 13 varijabli grupisano je u četiri faktora (F1 – hidroheminski faktor, F2 – faktor eutrofikacije, F3 – faktor tačkastih izvora zagađenja, F4 – ekološki faktor) na osnovu kojih je definisan najveći uticaj na variranje kvaliteta vode. U odnosu na ekstrahovane faktore izvršena je klaster analiza u cilju otkrivanje sličnosti i razlika fizičko hemijskog kvaliteta vode između mernih stanica značajno izmenjenih vodnih tela. Primenom faktorske analize/analize glavnih komponenti i klaster analize izdvojila su se vodna tela koja se nalaze pod najvećim pritiscima. U odnosu na faktor F1 to su: Plazović, Bosut, Studva, Zlatica, Stari Begej i Krivaja. U odnosu na faktor F2 to su: Krivaja i Kereš. U odnosu na faktor F3 to su: Studva, Krivaja i Kereš. U odnosu na F4 to su: Studva, Zlatica, Krivaja i Kereš. Na osnovu podataka RHMZ može se zaključiti da na vodnim telima (Plazović, Bosut, Studva, Zlatica, Tamiš, Stari Begej, Krivaja, Kereš) postoji opasnost od nedostizanja dobrog hemijskog statusa i dobrog ekološkog potencijala.

Ključne reči: multivarijacione statističke metode, faktorska analiza/analiza glavnih komponenti, klaster analiza, kvalitet vode.

Dostupno na Internetu sa adresu časopisa: <http://www.ache.org.rs/HI/>

Površinske vode su složeni višekomponentni sistemi za čije izučavanje je potreban multidisciplinarni pristup. On je zasnovan na sistemskom pristupu i uključuje primenu i usvajanje činjenica, principa i metoda hemije, fizike, geologije, hidrologije, meteorologije, matematike i drugih nauka, da bi se rešili problemi koji su u osnovi ekološke prirode. Specifičnost i kompleksnost hemijskog sastava površinskih voda i pokazatelja kvaliteta kao posledica u njoj rastvorenih mineralnih i organskih materija, gasova, suspendovanih čestica i mikroorganizama, naglašavaju značaj primene metoda za njihovo ocenjivanje iznalaženjem zajedničkog faktora koji obuhvata kvalitet kao celinu [1].

Procena stanja kvaliteta voda zahteva praćenje širokog spektra fizičkih, hemijskih i bioloških parametara. Uobičajena procedura je uzimanje uzorka na većem broju mernih stanica pri čemu se analizira veći broj parametara. Stoga je za procenu kvaliteta vode vodnih tela potrebna kompleksna matrica podataka [2]. Podaci

NAUČNI RAD

UDK 628.113(497.113):51

Hem. Ind. 67 (5) 823–833 (2013)

doi: 10.2298/HEMIND121002007V

dobijeni analizom parametara kvaliteta voda pružaju informacije o stanju vodnih tela. Klasifikacija, modelovanje i tumačenje podataka monitoringa predstavljaju najvažnije korake u postupku procene kvaliteta vode. Poseban problem kod monitoringa kvaliteta vode je kompleksnost povezana sa analizom velikog broja varijabli i visoka varijabilnost usled antropogenih i prirodnih uticaja [3]. Primena različitih multivarijacionih tehnika, kao što su faktorska analiza/analiza glavnih komponenti i klaster analiza, pomaže u interpretaciji kompleksnih matrica podataka u cilju boljeg razumevanja stanja kvaliteta vode ispitivanog područja. Ove tehnike omogućavaju identifikaciju mogućih izvora zagađenja koji utiču na vodna tela i predstavljaju korisne alate za pouzdano upravljanje vodnim resursima.

Kvalitet površinskih voda u Vojvodini pretežno je uslovjen antropogenim uticajem (ispuštanje otpadnih voda, tj. radom industrijskih postrojenja, poljoprivrednom proizvodnjom, ispuštanjem komunalnih otpadnih voda) i promenama uslovjenim klimatskim faktorima, od kojih su sušni periodi veoma važni. Ugroženost značajno izmenjenih i veštačkih vodnih tela zagađenjem biodegradabilnim organskim materijama naročito je izražena u blizini velikih gradova (Vrbas, Kula, Crvenka, Zrenjanin, Pančevo, Ruma i Bačka Topola) koji nemaju postrojenja za prečišćavanje gradskih otpadnih voda i

Prepiska: S. Vujović, Departman za građevinarstvo, Fakultet tehničkih nauka, Univerzitet u Novom Sadu, Novi Sad, Trg Dositeja Obradovića 6, 21 000 Novi Sad, Srbija.

E-pošta: vujojics@uns.ac.rs

Rad primljen: 2. oktobar, 2012

Rad prihvaćen: 17. januar, 2013

industrijskih postrojenja koja se bave proizvodnjom hrane (fabrike šećera, prerade voća i povrća, velike farme svinja, klanice, itd.). Ovaj problem posebno je izražen u periodu godine koji karakterišu niski vodostaji i povišene temperature. Novi Sad je izostavljen iz grupe gradova koji imaju značajan uticaj na kvalitet vode vodotoka jer se merna stanica Novi Sad nalazi uzvodno od mesta ispuštanja gradskih otpadnih voda, sa jedne strane, a sa druge strane, Dunav je velike moći samoprečiščavanja. Dunav, Sava, a delimično i Tisa, uspevaju, zahvaljujući moći samoprečiščavanja, da razgrade znatne količine organskih materija i održe zadoljavajući kvalitet voda. Nasuprot njima, u periodima rada fabrika punim kapacitetom prisutna je ugroženost malih vodotoka (Krivaja, Nadela, Kudoš i Bosut) i pojedine deonice HS DTD [4]. Na teritoriji Vojvodine registrovano je 511 zagađivača voda. Njihova struktura po delatnosti je sledeća: industrija (326 zagađivača), poljoprivreda (stočarstvo-farme) (113 zagađivača), naselja (44 zagađivača) i ostalo (20 zagađivača). U poslednju grupu spadaju medicinske ustanove (banje), korisnici termalnih voda, radionice za remont saobraćajnih sredstava, itd. Povećanje industrijske proizvodnje poslednjih godina uslovilo je povećanje količina otpadnih voda u odnosu na prethodni period, a samim tim i proporcionalno povećanje opterećenja vodotoka zagađujućim materijama iz ovih izvora. Značajno zagađenje voda u Vojvodini potiče iz prehrambene industrije. Emisija iz prehrambene industrije čini oko 80% ukupnog industrijskog zagađenja u Vojvodini [4].

Cilj ovog rada je da se primenom multivarijacionih statističkih metoda, faktorska analiza/analiza glavnih komponenti i klaster analiza, proceni stanje kvaliteta vode u pogledu hemijskih i fizičko-hemijskih parametara kvaliteta i da se u okviru grupe dobijenih klaster analizom utvrde uzroci za nedostizanje dobrog hemijskog statusa i dobrog ekološkog potencijala značajno izmenjenih vodnih tela na teritoriji Vojvodine.

EKSPERIMENTALNI DEO

Multivarijacione statističke metode

Procena kvaliteta površinskih i podzemnih voda i ekološka istraživanja primenom multivarijacionih metoda su dobro opisani u literaturi. Multivarijacione statističke metode se koriste za karakterizaciju i evaluaciju kvaliteta vode vodnih tela i predstavljaju koristan alat za utvrđivanje vremenskih i sezonskih varijacija usled prirodnih i antropogenih pritisaka. Faktorska analiza se koristi za objašnjenje korelacije između posmatranja preko osnovnih faktora koji nisu direktno uočljivi. Visoka korelisanost podataka u faktorskoj analizi (pozitivno ili negativno) pretpostavlja i veliku verovatnost da su podaci pod uticajem istih faktora, dok su relativno nekorelisani podaci pod uticajem različitih faktora, što je i aksiom faktorske analize [2,3,5].

U ovom radu su prema [6] korišćeni sledeći kriterijumi faktorskog opterećenja: >0,75 smatra se da je povezanost „visoka“, a ako se vrednost faktorskog opterećenja kreće od 0,75–0,5 povezanost je „srednja“. Takođe, u radu je prema [7] usvojeno da se sopstvena vrednost jednak 1 ili veća od 1 smatra značajnom. Kod izbora broja faktora je primenjen Kajzerov kriterijum [6] kojim se zadržavaju samo oni faktori koji imaju karakteristične vrednosti veće od 1, kao i test preloma (eng. *Scree-test*) koji predstavlja grafički prikaz sopstvenih vrednosti svih komponenti i sugerije da se u analizi zadrže one komponente koje obuhvatom varijanse znatno (vizuelno) odstupaju od ostalih. Kod izbora broja faktora Kajzerov kriterijum je bio odlučujući.

Klaster analiza je metoda koja se koristi za grupisanje podataka na osnovu sličnih karakteristika. Klaster analiza je objektivna statistička tehnika koja se koristi za identifikaciju prirodnog grupisanja u skupu podataka [8]. Kako bi se izračunala udaljenost između svih objekata u radu je primenjena Euklidска udaljenost (eng. *Euclidean distance*), a za povezivanje grupe objekata sa sličnim udaljenostima primenjena je metoda jednostrukog povezivanja (eng. *Single Linkage*) [9]. U radu se koristi metoda hijerarhijskog grupisanje (eng. *Hierarchical tree clustering*) koja predstavlja grafički prikaz grupisanja pojedinih grupa uz pomoć dendrograma.

Statistička obrada podataka

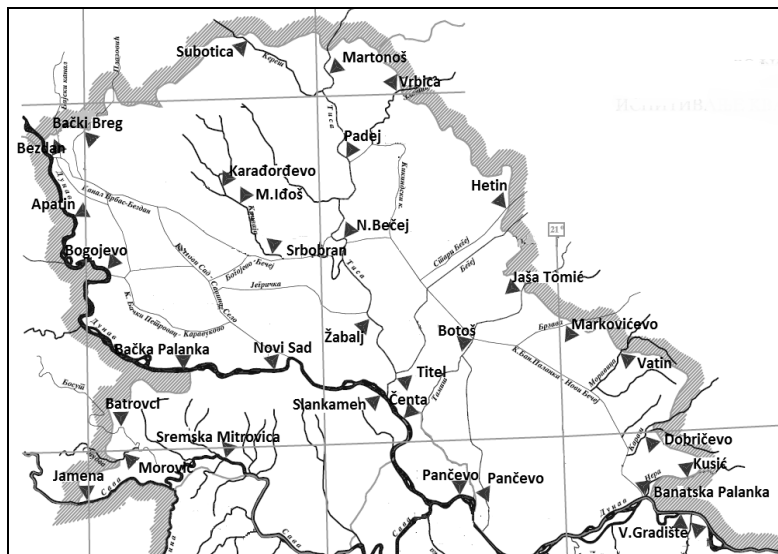
U radu su korišćeni podaci Republičkog Hidrometeorološkog zavoda (RHMZ) za 2010. godinu [10]. Na osnovu podataka RHMZ za izabrane parametre je izračunata srednja godišnja vrednost, minimalna i maksimalna vrednost. U tabeli 1 prikazane su srednja godišnja vrednost, minimalna i maksimalna vrednost za izabrane parametre.

Za faktorsku analizu/analizu glavnih komponenti i klaster analizu upotrebljene su srednje godišnje vrednosti izabranih parametara za 33 merne stanice. Hidrološka mapa Vojvodine sa mestima uzorkovanja prikazana je na slici 1. Podaci su obrađeni primenom statističkog softvera Statistica (Statistica, version 10.0).

Pravinikom o utvrđivanju vodnih tela površinskih i podzemnih voda, u cilju planiranja mera za očuvanje ili dostizanje dobrog statusa površinskih voda, identifikovana su vodna tela koja su razvrstana u kategorije (stačne vode, tekuće vode, značajno izmenjena vodna tela, veštačka vodna tela) [11]. Značajno izmenjena i veštačka vodna tela predstavljaju specifične kategorije vodnih tela. „Značajno izmenjeno vodno telo“ jeste telo površinske vode koje je, kao rezultat fizičkih izmena usled ljudskih aktivnosti bitno izmenjeno po svojim karakteristikama i razvrstano u skladu sa posebnim propisom. Veštačko vodno telo jeste telo površinske vode stvoreno ljudskom aktivnošću [12]. Veštačka vodna tela su stvorena na mestu gde ranije nije bilo vode, te se ne mogu valorizovati kao prirodni vodotoci [13].

Tabela 1. Srednja vrednost, minimum, maksimum fizičko-hemijskih parametara kvaliteta vode vodnih tela za period 2010. godine
Table 1. Mean, minimum, maximum of physical and chemical water quality parameters of the water bodies during 2010

Vodno telo	Ds	T °C	SM mg/l	Ras. O ₂ mgO ₂ /l	UT mg/l	pH	EP μS/cm	NH ₄ -N mg/l	NO ₃ -N mg/l	TP mg/l	Ca ²⁺ mg/l	Mg ²⁺ mg/l	BPK ₅ mg/l	PAM mg/l
Dunav	Mean	13,10	34,34	9,74	201,65	8,19	464,93	0,08	1,83	0,13	54,53	15,97	2,09	0,01
	Min	0,30	3,00	3,20	152,00	7,50	338,00	0,02	0,10	0,05	35,00	5,00	0,70	0,01
	Max	25,40	222,00	13,70	295,00	8,70	574,00	0,30	3,77	0,27	81,00	31,00	5,30	0,06
Tisa	Mean	13,52	90,46	8,63	170,22	7,93	458,79	0,10	1,07	0,18	48,99	11,77	2,09	0,01
	Min	0,20	14,00	4,80	124,00	7,70	279,00	0,02	0,51	0,08	37,00	8,00	1,00	0,01
	Max	26,70	340,00	12,60	223,00	8,20	601,00	0,80	1,61	0,46	62,00	18,00	5,10	0,03
Plazović	Mean	13,58	12,50	6,34	501,00	8,20	1314,00	0,08	1,46	0,41	82,10	72,00	2,08	0,02
	Min	1,80	2,00	1,10	442,00	7,90	1151,00	0,02	0,15	0,12	72,00	58,00	1,00	0,01
	Max	23,40	33,00	13,50	566,00	8,70	1436,00	0,30	3,68	0,70	91,00	83,00	4,40	0,05
Sava	Mean	12,81	21,50	9,60	220,08	8,08	379,00	0,06	0,73	0,23	64,25	13,65	1,32	0,01
	Min	2,60	1,00	6,10	133,00	7,80	300,00	0,01	0,30	0,04	34,00	8,00	0,50	0,01
	Max	27,20	53,00	22,50	467,00	8,70	805,00	0,82	2,60	2,90	111,00	70,00	7,90	0,02
Bosut	Mean	13,69	5,67	11,02	375,00	8,18	688,42	0,23	0,58	1,23	91,58	38,52	3,82	0,01
	Min	1,60	1,00	4,20	287,00	7,80	395,00	0,03	0,20	0,18	70,00	8,70	0,90	0,01
	Max	27,20	13,00	22,50	467,00	8,70	805,00	0,82	2,60	2,90	111,00	70,00	7,90	0,02
Studva	Mean	14,48	3,83	13,74	347,00	8,55	629,08	0,13	0,42	0,50	78,67	36,48	6,16	0,02
	Min	1,00	1,00	10,40	287,00	8,20	545,00	0,01	0,10	0,11	65,00	26,40	2,30	0,01
	Max	30,80	7,00	17,30	418,00	9,00	747,00	0,72	1,20	1,56	98,00	49,50	9,80	0,02
Zlatica	Mean	13,87	19,17	5,68	365,58	7,73	1421,33	0,06	0,75	0,49	82,67	38,92	3,98	0,03
	Min	4,50	5,00	0,40	249,00	7,30	866,00	0,02	0,04	0,12	63,00	22,00	1,20	0,01
	Max	28,60	41,00	13,80	540,00	8,30	1840,00	0,09	2,39	0,98	119,00	59,00	8,60	0,05
Star Begej	Mean	13,87	28,33	8,31	434,00	8,21	1247,00	0,08	1,49	0,52	81,42	57,00	2,54	0,02
	Min	0,30	2,00	4,20	257,00	7,90	720,00	0,03	0,31	0,23	63,00	34,00	1,00	0,01
	Max	26,80	80,00	11,80	610,00	8,50	1923,00	0,16	3,83	0,87	104,00	85,00	6,40	0,03
Tamiš	Mean	14,05	33,58	8,40	130,26	7,81	401,00	0,17	0,74	0,21	33,58	11,44	1,97	0,02
	Min	0,50	6,00	1,00	71,00	7,40	167,00	0,02	0,04	0,04	18,00	5,00	0,80	0,01
	Max	26,30	89,00	12,50	167,00	8,10	637,00	0,56	1,30	0,52	45,00	18,00	4,40	0,06
Brzava	Mean	15,02	43,90	8,94	121,70	7,76	310,30	0,10	1,37	0,24	32,60	9,90	1,54	0,02
	Min	7,40	15,00	7,20	81,00	7,50	205,00	0,02	0,93	0,07	21,00	7,00	1,00	0,01
	Max	21,10	78,00	11,00	172,00	8,00	448,00	0,16	1,90	0,48	40,00	18,00	2,10	0,04
Moravica	Mean	16,17	24,90	8,12	294,80	8,08	705,40	0,05	0,71	0,22	62,40	33,80	2,46	0,01
	Min	7,20	5,00	3,90	178,00	7,70	417,00	0,02	0,08	0,04	40,00	19,00	1,00	0,01
	Max	23,80	104,00	15,50	382,00	8,70	878,00	0,06	2,35	0,64	81,00	50,00	4,50	0,03
Karaš	Mean	14,72	45,70	9,37	212,60	8,02	454,80	0,10	1,11	0,21	72,70	7,60	2,16	0,02
	Min	8,20	5,00	7,50	165,00	7,90	368,00	0,03	0,48	0,06	56,00	5,00	1,00	0,01
	Max	19,80	158,00	10,50	248,00	8,20	512,00	0,30	3,24	0,59	84,00	10,00	5,50	0,04
Nera	Mean	11,96	24,42	10,62	144,75	8,13	297,92	0,04	0,60	0,07	49,08	5,50	1,40	0,02
	Min	3,10	3,00	8,00	127,00	7,70	249,00	0,02	0,17	0,03	44,00	4,00	0,80	0,01
	Max	22,50	51,00	13,00	160,00	8,40	338,00	0,10	0,98	0,16	53,00	7,00	2,40	0,03
Krivaja	Mean	14,73	17,77	7,32	454,00	8,25	1290,93	1,43	4,54	0,64	68,23	69,13	4,35	0,04
	Min	0,20	2,00	3,80	416,00	7,80	1011,00	0,02	0,05	0,03	43,00	60,00	1,50	0,03
	Max	28,10	125,00	16,80	528,00	8,90	1586,00	8,93	14,14	2,29	85,00	79,00	10,10	0,08
Kereš	Mean	13,25	48,82	7,74	289,80	8,49	991,91	0,69	0,57	0,35	47,60	41,80	10,53	0,07
	Min	1,70	2,00	2,90	264,00	7,90	905,00	0,04	0,26	0,17	36,00	28,00	2,10	0,04
	Max	28,10	96,00	13,80	315,00	9,50	1098,00	2,47	1,15	0,63	71,00	51,00	22,80	0,09



Slika 1. Hidrološka mapa Vojvodine sa mestima uzorkovanja.
Figure 1. Hydrological map of Vojvodina with monitoring stations.

Uredbom o graničnim vrednostima zagađujućih materija u površinskim i podzemnim vodama i sedimentu, kao i rokovi za njihovo dostizanje (u daljem tekstu Uredba) su u Srbiji vodotoci razvrstani u pet klasa [14]. Pravilnikom o parametrima ekološkog i hemijskog statusa površinskih voda i parametrima hemijskog i kvantitativnog statusa podzemnih voda (u daljem tekstu Pravilnik) propisani su parametri ekološkog i hemijskog statusa za reke i jezera, parametri ekološkog potencijala za veštačka vodna tela i značajno izmenjena vodna tela i parametri hemijskog i kvantitativnog statusa podzemnih voda na osnovu kojih se za vodna tela površinskih i podzemnih voda vrši ocena statusa [15]. Prema Pravilniku, "Ekološki potencijal" je status značajno iz-

menjenog, ili veštačkog vodnog tela, a „Hemijski status“ pokazuje da li je vodno telo pod uticajem zagađivanja prioritetnim i prioritetnim hazardnim supstancama, kao i drugim zagađujućim supstancama. U radu su prema Uredbi, na osnovu određenih parametara, definisane klase vodnih tela. Hemijski status vodnih tela procjenjen je na osnovu podataka monitoringa RHMZ i to poređenjem određenih vrednosti sa graničnim vrednostima zagađujućih materija propisanih Uredbom. Ekološki potencijal vodnih tela, razvrstanih u tipove, definisan je na osnovu parametara propisanih Pravilnikom. U tabeli 2 prikazana su vodna tela sa pripadajućom oznakom, tipom [13] i monitoring stanicama.

Tabela 2. Vodna tela sa pripadajućom oznakom, tipom i monitoring stanicama
Table 2. Water bodies with associated label, type, and monitoring stations

Vodno telo	Oznaka	Tip	Monitoring stanice
Dunav	D1-D10	1	Bezdan, Apatin, Bogojevo, Bačka Palanka, Novi Sad, Slankamen, Čenta, Pančevo, Banatska Palanka, Veliko Gradište
Tisa	TIS_1, TIS_2	1	Martonoš, Padej, Novi Becej, Žabalj, Titel
Plazović	PLA	5	Bački Breg
Sava	SA_1	1	Jamena, Sremska Mitrovica
Bosut	BOS	2	Batočci
Studva	–	–	Morović
Zlatica	ZLA	2	Vrbica
Stari Begej	STBEG	1	Hetin
Tamiš	TAM_1, TAM_2	1	Jaša Tomić, Botoš, Pančevo
Brzava	BRZ	5	Markovićovo
Moravica	MORBAN	5	Vatin
Karaš	KAR	5	Dobričev
Nera	NER_1	2	Kusić
Krivaja	KRIVJ_1, KRIVJ_3	5	Karađorđevo, Mali Idoš, Srbobran
Kereš	KER	5	Subotica

REZULTATI I DISKUSIJA

Rezultati faktorske analize/analize glavnih komponenti

Na osnovu podataka o kvalitetu voda, izvršena je faktorska analiza/analiza glavnih komponenti 13 parametara kvaliteta voda: temperatura (T), suspendovane materije (SM), rastvoreni kiseonik, ukupna tvrdoća (UT), pH, elektroprovodljivost (EP), amonijačni azot (NH_4-N), nitratni azot (NO_3-N), ukupni fosfor (TP), kalcijum (Ca^{2+}), magnezijum (Mg^{2+}), biološka potrošnja kiseonika (BPK_5) i prirodne anjon aktivne materije (PAM). Faktorska analiza/analiza glavnih komponenti je primenjena za identifikaciju skrivenih faktora koji su odgovorni za varijabilnost kvaliteta vode. Klaster analiza je primenjena za otkrivanje sličnosti i razlika fizičko-hemijskog stanja vode između mernih stanica vodnih tela u odnosu na identifikovane faktore. Na osnovu Kajzerovog kriterijuma izdvojena su četiri faktora.

U tabeli 3 dati su rezultati faktorske analize/analize glavnih komponenti, koja je izvršena uz ortogonalnu (Varimax normalizovanu) rotaciju.

Primenom faktorske analize/analize glavnih komponenti za značajna izmenjena vodna tela za 2010. godinu dobijena su četiri faktora koja objašnjavaju oko 78 % ukupnog varijabilitet.

Prvi faktor F1 doprinosi oko 28% u ukupnom varijabilitetu i najviše je korelisan sa parametrima: SM , UT , EP , pH, TP , Ca^{2+} i Mg^{2+} . Prvi faktor ima visoko pozitivno opterećenje za UT , EP , Ca^{2+} i Mg^{2+} , srednje negativno opterećenje za SM i srednje pozitivno opterećenje za pH i TP . Prvi faktor se može označiti kao hidrohemski faktor.

Tabela 3. Rezultati faktorske analize/analize glavnih komponenti; ^(a)vrednost faktorskog opterećenja veća od 0,75 – povezanost „visoka“; ^(b)vrednost faktorskog opterećenja od 0,75–0,5 – povezanost „srednja“
Table 3. Results of factor analysis/principal component analysis

Varijable	F1	F2	F3	F4
T	0.192265	-0.189630	0.121353	0.625316^(b)
SM	-0.733417^(b)	0.034387	-0.055012	0.187706
Rast. O ₂	0.062293	-0.520684^(b)	-0.132752	-0.743538^(b)
UT	0.854074^(a)	0.280454	0.321364	0.229167
pH	0.513915^(b)	-0.165045	0.482668	-0.562504^(b)
EP	0.636274^(b)	0.344388	0.442136	0.436012
NH ₄ -N	0.109922	0.824190^(a)	0.164661	-0.020774
NO ₃ -N	0.172304	0.866499^(a)	0.062675	0.035442
TP	0.579872^(b)	0.514314^(b)	0.136349	0.183537
Ca ²⁺	0.899685^(a)	0.099815	-0.018403	0.029819
Mg ²⁺	0.731311^(b)	0.326368	0.431771	0.289341
BPK ₅	0.209772	0.197047	0.873390^(a)	-0.077124
PAM	0.056926	0.097067	0.859537^(a)	0.277892
Eigenvalue	3.746657	2.392109	2.305114	1.741290
Varijabilitet (%)	28.820441	18.400841	17.731648	13.394536
Kumulativni varijabilitet, (%)	28.820441	47.221282	64.952930	78.347466

Drugi faktor doprinosi 18% ukupnom varijabilitetu

i najviše je korelisan parametrima: rastvoreni kiseonik, NH₄-N, NO₃-N i TP. Drugi faktor ima visoko pozitivno opterećenje za parametre NH₄-N i NO₃-N, srednje pozitivno opterećenje za TP i srednje negativno opterećenje za rastvoreni kiseonik. Drugi faktor se može označiti kao faktor eutrofikacije.

Treći faktor F3 doprinosi 17% ukupnom varijabilitetu i najviše je korelisan sa parametrima: BPK₅ i PAM. Treći faktor ima visoko pozitivno opterećenje za navedene parametre. Treći faktor se može označiti kao faktor tačkastih izvora zagađenja.

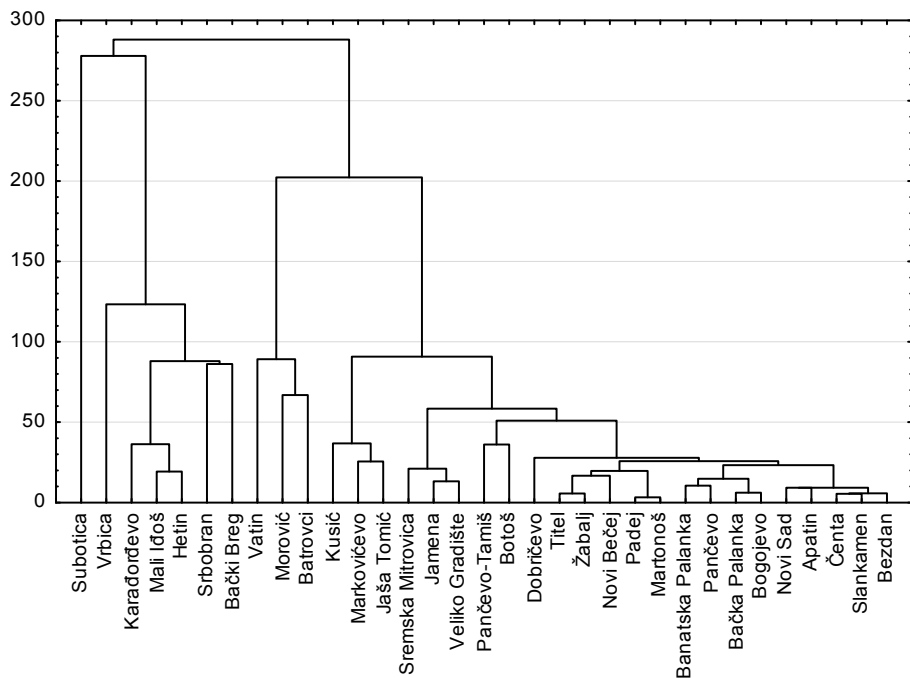
Četvrti faktor F4 doprinosi oko 13% u ukupnom varijabilitetu i najviše je korelisan sa parametrima: T, rastvoreni kiseonik i pH. Četvrti faktor ima srednje pozitivno opterećenje za T i srednje negativno opterećenje za rastvoreni kiseonik i pH. Četvrti faktor se može označiti kao ekološki faktor.

Rezultati klaster analize

Rezultati klaster analize prikazani su u grafički, preko dendrograma. Dendrogram klaster analize monitoring stanica u odnosu na prvi faktor F1 prikazan je na slici 2.

Prvoj grupi pripadaju merne stanice Zlatice (Vrbica), Plazovića (Bački Breg), Starog Begeja (Hetin), Krivaje (Karađorđevo, Mali Idoš i Srbobran) i Kereša (Subotica).

Merne stanice su izdvojene u I grupu na osnovu najvećih izmerenih vrednosti UT, EP, Ca²⁺ i Mg²⁺. Izmerene vrednosti UT na mernim stanicama se kreću od 289,8–501 mg/l. Najveća vrednost izmerena je na mernoj stanici Plazović. Izmerene vrednosti EP na mernim



Slika 2. Dendrogram klaster analize monitoring stanica u odnosu na prvi faktor F1.

Figure 2. Cluster analysis dendrogram of the monitoring stations in relation to the first factor F1.

stanicama se kreću od 991–1421 µS/cm. Najveća vrednost izmerena je na mernoj stanici Vrbica. Prema Uredbi, na osnovu izmerenih vrednosti EP, kvalitet vode vodnog tela Kereš pripada II klasi, dok za sva ostala vodna tela vrednost EP pripada III klasi.

Izmerene vrednosti TP na mernim stanicama se kreću od 0,05–1,07 mg/l. Vrednost od 1,07 mg/l izmerena je na mernoj stanici Srbobran i prema Uredbi pripada V klasi. Najniža vrednost izmerena je na mernoj stanici Karađorđevo i prema Uredbi pripada I klasi. Vrednost TP na mernoj stanici Subotica pripada III klasi, dok za ostale merne stanice I grupe vrednost pripada IV klasi.

Prema podacima RHMZ, na osnovu srednjih godišnjih vrednosti EP i TP, može se zaključiti da za vodna tela I grupe postoji opasnost od nedostizanja dobrog hemijskog statusa, a prema Pravilniku vodna tela ne ispunjavaju uslove za dobar ekološki potencijal.

Najveće vrednosti UT, Ca²⁺ i Mg²⁺ izmerene su na mernim stanicama u zimskom periodu, što može biti posledica spiranja terena. Najveće srednje godišnje vrednosti EP i TP izmerene su u prolećnom i letnjem periodu.

Drugoj grupi pripadaju merne stanice Bosuta (Batrovci), Studve (Morović) i Moravice (Vatin).

Merne stanice su se izdvojile u II grupu na osnovu najvećih izmerenih vrednosti TP i Ca²⁺ i najnižih izmerenih vrednosti SM.

Vrednost SM se kreće od 3,83–24,9 mg/l. Kako je prema Uredbi granična vrednost SM za I i II klasu vode 25 mg/l, može se zaključiti da za vodna tela II grupe ne postoji opasnost od dostizanja dobrog hemijskog statusa.

Merna stanica Batrovci izdvaja se po najvećoj izmerenoj vrednosti TP od 1,23 mg/l, što odgovara V klasi prema Uredbi. Srednja godišnja vrednost TP na mernoj stanici Studve pripada III klasi, a na mernoj stanici Vatin II klasi.

Izmerena vrednost TP na mernim stanicama Batrovci i Morović značajno prevazilazi kritičnu vrednost od 0,15 mg/l koja predstavlja minimum zahteva za sprečavanje procesa eutrofikacije [16]. Stoga, vodna tela Bosut i Studva ne ispunjavaju uslove za dobar ekološki potencijal.

Trećoj grupi pripadaju sve ostale merne stanice.

Merne stанице III grupe izdvajaju se po najvećim izmerenim vrednostima SM. Izmerene vrednosti SM se kreću od 20,58–101,44 mg/l. Najveća vrednost izmerena je na mernoj stanici Titel. Najveće srednje godišnje vrednosti SM su izmerene u prolećnom periodu što može biti posledica spiranja terena.

Prema podacima RHMZ, može se zaključiti da je klaster analizom izvršeno grupisanje mernih stanicama u treću grupu u kojoj vrednost SM na mernim stanicama prevazilazi graničnu koncentraciju za I i II klasu od 25 mg/l, prema Uredbi, sa izuzetkom sledećih mernih stanic: Veliko Gradište, Jajinci, Sremska Mitrovica, Pančevo-Tamiš i Kusić.

Generalno gledano, prema podacima RHMZ, na svim mernim stanicama na vodnom telima povećane vrednosti hidrohemski parametara (EP, UT, Ca²⁺ i Mg²⁺) prate niže vodostaje u toku godine, te se može zaključiti da klima ima značajan uticaj na variranje kvaliteta vode.

Na primer, na mernim stanicama Dunava srednji godišnji vodostaji se kreću od 321–774 cm. U periodima minimalnih vodostaja, koji se kreću od 53–754 cm, izmerene su povećane vrednosti hidrohemihjskih parametara (EP , UT , Ca^{2+} i Mg^{2+}). Najniži vodostaji u toku godine izmereni su u mesecima februar, mart, oktobar i novembar. U periodima maksimalnih vodostaja, koji se kreću od 490–796 cm izmerene su niže vrednosti parametara.

Dendrogram klaster analize monitoring stanica u odnosu na drugi faktor F2 prikazan je na slici 3.

Prvoj grupi pripadaju merne stanice Krivaje (Mali Iđoš i Srbobran).

Na mernim stanicama Krivaje izmerene su najveće srednje godišnje koncentracije NO_3-N što je bio razlog njenog izdvajanja u prvu grupu. Izmerene vrednosti NO_3-N se kreću od 6,13–7,25 mg/l, koje prema Uredbi pripadaju III klasi, a prema Pravilniku vodno telo ne ispunjava uslove za dobar ekološki potencijal. Najveće vrednosti NO_3-N izmerene su na mernoj stanici Krivaje u toku zimskog perioda. Koncentracije nitrata su niske u letnjem periodu jer se pri manjoj količini atmosferskih padavina, nitrati koji dospevaju ispiranjem sa poljoprivrednog zemljišta, više zadržavaju u zemljištu i na taj način se smanjuje njihov priliv u površinske vode [16]. Izmerene vrednosti NH_4-N se kreću od 0,60–3,66 mg/l. Minimalna vrednost NH_4-N prema Uredbi pripada III klasi, a maksimalna vrednost pripada V klasi. Stoga, prema Pravilniku vodno telo Krivaja ne ispunjava uslove za dobar ekološki potencijal.

Koncentracija nitrata u vodi retko je veća od 0,1 mg/l. Povećane vrednosti su uglavnom posledica ispuš-

tanja komunalnih i industrijskih otpadnih voda i primena nitratnih đubriva. Nezagađene vode uglavnom sadrže manje od 0,1 mg NH_4-N , a veće vrednosti mogu da budu posledica ispuštanja komunalnih otpadnih voda [17,18].

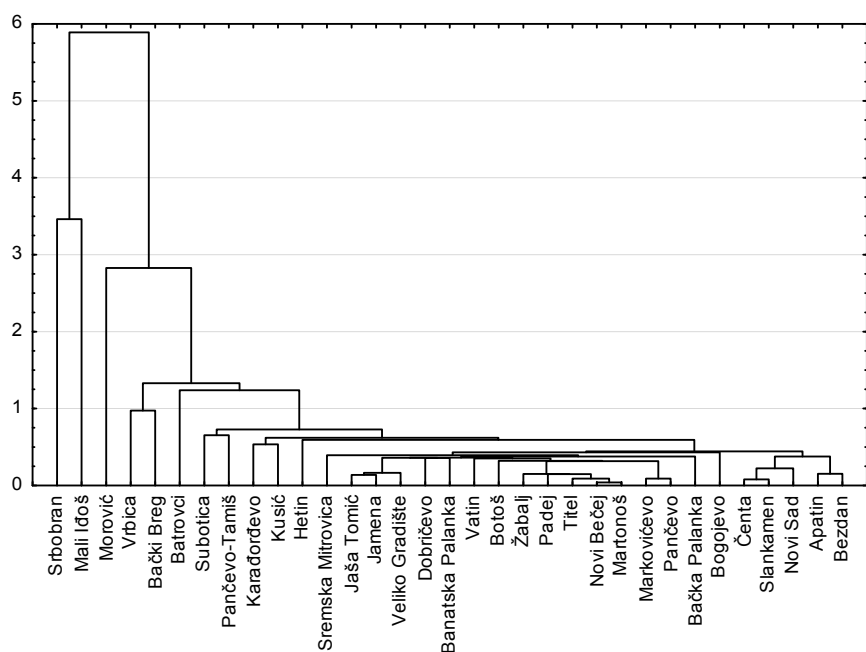
Drugoj grupi pripadaju sve ostale merne stanice.

Uticaj tzv. eutrofikacije je slabiji na mernim stanicama II grupe u poređenju sa uticajem na mernim stanicama I grupe, što je i utvrđeno njihovim grupisanim primenom klaster analize. Izmerene vrednosti NO_3-N se kreću od 0,24–2,12 mg/l. Na mernoj stanici Bezdan izmerena je najveća vrednost koja pripada II klasi, a prema Pravilniku vodno telo Dunav ispunjava uslove za dobar ekološki potencijal. Izmerene vrednosti NH_4-N se kreću od 0,03–0,69 mg/l. Na mernoj stanici Subotica izmerena je najveća vrednost koja prema Uredbi pripada IV klasi, te za vodno telo Kereš postoji opasnost od nedostizanja dobrog hemijskog statusa, a Prema Pravilniku vodno telo ne ispunjava uslove za dobar ekološki potencijal. Na ostalim mernim stanicama vrednost NH_4-N prema Uredbi pripada I i II klasi.

Dendrogram klaster analize monitoring stanica u odnosu na treći faktor F3 prikazan je na slici 4.

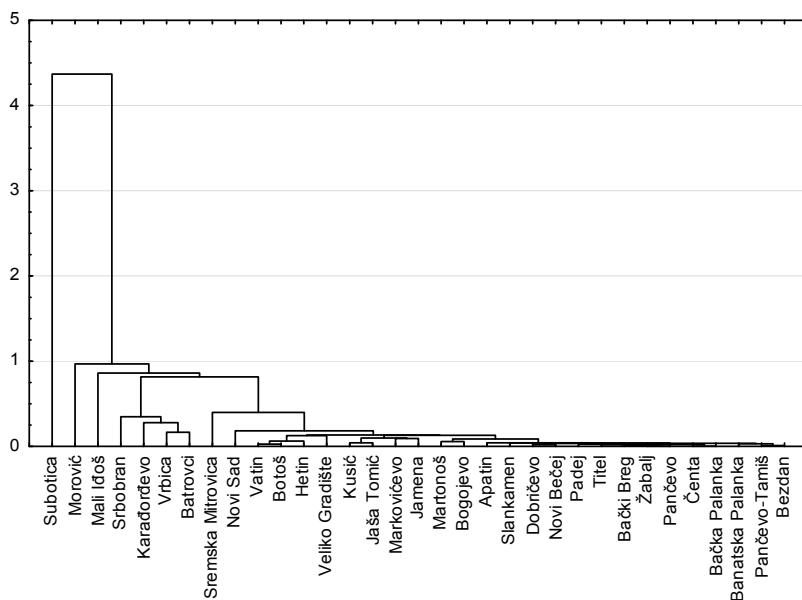
Prvoj grupi pripada merna stanica Kereša (Subotica).

Prema Uredbi, najveća izmerena vrednost BPK_5 od 10,53 mg/l na mernoj stanici Subotica pripada IV klasi. Prema Pravilniku vodno telo ne ispunjava uslove za dobar ekološki potencijal. Prema Uredbi, izmerena vrednost PAM od 0,07 mg/l pripada I klasi. Veće vrednosti PAM ukazuju na veći antropogeni uticaj. Na osnovu navedenih podataka može se zaključiti da je kvalitet



Slika 3. Dendrogram klaster analize monitoring stanica u odnosu na drugi faktor F2.

Figure 3. Cluster analysis dendrogram of the monitoring stations in relation to the second factor F2.



Slika 4. Dendrogram klaster analize monitoring stanica u odnosu na treći faktor F3.

Figure 4. Cluster analysis dendrogram of the monitoring stations in relation to the third factor F3.

vode vodotoka Kereš značajno ugrožen ispuštanjem komunalnih otpadnih voda i da za vodo telo postoji opasnost od nedostizanja dobrog hemijskog statusa.

Drugoj grupi pripadaju sve ostale merne stanice.

Izmerene vrednosti BPK_5 se kreću od 1–6,16 mg/l, a najveća vrednost izmerena je na mernoj stanici Morović i prema Uredbi odgovara III klasi. Vrednost BPK_5 na ostalim mernim stanicama prema Uredbi pripada I i II klasi.

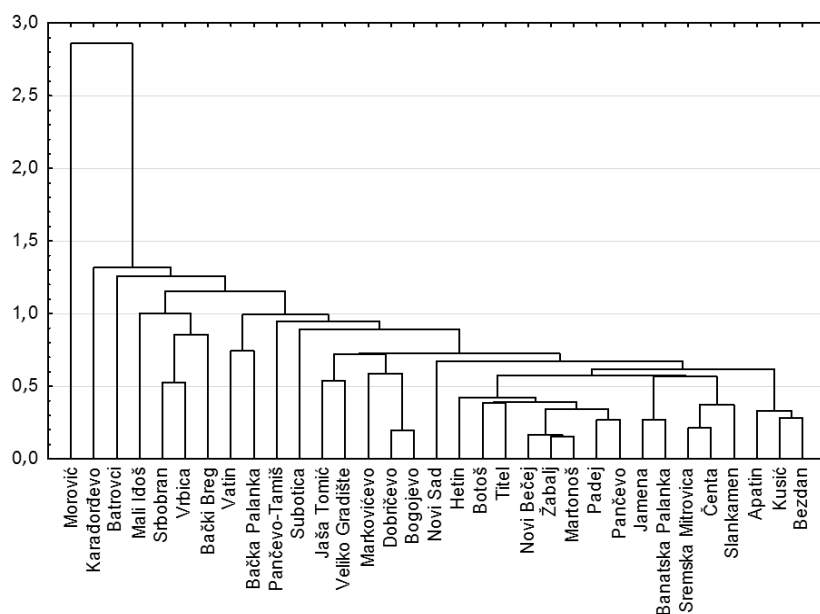
Izmerene vrednosti PAM se kreću od 0,01–0,06 mg/l. Najveća vrednost izmerena je na mernoj stanici

Srbobran što prema Uredbi odgovara I klasi. Takođe, vrednost PAM na svim ostalim mernim stanicama druge grupe prema Uredbi odgovara I klasi.

Može se zaključiti da za vodna tela Krivaja i Studva postoji opasnost od nedostizanja dobrog hemijskog statusa.

Dendrogram klaster analize monitoring stanica u odnosu na četvrti faktor F4 prikazan je na slici 5.

Prvoj grupi pripada merna stanica Studve (Morović).



Slika 5. Dendrogram klaster analize monitoring stanica u odnosu na četvrti faktor F4.

Figure 5. Cluster analysis dendrogram of the monitoring stations in relation to the fourth factor.

Uticaj ekološkog faktora najizraženiji je na mernoj stanici Morović koja je klaster analizom izdvojena u prvu grupu na osnovu najveće izmerene vrednosti rastvorenog kiseonika, od 13,74 mg/l, i na osnovu najveće vrednosti pH od 8,55. Prema Uredbi izmerena vrednost pH pripada V klasi, a prema Pravilniku vodno telo Studva ne ispunjava uslove za dobar ekološki potencijal.

Drugoj grupi pripadaju sve ostale merne stanice.

Izmerene vrednosti pH se kreću od 7,42–8,53. Najveća vrednost izmerena je na mernoj stanici Karađorđevo i prema Uredbi pripada V klasi, a za vodno telo postoji opasnost od nedostizanja dobrog hemijskog stanusa. Prema Pravilniku, vodno telo Krivaja ne ispunjava uslove za dobar ekološki potencijal.

Visoka vrednost pH, od 8,49, izmerena je na mernoj stanici Kereša, što odgovara IV klasi, a prema Pravilniku vodno telo ne ispunjava uslove za dobar ekološki potencijal.

Na pojedinim mernim stanicama izmerene su niže koncentracije rastvorenog kiseonika u odnosu na merne stanice I grupe. Najniže vrednosti rastvorenog kiseonika izmerene su na mernim stanicama Zlatice i Krivaje, na osnovu kojih vodotoci pripadaju III klasi. Na vodotocima Studva, i Krivaja izmerene su visoke vrednosti pH > 8,5. Radi se o vodotocima malog protoka, tako da su u pojedinim periodima godine po kvalitetu vode uslovi slični uslovima koji su karakteristični za stajaće vode.

Niske vrednosti rastvorenog kiseonika i pH utiču na smanjenje diverziteta flore i faune akvatičnih ekosistema [19]. Za većinu akvatičnih organizama optimalna pH vrednost se kreće od 7,2–8,7.

Povećanje pH vrednosti površinskih voda može biti posledica uticaja industrijskih otpadnih voda.

Kako visoke vrednosti pH utiču na rastvorljivost teških metala, a samim tim i na njihovu toksičnost, postoji opasnost od oslobođanja metalnih jona (npr. aluminija) iz kompleksa sa drugim katjonima. pH vrednost vode određuje rastvorljivost i biološku raspoloživost hemijskih konstituenata azota. Ukoliko su vrednosti pH niske u vodi su prisutni amonijum ion (NH_4^+) i hidronijum ion (H_3O^+). Amonijum ion nije toksičan za žive organizme. Međutim, opasnost za živi svet postoji u slučaju većih vrednosti pH (iznad 9) kada je dominantan NH_3 kao toksična komponenta. Temperatura može uticati na hemijske i biološke procese i samim tim na uslove života akvatičnih organizama. Na osnovu navedenih podataka može se zaključiti da su temperature vode na mernim stanicama uslovljene sezonskim varijacijama [17–19].

ZAKLJUČAK

Primenom faktorske analize/analize glavnih komponenti za značajno izmenjena vodna tela na teritoriji Vojvodine, na osnovu 13 parametara kvaliteta vode, ekstrahovana su četiri faktora koja objašnjavaju oko

78% ukupnog varijabiliteta. Prvi faktor F1 (hidrohemski faktor) doprinosi oko 28% ukupnom varijablitetu i najviše je korelisan parametrima: SM , UT , pH , EP , TP , Ca^{2+} i Mg^{2+} . Drugi faktor F2 (faktor eutrofikacije) doprinosi 18% ukupnom varijabilitetu i najviše je korelisan parametrima: rastvoren kiseonik, $\text{NH}_4\text{--N}$, $\text{NO}_3\text{--N}$ i TP . Treći faktor F3 (faktor tačkastih izvora zagađenja) doprinosi 17% ukupnom varijabilitetu i najviše je korelisan sa parametrima: BPK_5 i PAM . Četvrti faktor, F4 (ekološki faktor), doprinosi oko 13% u ukupnom varijabilitetu i najviše je korelisan sa parametrima: T , rastvoren kiseonik i pH. U odnosu na ekstrahovane faktore izvršena je klaster analiza u cilju otkrivanje sličnosti i razlika fizičko-hemijskog stanja vode između 33 merne stanice značajno izmenjenih vodnih tela.

Iz faktorske analize sledi da postoje pritisci, prirodni i antropogeni na variranje kvaliteta vode vodotoka. Primenom faktorske analize/analize glavnih komponenti i klaster analize izdvojila su se vodna tela koja se nalaze pod najvećim pritiscima. U odnosu na faktor F1 to su: Plazović, Bosut, Studva, Zlatica, Stari Begej i Krivaja. U odnosu na F2 to su: Krivaja i Kereš. U odnosu na faktor F3 to su: Studva, Krivaja i Kereš. U odnosu na faktor F4 to su: Studva, Zlatica, Krivaja i Kereš. Na osnovu navedenih podataka može se zaključiti da za vodna tela postoji opasnost od nedostizanja dobrog hemijskog stanusa i dobrog ekološkog potencijala.

Primenom multivarijacionih statističkih metoda za procenu stanja vodnih tela identifikovani su faktori/izvori koji su odgovorni za varijabilnost kvaliteta vode. Takođe, metodama je identifikovan raspored izvora zagađenja. Prikazano je da su faktorska analiza/analiza glavnih komponenti i klaster analiza koristan alat za razvoj odgovarajuće strategije za efikasnije upravljanje vodnim resursima.

LITERATURA

- [1] M. Gocić, S. Stanković, S. Trajković, Monitoring baziran na Webu za ocenjivanje kvaliteta površinskih voda, Zbornik radova Građevinsko-arkitektonskog fakulteta, Niš, **22** (2007) 149–158.
- [2] M. Adamu, A.Z. Aris, Spatial aspect of Surface Water Quality using chemometric analysis, *J. Appl. Sci. Environ. Sanit.* **6** (2011) 411–426.
- [3] H. Boyacioglu, H. Boyacioglu, Surface Water Quality Assessment by Environmetric Methods, *Environ. Monit. Assess.* **31** (2007) 371–376.
- [4] B. Dalmacija, Strategija vodosnabdevanja i zaštite voda AP Vojvodina, Pokrajinski sekreterijat za nauku i tehnološki razvoj, Novi Sad, 2009.
- [5] K.P. Singh, A. Malik, S. Sinha, Water quality assessment and apportionment of pollution sources of Gomti river (India) using multivariate statistical techniques – A case study, *Anal. Chim. Acta* **538** (2005) 355–374.
- [6] C.W. Liu, K.H. Lin, Y.M. Kuo, Application of factor analysis in the assessment of groundwater quality in a

- blackfoot disease area in Taiwan, *Sci. Total Environ.* **313** (2003) 77–89.
- [7] M.Varol, B. Sen, Assessment of surface water quality using multivariate statistical techniques: A case study of Behrimaz Stream, Turkey – *Environ Monit Assess*, **159** (2009) 543–553.
- [8] M.M. Prakash, A. Dagaonkar, Application of cluster analysis to phisicochemical parameters of Munj Sagar Talab, Dhar (Madhya Pradesh, India), *Recent Res. Sci. Technol.* **3** (2011) 41–50.
- [9] V. Simeonov, J. W. Einax, I. Stanimirova, J. Kraft, Environmetric modeling and interpretation of river water monitoring data, *Anal. Bioanal. Chem.* **374** (2002) 898–905.
- [10] Anon.: Hidrološki godišnjak 3, Kvalitet voda 2010, Republički hidrometeorološki zavod, 2011, Beograd.
- [11] Anon.: Pravilnik o utvrđivanju vodnih tela površinskih i podzemnih voda (Sl. Glasnik RS, br. 96/2010).
- [12] Anon.: Zakon o vodama (Sl. Glasnik RS, br. 30/2010).
- [13] Anon.: Plan upravljanja vodama za sлив реке Дунав, део 1: Анализа карактеристика слива Дунава у Србији – радна верзија, Институт за водопривреду Јарослав Черни, Београд, децембар, 2011.
- [14] Anon.: Uredba o graničnim vrednostima zagađujućih materija u površinskim i podzemnim vodama i sedimentu, kao i rokovi za njihovo dostizanje (Sl. Glasnik RS, br. 50/2012).
- [15] Anon.: Pravilnik o parametrima ekološkog i hemijskog statusa površinskih voda i parametrima hemijskog i kvantitativnog statusa podzemnih voda (Sl. Glasnik RS, br. 74/2011).
- [16] E. Perona, I. Bonilla, P. Mateo, Spatial and temporal changes in water quality in a Spanish river, *Sci. Total Environ.* **241** (1999) 75–90.
- [17] B. Dalmacija, I. Ivančev-Tumbas, Analiza vode-kontrola kvaliteta, tumačenje rezultata, Prirodno-matematički fakultet, Novi Sad, 2004.
- [18] V. Gvoždić, J. Brana, D. Puntarić, D. Vidovavljević, D. Roland, Changes in the Lower Drava River Water Quality Parameters Over 24 Years, *Arh. Hig. Rada Toksikol.* **62** (2011) 325–323.
- [19] M. Varol, B. Gököt, A. Bekleyen, B. Sen, Water quality assessment and apportionment of pollution sources of Tigris River (Turkey) using, multivariate statistical techniques – a case study, *River Res. Applic.* **27** (2011), <http://dx.doi.org/10.1002/rra.1553>.

SUMMARY**EVALUATION OF HEAVILY MODIFIED WATER BODIES IN VOJVODINA BY USING MULTIVARIATE STATISTICAL TECHNIQUES**Svetlana R. Vujović¹, Srđan R. Kolaković¹, Milena R. Bečelić-Tomin²¹*Faculty of Technical Sciences, Department of Civil Engineering, University of Novi Sad, Novi Sad, Serbia*²*Faculty of Sciences, Department of Chemistry, Biochemistry and Environmental Protection, University of Novi Sad, Novi Sad, Serbia*

(Scientific paper)

This paper illustrates the utility of multivariate statistical techniques for analysis and interpretation of water quality data sets and identification of pollution sources/factors the aim of getting better information about the water quality and design of a monitoring network for effective management of water resources. Multivariate statistical techniques, such as factor analysis (FA)/principal component analysis (PCA) and cluster analysis (CA), were applied to the evaluation of variations and the interpretation of water quality data of heavily modified water bodies, obtained during 2010 by the monitoring of 13 parameters at 33 different sites. FA/PCA attempts to explain the correlations between the observations in terms of the underlying factors, which are not directly observable. Factor analysis is applied to physicochemical parameters of heavily modified water bodies with the aim classification and data summation as well as segmentation of heterogeneous data sets into smaller homogeneous subsets. Factor loadings were categorized as strong and moderate corresponding to the absolute loading values of >0.75, 0.75–0.50, respectively. Four principal factors were obtained with Eigenvalues >1 summing more than 78% of the total variance in the water data sets, which is adequate to give good prior information regarding data structure. Each factor that is significantly related to specific variables represents a different dimension of water quality. The first factor F1 accounts for 28% of the total variance and represents the hydrochemical dimension of water quality. The second factor F2 accounts for 18% of the total variance and may be taken factor of water eutrophication. The third factor F3 accounts for 17% of the total variance and represents the influence of point sources of pollution on water quality. The fourth factor F4 accounts for 13% of the total variance and may be taken as an ecological dimension of water quality. Cluster analysis (CA) is an objective technique to identify natural groupings in the set of data. CA divides a large number of objects into smaller number of homogenous groups on the basis of their correlation structure. CA combines the data objects together to form the natural groups involving objects with similar cluster properties and separates the objects with different cluster properties. CA showed similarities and dissimilarities among the sampling sites and explained the observed clustering in terms of affected conditions. Using FA/PCA and CA, water bodies that are under the highest pressure were identified. With regard to the factors, the identified water bodies were: for factor F1 – Plazović, Bosut, Studva, Zlatica, Stari Begej and Krivaja; for factor F2 – Krivaja and Kereš; for factor F3 – Studva, Krivaja and Kereš; for factor F4 – Studva, Zlatica, Krivaja and Kereš.

Keywords: Multivariate statistical techniques • Factor analysis/Principal component analysis • Cluster analysis • Water quality

Investigation of whey protein concentration by ultrafiltration elements designed for water treatment

Miroslav Đ. Kukučka, Nikoleta M. Kukučka

Envirotech, d.o.o., Kikinda, Serbia

Abstract

The suitability of polysulfone ultrafiltration membranes (UFM) designed for commercial water treatment has been investigated for separation of protein (PR) from sweet whey. Ultrafiltration (UF) of whey originated from dairy has been realized by a self-made pilot plant, which has been in service for about one year. The influence of two whey temperatures (9 and 30 °C) on the efficiency of protein concentration has been examined. Application of investigated UF elements gave whey protein concentrate (WPC) with 5 to 6 times excess amount of protein content compared to the initial. At the same time, the prevalent content of lactose was removed to permeate. Better results were obtained with cold whey filtration. Besides the fact that the molecular weight cut-off (MWCO) of the investigated membranes was 50–100 kDa, the results showed very successful concentrating of whey proteins of dominantly lower molar weights than 50–100 kDa. Investigated membranes are beneficial for design and construction of UF plants for exploitation in small dairies.

Keywords: Ultrafiltration membranes for water treatment, whey protein concentration, temperature influence.

Available online at the Journal website: <http://www.ache.org.rs/HI/>

Cheese whey contains significant amount of proteins, lactose (L) and minerals that can be extracted and reused in food industry and biotechnologies. Water also presents great percentage of cheese whey, which can also be separated and reused in a function of dairy wastewater purification hence leading to environmental protection [1]. Purifying dairy wastewater has been investigated using membrane processes such as reverse osmosis [2], nanofiltration and ultrafiltration [3,4] as well as coagulation and adsorption [5].

The β -lactoglobulin (β -LG) and α -lactalbumin (α -LA) are the two biggest protein fractions in cheese whey. These fractions, together, account for 70 to 80% of total proteins in whey, but concentration of β -LG is twice that of α -LA. The molecular weight (MW) of α -LA is 14 kDa and MW of β -LG (as dimer) is 36.8 kDa [6]. The rest of the whey proteins are serum albumin in percentage of \approx 10% with MW of 69 kDa and immunoglobulin (MW 160–1000 kDa) with share of \approx 10% [7].

Extracting proteins from whey by membrane filtration has been investigated in previous studies using different types of membranes, such as ceramic micro-filters combined with polyetersulfone UFM [8–10] and tangential flow filtration modules [11,12]. The fractionation of whey into lactose enriched and protein-enriched streams using UFM of regenerated cellulose materials has also been investigated [13]. More

SCIENTIFIC PAPER

UDC 637.1/3:66.081.63

Hem. Ind. **67** (5) 835–842 (2013)

doi: 10.2298/HEMIND121016008K

research was done using commercial UFM designed for the separation of protein from milk [14–18]. The contribution of tubular ceramic membrane research [19,20] to study the mechanism of separation of protein from whey is also very significant. There have also been recent investigations on the removal of whey proteins using ultrafiltration membranes with molecular weight cut-off (MWCO) of 50–100 kDa [6].

Whey protein is concentrated by ultrafiltration on a daily basis in many industrial plants in the world. The goal of WPC separation from whey is to obtain a solution rich in protein that can be used to get various types of cheese [21], such as ricotta [22], cheddar [23] and white cheese [24]. By drying of WPC is obtained whey powder, which is an excellent additive in food products [25]. Also, whey protein can be disassociated to building components that are used for sophisticated applications [10]. UF permeate is practically used to obtain the crystalline lactose [26], or enzymatic digestion of lactose to monosaccharides gets a sweet solution to substitute the water and sucrose and is a great base for manufacturing the entire range of soft drinks rich in natural minerals derived from milk [27].

Industrial ultrafiltration takes place on specially designed flat-sheet membranes at relatively high transmembrane pressure (from 2.5 to 5 bar). Special UF membranes for filtration of milk and whey are differ from UF ultrafiltration membranes designed for water, in that they do not contain anti-telescoping caps and that their diameters and lengths are made according to special standards. These standards include the most common sizes of \varnothing 3.8" \times 38" length and \varnothing 8" \times 38" and

Correspondence: N.M. Kukučka, Envirotech, d.o.o., S. Popovića 42, Kikinda, Serbia.

E-mail: nikol@envirotech.rs

Paper received: 16 October, 2012

Paper accepted: 14 December, 2012

require special housing. Since the production of UFM for treatment of whey is in significantly smaller amounts than those for the ultrafiltration of water, the cost of making devices for filtration of UF whey special membranes are significantly higher. In addition, it is quite complicated (complex) to obtain special UFM with housings, but the world's leading manufacturers insist on a purchase a complete UF device.

Due to their whey content, dairy wastewaters are significant polluters with BOD₅ content of several thousand to tens of thousands mg O₂/L. Small dairies processing up to 50000 L of milk a day, due to the high cost of equipment for ultrafiltration, are not able to obtain specialized equipment designed to extract the proteins from whey. Currently, the unprocessed whey is being discharged as waste in most dairies in Serbia, directly affecting the environment. Thus, one of the goals of this work was to design cheaper equipment that can be used in small dairies across Serbia.

The aim of the investigation was to determine the ability of whey protein concentration using commercial UFM provided for ultrafiltration of water. A UF pilot plant was designed and built in the company "Enviro-tech", Kikinda, Serbia, and installed in the dairy "Kikinda industry of milk", part of the French Bongrain group in Kikinda, Serbia. This dairy processed daily up to 50000 L of milk to semi-hard cheeses (Gouda, Edam and Trappe). The formed part of the sweet whey was used in experiments at the pilot unit. Defining the technical design of pilot devices and basic investigation of

the potential concentration of whey protein lasted for two years. In the third year, a series of studies were conducted with hot and cold ultrafiltration of whey. The obtained WPC was used daily in a period of six months in dairy production of ricotta and mixed with the milk for the production of semi-hard cheeses.

MATERIALS AND METHODS

Design of the pilot plant and operating conditions

The pretreatment of whey before entering the collection tank (WM, Figure 1) consisted of centrifugal separation of milk fat and dispersed particles, as well as temperature settings. The operations were carried out by existing equipment of the dairy. In accordance with the experimental procedure, the whey temperature was 9 °C – cold whey (CW) or 30 °C – hot whey (WW). The average concentration of milk fat in whey after the milk fat centrifugal separation and the average pH was 0.04% and 6.7, respectively. Commercial spiral wound UFM designed for ultrafiltration of water (Woongjin Chemical Co., Ltd., Korea) was investigated. The UFM characteristics are shown in Table 1. The pilot plant contained two serial connected UF membranes.

The operating regime of the pilot unit was run by a programmable controller ZEN (Omron, Japan). Before the start of whey UF, back-flushing of UFM using demineralized water automatically took place for 2 min. Then the process of cross-flow filtration of whey was initiated using pumps CP1 and CP2 and MF (Figure 1).

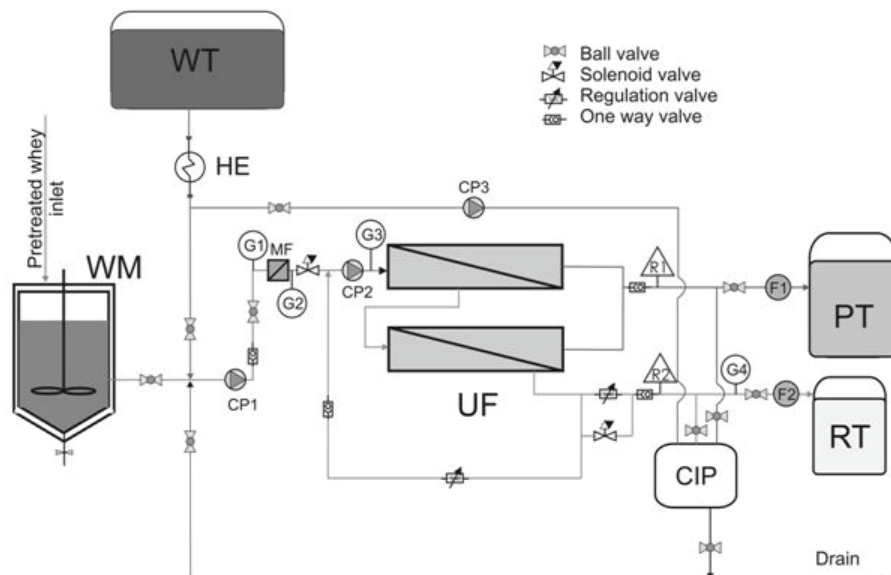


Figure 1. The flow sheet of an ultrafiltration pilot plant; WM – thermally insulated tank with a mixer for whey; WT – tank with demineralized water; HE – heat exchanger; MF – polypropylene microfilter of 5 µm; UF – ultrafiltration modules; PT – tank of permeate; RT – tank of retentate; CIP – vessel for the storage of the solutions for UF membrane cleaning; CP1 – feed pump; CP2 – booster pump of UF modules; CP3 – pump for demineralized water transport; R1 – continuous flow meter of permeate, R2 – continuous flow meter of retentate; G1/2 – pressure gauges before and after MF; G3/4 – pressure gauges before and after the membranes; F1 – cumulative permeate volume meter; F2 – cumulative retentate volume meter.

Table 1. Characteristics of UF membrane

Type	Material	Configuration	Dimensions Ø/mm×H/mm	Molecular weight cut off, kDa	Membrane area, m ²	Permeate flow rate, m ³ /h	Average flux L/(h m ²)
Homogenous asymmetric flat sheet	Polysulfone (PSF)	Spiral-wound, FRP wrapping	203×1,016	50–100	33.9	2.2	64.90

Upon termination of service modes, the membranes were again back-flushed with water for 2 min. Permeate from the UF unit was collected in the tank, PT, and retentate was stored in the reservoir, RT. Part of the retentate through the valve inlet mixed with whey.

During each test series, the following operating conditions (OC) of the pilot device were measured: pressure before and after MF and UF, permeate and retentate flow rates.

Sampling of whey from tank WM was performed at the beginning of each investigated batch. After each series with CW and WW, permeate and retentate volumes were measured and permeate and retentate aggregate samples were taken from the tanks PT and RT. In all samples, the contents of chemical composition parameters (CP) of whey, permeate and retentate: temperature (T), protein, lactose and total solids (TS) were measured (Table 2).

The first 10 series of WPC separation were carried out by filtration of CW. The following 10 series were dedicated to concentration of proteins from WW. For the duration of the filtration every series contained 10 check points of operating parameters measurements and sampling of permeate and retentate.

Processes of UFM washing and cleaning with water and chemicals were manually operated. Centrifugal pump CP3 supplied water for solutions preparation from the tank WT. In the CIP container different cleaning solutions were formed, which were circulated in a closed cycle using centrifugal pump CP1 through the membranes back into the CIP container, at a pressure of 2.5 bar and flow rate of 2000 L/h. The membranes were washed in the first phase with hot water (at 50 °C) for 20 min. Then came the enzymatic cleaning solution by combining of Ultrasil 67 and 69 [28], at a temperature of 55 °C for 20 min. The membranes were again washed with hot water (at 50 °C) for 10 min and

then treated using Ultrasil 11 [29], at 50 °C for 60 min. The final washing of the membranes was done with cold water at 18 °C for 30 min.

Physicochemical methods and analytical instruments used in the sample analyses

For the investigated whey, permeate and retentate, general quality parameters, such as fat, protein, lactose and TS were measured on a MilkoScan Minor instrument (Foss, Denmark) by photometric analytical methods [30]. Control values of these parameters were obtained by analysis of ten random samples of whey, permeate and retentate in an accredited laboratory Sojaprotein (Bečej, Serbia). The measured values using MilkoScan differed from values obtained in the accredited laboratory by ±1.1%.

Calculation of the cross-flow filtration parameters

Normalized differential pressure NDP (bar) as a function of permeate and retentate flow rates was calculated by the following equation:

$$NDP = \Delta p \frac{(2Q_{R0} + Q_{P0})^{1.5}}{(2Q_R + Q_P)^{1.5}} \quad (1)$$

where Δp – differential pressure on UF membranes; Q_{R0} – initial retentate flow rate (L/h); Q_{P0} – initial permeate flow (L/h), Q_R – retentate flow rate (L/h), Q_P – flow of permeate (L/h).

The flux - flow of filtrate per unit area of membrane was calculated as follows:

$$J = \frac{Q_p}{A_m} \quad (2)$$

where J (L/h/m²) – flux, A_m (m²) – surface of the UFM.

Temperature compensated specific flux TCSF defines the permeability of the membrane depending on

Table 2. The results of measurements of whey and UF effluents parameters

Sample	T / °C	Protein, %	Lactose, %	TS / %	Volume, L
Whey	9	1.03	4.51	5.99	11,657
Retentate		5.22	4.41	11.79	1,199
Permeate		0.21	3.79	5.78	10,458
Whey	30	0.99	4.12	5.33	4,460
Retentate		5.24	4.68	12.03	424
Permeate		0.21	3.65	5.67	4,036

the transmembrane pressure TMP and whey temperature (°C). TCSF indicates the chemical degradation or membrane fouling:

$$TCSF = \frac{J}{TMP} e^{(-0.031(T-20))} \quad (3)$$

The yield of protein, PY, in the retentate was calculated from the ratio of protein content in the retentate, C_r (%), and whey protein content, C_0 (%), by the expression:

$$PY = \frac{C_r}{C_0} \quad (4)$$

Rate changes of $NDP - RC_{NDP}$ (bar/min), during the UF process is calculated as follows:

$$RC_{NDP} = \frac{(NDP_f - NDP_s)}{t} \quad (5)$$

where NDP_f (bar) – NDP in the final point of UF; NDP_s (bar) – NDP in the starting point of UF; t (min) – lasting time of UF.

Rate change of $TMP - RC_{TMP}$ (bar/min) during the UF is calculated as:

$$RC_{TMP} = \frac{(TMP_f - TMP_s)}{t} \quad (6)$$

where TMP_f (bar) – TMP in the final point of UF; TMP_s (bar) – TMP in the starting point of UF; t (min) – duration of UF.

Membrane efficiency, η (%), was calculated as:

$$\eta = 100 \left(1 - \frac{C_p}{C_0} \right) \quad (7)$$

RESULTS AND DISCUSSION

During the course of the cold filtration of whey, microfilter MF differential pressures were equally

about 1 bar. The range of inlet and outlet pressures was from 7 to 6 bar. Inlet and outlet pressures of membrane elements were in the range of 9.5 to 9.8 bar and 8.5 to 8.8 bar, respectively. UFM differential pressures were constant of 1 bar. The average duration of CW ultrafiltration series was 630 min.

UF testing of hot whey have played at inlet pressures of pump CP1 of 6.9 bar at the beginning to 5.8 bar in the end of process. MF pressure drops were from 0.9 to 1.4 bar. Cross flow filtration processes have carried out under booster pump CP2 pressures of 9.1 bar in the start to 7.9 bar at the final check point. Membrane elements differential pressures were in the range 0.6 to 1.1 bar. Separation of WW protein lasted 250 min in average.

Mean values of changes NDP, TMP and WPC depending on the duration of UF process are shown in Figures 2 and 3. Figure 4 presents the membrane efficiency for the removal of proteins with regard to flux change, while Figure 5 describes the L/Pr ratio during the ultrafiltration of CW and WW. Figure 6 shows the dependence of the mean values of flux and TCSF during the lasting time of the ultrafiltration process.

Figures 2, 3 and 6 show that the ultrafiltration of CW successfully took place in about 2.5 times longer period of WW cross-flow filtration.

All ultrafiltration experiments took place until the appearance of fouling. The beginning of fouling was followed by the decrease in flux with increasing of differential pressure (Figures 2 and 6). Fouling was manifested in significantly reduction of protein yield (PY) in the retentate (Figure 3). Using the above-described procedure, membranes were chemically and enzymatically cleaned 154 times during the six months. After each cleaning, the UFM have renewed their flux, and the initial permeate flow. After last cleaning the total flux decline was 2.4% compared to the pre-flux of new membranes.

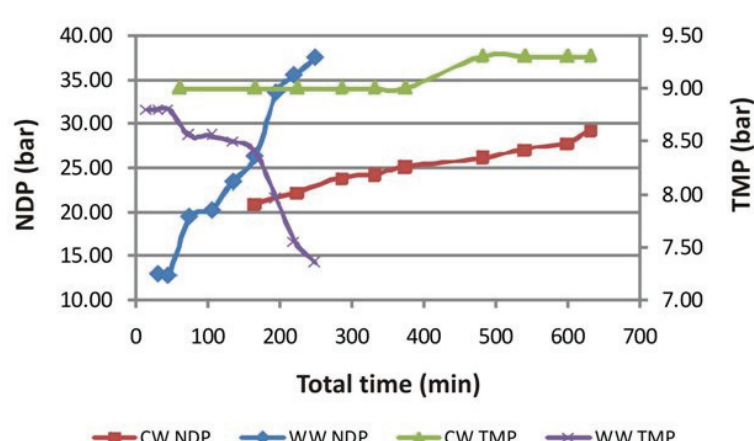


Figure 2. The differences between the changes of the NDP and TMP during the filtration of hot and cold whey.

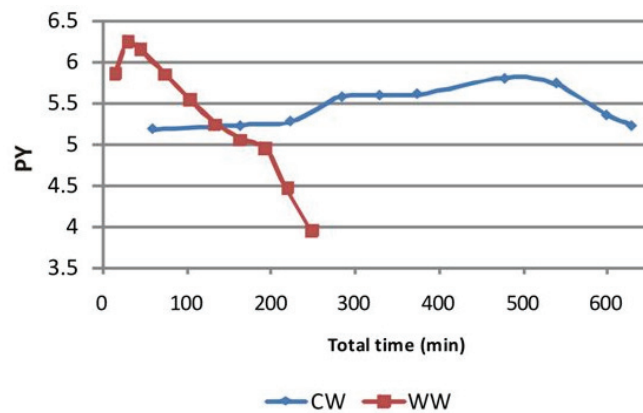


Figure 3. Changes of protein yield during the lasting time of filtration.

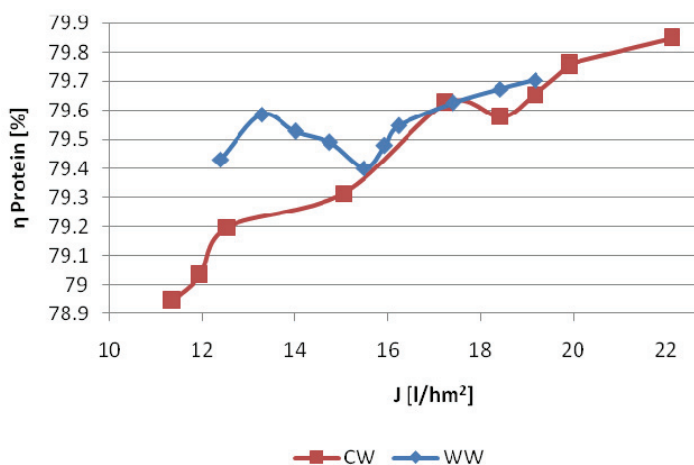


Figure 4. Protein removal membrane efficiency vs. flux during the CW and WW ultrafiltration.

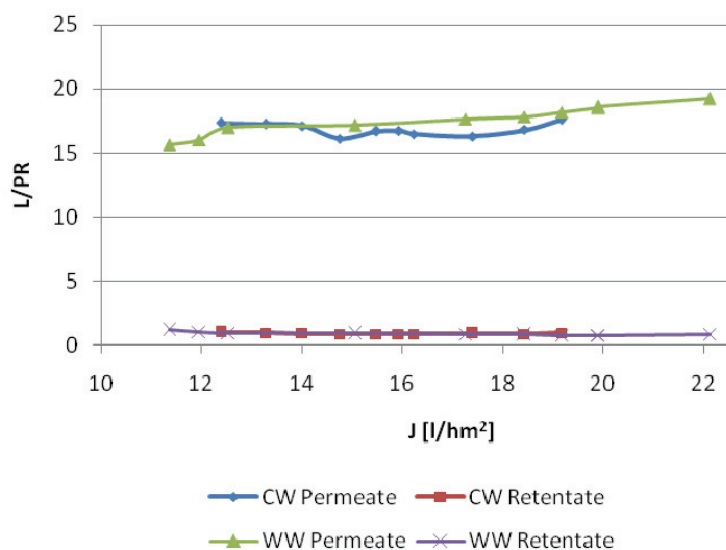


Figure 5. Lactose and protein ratio with regard to flux change.

During the CW and WW ultrafiltrations, the volume of obtained retentate was 10.29 and 9.51%, respectively, compared to the volume of incoming whey.

For the duration of the process of protein separation from the CW, TMP increased very slightly with a mean rate of $RC_{TMP} = 5.3 \times 10^{-4}$ bar/min. In CW filtration NDP also grew over the time at a mean rate of $RC_{NDP} =$

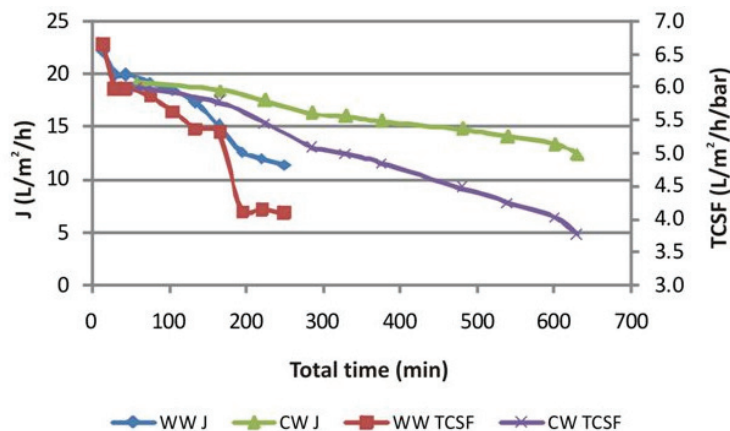


Figure 6. Comparison of flux and TCSF for the duration of the CW and WW ultrafiltrations.

= 0.015 bar/min. UFM differential pressure was constant during the course of UF. TMP was almost constant and the difference between the NDP from the beginning and end of the process was 8.28 bar.

During the filtration of hot whey, NDP sharply increased in a short period at an average rate of $RC_{NDP} = 0.11$ bar/min, while reducing the TMP of approximately $RC_{TMP} = -7 \times 10^{-3}$ bar/min.

Test series with WW were characterized by anomalies that with increase of the NDP the TMP decreased. The difference in differential pressure of UFM during WW filtration of 0.5 bar produced a large NDP difference of 24.6 bar, which originated as a consequence of decrease of the flow of permeate and retentate (Eq. (1)). These results mean that the UFM are more permeable at 30 °C than at the temperature of 9 °C. Increased permeability at the hot process of UF caused faster flux reduction followed by growth of the NDP, which are a consequence of fouling.

The protein content in the retentate during the ultrafiltration of CW through the cycle was 5 to 5.8 times higher than in the starting whey. In CW ultrafiltration WPC reaches a maximum value of the NDP of 26 bar at 480 min of filtration. At the beginning and end of the process yield of protein is approximately equal. During CW filtration mean protein content in the retentate is 5.32 times higher than in whey.

Concentration of protein from WW characterized by a rapid decrease in protein yield decreased in direct proportion to TMP. With an increase of the NDP, PY for 250 min reduced 1.6 times compared to the start of UF process.

As can be seen from Figure 4, protein removal membrane efficiency was extremely high and constant which was documented by average η values of 79.47 and 79.54% in WW and CW, respectively. Obtained results testify that investigated membranes can be used, with great efficiency, for removal of proteins from whey. The protein removal membrane efficiency curve, during the experiment with CW, exhibits great

linear correlation ($R^2 = 0.964$) while η protein curve in experiment with WW has an uneven trend during the flux change ($R^2 = 0.506$).

Ratio of lactose and protein contents in the whey amounted 4.38. In the course of ultrafiltration this ratio has been remarkably changed. The L/PR ratios have been calculated to obtain the results of transition effects of lactose and protein during the ultrafiltration. Figure 5 shows low L/PR ratios for retentates and high L/PR ratios for permeates. The average L/PR ratios in permeate and retentate were found to be 3.82 and 4.01 times higher and 4.87 and 4.92 times lower in CW and WW, respectively, than that in the inlet whey. Thus, lactose was prevalent in permeate and protein was dominant in retentate.

During the time course of protein separations with increasing NDP, TCSF and flux declined at both operating temperatures, with almost linear decrease in the separation of proteins from the CW. Reduction in flux and TCSF in WW investigation was in relation to the duration of the filtration 4 and 2.78 times larger, respectively.

CONCLUSION

Ultrafiltration membranes designed for water filtration have been successfully applied to whey protein concentrating. The average fluxes of CW and WW ultrafiltration were 16.77 and 15.71 L/m², respectively. These J values were 3.87 and 4.13 times lower than the average flux of investigated UF membranes in the case of water ultrafiltration. The average volume of obtained retentate was 10 times smaller than the initial volume of whey. Ultrafiltration process is successfully taking place at relatively low trans-membrane pressures in relation to TMP that are necessary for the functioning of special membranes designed for ultrafiltration of whey. Cross-flow filtration of whey cooled to 9 °C is more efficient with obtained equal yield of protein in the retentate 5.5 to 6 times higher than the protein

content in whey. At the same time, the prevalent content of lactose was removed to permeate. The duration of the ultrafiltration of more than 10 h before fouling appearance and the downtime for membrane cleaning is practically very acceptable.

In order for the process of protein concentration to last at least 10 h with a steady yield of protein in the retentate, it is necessary to provide a constant differential pressure on the UFM and almost equal *TMP* in the process. The slight decrease of permeate and retentate contributes to a small difference in the *NDP* during UF.

Ultrafiltration of hot whey at 30 °C was able to run at most 4.5 h before the emergence of fouling and rapid decline in the yield of protein.

Besides the fact that MWCO of investigated membranes were 50–100 kDa, the results showed very successfully concentrating of whey proteins of dominantly lower molar weights than 50–100 kDa. These results are similar to the recently published results [6]. It is known that there are many factors affecting membrane-based process, like type of membrane and its MWCO, *TMP*, temperature of operation, feed pH and so on, which are important operating variables that influence process efficiency. The scope of the further investigations will be focused to finding explanations for the obtained phenomena.

Acknowledgments

The authors would like to thank the dairy „Kikinda industry of milk“, part of French Bongrain group, specifically to Mr. Saša Mančić and Mrs. Tanja Barnić, for their support during the investigation.

REFERENCES

- [1] M. Kukučka, S. Mančić, N. Kukučka, Nova membranska tehnologija za prerađu surutke, Aktuelna problematika u vodoopskrbi i odvodnji. Sv. Martin, Hrvatska, 2009, pp. 299–305 (in Serbian).
- [2] M. Vourch, B. Balannec, B. Chaufer, G. Dorange, Treatment of dairy industry wastewater by reverse osmosis for water reuse, Desalination **219** (2008) 190–202.
- [3] F.A. Riera, A. Suárez, C. Muro, Nanofiltration of UHT flash cooler condensates from a dairy factory: Characterisation and water reuse potential, Desalination **309** (2013) 52–63.
- [4] J. Luo, L. Ding, B. Qi, M.Y. Jaffrin, Y. Wan, A two-stage ultrafiltration and nanofiltration process for recycling dairy wastewater, Biore. Technol. **102** (2011) 7437–7442.
- [5] B. Sarkar, P.P. Chakrabarti, A. Vijaykumar, V. Kale, Wastewater treatment in dairy industries — possibility of reuse, Desalination **195** (2006) 141–152.
- [6] C. Marella, K. Muthukumarappan, L. E. Metzger, Evaluation of commercially available, wide-pore ultrafiltration membranes for production of α -lactalbumin-enriched whey protein concentrate, J. Dairy Sci. **94** (2011) 1165–1175.
- [7] D. Gavarić, Principi membranske filtracije sa primenom u tehnologiji mleka, Tehnološki fakultet, Novi Sad, 1995 (in Serbian).
- [8] Beatriz Cancino, Valentina Espina, Claudia Orellana, Whey concentration using microfiltration and ultrafiltration, Desalination **200** (2006) 557–558.
- [9] M.S. Yorguna, I. Akmeđet Balcioglu, O. Sayginb, Performance comparison of ultrafiltration, nanofiltration and reverse osmosis on whey treatment, Desalination **229** (2008) 204–216.
- [10] O. Glagovskaia, F. Janakievski, K. De Silva, Comparison of Ceramic, Polymeric and Stainless Steel Microfiltration Membranes for the Fractionation of Whey and Casein Proteins from Skim Milk, Procedia Eng. **44** (2012) 1317–1320.
- [11] Beelin Cheang, Andrew L. Zydny, A two-stage ultrafiltration process for fractionation of whey protein isolate, J. Membrane Sci. **231** (2004) 159–167.
- [12] K. Pan, Q. Song, L. Wang, B. Cao, A study of demineralization of whey by nanofiltration membrane, Desalination **267** (2011) 217–221.
- [13] A. Chollangi, Md. M. Hossain, Separation of proteins and lactose from dairy wastewater, Chem. Eng. Process. **46** (2007) 398–404.
- [14] A. Hinkova, P. Zidova, V. Pour, Z. Bubnik, S. Henke, A. Salova, P. Kadlec, Potential of Membrane Separation Processes in Cheese Whey Fractionation and Separation, Procedia Eng. **42** (2012) 1425–1436.
- [15] A. Rektor, G. Vatai, Membrane filtration of Mozzarella whey, Desalination **162** (2004) 279–286.
- [16] M. O. Nigam, B. Bansal, X. D. Chen, Fouling and cleaning of whey protein concentrate fouled ultrafiltration membranes, Desalination **218** (2008) 313–322.
- [17] A. Macedo, E. Duarte, M. Pinho, The role of concentration polarization in ultrafiltration of ovine cheese whey, J. Membrane Sci. **381** (2011) 34–40.
- [18] K.W.K. Yee, D. E. Wiley, J. Bao, A unified model of the time dependence of flux decline for the long-term ultrafiltration of whey, J. Membrane Sci. **332** (2009) 69–80.
- [19] S. Popović, S. Milanović, M. Iličić, M. Djurić, M. Tekić, Flux recovery of tubular ceramic membranes fouled with whey proteins, Desalination **249** (2009) 293–300.
- [20] P. Narong, A.E. James, Efficiency of ultrafiltration in the separation of whey suspensions using a tubular zirconia membrane, Desalination **219** (2008) 348–357.
- [21] J. Hinrichs, Incorporation of whey proteins in cheese, Int. Dairy J. **11** (2001) 495–503.
- [22] M. El-Sheikh, A. Farrag, A. Zaghloul, Ricotta Cheese from Whey Protein Concentrate, J. Am. Sci. (2010) 321–325.
- [23] S. Pinto, A.K. Rathour, J.P. Prajapati, A.H. Jana, M.J. Solanky, Utilization of whey protein concentrate in processed cheese spread, Nat. Prod. Rad. **6** (2007) 398–401.
- [24] H. Jooyandeh, Impact of fermented whey protein concentrate on texture of Iranian white cheese, 18th Natio-

- nal congress on food technology, Mashhad, Iran, 2008, pp. 1–6.
- [25] J. Písecký, Spray Drying in the Cheese Industry, IDF Symposium on Cheese, Prague, Czech Republic, 2004, pp. 1–10.
- [26] P Schuck, A. Mimouni, MH Famelart, D. Naegele, S Bouhallab, Recent improvements in lactose crystallization and in drying parameters for improving quality and uses of acid whey and of related powders, 5th International whey conference, Paris, France, 2008, pp. 1–23.
- [27] S.T. Yang, E.M. Silva, Novel Products and New Technologies for Use of a Familiar Carbohydrate, Milk Lactose, *J. Dairy Sci.* **78** (1995) 2541–2562.
- [28] Ultrasil 67, Materials safety data sheet, Code 903456-03, Ecolab Food and Beverages, USA, 2010.
- [29] Ultrasil 11, Materials safety data sheet, Code 987404-02, Ecolab Food and Beverages, USA, 2008.
- [30] MilkoScan data sheet, P/N 1025570, Issue 7GB, Foss, Denmark, 2010.

IZVOD

ISPITIVANJE KONCENTRISANJA PROTEINA SURUTKE ULTRAFILTRACIONIM ELEMENTIMA DIZAJNIRANIM ZA FILTRACIJU VODE

Miroslav Đ. Kukučka, Nikoleta M. Kukučka

Envirotech, d.o.o., S. Popovića 42, Kikinda

(Naučni rad)

Ispitivana je pogodnost ultrafiltracionih membrana (UFM) od polisulfona koje se komercijalno proizvode za tretman vode, za izdvajanje proteina iz slatke surutke. Ultrafiltracija (UF) surutke poreklom iz mlekare je izvedena pomoću pilot uređaja sopstvene konstrukcije u trajanju od oko jedne godine. Određivan je uticaj temperature surutke (9 i 30 °C) na efikasnost koncentrovanja proteina. Primenom ispitivanih UFM je dobijen koncentrat proteina surutke koji je sadržao 5–6 puta više proteina u odnosu na polaznu surutku. Istovremeno je veći deo lakoze izdvojen u permeatu. Bolji rezultati su dobijeni filtracijom hladne surutke. Pored činjenice da su ispitivane membrane imale MWCO od 50–100 kDa, dobijeni rezultati ukazuju na uspešno koncentrisanje proteina surutke čija je molarna masa najvećim delom manja od 50–100 kDa. Ispitivane membrane su pogodne za projektovanje i izradu UF postrojenja za koncentrovanje susrutke u malim mlekarama.

Ključne reči: Ultrafiltracione membrane za tretman vode • Koncentrovanje proteina surutke • Uticaj temperature

Modeling the kinetics of essential oil hydrodistillation from plant materials

Svetomir Ž. Milojević¹, Dragana B. Radosavljević¹, Vladimir P. Pavićević², Srđan Pejanović², Vlada B. Veljković³

¹Faculty of Technical Sciences, University of Priština, Kosovska Mitrovica, Serbia

²Faculty of Technology and Metallurgy, University of Belgrade, 11000 Belgrade, Karnegijeva 4, Serbia

³Faculty of Technology, University of Niš, 16000 Leskovac, Bul. Oslobođenja 124, Serbia

Abstract

The present work deals with the modeling of the kinetics of essential oils extraction from plant materials by water and steam distillation. The experimental data were obtained by studying the hydrodistillation kinetics of essential oil from juniper berries. The literature data on the kinetics of essential oils hydrodistillation from different plant materials were also included into the modeling. A physical model based on simultaneous washing and diffusion of essential oil from plant materials were developed to describe the kinetics of essential oils hydrodistillation, and two other simpler models were derived from this physical model assuming either instantaneous washing followed by diffusion or diffusion with no washing (*i.e.*, first-order kinetics). The main goal was to compare these models and suggest the optimum ones for water and steam distillation and for different plant materials. All three models described well the experimental kinetic data on water distillation irrespective of the type of distillation equipment and its scale, the type of plant materials and the operational conditions. The most applicable model is the one involving simultaneous washing and diffusion of the essential oil. However, this model was generally inapplicable for steam distillation of essential oils, except for juniper berries. For this hydrodistillation technique, the pseudo first-order model was shown to be the best one. In a few cases, a variation of the essential oil yield with time was observed to be sigmoidal and was modeled by the Boltzmann sigmoid function.

Keywords: diffusion, modeling, physical models, steam distillation, washing, water distillation.

Available online at the Journal website: <http://www.ache.org.rs/HI/>

Essential oils are secondary metabolites of aromatic plants that are formed by all plant organs, such as buds, flowers, leaves, stems, twigs, seeds, fruits, roots, wood or bark. They are stored in secretory cells, cavities, canals, epidermic cells or glandular trichomes. At present, about 3000 essential oils are known, but only 10% of them are commercially important [1]. According to their chemical composition, essential oils are natural, complex mixtures of volatile compounds present at quite different concentrations and have a strong aroma and flavor. These mixtures are usually characterized by two or three major compounds at fairly high concentrations (20–70%), while the other compounds are present in trace amounts. For example, α -pinene (38–54%), limonene (16–18%) and myrcene (9–19%) are the major compounds of *Juniper communis* essential oil, which is 70–80% of the essential oil [2]. Generally, these major compounds determine the biological properties of essential oils [1].

Correspondence: V.B. Veljković, Faculty of Technology, University of Niš, Bul. oslobođenja 124, 16000 Leskovac, Serbia.

E-mail: veljkovicvb@yahoo.com

Paper received: 26 October, 2012

Paper accepted: 11 January, 2013

SCIENTIFIC PAPER

UDC 665.52.048:66.048

Hem. Ind. **67** (5) 843–859 (2013)

doi: 10.2298/HEMIND121026009M

The essential oil from a plant or its parts has an identifiable aroma, flavor or other feature of that plant or part that is of practical use. Essential oils and their individual components are used as food and drink flavorings, perfumes, deodorants, pharmaceuticals, pesticides, etc. Their use is determined by their specific chemical, physical and sensory properties. It is obvious that the content, composition and character of essential oils extracted from different plant species, the same plant species or from different parts of a plant species could differ to each other due to different geographical locations, climate, soil factors as well as plant organ, age and vegetative stage.

The production of essential oil involves several, closely connected steps. The raw plant material is obtained by manual collection of wild plant populations or by the harvesting of cultivated plants in the stage of development that gives the best yield of the essential oil having the desired features. The raw plant materials are used as fresh or after drying in the dark, sun or convective dryers, and some of them are comminuted before further processing. The state of the employed raw plant material significantly influences the yield, composition and features of the essential oil that can be extracted. The essential oil is usually present in the

raw plant material at a low concentration and a high performance separation method is employed to recover it in a high yield. Both traditional and novel methods, such as hydrodistillation, solvent extraction or supercritical carbon dioxide extraction, are used for essential oil recovery. Like the pretreatment of the raw plant material (drying, comminution, etc.), the recovery method applied affects the yield, composition and character of the obtained essential oil. Sometimes, a particular feature is reinforced by eliminating unwanted fractions or by extracting desired fractions of the essential oil through further processing employing physical or chemical methods. Due to the novel separation techniques, essential oils are regarded as industrial raw materials for the production of the individual compounds or fractions with particular flavor and aroma characteristics.

Each of the traditional essential oil separation methods has its particular advantages and disadvantages. Solvent extraction produces extracts that contain solvent residues and non-volatile waxy components. The extracting solvents are usually toxic and flammable, while their recovery entails additional costs and environmental risks. Although hydrodistillation provides essential oils in low yields containing several by-products of the distillation process, this method is most frequently used for essential oil extraction from raw plant materials. The essential oil is extracted at temperatures lower than the boiling points of its constituents, enabling the separation of thermo-sensitive compounds. Hydrodistillation, which provides good quality essential oil, is operated in a relatively simple and safe manner and is environmentally friendly. The advantages of this method are also that the volatile constituents are condensed into water, and the steam displaces atmospheric oxygen protecting the volatiles from oxidation. Its disadvantages are a high-energy consumption and heating the raw plant material to high temperatures. Compared with supercritical carbon dioxide extraction, which is technologically more advanced, hydrodistillation is much cheaper with respect to the capital cost. It is performed as a water, steam or water-steam distillation.

In the laboratory, a Clevenger-type apparatus is normally used for extracting essential oils from raw plant materials, while at the pilot or industrial level, different types of distillation units (distillers) with or without direct steam supply are employed. Hydrodistillation under atmospheric pressure remains the most widely employed technique for the extraction of essential oil on the industrial level because of its economic viability [3]. Other types of distillation have also been tried for extracting the essential oil from raw plant materials, such as vacuum distillation of essential oil

from heated pulverized plant materials, known as "dry" distillation [4] and water distillation under vacuum [3].

There have been numerous studies dealing with the yield, composition and biological activities of essential oils obtained by hydrodistillation from different plant species grown all over the world. However, the kinetics of essential oil hydrodistillation has been studied to a much smaller extent despite its importance not only for the fundamental understanding but also for operation, optimization, control and design of industrial hydrodistillation processes. Kinetic models along with essential oil yield and composition are important for hydrodistillation processes from both technological and economical viewpoints.

Surveys of the reports on the kinetics of water and steam distillation of essential oil are given in Tables 1 and 2, respectively. Aerial parts and leaves were mainly employed as the raw plant materials in these studies, although other plant organs, such as flowers, seeds, fruits, peals and branches with needles and wood, were also used. Intact and fresh raw plant materials are more rarely used than processed ones. After harvesting, the raw plant materials are usually dried to preserve/conserve their qualities. To protect the sensitive constituents, low drying temperatures (30 to 50 °C) are most frequently applied. Small quantities of collected plant materials are naturally dried in the field or in a well-aired, dark and dry place at room temperature, while large quantities of raw plant materials on the industrial scale are convectively dried by warm air in special dryers, corresponding to the plant parts to be dried. After drying, the plant material is comminuted (chopped, milled, ground, etc.).

Water and steam distillations are mainly used for extracting essential oils from aerial parts, leaves, flowers, seeds, fruits, needles, peals and wood (Tables 1 and 2, respectively), while the employment of water-steam distillation has not yet been reported. The kinetics of hydrodistillation process as well as the oil yield and composition were the main subjects of the studies performed. In several studies, various kinetic models were presented. The maximum essential oil yield and the duration of hydrodistillation to attain it varied from one plant material to another and on the applied operational conditions.

When using a water distillation, the plant material is completely immersed in water in a heated still. On the laboratory scale, the apparatus according to Clevenger was usually employed to perform water distillation under atmospheric pressure, and a reduced pressure was used in only one study. Different solid-to-water ratios up to 1:50 g/mL were applied in the studies. The suspension was usually held at the boiling temperature (about 100 °C), although a water distillation can be performed under vacuum at a reduced temperature. The

Table 1. Literature survey on studying the kinetics of water distillation of essential oils from plant materials; na – not available

Plant/part	Technique/level	Operating conditions	Essential oil yield	Objective of study	Reference
Lavender (<i>Lavandula angustifolia</i>); flowers	50 g/3 L of buffered aqueous medium (pH 7.0).	100°C, 15 min to 7 h	1.61%, 2 h	Kinetics of the essential oil constituents	Morin <i>et al.</i> [5]
<i>Ridolfia segetum</i> , flowers, fresh	Clevenger; 500 g/500 mL of distilled water	B.p., up to 150 min	5.0%, 1.5 h	Kinetics; composition and antibacterial activity of the oil	Jannet and Mighri [6]
Common lavender (<i>Lavandula officinalis</i>); flowers, dried and milled ($d_p=0.5$ mm)	Clevenger; 15 g/150 mL of water or cohobation water	B.p., up to 240 min	5.73 mL/100 g	Kinetics; composition and antimicrobial activity of the oil	Stanojević <i>et al.</i> [7]
Wild marigold (<i>Target es minuta</i>); flowering tops, fresh	Clevenger; 500 g Portable distillation unit; 2 kg/8 kg of water	B.p., 3 h B.p. under vaccum (to 225 mmHg), up to 3.5-4.5 h	1.56%, 3 h 0.91-1.16%, about 3 h	Kinetics; oil yield and composition; kinetic model.	Babu and Kaul [3]
Sage (<i>Salvia officinalis</i>), flowers, leaves and stems, dried	Clevenger 400 g of plant sample / 5 dm ³ of water	B.p., 2 h	Flower: 1.8% Leaf: 2.0% Stem: 0.4%	Kinetics; oil yield	Veličković <i>et al.</i> [8]
Savory (<i>Satureja hortensis</i> , <i>Satureja montana</i>); dried aerial parts	Clevenger; 1:20 w/w (6 or 30 g of plant materials)	B.p., 4 h	3.1% for <i>S. hortensis</i> , 0.7% for <i>S. montana</i> , 3 h	Kinetics; oil yield	Rezvanpanah <i>et al.</i> [9]
Spearmint (<i>Mentha spicata</i>); leaves, fresh	na; 100 g/? g of water	B.p., up to 3 hours	0.89%, 2 h	Kinetics; composition vriation with time	Benyoussef <i>et al.</i> [10]
<i>Eucalyptus cinerea</i> , leaves, fresh and dried	Clevenger; 4 kg/8 L of water	B.p., up to 8 h 24 h at ambient conditions	2.56% (fresh leaves), 2.87% dried leaves, 8 h	Effect of drying on the kinetics and the oil composition; modeling by the Langmuir equation	Babu and Singh [11]
Rosemary (<i>Rosmarinus officinalis</i>); leaves	na	B.p., up to 2 h	0.44%, 2 h.	Kinetics; modeling (diffusional model based on the Fick's second law)	Boutekejdjiret <i>et al.</i> [12]
Rosemary (<i>Rosmarinus officinalis</i>); leaves	Clevenger; 500 g/3 L of water	B.p., up to 1.5 h	0.35%, 1.5 h	Kinetics; oil composition	Bousbia <i>et al.</i> [13]
Thyme (<i>Thymus vulgaris</i>); aerial parts, dried	Clevenger; 60 g/1.2 L of water	B.p., up to 4 h	2.39%, 4 h.	Kinetics; oil composition	Golmakani and Rezaei [14]
Creeping thyme (<i>Thymus serpyllum</i>); herba, dried, crushed (<1 mm)	Unger; 1:10, 1:20, 1:30, 1:40 and 1:50	B.p., up to 3 h	0.8-1.0%, 3 h	Kinetics; modeling (a phenomenological model including intact and broken plant cells)	Sovová and Aleksovská [15]
Shirazi thyme (<i>Zataria multiflora</i>); aerial parts, dried	na ^a ; 30 g/0.5 L of water	B.p., up to 4 h.	3.23%, 3.64% (salted, 1% NaCl), 60 min.	Kinetics; oil yield, composition and properties	Gavahian <i>et al.</i> [16]
Lemon grass (<i>Cymbopogon citratus</i>); leaves.	na; 250 g/2 L of water.	B.p., up to 45 min	0.84% (v/w), 45 min.	Kinetics; process optimization	Silou <i>et al.</i> [17]
Cherry laurel (<i>Prunus laurocerastis</i> L. var. <i>serbica</i> Pančić); leaves	Clevenger; 0.5 kg/5 kg of water	B.p., up to 2.5 h	0.432% (v/w), 2.5 h	Kinetics; oil composition	Stanislavljević <i>et al.</i> [18]
Coriander (<i>Coriandrum sativum</i> L.); seeds	Clevenger; 60 g.	B.p., up to 9 h	0.057%, 9 h	Modeling (difusional model and model based on first order kinetics)	Benyoussef <i>et al.</i> [19]
Cumin (<i>Cuminum cyminum</i>); seeds, ground	Clevenger; 200 g (small batch)	B.p., up to 5 h	3.4-3.8% (small batch), 5h	Kinetics; oil yield; modeling (model based on first order kinetics)	Sowbhagya <i>et al.</i> [20]

Table 1. Continued

Plant/part	Technique/level	Operating conditions	Essential oil yield	Objective of study	Reference
Celery (<i>Apium graveolens</i> Linn.); seeds, milled	Clevenger; 200 g (small batch)	B.p., up to 5 h	1.8–2.2% (small batch), 5 h	Kinetics; oil yield; modeling (model based on first order kinetics)	Sowbhagya <i>et al.</i> [21]
Fennel (<i>Foeniculum vulgare</i>); seeds, crushed	Clevenger; 25 g/200 mL	B.p., up to 20 min; 300 W	2.12% (v/w), 20 min	Kinetics; modeling (model including washing and diffusion)	Kapas <i>et al.</i> [22]
Parsly (<i>Petroselinum crispum</i>); seeds, intact, non-fermented	Clevenger; 2000 mL	B.p., up to 270 min	2.17% (v/w), 270 min	Kinetics; effects of different hydrodistillation techniques on the oil yield	Stanković <i>et al.</i> (2004)
Parsly (<i>Petroselinum crispum</i>); seeds.	Clevenger	B.p., up to 270 min	3.28% (v/w) intact; 4.51% (v/w) crushed; 270 min	Kinetics; effects of seed fermentation on the oil yield	Stanković <i>et al.</i> [23]
Intact, feremented at 28 °C for 4 h	20 g/200 mL	—	—	—	—
	20 g/300 mL	—	—	—	—
	20 g/400 ml	—	—	—	—
	20 g/500 ml	—	—	—	—
Intact, feremented at 30°C for 4 h	20 g/400 ml	—	—	—	—
Crushed, feremented at 28°C for 4 h	20 g/400 ml	—	—	—	—
Parsly (<i>Petroselinum crispum</i>); seeds	Clevenger	B.p., up to 270 min	—	—	Stanković <i>et al.</i> [24]
Juniper (<i>Juniperus communis</i> L.); berries, dried, milled	Clevenger; 364 or 1000 g; 1:3 or 1:10 g/mL	B.p., up to 100 min; 150-700 W	0.56-1.68% (v/w), 90 min	Kinetics; modeling (model based on washing and diffusion)	Milojević <i>et al.</i> [2]
<i>Abies grandis</i> , <i>Picea abies</i> , <i>Pinus sylvestris</i> , <i>Pseudotsuga menziesii</i> , branches with needles, chopped; <i>Juniper communis</i> , fruits, ground	Unger; 100 g/300 mL of water; for some experiments, the plant materials were microwave-pretreated (10 min)	na	0.53-1.68% (v/w), 2 h	Kinetics; oil yield	Miletić <i>et al.</i> [26]
Lime (<i>Citrus latifolia</i> Tanaka); peals, dried, whole/milled (2 mm)	Clevenger; 60 g	B.p., up to 8 h	3.4% (v/w), 5 h	Kinetics; oil yield and composition	Atti-Santos <i>et al.</i> [27]
Lemon (<i>Citrus limon</i>), peals, fresh	Clevenger; 200 g/2 L of water	B.p., up to 3 h	0.21%, 3 h	Kinetics; oil yield, composition and antimicrobial activity	Ferhat <i>et al.</i> [28]
Agarwood (<i>Aquilaria crasna</i>), wood, dried, comminuted, sieved (0.7 cm)	3 kg/27 kg of water; wood was soaked in water for 7 days	Operating temperature: 80, 100 and 120 °C; up to 64 h	0.046-0.061%, 64 h	Kinetics; oil yield and composition; modeling (model based on washing and diffusion)	Pornpunyapat <i>et al.</i> [29]

Table 2. Literature survey on studying the kinetics of steam distillation of essential oils from plant materials; na – not available

Plant/part	Level	Operating conditions	Essential oil yield	Objective of study	Reference
Lavender (<i>Lavandula angustifolia</i>); flowers, dried	50 g per batch	na	8.75%, 1.5 h	Kinetics; yield and composition of the essential oil	Chemat <i>et al.</i> [30]
Sage (<i>Salvia officinalis</i>), flowers, leaves and stems, dried	Clevenger 400 g per batch	2 h	Flower: 1.6 Leaf: 1.7% Stem: 0.2%	Kinetics; oil yield	Veličković <i>et al.</i> [8]

Table 2. Continued

Plant/part	Level	Operating conditions	Essential oil yield	Objective of study	Reference
Lavandin super (<i>Lavandula angustifolia</i> x <i>latifolia</i>); aerial parts, fresh	Bench scale unit; 2175 g per batch	Steam pressure: 2 bar	1.186–1.468%	Kinetics; modeling (a phenomenological model)	Cerpa <i>et al.</i> [31]
Aniseed (<i>Pimpinella anisum</i>); leaves, dried	Pilot plant, 2 and 5 kg per batch	140 and 200 kPa; steam flow rate: 6 kg/h; up to 2.5 h	2.55%, 2.5 h	Kinetics; modeling of steam distillation; oil yield	Romdhane and Tizaoui [32]
Thyme (<i>Thymus spicata</i>); leaves, dried; whole: 2.05 mm; ground: 0.50 and 1.00 mm	150 g per batch	Steam of atmospheric pressure, flow rate: 0.64 and 1.03 L/h; up to 2.5 h	1.3%, 2.5 h	Effects of milling, process time and steam flow rate on essential oil yield and composition; kinetics	Hanci <i>et al.</i> [33]
Rosemary (<i>Rosmarinus officinalis</i>); leaves	na	Steam of atmospheric pressure	1.2%, 2 h	Kinetics; modeling (diffusional model based on the Fick's second law)	Boutekedjiret <i>et al.</i> [12]
Lavander (<i>Lavandula angustifolia</i>), flowers; Artemisia (<i>Artemisia annua</i>), leaves	750 g per batch	na	6-10%, 5 h 0.3-0.9%, 4 h	Kinetics; oil yield and composition	Masango [34]
<i>Artemisia judaica</i> , aerial parts (flowers, leaves and small stems), fresh	1 kg per batch	na	1.42%, 2 h	Kinetics; oil yield and composition	Charchari and Hamadi [35]
Rosemary (<i>Rosmarinus officinalis</i>); leaves and caulis together, dried (lot A) and fresh (lot B).	Pilot plant, 9.9–23.0 (lot A) and 8.6–29.9 kg (lot B) per batch	Steam pressure: 3 bar; steam flow rate: 0.89 and 0.75 kg/min for lots A and B, respectively	Mean 0.62% and 0.49% for lots A and B, respectively	Economic evaluation of an industrial steam distillation; kinetics; oil yield and composition	Mateus <i>et al.</i> [36]
Citronella (<i>Cymbopogon winterianus</i>); aerial parts (leaves and twigs), dried and fresh	50 g per batch	na	0.776%, 4 h (dried) 0.942%, 2 h (fresh)	Kinetics; oil yield and composition; process optimization; modeling (diffusional model based on the Fick's second law)	Cassel and Vargas [37]
<i>Baccharis anomala</i> , <i>Baccharis dentata</i> , <i>Baccharis uncinella</i> , aerial parts (leaves and twigs)	200 g per batch	na	0.06% (v/w), 0.05% (v/w), 0.24% (v/w), 40 min	Kinetics; oil yield and composition; modeling (model of Sovova based on mass transfer fundamentals)	Xavier <i>et al.</i> [38]
Rosemary (<i>Rosmarinus officinalis</i>), basil (<i>Ocimum basilicum</i>), lavender (<i>Lavandula dentata</i>), fresh leaves	213-313 g per batch	Steam pressure: 1.01.bar; steam flow 3.4 mL/min; 213-313 g; no pre-processing of leaves	0.51%, 0.38%, 0.32%, 30 min	Kinetics; oil yield and composition; modeling (diffusional model)	Cassel <i>et al.</i> [39]
Lemon grass (<i>Cymbopogon spp.</i>), leaves, chopped or unchopped; 70-1000 kg	Pilot plant	Steam flow rate: 12- 16 L/h	0.31-0.53% (v/w), 5 h	Kinetics at pilot scale; modeling (model based on first order kinetics)	Kaul <i>et al.</i> [40]
Peppermint (<i>Mentha piperita</i>), leaves, dried, crushed	Steam distillation	Steam pressure: 1 atm (100 °C)	na	Kinetics of oil constituent distillation	Ammann <i>et al.</i> [41]

produced water steam and the essential oil leave the hot suspension, condense and are collected and separated by decantation. Two products are obtained – the essential oil and the condensed water containing water-soluble constituents of the essential oil, known as floral water or hydrosol. The plant materials are usually comminuted to decrease the particle size and to increase the particle surface area.

When employing a steam distillation, the plant material is placed in a still and steam is forced to pass through the material and the essential oil is released from the plant material. Different batches of plant materials and steam flow rates are used on scales from laboratory to industrial. The pressure of steam is usually greater than atmospheric pressure; hence, the operational temperature is higher than 100 °C. The steam containing the essential oil is cooled down, collected and separated into two products – the essential oil and the floral water. Water-steam distillation is a combination of the previous two methods. The plant material is immersed in water in a still, which is heated, and steam is fed into the suspension.

During a hydrodistillation, the increase of temperature causes an increase of pressure within the plant organs containing the essential oil. Once the pressure increases above a certain level, the cell walls break and the essential oil is released. A part of the essential oil is released from the external surfaces of the plant particles, but the remaining part must diffuse from the interior of the plant particles to their external surfaces. Then, the steam carries away the essential oil from the external surface of plant particles. This mechanism is the basis for modeling the kinetics of essential oil hydrodistillation processes.

The present work deals with the modeling of the kinetics of the extraction of essential oils from a number of plant materials and their parts by hydrodistillation (water and steam distillation). The experimental data were obtained by studying the hydrodistillation kinetics of the essential oil from juniper berries using a pilot distillation unit. In addition, data on the kinetics of the hydrodistillation of essential oils collected from the literature (Tables 1 and 2) were included in the modeling. A three-parameter physical model was developed assuming simultaneous essential oil washing and diffusion processes. Two simpler exponential models, the first assuming instantaneous washing followed by diffusion of essential oil and the second assuming only diffusion of essential oil, were derived from the three-parameter model. Furthermore, a sigmoid model was used to describe the kinetics of essential oils deviating from the exponential pattern. The main goal was to compare these physical models and suggest the optimum ones for the two methods of hydrodistillation and for different plant materials.

Modeling of the kinetics of essential oils hydrodistillation

Model of simultaneous washing and diffusion

The mathematical model describing the kinetics of essential oil hydrodistillation is derived for a batch distillation vessel in which a plant material and water are added. For water distillation of the essential oil, the plant material is immersed in water, while for steam distillation the plant material as a porous bed is placed on a perforated plate above the water. The produced water vapor (steam) heats the plant material and carries the essential oil from the external surface of the plant particles. The mixture of water and essential oil vapors is condensed in a heat exchanger and then separates into the floral water and the essential oil. In the case of water distillation the floral water is usually returned to the distillation vessel.

The mathematical model is based on the following assumptions:

- i) in the case of water distillation, the suspension in the distillation vessel is perfectly mixed. In the case of steam distillation, the porous bed of plant material is considered as a batch and is stable, with no changes in form or disposition during the process, and the vapor phase flow is plug flow, with a constant rate;
- ii) the essential oil is considered as a single component;
- iii) plant particles are isotropic, equal in size, shape and initial essential oil content;
- iv) the effective coefficient of diffusion through plant particles is constant;
- v) there is no resistance to the mass transfer of essential oil from the external surfaces of the plant particles;
- vi) the essential oil and the floral water are completely immiscible;
- vii) a fraction of the essential oil is located at the external surfaces of the plant particles, f , and the rest is uniformly distributed in the plant particles, $(1-f)$;
- viii) the isolation of essential oil occurs via two simultaneous mechanisms: a) "washing" of the essential oil from the external surfaces of the plant particles and b) the diffusion of essential oil from the interior of the plant particles towards their external surfaces. The kinetics of both processes is assumed to be the first order with respect to the essential oil in the plant particles:

$$-\frac{dq_p}{dt} = kq_p \quad (1)$$

where q_p is the average concentration of essential oil in the plant particles (g/100 g) at time t , and k is the process rate constant. Each process has a different rate constant: the diffusional process is much slower than

the washing and is responsible for limiting the overall extraction process rate.

ix) The amount of the essential oil available for hydrodistillation corresponds to the amount of the essential oil distilled off until saturation:

$$q_{po} = q_{\infty} \quad (2)$$

where q_{po} is the initial average concentration of essential oil in the plant particles, and q_{∞} is the amount of essential oil distilled off until saturation (in g/100 g of the plant materials).

By integrating Eq. (1), the following equations are derived for washing and diffusion, respectively:

$$\frac{q_{p1}}{q_{\infty}} = e^{-k_1 t} \quad (3)$$

and

$$\frac{q_{p2}}{q_{\infty}} = e^{-k_2 t} \quad (4)$$

where k_1 and k_2 are the rate constants for washing and diffusion processes, respectively.

Based on the assumption *vii)*, the total amount of essential oil remained in the plant particles until time t is as follows:

$$\frac{q_p}{q_{\infty}} = f \frac{q_{p1}}{q_{\infty}} + (1-f) \frac{q_{p2}}{q_{\infty}} \quad (5)$$

or:

$$\frac{q_p}{q_{\infty}} = fe^{-k_1 t} + (1-f)e^{-k_2 t} \quad (6)$$

The amount of essential oil recovered until time t , q , is connected to the amount of the essential oil present in the plant particles at the same time by the following equation:

$$q = q_{\infty} - q_p \quad (7)$$

By combining Eqs. (6) and (7), the following equation is derived:

$$\frac{q}{q_{\infty}} = 1 - fe^{-k_1 t} - (1-f)e^{-k_2 t} \quad (8)$$

Analyzing the hydrodistillation apparatus as a whole, Milojević *et al.* [2] showed that a direct relationship between the amount of the essential oil collected in the separator, divided by the amount of the plant material, and the essential oil yield from the plant material in the distillation vessel with the time delay. Therefore, Eq. (8) describes the variation of the dimensionless content of essential oil extracted from the plant material with the progress of extraction. The

parameters of Eq. (8) can be calculated by fitting this equation to the experimental q/q_{∞} ratios and minimizing the sum of the squared deviations between the experimental and calculated ratios.

Sovova and Aleksovski [15] have derived a kinetic expression basically the same to Eq. (8) from a phenomenological model for water distillation of essential oil for both particles with homogeneously distributed essential oil and particles with part of the essential oil deposited on their surface. In the former case, the essential oil from intact cells diffuses slowly to the particle surface, and in the latter case, the essential oil located in the cells with broken walls is rapidly extracted (washed out). According to the phenomenological model of Sovova and Aleksovski, the parameter f is the fraction of broken plant cells, while its two other parameters are time constants corresponding to the reciprocal values of the rate constants for washing and diffusion, k_1 and k_2 . The phenomenological model has been already tested for water distillation of essential oil from creeping thyme and intact coriander seeds [15].

Model of instantaneous washing followed by diffusion

The developed model can be further simplified by assuming that washing is very fast and occurs instantaneously ($k_1 \rightarrow \infty$), so Eq. (8) becomes:

$$\frac{q}{q_{\infty}} = 1 - (1-f)e^{-k_2 t} \quad (9)$$

Equation (9) is the same to the kinetic expression developed by Milojević *et al.* [2], where f is the washing coefficient, corresponding to the washable part of the essential oil that can be extracted, and k_2 is the coefficient of slow essential oil distillation. The model has been experimentally verified for the extraction of the essential oil from cherry juniper berries [2], laurel leaves [18], fennel seeds [22] and agarwood [29] by water distillation.

Model of pseudo-first order kinetics

If no washing of the essential oil occurs ($f = 0$), then Eq. (9) becomes a simple exponential function:

$$\frac{q}{q_{\infty}} = 1 - e^{-k_2 t} \quad (10)$$

This is the logarithmic equation based on the assumption of pseudo first-order kinetics with respect to the essential oil remaining in the plant material and is frequently used model for both water and steam distillations. For instance, the first-order kinetics was used to model the essential oil extraction from leaves of thyme (*Thymus spicata* L.) [33], lemon grass (*Cymbopogon* spp.) [40], celery (*Apium graveolens* Linn.) [21] and cumin (*Cuminum cyminum* L.) [20] seeds by

steam distillation, as well as from flowers of lavender (*Lavandula angustifolia* Mnch) by water distillation [5].

Sigmoid model

The kinetics of water and steam distillation of essential oils from some plant materials have been observed to deviate from the above-mentioned exponential kinetic models. An almost linear increase during the initial period of the water distillation of parsley seeds was noticed [23], while a sigmoid variation of the essential oil yield with time was observed for various plant materials exposed to either water or steam distillation, such as the aerial parts of *Artemisia judaica* [35], the flowers, leaves and stems of common sage [8], lavender flowers and leaves [34], as well as rosemary leaves and caulis [36]. In these cases, the variation of the essential oil yield from its lowest, A_1 , to the highest, A_2 , asymptotic value can be described by a Boltzmann sigmoid curve:

$$\frac{q}{q_\infty} = \frac{A_1 - A_2}{1 + \exp\left(\frac{t - t_0}{T_1}\right)} + A_2 \quad (11)$$

Since $A_1 = 0$ at $t = 0$ and $A_2 = 1$ when $t \rightarrow \infty$, Eq. (11) becomes:

$$\frac{q}{q_\infty} = 1 - \frac{1}{1 + \exp\left(\frac{t - t_0}{T_1}\right)} \quad (12)$$

where t_0 is the time at which the essential oil yield is halfway between the lowest and the highest value and T_1 is the steepness of the curve, which corresponds to the diffusion time constant. This model has not been used yet for the purpose of modeling the kinetics of essential oil hydrodistillation.

EXPERIMENTAL

Plant material

Mature juniper berries, originating from the Mountain Kopaonik, Leposavić, Serbia, were used. The berries were comminuted immediately before the pilot hydrodistillation by a hammer mill (5 kW).

Water distillation

The water distillation was performed in a pilot distillation unit. The comminuted berries (10 kg) were placed in the distillation vessel and distilled water (30 L) was added. The floral water flow rate was 46 mL/min. The essential oil was collected at different times and the volume recorded.

Steam distillation

The same pilot distillation unit was employed to recover the essential oil from juniper berries by steam

distillation. The comminuted berries (3 kg) were placed on a perforated plate, above the distilled water (10 L). The thickness of the juniper bed was about 30 mm. The floral water rate was 30 mL/min. The volume of the essential oil collected at different times was recorded.

Literature data

The published experimental data on the kinetics of hydrodistillation of essential oil from different plant materials were included into comparing the kinetic models. Tables 1 and 2 summarize the plant materials, the technique and the operating conditions used in the studies on water and steam distillation of essential oil, respectively.

Estimation of the parameter values

Values of the parameters of Eqs. (8)–(10) and (12) were estimated by a computer program using all measured values of the q/q_∞ ratio. The computer program employs the Levenberg-Marquardt algorithm, which combines the Gauss-Newton method and the steepest descent method, to adjust the parameter values in the iterative procedure. The “best-fit” parameter values were estimated by minimizing the deviation between the predicted and actual values of the q/q_∞ ratio.

Goodness of fit

The criterion used to evaluate the goodness of fit of each model was the mean relative percentage deviation between the predicted and actual values of the q/q_∞ ratio, $MRPD$, which is defined as follows:

$$MRPD = \frac{100}{n} \sum_{i=1}^n \left| \frac{(q/q_\infty)_{pi} - (q/q_\infty)_{ai}}{(q/q_\infty)_{ai}} \right| \quad (13)$$

where subscripts p and a denote predicted and actual, respectively.

RESULTS AND DISCUSSION

Hydrodistillation of juniper essential oil

The variations of the normalized juniper essential oil yields with the progress of the water and steam distillation processes are shown in Figure 1. The initial essential oil extraction was faster by steam than by water distillation. However, the essential oil yield and the process duration were larger for water than for steam distillations. A techno-economic analysis should be performed to distinguish whether water or steam distillation is more suitable for the recovery of the essential oil from juniper berries on a commercial scale.

According to the mean relative percentage deviation ($MRPD$) values (Tables 3 and 4), the model based on simultaneous washing and diffusion fits better the

experimental data than the model based on instantaneous washing followed by diffusion especially for the steam distillation. The pseudo-first order model appears to be the worst one because of the largest *MRPD* values. The values of the parameters of the employed models for water and steam distillation of essential oil from juniper berries are presented in Tables 3 and 4. Values of the rate constants k_1 and k_2 indicate that both diffusion and washing during steam distillation of juniper berries were faster than those during water distillation, and the difference was greater for washing than for diffusion. However, the fraction of washed essential oil was larger for the juniper berries subjected to water distillation. Compared to the laboratory water distillation of juniper berries [2] (Table 4), the pilot water distillation is characterized by smaller values of the rate constants k_1 and k_2 , indicating a slower process, which is probably due to more efficient heating applied in the former case.

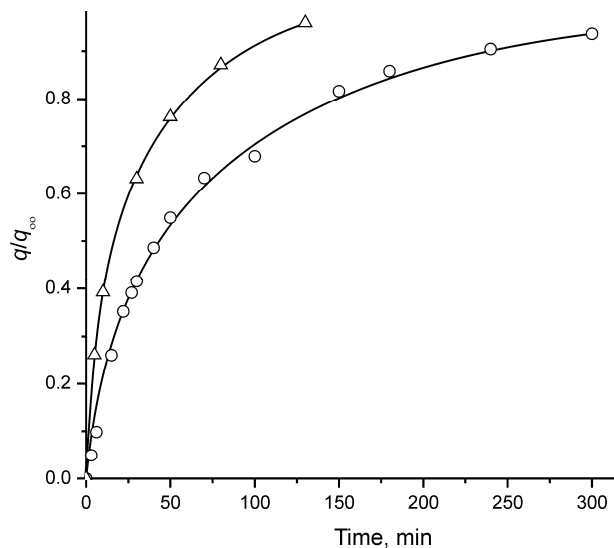


Figure 1. Variation of q/q_∞ with time during water and steam distillation of essential oil from ground, dried juniper berries (water distillation: O; solid batch: 10 kg; solid/liquid ratio: 1:3; floral flow rate: 46 mL/min; steam distillation: △; solid batch: 3 kg; steam flow rate: 30 g/mL).

The results for water and steam distillation of the essential oil from rosemary leaves can also be employed for comparing the two techniques. The results confirmed that the diffusion rate through the plant particles was much smaller for water (0.019 min^{-1} , Table 3) than for steam (0.154 min^{-1} , Table 4) distillation [11]. The same was also observed for dried thyme leaves ($0.010\text{--}0.020 \text{ min}^{-1}$ [15] and $0.030\text{--}0.052 \text{ min}^{-1}$ [33] for water and steam distillation presented in Tables 3 and 4, respectively. However, the diffusion rate constants for water and steam distillation of the essential oil from lavender flowers were approximately the same (about 0.050 min^{-1}) [5,30].

Water and steam distillation of essential from various plant materials

The results of the application of the simplified physical models for modeling the kinetics of essential oil extraction from different plant materials by water and steam distillation are summarized in Tables 3 and 4, respectively.

Water distillation

All the employed models fitted the kinetics of the experimental water distillation data quite well, independent of the type of distillation equipment and its scale, the type of plant and the plant part, and the operational conditions. The applicability of a model improved with its complexity, and the best model was the most complex model of simultaneous washing and diffusion, Eq. (8), involving the simultaneous washing and diffusion of the essential oil. As a rule, the lowest *MRPD*-values between the predicted and experimental values of the essential oil yield were observed with this model. In some cases, the fit did not converge for unknown reasons or for the over parameterization of the fitting model. In addition, in a few cases, it was observed that the rate constants k_1 and k_2 were very similar. In such cases, the simpler models were used to fit the experimental data. The worst model was shown to be that based on the pseudo-first order kinetics, Eq. (10). The model of Milojević and coworkers involving instantaneous washing followed by diffusion of the essential oil through the plant particles, Eq. (9), was

Table 3. Parameters of the kinetic models based on essential oil washing and/or diffusion: water distillation

Reference	Plant	q_∞ g/100 g	Pseudo-first order, Eq. (10)	Instantaneous washing and diffusion, Eq. (9)			Simultaneous washing and diffusion, Eq. (8)				
				$k_2 \times 10^3$ min^{-1}	MRPD %	f	$k_1 \times 10^3$ min^{-1}	$k_2 \times 10^3$ min^{-1}	MRPD %		
Morin et al. [5]	Lavender, flowers	1.61	54.0	± 5.1	46.1	0.406	± 1.1	0.456	268.8	48.3	± 0.2
Stanojević et al. [7]	Common lavender, flowers, dried	5.73 ^a	30.5	± 12.5	27.7	0.284	± 11.2	0.773	70.9	16.0	± 3.5
Jannet and Mighri [6]	<i>Ridolfia segetum</i> , flowers, fresh	5.0	38.7	± 10.5	35.5	0.213	± 2.7	0.669	73.0	25.1	± 1.3

Table 3. Continued

Reference	Plant	q_{∞} g/100 g	Pseudo-first order, Eq. (10)		Instantaneous washing and diffusion, Eq. (9)			Simultaneous washing and diffusion, Eq. (8)				
			$k_2 \times 10^3$ min ⁻¹	MRPD %	$k_2 \times 10^3$ min ⁻¹	f	MRPD %	f	$k_1 \times 10^3$ min	$k_2 \times 10^3$ min	MRPD %	
Babu and Kaul [3]	Vaccum distilled	0.91	23.3	±6.5	—	—	—	0.091	220.8	16.7	± 5.4	
Wild marigold, aerial parts	Distilled at NTP	1.56	19.5	±7.4	18.5	0.032	± 3.2	0.019	22222.2	20.8	± 3.7	
Rezvanpanah et al. [9]	<i>Satureja hortensis</i> , aerial parts, dried	3.1	21.3	±14.4	17.5	0.359	7.3	0.200	1091.7	20.1	± 9.7	
	<i>Satureja montana</i> , aerial parts, dried	0.7	20.8	±11.0	17.3	0.333	± 5.9	0.100	6493.5	20.0	± 14.7	
Gavahian et al. [16]	Shirazi thyme, aerial parts, dried	3.23 ^a	127.2	±7.1	126.4	0.016	± 6.7	0.254	561.8	98.2	± 3.5	
Golmakani and Rezaei [14]	Thyme, aerial parts, dried	2.39	53.8	±3.0	51.6	0.098	± 7.5	0.558	89.4	41.1	± 3.9	
Sovova and Aleksovski [15]	Particle size, mm	Liquid/ solid ratio, g/mL										
Thyme, aerial parts, dried	0.1	1:10	0.790	12.0	±19.1	8.8	0.283	±9.5	0.506	43.5	13.6	±1.5
		1:20	0.794	11.9	±17.3	9.4	0.222	±10.5	0.048	140.1	20.7	±2.2
		1:30	0.772	9.7	±10.4	—	—	—	1.0	—	—	—
		1:40	0.747	9.9	±15.4	9.3	0.055	±8.1	1.0	—	—	—
		1:50	0.687	10.1	±15.0	9.6	0.041	±13.7	1.0	—	—	—
	0.25	1:10	0.820	9.9	±12.9	9.1	0.094	±7.5	0.105	0.234	109.18	±3.5
		1:20	0.824	10.3	±8.4	9.6	0.081	±11.9	1.0	—	—	—
		1:30	0.815	9.6	±10.7	9.2	0.049	±7.4	1.0	—	—	—
		1:40	0.747	9.5	±19.0	—	—	—	1.0	—	—	—
		1:50	0.687	10.3	±23.1	9.9	0.030	±21.6	1.0	—	—	—
	0.315	1:10	0.858	12.5	±7.5	12.3	0.024	±6.4	1.0	—	—	—
		1:20	0.927	17.3	±7.4	16.4	0.085	±2.4	1.0	—	—	—
		1:30	0.815	11.4	±10.8	11.3	0.009	±7.6	1.0	—	—	—
		1:40	0.747	9.2	±15.4	8.6	0.059	±9.3	1.0	—	—	—
		1:50	0.687	7.9	±17.8	7.8	0.016	±15.4	1.0	—	—	—
	0.4	1:10	0.944	19.4	±10.5	15.7	0.316	±6.4	0.108	2304.1	25.5	±0.9
		1:20	0.961	21.9	±6.5	20.3	0.147	±4.9	0.175	2500.0	21.3	±2.0
		1:30	0.901	15.7	±5.3	15.2	0.049	±7.9	1.0	—	—	—
		1:40	0.841	13.0	±11.3	10.8	0.200	±13.3	1.0	—	—	—
		1:50	0.833	12.2	±5.2	11.2	0.096	±14.7	1.0	—	—	—
	0.5	1:10	0.880	13.0	±15.7	10.1	0.296	±7.0	0.425	56.8	8.1	±1.9
		1:20	0.913	15.2	±10.5	13.1	0.224	±6.9	0.131	7812.5	16.6	±2.0
		1:30	0.880	15.4	±11.8	12.7	0.246	±7.7	0.226	93.0	17.3	±1.0
		1:40	0.856	14.2	±14.3	11.0	0.276	±9.6	0.295	81.3	15.6	±0.6
		1:50	0.800	11.3	±13.3	9.3	0.186	±11.6	0.291	58.5	9.9	±1.9
	0.63	1:10	0.875	15.7	±14.1	12.0	0.317	±8.6	0.097	47619.0	24.1	±1.9
		1:20	0.910	18.8	±12.3	14.6	0.349	±8.8	0.097	1730.1	27.6	±0.9
		1:30	0.867	14.0	±8.9	12.3	0.155	±7.9	0.114	3745.3	15.1	±4.4
		1:40	0.850	13.6	±11.4	11.4	0.196	±9.8	0.086	15384.6	18.1	±2.1
		1:50	0.858	16.6	±7.2	16.3	0.027	±13.0	0.004	2681.0	19.0	±6.3
	0.8	1:10	0.858	12.4	±7.3	10.9	0.160	±3.9	1.0	—	—	—
		1:20	0.893	13.8	±11.6	11.4	0.24	±3.0	1.0	—	—	—
		1:30	0.858	13.8	±7.4	12.7	0.112	±6.6	0.058	1869.2	17.3	±2.7

Table 3. Continued

Reference	Plant	q_{∞} g/100 g	Pseudo-first order, Eq. (10)		Instantaneous washing and diffusion, Eq. (9)			Simultaneous washing and diffusion, Eq. (8)					
			$k_2 \times 10^3$ min ⁻¹	MRPD %	$k_2 \times 10^3$ min ⁻¹	f	MRPD %	f	$k_1 \times 10^3$ min	$k_2 \times 10^3$ min	MRPD %		
1.0		1:40	0.858	11.5	±16.9	8.9	0.273	±6.7	0.293	139.9	8.5	±0.9	
		1:50	0.858	13.1	±8.5	11.9	0.121	±10.6	0.012	2681.0	19.0	±4.8	
		1:10	0.840	14.2	±13.5	11.1	0.267	±9.3	0.131	65.3	22.2	±1.3	
		1:20	0.848	11.4	±10.3	10.1	0.154	±7.5	0.040	2932.6	19.1	±6.6	
		1:30	0.800	9.5	±8.3	8.7	0.090	±6.7	0.043	12820.5	9.9	±3.2	
		1:40	0.800	9.5	±8.6	8.5	0.117	±15.3	1.0	—	—	—	
Benyouseff <i>et al.</i> [10]	Spearmint, leaves, fresh	1:50	0.800	11.3	±13.3	9.3	0.186	±11.6	0.076	58.5	9.9	±7.0	
		0.89	22.7	±14.6	18.7	0.242	12.5	—	—	—	—	—	
		Babu and Singh [11]	Fresh	2.56	9.39	±5.7	8.53	0.236	±2.9	0.524	22.9	6.4	±1.0
		Eucalyptus cinerea, leaves	Dried	2.87	8.75	±4.2	8.81	0.134	±1.6	0.377	24.6	5.9	±0.4
		Boutekejiret <i>et al.</i> [12]	Rosemary, leaves	0.44	68.7	±2.4	67.5	0.010	±0.30	0.943	75.3	10.4	±2.3
		Stanisavljević <i>et al.</i> [18]	Cherry laurel; leaves	0.43 ^a	38.7	±11.8	34.2	0.294	±6.6	0.779	85.6	18.2	±1.7
Bousbia <i>et al.</i> [13]		Rosemary, leaves	0.35	19.35	±8.4	—	—	—	—	—	—	—	
		Silou <i>et al.</i> [17]	Cut, 1000 W	0.36 ^a	90.1	±29.7	—	—	—	—	—	—	
		Lemon grass	Cut, 1500 W	0.28 ^a	69.0	±24.8	—	—	—	—	—	—	
			Ground 1000 W	0.64 ^a	73.9	±9.3	—	—	—	—	—	—	
		Benyouseff <i>et al.</i> [19]	Corriander seeds	0.0566	5.20	±5.4	—	—	—	0.024	170.9	4.0	±2.7
		Sowbhagya <i>et al.</i> [20], Cumin seeds	Powder	1.92 ^a	63.4	±3.5	57.3	0.327	±1.0	0.752	111.6	42.5	±0.1
Sowbhagya <i>et al.</i> [21], Celery seeds		Flakes	2.19 ^a	56.2	±4.1	54.6	0.054	±3.8	0.544	4830.9	25.6	±1.3	
		Powder	1.320 ^a	44.8	±1.7	—	—	—	—	—	—	—	
		Flakes	1.623 ^a	40.6	±5.3	35.2	0.315	±3.5	—	—	—	—	
		Kapas <i>et al.</i> [22]	Fennel seeds, crushed	2.12 ^a	22.4	±28.1	3.4 ^b	0.084 ^a	na ^c	0.867	250.0	149.9	±5.8
		Milojević <i>et al.</i> [2], Juniper berries, dried	1:3 g/mL; 0.13 mL/min	0.56	22.5	±7.4	—	—	—	—	—	—	
			1:3 g/mL; 3.6 mL/min	1.52	38.2	±17.4	36.1	0.134	±9.0	0.443	107.8	8.6	±1.5
This work			1:3 g/mL; 10.0 mL/min	1.68	50.6	±10.6	50.3	0.199	±6.5	0.820	82.2	13.4	±2.2
			1:3 g/mL; 11.7 mL/min	1.68	56.4	±9.7	51.7	0.212	±5.1	0.172	247.5	56.1	±1.6
			1:10 g/mL; 10.0 mL/min	1.51	115.4	±22.3	89.3	0.549	±14.7	0.709	332.2	15.0	±4.6
		Juniper berries, dried	Batch of 10 kg, 1:3 kg/L; floral water rate: 46 mL/min	1.33 ^a	10.2	±16.7	8.0	0.350	±5.9	0.364	50.7	7.9	±5.5
		Miletić <i>et al.</i> [26]	Abies grandis, wooded greenery	0.65 ^a	26.8	±9.1	—	—	—	0.073	1712.3	11.9	±2.3
			Picea abies, branches with needles, fresh	0.63 ^a	30.9	±13.1	—	—	—	0.189	8.1	8.2	±5.9
Atti-Santos <i>et al.</i> [27]			Pinus sylvestris, branches with needles	0.53 ^a	33.4	±3.7	—	—	—	0.039	3759.4	26.2	±2.0
			Juniper berries, dried, microwave pretreated	1.68 ^a	21.5	±32.2	—	—	—	0.195	27777.8	24.3	±1.1
			Juniper berries, dried	1.50 ^a	32.9	±2.8	—	—	—	—	—	—	—
			Pseudotsuga menziesii, branches with needles	0.75 ^a	26.4	±5.0	—	—	—	—	—	—	—
		Lime, peals, dried	3.48 ^a	8.7	±5.5	8.43	0.040	±5.4	0.187	699.3	6.8	±2.8	
		Ferhat <i>et al.</i> [28]	Lemon, peals, fresh	0.21	11.6	±7.9	—	—	—	—	—	—	—

^amL/100 g; ^bThe value taken from the original paper; ^cNot available

Table 4. Parameters of the kinetic models based on essential oil washing and/or diffusion: steam distillation

Reference	Plant	q_{∞} g/100 g	Pseudo first-order, Eq. (10)		Instantaneous washing and diffusion, Eq. (9)		
			$k_2 \times 10^3$ min ⁻¹	MRPD %	f	$k_2 \times 10^3$ min ⁻¹	MRPD %
Chemat <i>et al.</i> [30] ^a	Lavender; flowers, dried	8.75	52.5	±4.6	0.030	51.2	± 3.4
Cerpa <i>et al.</i> [31], Lavandin super, aerial parts, fresh; floral water flow 35 ml/min	Bed porosity						
	0.721	1.324	131.3	±16.0	—	—	—
	0.762	1.654	84.3	±27.8	—	—	—
	0.805	1.410	114.0	±7.9	—	—	—
Hanci <i>et al.</i> [33], Thyme, dried leaves; steam flow rate: 0.64 L/h	Mean particle size, mm						
	2.05	1.33 ^d	55.4	±3.2	0.173	51.6	±2.6
	1.00	1.00 ^d	48.1	±4.3	0.172	44.3	±3.7
	0.50	1.00 ^d	31.4	±4.2	0.109	29.7	±5.5
Steam flow rate: 1.03 L/h							
	2.05	1.6 ^d	53.4	±3.6	0.139	50.9	±17.9
	1.00	0.9 ^d	47.9	±6.2	—	—	—
	0.50	0.8 ^d	39.9	±2.1	—	—	—
Cassel and Vargas [37]	Cymbopogon leaves; laboratory	2.55	30.0	±13.0	0.191	26.0	±5.0
Xavier <i>et al.</i> [38] <i>Baccharis anomala</i> , aerial parts	Autumn	0.040	70.8	±18.7	—	—	—
	Winter	0.042	64.1	±18.5	—	—	—
<i>Baccharis dentata</i> , aerial parts	Autumn	0.027	73.4	±9.5	—	—	—
	Winter	0.037	40.1	±22.0	—	—	—
<i>Baccharis uncinella</i> , aerial parts	Autumn	0.163	87.7	±5.8	—	—	—
	Winter	0.182	65.1	±18.5	—	—	—
Cassel <i>et al.</i> [39]	Rosemary, leaves	0.51	16.6	±4.9	0.128	15.56	±6.4
	Basil, leaves	0.38	17.4	±17.9	—	—	—
	Lavender, leaves	0.32	12.0	±30.9	—	—	—
Boutekedjiret <i>et al.</i> [12] ^b	Rosemary, leaves	1.20	154.4	±4.2	0.480	110.8	±2.6
Koul <i>et al.</i> [40], Lemon grass	100 kg, unchopped, tight packing, 12–15 L/h	0.31 ^d	12.2	±9.4	—	—	—
	86 kg, unchopped, loose packing, 12–15 L/h	0.49 ^d	10.8	±17.5	—	—	—
	70 kg, chopped, loose packing, 12 L/h	0.55 ^d	15.0	±5.1	—	—	—
	70 kg, chopped, loose packing, 15 L/h	0.47 ^d	14.5	±21.1	—	—	—
	1000 kg, unchopped, loose packing, 125 L/h	0.57 ^d	18.5	±4.0	—	—	—
	1000 kg, unchopped, loose packing, 140 L/h	0.52 ^d	18.8	±9.8	—	—	—
	1000 kg, unchopped, loose packing, 160 L/h	0.53 ^d	18.8	±11.8	—	—	—
Romdhane and Tizaoui [32]	1.4 kPa/2 kg	1.9	18.7	±4.3	—	—	—
Aniseed; steam pressure/batch	2.0 kPa/2 kg	2.1	25.8	±5.8	—	—	—
	2.0 kPa/5 kg	2.0	20.7	±8.7	—	—	—
This work ^c	Juniper berries, dried	0.73 ^d	25.5	±19.7	0.265	22.1	±6.4
	Batch of 3 kg; bed thickness: 3 cm; steam flow rate: 30 mL/min						

^aEquation (8) was applicable with a very small value of the fraction of broken plant cells ($f = 0.030$; $k_1 = 9.80 \text{ min}^{-1}$; $k_2 = 0.0522 \text{ min}^{-1}$); ^bEq. (8) was applicable with a very large value of the fraction of broken plant cells ($f = 0.901$; $k_1 = 0.240 \text{ min}^{-1}$; $k_2 = 0.0163 \text{ min}^{-1}$); ^cEq. (8) was applicable with the following parameters: $f = 0.299$, $k_1 = 0.200 \text{ min}^{-1}$ and $k_2 = 0.0215 \text{ min}^{-1}$ (MRPD :±0.3%); ^dmL/100 g

applicable only in the latter stage of water distillation and deviated from the experimental data in the initial period.

When the model involving the simultaneous washing and diffusion of the essential oil was applied to the distillation of the essential oil from flowers [5–7], a medium to large fraction of washed essential oil (0.46 to 0.77) was observed. The washing rate constant was 3 to 5 times larger than the diffusion rate constant, indicating that the washing was much faster than the diffusion. Thus, for water distillation of essential oils from flowers, washing is more important than diffusion. The fraction f was larger and the rate constants were lower for dried lavender flowers than for fresh ones, indicating that drying increases the availability of the essential oil for washing by rupturing the cell walls but decreases the rates of washing and diffusion, probably because of in-take of the solvent by the dry plant material followed by washing and diffusion through the liquid within the plant particles. Large, but similar values of fraction f were found for the fresh flowers of *L. officinalis* and *R. segetum* [6,7]; moreover, the values of the washing and diffusion rate constants were similar for these two flowers. Small to medium values of fraction f (up to 0.52) were determined for essential oil recovery from the aerial parts and leaves of different plants by water distillation [3,9–11,13–18]. The application of vacuum during the water distillation of wild marigold increased the fraction f and dramatically increased the washing rate constant, probably due to the reduced vapor pressure of the essential oil [3]. Values of the diffusion rate constant, k_2 , determined for the different types of plant materials were mainly of the same order, about 0.01 to 0.02 min^{-1} , although, some plant materials had smaller and others higher values of this rate constant under certain operating conditions. The phenomenological model was generally applicable for essential oil extraction from large particles ($> 0.5 \text{ mm}$) of thyme, independent of the solid-to-liquid ratio, while the exponential pseudo-first order model could be employed for small plant particles [15]. Smaller values of fraction f were observed for larger plant particles of the aerial parts of thyme, which were connected to the smaller degree of plant material comminution. This is in accordance to the very small values of fraction f observed for the largest plant particles (1.0 mm). Approximately the same values of model parameters were determined for fresh and dried *E. cinerea* leaves [11].

The model based on the first-order kinetics was found to be applicable for modeling the kinetics of water distillation of the essential oil from almost all the studied plant materials, as the MRPD was generally less than $\pm 20\%$ with a few exceptions, such as lemon grass, fennel seeds and juniper berries. The diffusion rate

constants for the essential oils from the aerial parts of wild marigold, *S. hortensis* and *S. montana* and the leaves of spearmint and rosemary were approximately the same (about 0.020 to 0.023 min^{-1}). Significantly higher values of the diffusion rate constant were found for aerial parts of shirazi thyme (0.127 min^{-1}) and thyme (0.054 min^{-1}) from Iran, the leaves of cherry laurel (0.040 min^{-1}) and rosemary (0.069 min^{-1}), and lemon grass (0.070 to 0.090 min^{-1}). The diffusion rate constants for flowers, being between 0.030 and 0.054 min^{-1} , were also higher than those for most of the aerial parts and leaves. However, smaller values (generally less than 0.015 min^{-1}) were determined for the aerial parts of thyme (collected from Macedonia) and the leaves of spearmint and *E. cinerea*. The effects of plant particle size and solid-to-liquid ratio in the case of the water distillation of the essential oil from the aerial parts of thyme were observed to be very complex. The values of the diffusion rate constant for fresh and dried leaves of *E. cinerea* were similar. As expected, cumin and celery seeds in the form of powder and flakes showed much higher values of the diffusion rate constant (0.040 to 0.063 min^{-1}) than intact coriander seeds (0.005 min^{-1}). Higher values of the diffusion rate constant were found for powdered seeds than for flakes due to the better degree of seed disintegration. In the case of juniper berries, the diffusion rate constant increased with increasing the floral flow rate and with decreasing solid-to-liquid ratio. According to the diffusion rate constant at a solid-to-liquid ratio of 1:3 g/mL, the comminution of dried juniper berries using a blender (0.023 to 0.056 min^{-1}) was more efficient than using a hammer mill (0.010 min^{-1}), as can be concluded from Tables 3 and 4, respectively. The rate of essential oil diffusion was increased after microwave pretreatment of dried juniper berries. The diffusion rate constant for the peals of lime and lemon were among the lowest ones (0.009 and 0.012 min^{-1}).

Steam distillation

For steam distillation, generally, the model based on the first-order kinetics, Eq. (10), appears to be the best model for all types of plant materials included in the present study [12,31–33,37–40]. The bed porosity seems not to influence the diffusion rate constant in the case of fresh aerial parts of lavandin super. The steam flow rate did not affect the diffusion rate constant for the distillation of essential oil from dried thyme leaves and lemon grass. However, surprisingly, the diffusion rate constant decreased with decreasing plant particle size, independently of the steam flow rate. It was observed that the diffusion rate constant for lemon grass increased with increasing the batch size from 100 to 1000 kg, but chopping and dense packing did not affect the diffusion rate constant. The increase

in steam pressure in the distillation of aniseed increased the diffusion rate constant.

The phenomenological model based on the simultaneous washing and diffusion was not applicable for the steam distillation of essential oils from plant materials, except from lavender flowers, rosemary leaves and juniper berries (Table 4). In the first two cases, either a very small ($f = 0.03$) or a very large ($f = 0.90$) value of the fraction f was determined, indicating that the kinetics of essential oil distillation was rather "pure" exponential.

It is also interesting that a washing stage was not observed for most of the plant materials included in the analysis. When the washing was a part of the kinetic model (flowers of lavender as well as leaves of thyme, *Cymbopogon* and rosemary), the lowest value of the washing coefficient f was found for dried flowers of lavender (0.03). Its values were mainly between 0.11 and 0.19, indicating that diffusion through plant material is a more important stage than washing. The diffusion rate constant was of the same order for flowers and leaves.

Sigmoid model

The parameters of the sigmoid kinetic model for water and steam distillation are presented in Tables 5 and 6, respectively. Approximately the same values of the diffusion time constant were observed for water and steam distillation of the essential oil of the flowers, leaves and stems of common sage [8]. However, the

time constant was larger for water (10.4 to 14.1 min) than for steam (6.6 to 8.8 min) distillation, indicating that the latter was faster than the former (Table 5). Smaller values of the diffusion time constant were determined for water distillation of crushed than of intact parsley seeds, regardless of whether the seeds were fermented or not [23–25]. However, the solid-to-liquid ratio did not affect the diffusion rate constant for water distillation of the essential oil from parsley seeds [24,25]. The steam flow rate greatly influenced the diffusion time constant for essential oils obtained from lavender flowers and Artemisia leaves by steam distillation (Table 6) [34]. With increasing steam flow rate, the diffusion time constant decreased, indicating the enhancement of the essential oil distillation rate [34].

CONCLUSIONS

Three physical models for describing the kinetics of the hydrodistillation of essential oil from different plant materials were compared in the present paper. These models were 1) a pseudo first-order model (logarithmic model), 2) an instantaneous washing followed by diffusion model and 3) a model based on simultaneous washing and diffusion. Although all models are applicable for the water distillation of essential oils, the model based on simultaneous washing and diffusion is the best choice for describing the kinetics of essential oil recovery from any type of plant material and on any scale. In the case of steam distillation, the best model is

Table 5. Parameters of the sigmoid kinetic models: water distillation

Reference	Plant	t_0 / min	T_1 / min	MRPD / %
Veličković <i>et al.</i> [8], Common sage	Flowers	30.00	12.06	±5.1
	Leaves	33.44	14.08	±3.2
	Stems	27.59	10.37	±5.1
Stanković <i>et al.</i> [23]	Parsley, seeds, intact	105.98	39.98	±5.8
Stanković <i>et al.</i> [24], Parsley, seeds, intact, fermented (28 °C, 4 h); Intact, fermented (30 °C, 4 h)	Solid/liquid ratio, g/ml			
	1:10	81.23	35.15	±7.2
	1:15	75.22	33.22	±5.9
	1:20	74.46	34.82	±7.0
	1:25	74.87	33.70	±7.1
Crushed, fermented (30 °C, 4 h)	1:20	74.87	33.70	±7.1
	1:20	53.98	25.12	±5.9
Stanković <i>et al.</i> [25], Parsley, seeds, intact	Solid/liquid ratio, g/ml			
	1:10	95.24	38.78	±6.4
	1:15	103.05	43.37	±8.3
	1:20	81.83	37.82	±6.5
	1:25	92.25	40.22	±7.8
Crushed	1:10	60.81	29.37	±7.6
	1:15	60.50	32.50	±14.7
	1:20	51.77	27.67	±8.2
	1:25	53.46	26.70	±8.2

Table 6. Parameters of the sigmoid kinetic models: steam distillation

Reference	Plant	t_0 / min	T_1 / min	MRPD / %
Veličković <i>et al.</i> [8], Common sage	Flowers	20.01	7.66	±7.8
	Leaves	21.98	8.80	±12.3
	Stems	21.28	5.59	±14.7
Masango [34], Lavander, flowers	Steam flow rate, ml/min			
	2	49.67	19.06	±2.3
	4	22.17	8.80	±2.6
Artemisia, leaves	20	4.83	2.25	±4.5
	2.5	33.52	10.12	±2.9
	5	17.39	5.58	±3.1
Charchari and Hamadi [35]	20	4.74	2.01	±3.9
	<i>Artemisia judaica</i> , aerial parts, fresh	41.43	8.95	±4.8
	Dried plant	5.58	2.40	±8.3
Mateus <i>et al.</i> [36], Rosemary, leaves and caulis	Fresh plant	4.54	1.91	±4.0

the pseudo-first-order model, while the model based on simultaneous washing and diffusion was non-applicable except in the case of a few plant materials. For certain plant materials, however, only the sigmoidal model fitted the experimental data. Further studies involving a number of operational variables should be performed to derive a general model applicable to all plant materials from laboratory to the industrial scale.

REFERENCES

- [1] F. Bakkali, S. Averbeck, D. Averbeck, M. Idaomar, Biological effects of essential oils – A review, *Food Chem. Toxicol.* **46** (2008) 446–475.
- [2] S.Ž. Milojević, T.D. Stojanović, R. Palić, M.L. Lazić, V.B. Veljković, Kinetics of distillation of essential oil from comminuted ripe juniper (*Juniperus communis* L.) berries, *Biochem. Eng. J.* **39** (2008) 547–553.
- [3] K.G.D. Babu, V.K. Kaul, Variations in quantitative and qualitative characteristics of wild marigold (*Tagetes minuta* L.) oils distilled under vacuum and at NTP, *Ind. Crops Prod.* **26** (2007) 241–251.
- [4] R.B. Inman, P.J. Dunlop, J.F. Jackson, Oils and waxes of eucalyptus: vacuum distillation methods for essential oils. In: Linskens, H.F., Jackson, J.F. (Eds.), *Modern Methods of Plant Analysis*, New series. Essential Oils and Waxes, Vol. 12, Springer-Verlag, Heidelberg, 1991, pp. 195–203.
- [5] P. Morin, C. Gunther, L. Peyron, H. Richard, Etude des phénomènes physico-chimiques intervenant lors du procédé d'hydrodistillation, *Bull. Soc. Chim. Fr.* **5** (1985) 921–930.
- [6] H.B. Jannet, Z. Mighri, Hydrodistillation kinetic and antibacterial effect studies of the flower essential oil from the Tunisian *Ridolfia segetum* (L.), *J. Essent. Oil Res.* **19** (2007) 258–261.
- [7] Lj. Stanojević, M. Stanković, M. Čakić, V. Nikolić, Lj. Nikolić, D. Ilić, N. Radulović, The effect of hydrodistillation techniques on yield, kinetics, composition and antimicrobial activity of essential oils from flowers of *Lavandula officinalis* L., *Hem. Ind.* **65** (2011) 455–463.
- [8] D. Veličković, M. Ristić, D. Stojiljković, A. Šmelcerović, Kinetics of obtaining the essential oil by different technological procedures from flowers, leaves and stems of sage (*Salvia officinalis* L.), *Lek. sirov.* **21** (2001) 67–72.
- [9] S. Rezvanpanah, K. Rezaei, S.H. Razavi, S. Moini, Use of Microwave-assisted Hydrodistillation to Extract the Essential Oils from *Satureja hortensis* and *Satureja montana*, *Food Sci. Technol. Res.* **14** (2008) 311–314.
- [10] E.-H. Benyoussef, N. Yahiaoui, A. Khelfaoui, F. Aid, Water distillation kinetic study of spearmint essential oil and of its major components, *Flavour Fragrance J.* **20** (2005) 30–33.
- [11] G.D.K. Babu, B. Singh, Simulation of *Eucalyptus cinerea* oil distillation: A study on optimization of 1,8-cineole production, *Biochem. Eng. J.* **44** (2009) 226–231.
- [12] C. Boutekedjiret, F. Bentahar, R. Belabbes, J. Bessiere, Comparative study of the kinetics extraction of rosemary essential oil by steam distillation and hydrodistillation, *Récents Progrès en Génie des Procédés (Lavoisier, Paris, France)* **92** (2005).
- [13] N. Bousbia, M.A. Vian, M.A. Ferhat, E. Petitcolas, B.Y. Meklati, F. Chemat, Comparison of two isolation methods for essential oil from rosemary leaves: Hydrodistillation and microwave hydrodiffusion and gravity, *Food Chem.* **114** (2009) 355–362.
- [14] M.-T. Golmakani, K. Rezaei, Comparison of microwave-assisted hydrodistillation with the traditional hydrodistillation method in the extraction of essential oils from *Thymus vulgaris* L., *Food Chem.* **109** (2008) 925–930.
- [15] H. Sovová, S.A. Aleksovski, Mathematical model for hydrodistillation of essential oils, *Flavour Fragrance J.* **21** (2006) 881–889.
- [16] M. Gavahian, A. Farahnaky, M. Majzoobi, K. Javidnia, M. J. Saharkhiz, G. Mesbahi, Ohmic-assisted hydrodistillation of essential oils from *Zataria multiflora* Boiss (Shirazi thyme), *Int. J. Food Sci. Technol.* **46** (2011) 2619–2627.

- [17] T. Silou, M. Malanda, L. Loubaki, Optimisation de l'extraction de l'huile essentielle de *Cymbopogon citratus* grâce à un plan factoriel complet 2³, *J. Food Eng.* **65** (2004) 219–223.
- [18] I.T. Stanisljević, S.S. Stojičević, D.T. Veličković, M.S. Ristić, M.L. Lazić, V.B. Veljković, Kinetics of hydrodistillation and chemical composition of essential oil from cherry laurel (*Prunus laurocerasus* var. *serbica* Pančić) leaves, *J. Essent. Oil Res.* **22** (2010) 564–567.
- [19] E.-H. Benyoussef, S. Hasni, R. Belabbes, J.-M. Bessiere, Modélisation du transfert de matière lors de l'extraction de l'huile essentielle des fruits de coriandre, *Chem. Eng. J.* **85** (2002) 1–5.
- [20] H.B. Sowbhagya, B.V. Sathyendra Rao, N. Krishnamurthy, Evaluation of size reduction and expansion on yield and quality of cumin (*Cuminum cyminum*) seed oil, *J. Food Eng.* **84** (2008) 595–600.
- [21] H.B. Sowbhagya, S.R. Sampathu, N. Krishnamurthy, Evaluation of size reduction on the yield and quality of celery seed oil, *J. Food Eng.* **80** (2007) 1255–1260.
- [22] Á. Kapás, C.D. András, T. Gh. Dobre, E. Vass, G. Székely, M. Stroescu, S. Lányi, B. Ábrahám, The kinetic of essential oil separation from fennel by microwave assisted hydrodistillation (MWHD), *Univ. Polytech. Bucharest. Sci. Bull., Ser. B* **73** (2011) 113–120.
- [23] M. Stanković, N. Nikolić, L. Stanojević, M.D. Čakić, The effect of hydrodistillation technique on the yield and composition of essential oil from the seed of *Petroselinum crispum* (Mill.) Nym. ex. A.W. Hill, *Chem. Ind. Chem. Eng. Q.* **10** (2004) 409–412.
- [24] M.Z. Stanković, N.Č. Nikolić, L.P. Stanojević, S.D. Petrović, M.D. Čakić, Hydrodistillation kinetics and essential oil composition from fermented parsley seeds, *Chem. Ind. Chem. Eng. Q.* **11** (2005) 25–29.
- [25] M.Z. Stanković, L.P. Stanojević, N.Č. Nikolić, M.D. Čakić, The effect of parsley (*Petroselinum crispum* (Mill.) Nym. ex. A.W. Hill) seeds milling and fermentation conditions on essential oil yield and composition, *Chem. Ind. Chem. Eng. Q.* **11** (2005) 177–182.
- [26] P. Miletić, R. Grujić, Ž. Marjanović-Balaban, The application of microwaves in essential oil hydrodistillation processes, *Chem. Ind. Chem. Eng. Q.* **15** (2009) 37–39.
- [27] A.C. Atti-Santos, M. Rossato, L. Atti Serafini, E. Cassel, P. Moyna, Extraction of Essential Oils from Lime (*Citrus latifolia* Tanaka) by Hydrodistillation and Supercritical Carbon Dioxide, *Braz. Arch. Biol. Technol.* **48** (2005) 155–160.
- [28] M.A. Ferhat, B.Y. Meklati, F. Chemat, Comparison of different isolation methods of essential oil from Citrus fruits: cold pressing, hydrodistillation and microwave "dry" distillation, *Flavour Fragrance J.* **22** (2007) 494–504.
- [29] J. Pornpunyapat, Pakamas Chetpattananondh, Chakrit Tongurai, Mathematical modeling for extraction of essential oil from *Aquilaria crassna* by hydrodistillation and quality of agarwood oil, *Bangladesh J. Pharmacol.* **6** (2011) 18–24.
- [30] F. Chemat, M. E. Lucchesi, J. Smadja, L. Favretto, G. Colnaghi, F. Visinoni, Microwave accelerated steam distillation of essential oil from lavender: A rapid, clean and environmentally friendly approach, *Anal. Chim. Acta* **555** (2006) 157–160.
- [31] M.G. Cerpa, R.B. Mato, M.J. Cocero, Modeling Steam Distillation of Essential Oils: Application to Lavandin Super Oil, *AIChE J.* **54** (2008) 909–917.
- [32] M. Romdhane, C. Tizaoui, The kinetic modelling of a steam distillation unit for the extraction of aniseed (*Pimpinella anisum*) essential oil, *J. Chem. Technol. Biotechnol.* **80** (2005) 759–766.
- [33] S.S. Hancı, S. Sahin, L. Yılmaz, Isolation of volatile oil from thyme (*Thymus spicata*) by steam distillation, *Nahrung/Food* **47** (2003) 252–255.
- [34] P. Masango, Cleaner production of essential oils by steam distillation, *J Clean Prod.* **13** (2005) 833–839.
- [35] S. Charchari, S. Hamadi, Kinetic study of *Artemisia judaica* L. essential oil steam distillation, *J. Essent. Oil Bear. Plants* **10** (2007) 304–309.
- [36] E.M. Mateus, C. Lopes, T. Nogueira, J.A.A. Lourenço, M.J. Marcelo Curto, Pilot Steam Distillation of Rosemary (*Rosmarinus officinalis* L.) from Portugal, *Silva Lusitana* **14** (2006) 203–217.
- [37] E. Cassel, R.M.F. Vargas, Experiments and Modeling of the *Cymbopogon winterianus* essential oil extraction by steam distillation, *J. Mex. Chem. Soc.* **50** (2006) 126–129.
- [38] V.B. Xavier, R.M.F. Vargas, E. Cassel, A.M. Lucas, M.A. Santos, C.A. Mondin, E.R. Santarem, L.V. Astaritac, T. Sartor, Mathematical modeling for extraction of essential oil from *Baccharis* spp. by steam distillation, *Ind. Crops Prod.* **33** (2011) 599–604.
- [39] E. Cassel, R.M.F. Vargas, N. Martinez, D. Lorenzo, E. Dellacassa, Steam distillation modeling for essential oil extraction process, *Ind. Crops Prod.* **29** (2009) 171–176.
- [40] V.K. Kaul, B.M. Gandotra, S. Koul, S. Ghosh, C.L. Tikoo, A.K. Gupta, Steam distillation of lemon grass (*Cymbopogon spp.*), *Ind. J. Chem. Technol.* **11** (2004) 135–139.
- [41] A. Ammann, D.C. Hinz, R.S. Addleman, C.M. Wai, B.W. Wenclawiak, Superheated water extraction, steam distillation and SFE of peppermint oil, *Fresenius' J. Anal. Chem.* **364** (1999) 650–653.

IZVOD

MODELovanje KINETIKE HIDRODESTILACIJE ETARSKOG ULJA IZ BILJNIH MATERIJALA

Svetomir Ž. Milojević¹, Dragana B. Radosavljević¹, Vladimir P. Pavićević², Srđan Pejanović², Vlada B. Veljković³

¹*Fakultet tehničkih nauka, Univerzitet u Prištini, Kosovska Mitrovica, Srbija*

²*Tehnološko–metalurški fakultet, Univerzitet u Beogradu, Karnegijeva 4, 11000 Beograd, Srbija*

³*Tehnološki fakultet, Univerzitet u Nišu, Bulevar oslobođenja 124, 16000 Leskovac, Srbija*

(Naučni rad)

Rad se bavi modelovanjem kinetike ekstrakcije etarskog ulja iz biljnih materijala primenom destilacija vodom i vodenom parom. Eksperimentalni podaci dobijeni su proučavanjem kinetike hidrodestilacije etarskog ulja ploda kleke. Literaturni podaci o kinetici hidrodestilacije etarskog ulja iz različitih biljnih materijala su, takođe, uključeni u modelovanje. Za opisivanje kinetike hidrodestilacije etarskog ulja razvijen je fizički model koji je zasnovan na istovremenom ispiranju i difuziji etarskog ulja iz biljnog materijala. Iz ovog modela izvedena su dva prostija modela od kojih je prvi zasnovan na trenutnom ispiranju praćenim difuzijom a drugi na difuziji bez ispiranja (tj. na kinetici prvog reda). Glavni cilj je bio poređenje ovih modela i predlaganje optimalnog za destilacije vodom i vodenom parom I za različite biljne materijale. Sva tri modela opisuju dobro eksperimentalne kinetičke podatke u slučaju destilacije vodom nezavisno od tipa destilatora i njegove veličine, tipa biljnog materijala i procesnih uslova, ali je najbolji model koji uključuje istovremeno ispiranje i difuziju etarskog ulja. Ovaj model je, međutim, neprimenljiv za vodeno-parnu destilaciju etarskog ulja, izuzev za etarsko ulje ploda kleke. Za ovu destilaciju etarskog ulja najbolji je kinetički model pseudo-prvog reda. U slučaju nekoliko biljnih materijala, promena prinosa etarskog ulja sa vremenom je sigmoidna, pa je modelovana Boltzmanovom sigmoidnom funkcijom.

Ključne reči: Destilacija vodenom parom

• Destilacija vodom • Difuzija • Fizički modeli • Ispiranje • Modelovanje